Universidad Autónoma de Madrid

Dpto. Bioquímica

MECANISMOS DE LA ACCIÓN ANTI-INFLAMATORIA DE DERIVADOS SINTÉTICOS DEL ÁCIDO ACANTOICO

MARÍA PIMENTEL SANTILLANA

TESIS DOCTORAL

MADRID, 2013

DEPARTAMENTO DE BIOQUÍMICA

FACULTAD DE MEDICINA

UNIVERDIDAD AUTÓNOMA DE MADRID

MECANISMOS DE LA ACCIÓN ANTI-INFLAMATORIA DE DERIVADOS SINTÉTICOS DEL ÁCIDO ACANTOICO

Memoria de Tesis Doctoral presentada por

MARÍA PIMENTEL SANTILLANA

Licenciada en Biotecnología,

para aspirar al grado de Doctor por la

Universidad Autónoma de Madrid

Directores de Tesis:

Dr. Lisardo Boscá Gomar

Profesor Investigación

Dra. Francisca González Través

Instituto de Investigaciones Biomédicas "Alberto Sols"

CSIC-UAM

Dr. Lisardo Boscá Gomar, Profesor de Investigación del Instituto de Investigaciones Biomédicas “Alberto Sols” CSIS-UAM y Dra. Francisca González Través

CERTIFICAN:

Que María Pimentel Santillana, Licenciada en Biotecnología, ha realizado bajo nuestra dirección el trabajo de investigación titulado: “MECANISMOS DE LA ACCIÓN ANTI-INFLAMATORIA DE DERIVADOS SINTÉTICOS DEL ÁCIDO ACANTOICO” en el Instituto de Investigaciones Biomédicas "Alberto Sols”.

Consideramos que el mencionado trabajo es satisfactorio y apto para poder optar al grado de Doctor por la Universidad Autónoma de Madrid.

Y para que conste a todos los efectos, firmamos el presente certificado en Madrid, a …. de Septiembre de 2013.

Fdo.: Lisardo Boscá Gomar

Director de Tesis

Profesor Investigación

Fdo.: Francisca Gonzáles Través

Co-directora de Tesis

VºBº Tutora

Margarita Fernández Martín

Profesora Titular, UAM

Este trabajo ha sido realizado en el Departamento de Bioquímica del Instituto de Investigaciones Biomédicas “Alberto Sols” (IIBM), centro mixto CSIC-UAM, con la ayuda de una beca de formación de personal investigador (FPI) del Ministerio de Economía y Competitividad de España.

“Para empezar un gran proyecto, hace falta valentía.

Para terminar un gran proyecto, hace falta perseverancia”

Anónimo

Para mi familia

AGRADECIMIENTOS

Ya han pasado cuatro años desde que entré por la puerta del B-11…Todo el mundo me decía que estos años pasaban volando, y a mí me parecían una eternidad y sin embargo, tengo que darles la razón a todos y cada uno de ellos. Ya han pasado y aquí me encuentro, escribiendo la Tesis Doctoral, quién me lo iba a decir!!!

El hecho de que estos años al final hayan pasado tan deprisa significa que han estado llenos, sobre todo, de buenos momentos gracias a toda la gente que me ha rodeado y arropado durante esta etapa. Por eso, no puedo ni quiero dejar de agradecer a todos ellos el apoyo y confianza que me han demostrado.

En primer lugar, como no podría ser de otra manera, al Dr. Lisardo Boscá, por haber depositado en mí toda su confianza, acogerme en su grupo y darme esta oportunidad. GRACIAS JEFE por contagiarme de tu optimismo y por dejarme libertad para tomar mis propias decisiones, aunque en alguna ocasión tuviera que oír “te lo dije, incrédula”; y porque a pesar de estar tan ocupado, siempre has tenido un hueco para escuchar lo que te tuviera que decir.

En segundo lugar, a mi co-directora de tesis, la Dra. Francisca González, para mí, Paqui. Gracias por haberme servido de guía en mi andadura científica, sobre todo los primeros años en los que compartíamos laboratorio, y por haber estado pendiente de mí a pesar de la distancia.

Por supuesto, gracias también a la Dra. Paloma Martín, la otra jefa del labo y con quien comencé mi camino en el mundo científico. Por todo lo enseñado en aquellos meses y en estos años y por tu interés en conocer mis resultados.

Al recordar mis comienzos me acuerdo también de la Dra. Sonsoles Hortelano, con la que también compartí un año de mi vida en su laboratorio antes de iniciar esta andadura. Gracias por todo lo que me transmitiste ese año, por tu comprensión y por la alegría que siempre demostrabas, anda que no nos reímos juntas… Por supuesto a Raquelita, Gaby y Alfonsito, de los cuales aprendí mucho.

Gracias al Dr. Antonio Castrillo por orientarme e interesarse en mi trabajo en sus múltiples y fugaces visitas a Madrid. Así como por habernos dejado unos de tus ratoncitos para realizar una serie de experimentos.

Quería agradecer a los servicios del IIB y de la Autónoma por su trabajo, a Laura de citometría, Lola, Ana y Diego de confocal… y en especial a Toño, de informática, por el pánico de estos meses anteriores a la escritura de la Tesis, en los que pensé que me quedaba sin

ordenador; ahora lo recuerdo y me río, por lo menos estuve entre los 5 primeros de tu lista!!! Jajaja. Tardé en darte guerra, pero lo hice y bien!!!

También a la gente de otros laboratorios que me han prestado su ayuda desinteresada en distintos momentos a lo largo de estos cuatro años, en especial a Carlos del B-15 por las charlas en el pasillo y por enseñarme esas fotos que me alegraban el día, jejeje.

A mi grupo americano de San Diego, gente a la que nunca olvidaré. Al Dr. Lemke, por recibirme en su laboratorio y mostrarse cercano durante esos tres meses. Ah! Y por ese pavo tan estupendo que nos preparaste en acción de gracias!!! A Paqui, por agilizar los trámites y porque tener a alguien allí siempre tranquiliza, a pesar de que igualmente fui con mucho miedo, y por soportarme, sobre todo los días antes de dar "mis adorados" seminarios. A Lawrence, por su paciencia conmigo y repetirme las frases una y otra vez; al final logró que la entendiera!!! A Joseph, Anna, Jennifer y Erin por estar siempre pendientes de mí y en especial a "mi técnico", Patrick, quien desde el momento uno se preocupó muchísimo por mí, por intentar aprender palabras en español conmigo, por los pequeños regalitos del principio, por haberme alimentado tan bien (gracias a ti, y a más personas, volví con algún kilito, jejeje) y por no haberte desesperado conmigo; y como no, por todo lo que me enseñaste, gracias!!! Y a toda la gente con la que compartí estos tres meses maravillosos, tanto al grupo de españoles, sobre todo a Sandrita, como a mis caseros, Lukas y Vanessa; y a Ben, mi alemán pirado, con quien compartí muchas risas a la hora de volver a casa, espero que hayas mejorado como portero…y cocinero, jajaja.

Y como no, ya os ha llegado el turno, A MIS NIÑAS DEL B-11!!!, los chicos ya sabéis que os consideramos una más, jejeje, por lo tanto, también estáis dentro del grupo. Unas de las personas más importantes durante estos cuatro años, con las que he trabajado codo con codo y que han hecho que mi etapa como pre-doctoral sea una época inolvidable. Si hablo de los inicios no me puedo olvidar de Paqui y Rafa, dos de "mis maestrillos", de los que aprendí gran parte de lo que hoy sé y con los que me he vuelto a reencontrar en San Diego. A Rafa, gracias por tu paciencia, por enseñarme cuando aún era estudiante y por todos los temas de ordenador; y a Paqui, por mostrarte cercana, por preguntarme y estar siempre pendiente de mí, gracias. A Cris, mi antecesora en todo esto, espero que todo te vaya genial en tu nueva etapa como post-doc. ¡Qué decir del resto que no sepáis ya, que me habéis aguantado durante todo este tiempo y con quienes he compartido tantas cosas! A María, hasta ahora la mami del grupo, por tus frases alentadoras en todo momento: "te va a ir genial, ya lo verás", "te va a salir"… gracias por apoyarme siempre que lo he necesitado, sobre todo en estos meses de escritura y por enseñarme que las cosas claras y bien hechas, bien parecen. A mis "churris", Patri y Vero, ¿os acordáis de

mis primeros días intentando coger un ratoncillo negro en el pasillo de la cámara fría? Cómo olvidarlo, no? Jajaja. A Patri, de la que me llevé una buena opinión en mi primera etapa en el B-11 debido a su entusiasmo contagioso, estos años he podido comprobar que no era solo una impresión; gracias por haber estado dispuesta a ayudarme siempre. A Vero, mi compañera de mesa durante un año, gracias por tu complicidad, apoyo, cariño, ayuda, por entenderme con solo mirarnos, por escucharme siempre y estar disponible cuando te he necesitado, tanto dentro como fuera del labo. Ahhh!!! Y por tu cartelito a la hora de separarnos, jejeje. A Noe, mi nueva compi, anda que no hemos compartido charletas tú y yo en el sitio y en el coche!, por preguntarme y asesorarme en todo momento, gracias por todo ello y por tus consejos. Por cierto, al final te he demostrado que "sí existe", jajaja. A María José, por mostrarte siempre tan servicial y dispuesta a ayudarnos. A Gemita, a la que ya conocía y con la que he vuelto a coincidir, gracias por todo. A Omar, ¿o tendría que decir "Monito"? jejeje, debido a tí desapareció la operación biquini en el labo!!! Gracias por interesarte por mí en estos meses de escritura y decirte que…prepárate que el siguiente eres tú!!! A Luuuiiiis, el mejicano del labo, gracias por los dos años compartidos y estaremos encantadas de "aguantarte" un año más, jajaja. A Silvia, la última adquisición del grupo. No me puedo olvidar tampoco de Dani, nuestro argentino, por los buenos momentos vividos durante tus seis meses en el laboratorio, solo decirte que estaremos esperándote de nuevo con los brazos abiertos. Debido a que este año no será recordado en el labo solo por mi tesis, no puedo dejar de acordarme de las pequeñas nuevas incorporaciones!!! También recuerdo los buenos momentos vividos fuera del labo, las comidas de navidad, en mi pueblo, en Pelayos, en las despedidas de soltera, en las bodas…han sido muchos los momentos compartidos con vosotros, por eso, a todos y cada uno muchas gracias por no ser meros compañeros de trabajo, si no por vuestra amistad, y terminar diciéndoos "hay que ver como sois!!": GENIALES!!!

A mis amigos de toda la vida, por mostrarme su apoyo en todo momento, en especial en estos meses, aunque muchos de ellos se han quedado solamente en que trabajo con ratones!!! Gracias por vuestro interés en conocer mi trabajo y por todos los momentos vividos junto a vosotros, y por los que nos quedan, entre ellos la primera boda!!! Jajaja. En especial a Celia, que ha tenido que soportar horas y horas de conversación conmigo, en ocasiones, sin enterarse de que hablaba, pero siempre ha estado ahí.

Y en último lugar, y no por ello menos importante, a mi familia. No os puedo nombrar a todos porque me faltarían páginas, pero sí tengo que nombrar de un modo especial al primo Enrique, que a pesar de que ya no está con nosotros, estoy segura de que nos sigue muy de cerca; Kike, mientras nosotros estemos aquí, tú seguirás con nosotros. A mis abuelos, a los que están y

no están, por preocuparse tanto por mí, por preguntarme que tal me van las cosas y por querer que disfrute de la vida.

Muy especialmente a mis padres y mi hermano, los mejores que nadie pueda soñar. A mi hermano, Carlos, con quien tanto me he peleado de pequeña y que el paso del tiempo ha hecho que estemos cada vez más unidos, gracias por soportarme, por los momentos y risas compartidos. Gracias también a “mi cuñaína”, Sara, con la que he compartido tantas y tantas cosas. A mis padres, por su apoyo y amor incondicional, por estar siempre ahí y darme en todo momento ánimos, cuando los he necesitado, para seguir adelante; por aconsejarme y apoyarme en todas y cada una de mis decisiones. A papá, por dejarme ser “tu princesa”, querías tener una niña y al final lo conseguiste!!! A mamá, por todo lo que te has sacrificado por nosotros. Gracias a los dos por estar siempre pendientes de nosotros y que no nos falte de nada. Os quiero!!!

ÍNDICE

ABREVIATURAS

ADN	Ácido desoxirribonucleico
AP-1	Proteína activadora 1
ARN	Ácido ribonucleico
BMDM	Macrófagos derivados de médula ósea
cADN	ADN complementario
COX	Ciclooxigenasa 2
DAPI	4',6-diamidino-2-fenilindol diclorohidrato
DE	Desviación estándar
DEPC	Dietilpirocarbonato
D-GalN	D-galactosamina
DKO	*Double knockout*
DMSO	Dimetilsulfóxido
dNTPs	Desoxinucleótidos
DTP	Diterpeno
ECL	Sistema intensificador de quimioluminiscencia para Western blot
EDTA	Ácido etilen-diamino tetra-acético
EGTA	Ácido etilen-bis tetra-acético
ERK	Quinasa regulada por señales extracelulares
IFN	Interferón
IKK	Quinasa IκB
IL	Interleuquina
IL-1R	Receptor de interleuquina 1
IP	Ioduro de propidio
i.p.	Intraperitoneal
IRAK	Quinasa asociada al receptor IL-1
IκB	Inhibidor *kappa* B

IRF3	Factor 3 regulador de interferón
JNK	Quinasa c-Jun N-terminal
KO	*Knockout* (deficiente)
LPS	Lipopolisacárido
LTA	Ácido lipoteicoico
LXR	Receptor X hepático
MAPK	Proteína quinasa activada por mitógenos
M-CSF	Factor estimulante de colonias de macrófagos
MPO	Mieloperoxidasa
mTOR	Diana de la rapamicina en mamíferos
MyD88	Factor 88 de diferenciación mieloide
NEDA	Naftiletilenodiamina
NF-κB	Factor nuclear κB
NLS	Secuencia de señalización nuclear
NO	Óxido nítrico
NOS	Óxido nítrico sintasa
PAMPs	Patrones moleculares asociados a patógeno
PBS	Tampón fosfato salino
PCR	Reacción en cadena de la polimerasa
PDK	Quinasa dependiente de fosfoinositoles
PI3K	Fostatidil inositol 3 quinasa
pI:C	Ácido poliinosítico-policitidílico
PIP	Fostatidil inositol fosfato
PMSF	Fenil-metil sulfonil fluoruro
PTEN	Fosfatasa homóloga a la tensina
RHD	Dominio de homología Rel

RNasa	Ribonucleasa
ROS	Especies reactivas de oxígeno
RT	Retrotranscripción
SDS	Dodecilsulfato de sodio
SFB	Suero fetal bovino
siARN	ARN de interferencia pequeño
SOCS	Supresor de la señalización por citoquinas
T1317	T0901317 (ligando comercial de LXRs)
TAD	Dominio de activación de la transcripción
TAK	Quinasa activada por factor de crecimiento transformante β (TGF-β)
TANK	Activador de NF-κB asociado a la familia TRAF
TBK1	Quinasa de unión a TANK1
TIR	Receptor Toll/interleuquina 1 (Toll/Il-1R)
TIRAP	Proteína adaptadora con dominio TIR
TLR	Receptores tipo Toll
TNF	Factor de necrosis tumoral
TPA	12-O-tetradecanoil-forbol-13-acetato
TRAF	Factor asociado al receptor TNF
TRAM	Molécula adaptadora relacionada con TRIF
TRIF	Adaptador que contiene el dominio TIR e induce IFN-β
vs.	*Versus*
WT	*Wild type* (silvestre)

RESUMEN

En los últimos años ha habido un gran interés científico en el estudio de las propiedades terapéuticas, sobre todo anti-inflamatorias, de compuestos naturales como son los diterpenos, sin embargo, son pocos los trabajos que se han centrado en los mecanismos de acción de estas moléculas a través de los cuales ejercen sus acciones anti-inflamatorias.

Evaluamos la capacidad anti-inflamatoria de cinco moléculas derivadas del ácido acantoico. Tres de ellas, DTP1, DTP3 y DTP5, fueron seleccionadas para evaluar sus efectos en la generación de mediadores inflamatorios en macrófagos peritoneales y macrófagos derivados de médula ósea activados con diferentes ligandos de los receptores tipo Toll (TLRs). Los resultados obtenidos mostraron que estos DTPs ejercen un gran efecto inhibitorio en la expresión de genes regulados por NF-κB, tales como NOS-2 y COX-2, inducidos tras la estimulación con ligandos de TLR2, TLR3 y TRL4. Además, se observó una clara inhibición de citoquinas pro-inflamatorias después de la estimulación con diferentes ligandos de los TLRs. Al analizar el efecto de los DTPs sobre la vía de señalización de NF-κB, se observó que fueron capaces de reducir la degradación de IκB-β, inhibiendo la fosforilación de IKK, tras la activación con LPS, LTA o pI:C. El análisis de la vía de las MAPKs mostró que los niveles p-p38 y p-ERK estaban reducidos en los macrófagos estimulados con ligandos de los TLRs y pre-tratados con DTPs, mientras que la fosforilación de JNK no se vio alterada. Por otra parte, estudios realizados macrófagos de ratones deficientes en MyD88 mostraron que estos DTPs son capaces de actuar tanto a través de la vía dependiente de MyD88 como de la vía dependiente de TRIF, lo que sugiere la existencia de una vía de señalización común, que comprometa los TLRs, a través de la cual los DTPs ejercen su efecto. También se demostró que ejercen una rápida y potente activación de la vía PI3K/Akt, que conduce a la inhibición de la vía de NF-κB y de las MAPKs p38 y ERK. La inhibición de PI3K suprimió el efecto de los DTPs en las vías de NF-κB y de las MAPKs.

Estudios *in vivo* realizados en ratones con DTPs, demostraron que éstos son capaces de ejercer acciones anti-inflamatorias en el edema de la oreja inducido por TPA, además, redujeron los niveles de TNF-α en plasma, mejoraron la supervivencia de los animales en un modelo de letalidad inducida por LPS/D-galactosamina e inhibieron la actividad mieloperoxidasa inducida por zimosán.

Los efectos anti-inflamatorios de estos DTPs y su baja toxicidad, los convierten en moléculas con un gran potencial terapéutico para el tratamiento de enfermedades inflamatorias.

SUMMARY

During the last years, the level of research activity related to diterpenes (DTPs) has significantly increased, trying to provide evidence on the therapeutic properties of natural products, mainly for their use as anti-inflammatory drugs; however, only few reports have examined the mechanisms involved in the anti-inflammatory actions of these molecules.

In the present study, five acanthoic acid-derived molecules (DTPs) were tested for potential anti-inflammatory activity. Three of these compounds, DTP1, DTP3 and DTP5, were selected to evaluate their effects on the generation of inflammatory mediators in peritoneal macrophages and bone marrow derived macrophages activated with different Toll-like receptor (TLR) ligands. The results obtained showed that these DTPs exert potent inhibitory effects on the expression of NF-κB responsive genes, such as NOS-2 and COX-2, after stimulation with TLR2, TLR3 and TLR4 ligands. In addition, we observed a clear inhibition of the release of pro-inflammatory cytokines after stimulation with TLR ligands. Examination of the effects of these DTPs on NF-κB signaling showed that DTPs inhibit IKK phosphorylation, preventing the IκBβ degradation, after activation with LPS, LTA and pI:C. Modulation of MAPKs pathways by DTPs, was also analyzed. p-p38 and p-ERK were reduced in macrophages stimulated with TLR ligands and pre-treated with DTPs, while JNK phosphorylation induced by LPS, LTA and pI:C was unaffected by DTPs. Moreover, studies in macrophages from MyD88-deficient mice indicated that DTPs act both in MyD88- and TRIF-dependent pathways point to the presence of "shared" signaling pathways upon TLR2, TLR3 and TLR4 engagement. DTPs display a rapid and potent activation of the PI3K/Akt pathway. PI3K/Akt activation block of the LPS-dependent stimulation of IKK/NF-κB and p38 and ERK MAPKs. Inhibition of PI3K suppressed the effect of these DTPs on IKK/NF-κB and MAPKs signaling after stimulation with TLR2, TLR3 and TLR4 ligands.

DTP1 and DTP5 displayed significant anti-inflammatory activity *in vivo*, suppressing mouse ear edema induced by TPA and decreasing the TNF-α plasma levels. Furthermore, intraperitoneal injection of these DTPs improved mice survival in a model of D-galactosamine/LPS-dependent lethality and reduced myeloperoxidase activity induced by zymosan.

In conclusion, the anti-inflammatory effects of these compounds, together with their low cell toxicity, suggest potential therapeutic applications in the regulation of the inflammatory response.

INTRODUCCIÓN

1. El sistema inmune.

Todos los organismos están expuestos constantemente a microorganismos infecciosos presentes en el entorno y necesitan hacer frente a la invasión de estos patógenos, para no sufrir constantemente las enfermedades que éstos ocasionan. La defensa del organismo frente a agentes extraños está mediada por el sistema inmune, dentro del cual podemos distinguir entre las llamadas respuesta inmune innata y respuesta inmune adaptativa.

La respuesta inmune innata engloba una serie de mecanismos de defensa celulares y bioquímicos que constituyen la primera barrera de defensa del organismo frente a la infección de agentes patógenos. Es el mecanismo de defensa más antiguo y conservado evolutivamente y está presente en todos los organismos pluricelulares. La inmunidad innata depende de receptores codificados por genes de la línea germinal (Medzhitov and Janeway, 1997) (Turvey and Broide, 2010), que reconocen características comunes a muchos agentes patógenos.

El sistema inmune adaptativo distingue moléculas específicas incluso de microorganismos muy relacionados entre sí, gracias a receptores específicos de antígeno que se generan por reordenamiento genético. Aquella célula capaz de reconocer al antígeno se expande clonalmente (Turvey and Broide, 2010). Además, el sistema inmune adaptativo se caracteriza por poseer capacidad de memoria, aumentando la capacidad de defensa frente a exposiciones posteriores del microorganismo.

1.1. La respuesta inflamatoria.

La enfermedad infecciosa se produce cuando un microorganismo supera las barreras físicas de defensa del huésped para establecer un sitio de infección y su posterior transmisión. Esta expansión del agente patógeno se controla normalmente por una respuesta inflamatoria, la cual tiene lugar en el sitio de infección y es llevada a cabo gracias a la respuesta de los macrófagos frente a los microorganismos invasores. La inflamación se define por cuatro signos, que son calor, dolor, rubor o enrojecimiento y tumor o hinchazón (Bosca et al., 2005), siendo todos ellos consecuencia de los efectos que producen mediadores inflamatorios al actuar sobre los vasos sanguíneos locales. La dilatación y el aumento de permeabilidad de los vasos sanguíneos locales durante la inflamación conllevan un aumento del flujo sanguíneo y del flujo de células y plasma desde los capilares al tejido, lo cual explica el calor, el enrojecimiento y la hinchazón. A su vez, también se producen cambios en las propiedades adhesivas del endotelio, provocando que células circulantes se adhieran a las células endoteliales de la pared vascular y

migren entre ellas hasta el foco de infección. Esta migración de las células y sus efectos locales explican el dolor.

En definitiva, el objetivo de la respuesta inflamatoria es destruir a los patógenos invasores poniendo en contacto a dichos microorganismos con células efectoras.

El tipo celular que se observa de forma predominante en las primeras fases de la respuesta inflamatoria son los neutrófilos. El flujo de neutrófilos va seguido poco después por la infiltración de los monocitos, que se diferencia rápidamente a macrófagos los cuales constituyen las principales células efectoras de la respuesta inflamatoria.

1.2. Implicación de los macrófagos en la respuesta inflamatoria.

Los macrófagos son células que maduran a partir de los monocitos circulantes que abandonan la circulación sanguínea para migrar al interior de los tejidos. Su desarrollo comienza en la médula ósea, donde una célula madre se diferencia a un progenitor mieloide, que es el precursor de los granulocitos (basófilos, eosinófilos y neutrófilos), monocitos (que posteriormente darán lugar a los macrófagos) y células dendríticas (Taylor and Gordon, 2003) (Gordon and Taylor, 2005).

Los macrófagos tienen un papel clave en la inmunidad innata, ya que reconocen, ingieren y destruyen muchos patógenos. Además, también intervienen en la reparación de los tejidos dañados durante el proceso inflamatorio evitando así el daño tisular, por lo que se puede decir que también controlan la homeostasis celular (Stout and Suttles, 2004) (Murray and Wynn, 2011). Estas evidencias ponen de manifiesto que existe un sistema capaz de controlar la magnitud y duración de la respuesta inflamatoria, haciendo que ésta sea suficiente para eliminar los agentes extraños, pero no excesiva, de modo que no cause daño tisular e incluso sepsis.

La principal función de los macrófagos es la fagocitosis, para ello los macrófagos reconocen agentes patógenos mediante diversos receptores de membrana, como son los receptores tipo Toll (TLRs), que son capaces de diferenciar entre las moléculas de superficie expresadas por el organismo invasor y las del propio organismo (Akira et al., 2001) (Turvey and Broide, 2010). Una vez que se ha producido el reconocimiento del patógeno, éste es internalizado en una vesícula denominada fagosoma. Los fagosomas se fusionan con los lisosomas de los macrófagos, los cuales contienen enzimas, proteínas y péptidos, para llevar a cabo la destrucción de los patógenos ingeridos.

2. Receptores tipo Toll (TLRs).

La inmunidad innata, altamente conservada desde un punto de vista filogenético, ha sido considerada como un sistema inespecífico. Sin embargo, estudios posteriores han demostrado que dicho sistema tiene cierto grado de especificidad (Akira et al., 2001) (Kawai and Akira, 2006) (Turvey and Broide, 2010), que se debe en gran medida a los receptores tipo Toll, denominados así por su homología con la proteína Toll.

En 1988 se descubrió la proteína Toll y se describió su papel en el desarrollo embrionario de *Drosophila melanogaster* (Hashimoto et al., 1988) (Morisato and Anderson, 1995). Sin embargo, estudios posteriores han demostrado que también juega un papel importante en la respuesta inmune innata (Lemaitre et al., 1996) (Kawai and Akira, 2007a) (Lu et al., 2008) (Lemaitre et al., 2012).

Los TLRs son una familia de proteínas transmembrana que, como se ha descrito anteriormente, reconocen estructuras muy conservadas de los microorganismos. Estas estructuras conservadas resultan ser vitales para la supervivencia de los patógenos y reciben el nombre de patrones moleculares asociados a patógenos (PAMPs). Cuando los TLRs interaccionan con los PAMPs, activan una serie de vías de señalización como respuesta inmune innata; que, a su vez, resultan ser esenciales para el desarrollo de una adecuada respuesta por parte del sistema inmune adaptativo. De este modo, se logra la erradicación de los microorganismos infecciosos (Pasare and Medzhitov, 2004) (Kawai and Akira, 2007b) (Kumar et al., 2009).

2.1. Estructura de los TLRs.

Los TLRs son proteínas transmembrana conservadas evolutivamente. Se caracterizan por poseer un dominio extracelular, que contiene repeticiones en tándem de motivos ricos en leucina (LRR), y una región intracelular, la cual presenta una gran homología con la familia de receptores de IL-1 (IL-1R), conocida como dominio TIR (Akira and Takeda, 2004), (Kumar et al., 2009, Kawai and Akira, 2011) (Figura I).

El dominio extracelular es el encargado de mediar el reconocimiento de los PAMPs; mientras que el dominio TIR es requerido para reclutar diversas proteínas adaptadoras y activar las vías de señalización, que culminarán con la síntesis de citoquinas y quimioquinas inflamatorias y de interferones (IFN) tipo I (Kawai and Akira, 2006).

Los distintos TLRs usan diferentes combinaciones de proteínas adaptadoras, entre las que destacan MyD88 (factor 88 de diferenciación mieloide), TIRAP (proteína adaptadora con

dominio TIR), TRIF (adaptador que contiene el dominio TIR e induce IFN-β) y TRAM (molécula adaptadora relacionada con TRIF) (Lu et al., 2008); para determinar la señalización que va a ser desencadenada (Jin and Lee, 2008), (Abreu and Arditi, 2004).

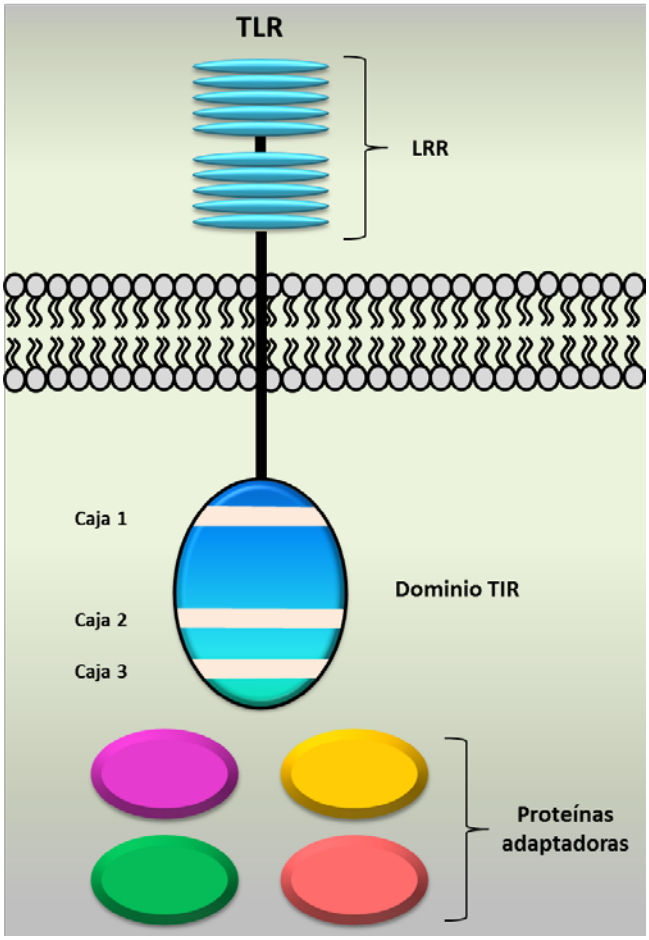

Figura I. Estructura de los TLRs. *Los TLRs tienen un dominio citoplasmático muy conservado conocido como dominio TIR, el cual se caracteriza por la presencia de 3 regiones de gran homología conocidas como cajas 1, 2 y 3. En sus regiones extracelulares presentan repeticiones en tándem de regiones ricas en leucina (LRR).*

2.2. Tipos de TLRs.

En mamíferos, han sido identificados hasta 13 receptores (10 en humanos y 12 murinos) (Kumar et al., 2011) (Kawai and Akira, 2011) (Qian and Cao, 2013), que se diferencian entre sí tanto por su localización en diversos compartimentos celulares como por los motivos que reconocen de los microorganismos (Tabla I).

Los diferentes TLRs pueden ser clasificados en tres grupos en función de los PAMPs que reconocen (Kawai and Akira, 2007b):

- TLRs que reconocen componentes lipídicos: TLR1, 2, 4 y 6.
- TLRs que reconocen ligandos proteicos: TLR5.
- TLRs que detectan ácidos nucleicos procedentes de virus y bacterias: TLR3, 7, 8 y 9.

TLRs	Localización celular	Ligandos
TLR1	Membrana plasmática	Triacil-lipopéptidos. Factores solubles bacterianos.
TLR2	Membrana plasmática	Ácido lipoteicoico (LTA). Peptidoglicanos. Zymosan.
TLR3	Endosoma	ARN de doble cadena. Ácido poliinosínico-policitidílico (Poly I:C).
TLR4	Membrana plamática	Lipopolisacárido (LPS). Manano. Proteínas virales.
TLR5	Membrana plasmática	Flagelina.
TLR6	Membrana plasmática	Diacil-lipopéptidos. Ácido lipoteicoico (LTA). Zymosan.
TLR7	Endosoma	ARN de cadena sencilla prodecente de virus de ARN.
TLR8	Endosoma	ARN de cadena sencilla .
TLR9	Endosoma	ADN bacterianos y víricos (islas CpG).
TLR10	- - - - -	Desconocido
TLR11	Membrana plasmática	Moléculas tipo profilina.
TLR12	- - - - -	Desconocido
TLR13	- - - - -	Desconocido

Tabla I. Localización y ligandos de los distintos TLRs. *Los TLRs1-9 están conservados en humanos y ratones y están perfectamente caracterizados. Sin embargo TLR10 solamente se expresa en humanos, mientras que los TLR11, 12 y 13 solo están presentes en animales murinos. TLR10, al igual que TLR12 y 13, no están caracterizados y sus funciones se desconocen.*

2.3. Vías de señalización de los TLRs.

Cuando un ligando se une a su receptor TLR, éste dimeriza, pudiéndose formar tanto homodímeros (TLR4) como heterodímeros (TRLR1 y 2). De este modo se induce un cambio conformacional necesario para reclutar las moléculas implicadas en la transmisión de la señal (Akira and Takeda, 2004). Según las proteínas adaptadoras que reclute, la señalización celular mediada por los TLRs se divide en dos grandes grupos: señalización dependiente de MyD88 y señalización independiente de MyD88 (Takeda and Akira, 2004) (Lim and Staudt, 2013) (Figura II).

Vía dependiente de MyD88.

Todos los TLRs, excepto TLR3, reclutan la proteína adaptadora MyD88 cuando son activados. En esta ruta, la unión del ligando al receptor origina el reclutamiento de MyD88 a través del dominio TIR. A continuación, MyD88 recluta a IRAK4 (quinasa 4 asociada al receptor IL-1) y a IRAK1. IRAK4 fosforila a IRAK1, lo que facilita la unión de TRAF6 (factor 6 asociado al receptor de TNF). Posteriormente, el complejo IRAK1-TRAF6 se disocia del receptor e interacciona con la quinasa TAK1 (quinasa 1 activada por el factor de crecimiento transformante β) favoreciendo su activación. A continuación, TAK1 es capaz de fosforilar a las quinasas activadas por mitógenos (MAPKs): ERK, p38 y JNK; y al complejo IKK (quinasas IκB); promoviendo en último término la translocación de los factores de transcripción AP-1 (proteína activadora 1) y NF-κB (factor nuclar κB), respectivamente, desde el citoplasma al núcleo, donde median la expresión de genes pro-inflamatorios (Lu et al., 2008) (Kawai and Akira, 2007b) (Wells et al., 2010).

Vía independiente de MyD88.

TLR3 ejerce su función a través de una vía independiente de MyD88. Dicha vía de señalización también es conocida como vía dependiente de TRIF, ya que ha sido identificada como la proteína adaptadora más importante de esta vía (Kawai and Akira, 2007b). Además se sabe que la señalización de TLR4 puede desencadenar una respuesta a través de la vía independiente de MyD88, lo que lo convierte en el único receptor capaz de mediar una respuesta por ambas vías.

TLR3 y 4 reclutan al adaptador TRIF, el cual interacciona con TBK1 (quinasa de unión a TANK1) y una vez que TBK1 está activada, interacciona con IKKε y fosforila al factor de transcripción IRF3 (factor regulador de interferón). IRF3 fosforilado dimeriza y se transloca al

núcleo induciendo la transcripción de genes IFN tipo I. Además, TRIF interacciona con TRAF6 activando a TAK1 y por tanto induce también la activación tardía del factor de transcripción NF-κB y de las MAPKs (Kawai and Akira, 2007b), (Lu et al., 2008), (Wells et al., 2010).

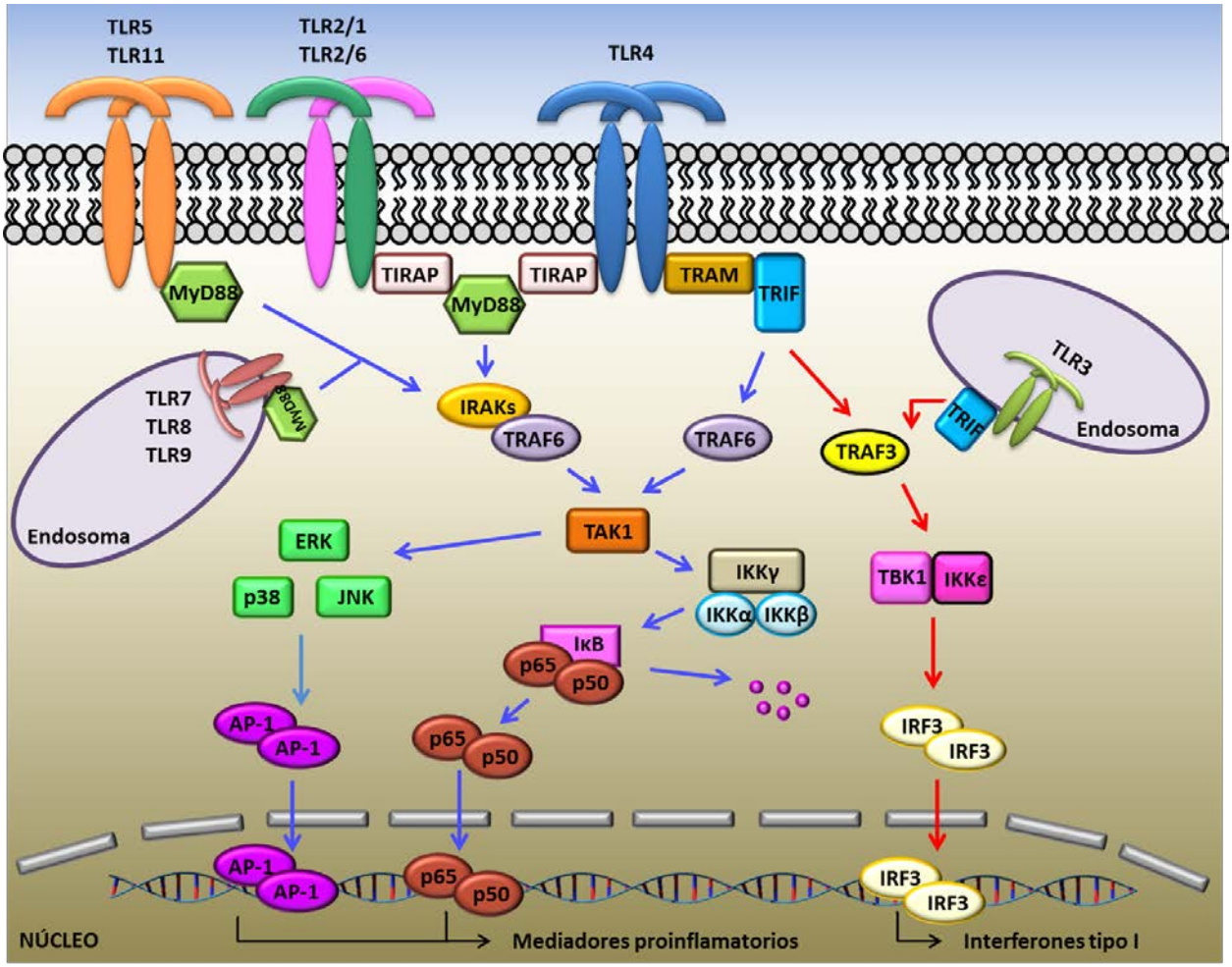

Figura II. Vías de señalización mediadas por los TLRs. *El reconocimiento de los PAMPs por los TLRs ocasiona su dimerización y activa las vías de señalización. Vía dependiente de MyD88 (mostrada con flechas azules): Todos los TLRs, a excepción de TLR3, reclutan a la proteína adaptadora MyD88, la cual interacciona con IRAKs y TRAF6 para activar a TAK1, que posteriormente activa al complejo IKK. Este complejo media la fosforilación de las proteínas IκB, que serán degradadas en el proteasoma permitiendo la translocación de NF-κB al núcleo. TAK1 también activa la vía de las MAPKs, la cual media la activación de AP-1. Ambos factores de transcripción, NF-κB y AP-1, promueven la transcripción de citoquinas pro-inflamatorias. Vía independiente de MyD88 (mostrada con flechas rojas): Es llevada a cabo por TLR3 y TLR4 y es dependiente de TRIF. La activación de IRF3 se produce al ser fosforilado por TBK1 e IKKε, lo que favorece la dimerización de IRF3 y su translocación al núcleo donde media la transcripción de IFN tipo I. De manera más tardía, esta vía de señalización también induce la activación de NF-κB y AP-1. Modificado de Kumar y colaboradores (Kumar et al., 2009).*

Inhibición de la señalización mediada por los TLRs.

La estimulación de los TLRs es esencial para la activación de la respuesta inflamatoria y la erradicación de los microorganismos infecciosos. Sin embargo, una activación de la respuesta inmune prolongada y excesiva es perjudicial para el huésped, pudiendo ocasionar daños sistémicos.

Existen dos mecanismos de regulación negativa de la señalización mediada por los TLRs durante la respuesta inmune innata: la inhibición temprana, regulada por modificaciones post-traduccionales de proteínas, y la inhibición tardía, regulada por la expresión de genes específicos (Fukao and Koyasu, 2003).

- Inhibición temprana de la señalización por TLRs: PI3K.

La mayoría de los TLRs tras el reconocimiento del patógeno activan también la vía de señalización de la fosfatidil inositol 3 quinasa (PI3K). PI3K es una enzima que cataliza la conversión del fosfatidil inositol-4,5-bifosfato (PIP2) a fosfatidil inositol-3,4,5-trifosfato (PIP3), activando en último término a Akt/PKB. Akt inhibe la activación de las MAPKs p38, JNK y ERK, así como la translocación de NF-κB al núcleo, inhibiendo de este modo la transcripción de mediadores pro-inflamatorios, como las citoquinas, las cuales son producidas en respuesta a diferentes antígenos y actúan regulando procesos inmunes e inflamatorios.

- Inhibición tardía de la señalización por TLRs: SOCS.

La activación de los TLRs induce un segundo mecanismo de retroalimentación negativa, estimulando la transcripción de genes supresores de la señalización por citoquinas denominados SOCS. Las proteínas SOCS modulan negativamente la señalización mediada por los TLRs actuando en diferentes puntos de la vía de señalización de estos receptores.

3. Factor nuclear κB (NF-κB).

NF-κB fue descrito por primera vez en 1986 por Sen y Baltimore (Sen and Baltimore, 1986) como un factor de transcripción que regulaba la expresión de cientos de genes implicados en numerosos procesos fisiológicos, como inmunidad, inflamación, supervivencia, etc.

NF-κB es una proteína dimérica compuesta por varias combinaciones de proteínas de la familia Rel. En mamíferos se han identificados 5 miembros de esta familia: Rel (c-Rel), RelA (p65), RelB, NF-κB1 (p50 y su precursor p105) y NF-κB2 (p52 y su precursor p100) (Siomek, 2012). Estas proteínas poseen una región de unos 300 aminoácidos, conservada evolutivamente, denominada dominio de homología Rel (RHD). Este dominio es el responsable de la unión al ADN, dimerización y asociación con las proteínas inhibidoras IκB (Ghosh and Karin, 2002).

NF-κB se une a los promotores de genes que contienen los llamados elementos κB, cuya secuencia consenso es 5'GGGRNWYYCC3' (N: cualquier base, R: base púrica, W: guanina o timidina y Y: pirimidina). Tres miembros de la familia, RelA, RelB y c-Rel poseen un dominio de activación de la transcripción (TAD) a través del cual regulan positivamente la expresión génica; mientras que p50 y p52 carecen de dicho dominio, por lo que reprimen la transcripción de sus genes diana, a menos que se asocien con otros miembros de la familia Rel. De este modo, se formarían heterodímeros que actuarían como potenciadores de la transcripción (Siomek, 2012) (Napetschnig and Wu, 2013). En general, p50 y p65 son los miembros más distribuidos, por lo que el término NF-κB es comúnmente empleado para describir a la proteína heterodimérica p50/p65.

Las proteínas de esta familia residen en el citoplasma, interaccionando con las proteínas IκBs, y deben ser activadas y translocadas al núcleo para llevar a cabo su función principal.

La familia de proteínas IκB incluye IκBα, IκBβ, IκBε, IκBγ y Bcl-3. Estas proteínas se caracterizan por la presencia de múltiples repeticiones de anquirina, a través de las cuales interaccionan con el dominio RHD de NF-κB y, de este modo, enmascaran la secuencia de localización nuclear (NLS) (Verma et al., 1995). Dentro de esta familia también se pueden incluir a los precursores p100 y p105, ya que contienen repeticiones de anquirina que les permite interaccionar con su propio RHD (Kawai and Akira, 2007a). Tras la activación dependiente de estímulo, las IκBs son fosforiladas. Dicha fosforilación conlleva la ruptura de la interacción NF-κB/IκB y a la posterior ubiquitinación y degradación de IκB; mientras que NF-κB se transloca al núcleo, donde induce la expresión de citoquinas y quimioquinas pro-inflamatorias, enzimas efectoras inducibles, etc. (Ghosh and Karin, 2002) (Siomek, 2012).

Un hallazgo relevante, relativo a la vía de activación de NF-κB, fue la identificación del complejo IκB quinasa (IKK), el cual consiste en dos subunidades catalíticas (IKKα e IKKβ o IKK1 e IKK2 respectivamente) y una subunidad reguladora (IKKγ, también conocida como NEMO). Este complejo es el responsable de la fosforilación de las IκBs (Ser 32 y 36 para IκBα,

Ser 19 y 23 para IκBβ), y su función principal es la de conectar señales desencadenadas por los PAMPs para activar a NF-κB (Napetschnig and Wu, 2013). (Figura III).

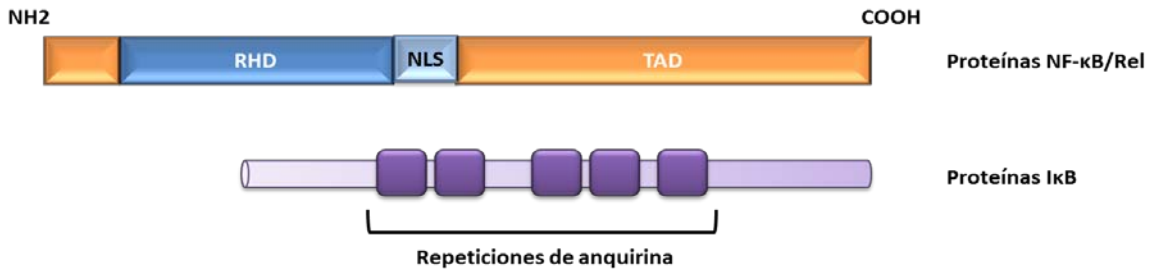

Figura III. Dominios estructurales de la familia de proteínas NF-κB e IκB. *Todos los miembros de la familia NF-κB contienen el dominio de homología RHD, responsable de la unión al ADN; y una secuencia de localización nuclear (NLS). Además, las proteínas c-Rel, RelA y RelB contienen un dominio de activación de la transcripción (TAD), ausente en los precursores p100 y p105. Las proteínas IκB se caracterizan por la presencia de múltiples repeticiones de anquirina, a través de las cuales interaccionan con el dominio RHD de NF-κB, enmascarando la secuencia NLS. Modificado de Ghosh y colaboradores (Ghosh et al., 1998).*

4. Proteínas quinasas activadas por mitógenos (MAPKs).

La vía de señalización de las proteínas quinasas activadas por mitógenos (MAPKs), junto con la vía NF-κB, juega un papel muy importante en la liberación de citoquinas pro-inflamatorias, implicadas en la respuesta inflamatoria (Zhu et al., 2013).

Las MAPKs pueden ser activadas por una amplia variedad de estímulos, tales como factores de crecimiento, mitógenos, estrés y citoquinas pro-inflamatorias principalmente, llevando a cabo multitud de procesos celulares como regulación de la expresión génica, desarrollo, crecimiento y diferenciación celular, apoptosis e inflamación (Krishna and Narang, 2008).

Actualmente, en mamíferos se han descrito seis grupos de MAPKs: quinasas reguladas por receptor extracelular (ERK1/2), quinasas c-Jun N-terminal (JNK1/2/3), p38 (p38α/β/γ/δ), ERK7/8, ERK3/4 y ERK5, de las cuales las más estudiadas son ERK1/2, JNKs y p38.

4.1. Características generales de las vías de las MAPKs.

Las vías de señalización de las distintas MAPKs poseen una serie de características que son comunes a todas ellas. Cada vía de señalización consiste en un conjunto de tres quinasas, evolutivamente conservadas, que son activadas de manera secuencial: MAPK quinasas quinasas (MAPKKK, MAP3Ks o MEKK), MAPK quinasas (MAPKK, MAP2Ks o MEK) y las MAPK. (Figura IV).

De esta forma, las MAP3Ks, activadas por fosforilación en respuesta a diversos estímulos, promueven la fosforilación de las MAP2Ks en residuos de serina y/o treonina, y éstas a su vez fosforilan a las MAPKs en residuos de treonina y tirosina del motivo conservado T-X-Y, promoviendo de este modo su activación. En este dominio, X es glutamato, prolina y glicina en el caso de ERK, JNK y p38, respectivamente (Huang et al., 2009).

Una vez activadas, las MAPKs fosforilan a sus dianas correspondientes, ya sean factores de transcripción u otras quinasas, en residuos de serina o treonina siempre que vayan seguidos de una prolina (Pimienta and Pascual, 2007).

Las vías de señalización de las distintas MAPKs pueden ser inhibidas por la acción dual de fosfatasas que eliminan los grupos fosfato de los motivos T-X-Y.

4.2. Vía ERK1/2.

Esta vía de señalización puede ser activada por factores de crecimiento, así como por agonistas de los TLR y citoquinas (Cohen, 2009). Señales a través de los PAMPs inducen su activación a través de Cot/tpl2.

Se conocen dos isoformas, ERK1 y ERK2 que se expresan en todos los tejidos.

La señalización normalmente se inicia a través de receptores de superficie que activan a Ras, el cual recluta a la MAP3K a la membrana plasmática, donde es activada. La MAP3K fosforila a MEK1 y MEK2, las cuales activan a ERK1/2 promoviendo su fosforilación en el dominio conservado Thr-Glu-Tyr. ERK1/2 pueden llevar a cabo la fosforilación de varios sustratos como proteínas de membrana y citosólicas, así como factores de transcripción o bien activar a otras proteínas quinasas (Broom et al., 2009).

4.3. Vía JNK.

Originalmente fueron identificadas como proteínas quinasa activadas por estrés (SAPKs), aunque también pueden ser activadas por citoquinas. Esta vía se caracteriza por la activación del factor de transcripción c-jun.

Se conocen tres isoformas: JNK1, JNK2 y JNK3, las cuales se diferencian por los tejidos donde son expresadas. JNK1 y 2 tienen una expresión ubicua mientras que JNK3 se expresa en el cerebro, corazón y testículos.

Las MAPKK que promueven la vía de JNK son MKK4 y MKK7, las cuales pueden activarse por la acción de una gran diversidad de MAP3Ks, entre las que se encuentra TAK1, que es activada en respuesta a citoquinas inflamatorias y a los TLRs. La activación de una u otra MAP3K dependerá de los estímulos externos. JNK influye en numerosos procesos celulares como en la alteración de la proliferación o de la expresión génica, ya que promueven la actividad transcripcional de AP-1 (Chen et al., 2001).

8.4. Vía p38.

Se han descrito cuatro isoformas de p38: α, β, γ y δ; que son activadas en respuesta a estrés y citoquinas inflamatorias. La más estudiada es la isoforma α.

p38 se activa en respuesta a MKK3 y MKK6, que son fosforiladas por diversas MAP3Ks, entre las que destaca TAK1. MKK6 es capaz de activar todas las isoformas de p38, mientras que MKK3 no puede fosforilar a p38β. La principal función de p38 está relacionada con la inflamación, ya que interviene en la producción de citoquinas pro-inflamatorias, en la inducción de enzimas como la ciclooxigenasa-2 (COX-2) y la óxido nítrico sintasa inducible (NOS-2), así como en la inducción de proteínas adherentes (Kaminska, 2005).

5. Fosfoinositol 3-quinasa (PI3K).

La PI3K es una quinasa que juega un papel fundamental a nivel celular regulando crecimiento y supervivencia, metabolismo, comunicación intercelular y respuesta inflamatoria; donde constituye uno de los mecanismos de regulación negativa de la señalización mediada por los TLRs (Fukao and Koyasu, 2003) (Troutman et al., 2012).

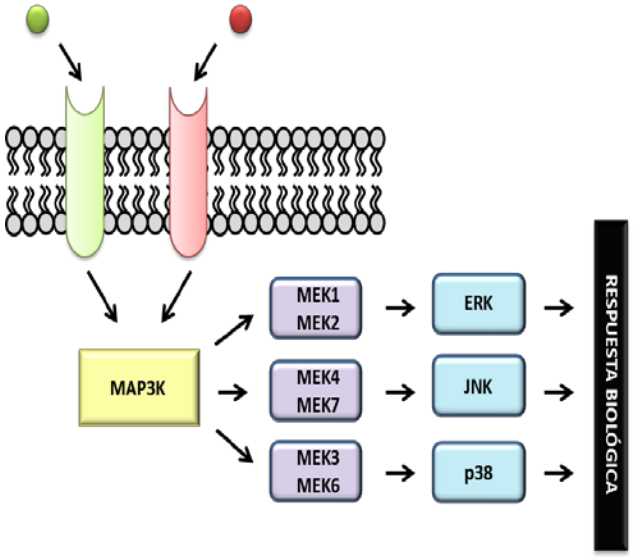

Figura IV. Activación de las MAPKs. *La cascada de señalización de las MAPKs comprende tres proteínas quinasas que son activadas de manera secuencial. Esta vía de señalización se desencadena en respuesta a diversos estímulos. Las MAP3Ks median la fosforilación y activación de las MAP2Ks, las cuales activan a las MAPKs. Las MAPKs fosforilan varios sustratos, incluyendo factores de transcripción que regulan una gran variedad de procesos celulares como proliferación, migración y respuesta inflamatoria.Modificada de Chen y colaboradores (Chen et al., 2001)*

La familia de las enzimas PI3K cataliza la fosforilación de lípidos de inositol en posición 3 generando 3-fosfoinositoles: fosfatidilinositol 3-fosfato (PIP3), fosfatidilinositol (3,4)-bifosfato (PIP2) y fosfatidilinositol (3,4,5)-trifosfato (PIP3), los cuales actúan como segundos mensajeros en numerosos procesos de señalización intracelular (Kingham and Welham, 2009), destacando las vías de supervivencia, proliferación y migración.

Los miembros de esta familia están agrupados en tres clases en función de sus características estructurales (Hazeki et al., 2007):

- ***Clase I:*** Se tratan de proteínas heterodiméricas formadas por una subunidad reguladora y una subunidad catalítica (p110), de la que existen cuatro isoformas: α, β, γ y δ, que a su vez han sido reagrupadas en dos subgrupos:
  - Clase IA: p110α, p110β y p110δ, cuya subunidad reguladora es p85.
  - Clase IB: p110γ. En este caso la subunidad reguladora es p101.
- ***Clase II:*** Son proteínas monoméricas (carecen de subunidad reguladora) que presentan una elevada especificidad de sustrato por fosfoinositoles y por fofatidilinositol 4-fosfato.
- ***Clase III:*** Son proteínas monoméricas que presentan una gran homología con Vps34p de *S. cerevisiae* y únicamente fosforilan fosfatidilinositoles.

Los principales estudios de esta vía de señalización se han centrado en las PI3K de clase I, caracterizadas por llevar a cabo la fosforilación de PIP2 para generar PIP3, que actúa como segundo mensajero permitiendo la unión a la membrana plasmática de proteínas que poseen un dominio de homología a la pleckstrina (dominio PH), lo que provoca la activación de toda una cascada de transducción de señales (Foster et al., 2012). Entre las proteínas con un domino PH que son reclutadas por el PIP3 destaca la serina-treonina quinasa Akt, también conocida como proteína quinasa B (PKB).

Las PI3Ks son activadas durante la señalización de los TLRs/IL-1R (Akira and Takeda, 2004) y diversos receptores tirosina quinasa de distintas citoquinas (Foster et al., 2012). Tras la unión del ligando a su receptor, se induce la fosforilación de residuos de tirosina en la región citoplasmática del receptor o de la proteína adaptadora en un dominio que contiene el motivo Tyr-Xaa-Xaa-Met (Xaa corresponde a cualquier aminoácido), lo que produce el reclutamiento y activación de la PI3K como resultado de una interacción directa entre el dominio SH2 (homología con el dominio 2 de la proteína Src) de la subunidad reguladora p85 y los residuos de tirosina fosforilados (Akira and Takeda, 2004) (Duronio, 2008). Esta asociación resulta en una completa activación de la PI3K, que convierte el PIP2 en PIP3, permitiendo la unión de Akt a la membrana plasmática. Akt se transloca a la membrana sufriendo un cambio conformacional, de modo que dos de sus residuos quedan expuestos para ser fosforilados por la quinasa dependiente de fosfoinositoles (PDK1, la cual también posee un dominio PH) en treonina 308 (Thr308) y por el complejo 2 de la diana de rapamicina en mamíferos (mTORC2) en serina 473 (Ser473), resultando en la activación completa de Akt (Alessi et al., 1997) (Dong and Liu, 2005) (Sarbassov et al., 2005) (Duronio, 2008). (Figura V).

La vía de señalización de la PI3K puede ser regulada de manera negativa por acción de la fosfatidilinositol-3,4,5-trifostato 3-fosfatasa (PTEN) que elimina el grupo fosfato de la posición 3 del anillo inositol del PIP3, generándose PIP2, y reprimiendo por tanto los diversos procesos de señalización en los que la PI3K está implicada (Kingham and Welham, 2009).

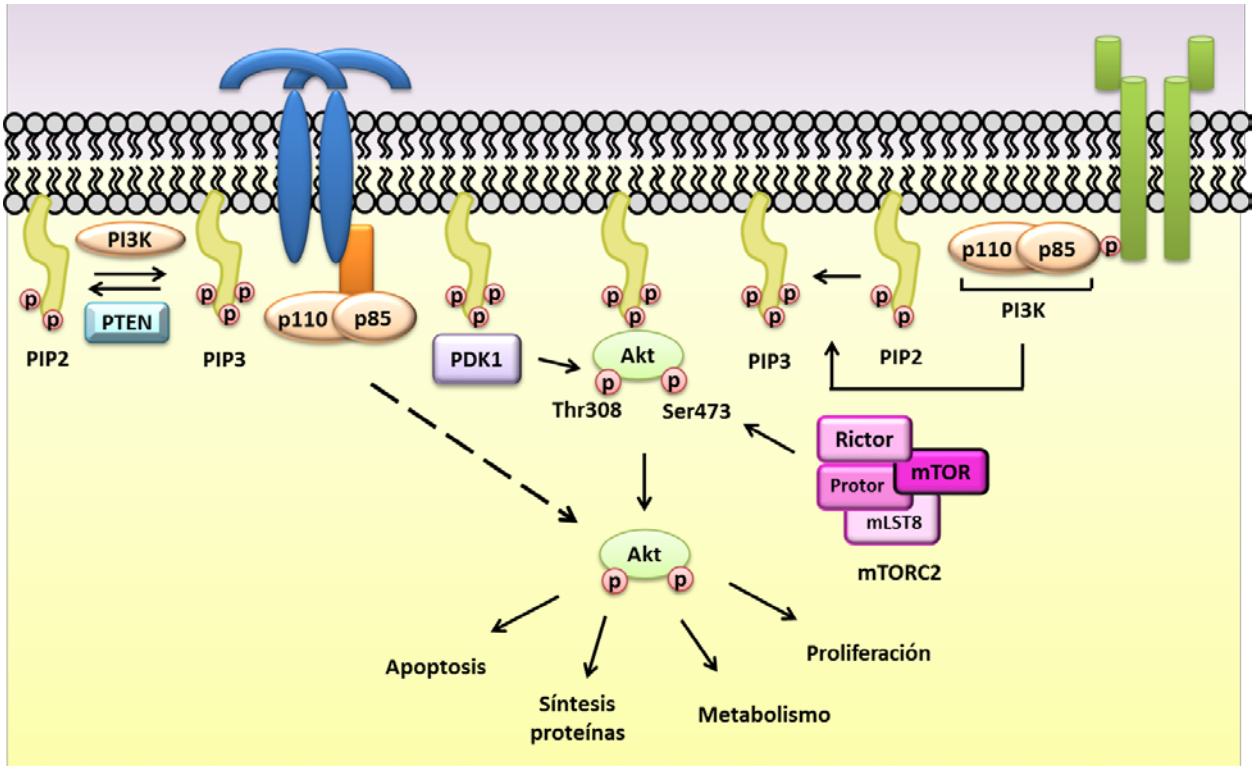

Figura V. Representación esquemática de la vía de señalización PI3K/Akt. *La activación de la PI3K tras la estimulación del receptor conlleva a la producción de PIP3 en la membrana plasmática. Akt se transloca a la membrana donde es fosoforilada por PDK1 y el complejo mTORC2. Tras la fosforilación, Akt se libera al citoplasma donde lleva a cabo la activación o inhibición de diversas proteínas o factores de transcripción, regulando de este modo multitud de procesos biológicos. Modificada de Polak y Buitenhuis (Polak and Buitenhuis, 2012)*

6. Plantas medicinales.

A pesar del creciente desarrollo tecnológico que ha tenido lugar en las últimas décadas, existe un renovado interés en el estudio del potencial farmacológico de compuestos naturales, empleados a lo largo de la historia como recursos terapéuticos, entre los que destacan las plantas medicinales.

La definición de planta medicinal incluye partes (hojas, semillas, flores, cortezas y raíces) o extractos que se utilizan como drogas o medicamentos para el tratamiento de alguna afección. El uso de estos remedios de origen natural se remonta a la época prehistórica, y es una de las formas más extendida de medicina en todo el mundo.

Actualmente, la industria farmacéutica se ha basado en los conocimientos tradicionales para la síntesis y elaboración de fármacos, con el objetivo de que la mayoría contengan únicamente los principios activos responsables de las propiedades medicinales de dichas plantas. En algunos casos, los principios activos se obtienen del procesamiento de las plantas medicinales y en otros casos se sintetizan de manera artificial. Se sabe que al menos 23 medicamentos derivados de productos naturales han sido lanzados al mercado en Europa, Japón y Estados Unidos entre 2001 y 2005, con diversas propiedades terapéuticas: anti-fúngica, anti-bacteriana, anti-cancerígena, etc. (Lam, 2007).

Hoy en día, continúa el proceso de verificación científica de los principios activos, tanto para llevar a cabo su aislamiento y purificación, como para descubrir novedosas aplicaciones de los mismos.

7. *Acanthopanax koreanum*, Nakai.

La especie *Acanthopanax* (araliácea) está ampliamente distribuida en Corea, Japón, China y el este de Rusia (Phuong et al., 2006). En la actualidad se conocen alrededor de 40 subespecies de *Acanthopanax*, 15 de las cuales crecen en la península de Corea.

En concreto, *A. koreanum* es una planta nativa que se encuentra ampliamente distribuida en la isla de Jeju, en Corea del Sur. Extractos procedentes de la raíz y del tallo de esta planta han sido empleados tradicionalmente como tónicos y sedantes, así como para el tratamiento del reumatismo y la diabetes (Kim et al., 2011). Diversos estudios han demostrado que esta subespecie presenta un elevado contenido de diterpenos (entre los que se encuentra el ácido acantoico, objeto de nuestro estudio) (Kim, 1988), triterpenos (Kim et al., 2011), fenilpropanoides, ligninas y flavonoides (Hahn, 1985), aislados a partir de distintas partes de la planta, a los que diferentes estudios farmacológicos han atribuido actividades anti-inflamatorias (Chao et al., 2005) (Suh et al., 2004) (Lam et al., 2003)}, inmunoestimuladoras (Han et al., 2003) y anti-oxidantes (Park et al., 2004).

Existen varios triterpenos y diterpenos procedentes de *A. koreanum* capaces de inhibir la actividad del factor de transcripción NFAT (Cai et al., 2004) y la síntesis del factor de necrosis tumoral α (TNF-α) (Kim et al., 2010) así como diversas citoquinas pro-inflamatorias (Cai et al., 2003).

8. El ácido acantoico.

El ácido acantoico, ácido (-)-pimara-9(11),15-diene-19-oico, se aisló por primera vez de la raíz de *A. koreanum* en 1988 (Kim, 1988). Se trata de un diterpeno de tipo pimarano, caracterizado por poseer una estructura básica de veinte carbonos (Wagner and Elmadfa, 2003), que ha sido descrito en los últimos años como un potente anti-inflamatorio.

Estudios previos realizados con el ácido acantoico en monocitos y macrófagos humanos de sangre periférica, demuestran que es capaz de reducir la producción de interleuquina (IL)-1 y TNF-α de manera dosis-dependiente (Kang et al., 1998). Además, también es capaz de suprimir la producción de especies reactivas de oxígeno (ROS), uno de los principales mediadores inflamatorios que causan inflamación y daño tisular (Kang et al., 1996). En otros trabajos realizados con la línea celular HT29 (células epiteliales humanas de colon), se demuestra que este diterpeno inhibe la activación de NF-κB y de las MAPKs (Kim et al., 2004).

Algunos autores han evaluado los efectos *in vivo* del ácido acantoico en diversos modelos experimentales de inflamación. Así, en un modelo murino de daño hepático inducido por lipopolisacárido (LPS) y D-galactosamina (D-GalN), el pre-tratamiento con el ácido acantoico es capaz de inhibir el aumento de los niveles de TNF-α en suero, así como la apoptosis de los hepatocitos promovida por LPS/D-GalN (Nan et al., 2008). Este efecto hepatoprotector ha sido recientemente corroborado en otro modelo murino de daño hepático inducido por acetaminofén. En este estudio se observa que los niveles de alanino transaminasa y aspartato transaminasa, inducidos por este fármaco, están reducidos en el suero de los animales pre-tratados con ácido acantoico (Wu et al., 2010).

Numerosos antecedentes coinciden en la idea de que la inusual estructura del ácido acantoico, debido a su cuerpo tricíclico rígido, podría ser la responsable de su perfil farmacológico; lo que favoreció el desarrollo de programas de síntesis química de este diterpeno (Ling et al., 2000) (Figura VI). Esta estrategia establece las bases para la preparación de análogos sintéticos, diseñados con el objetivo de mejorar sus propiedades farmacológicas.

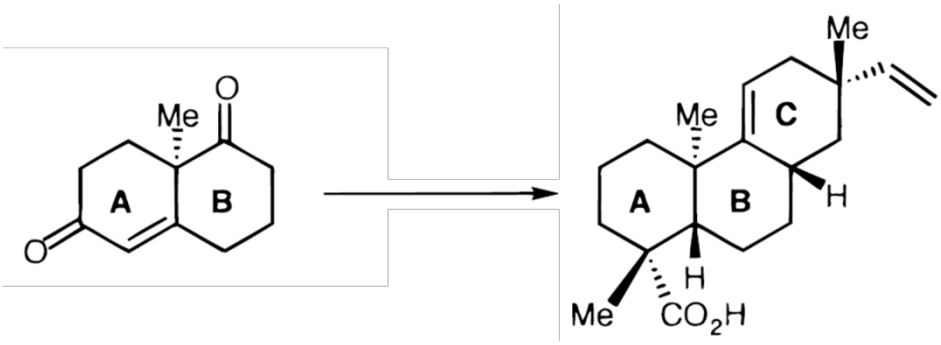

Figura VI. Síntesis química del (-)ácido acantoico. *El punto de partida para la síntesis del ácido acantoico es una diacetona bicíclica. El proceso consta de 14 pasos y culmina con la construcción del anillo C. Su inusual estructura junto con los datos que lo señalan como un compuesto de interés farmacológico, lo convierten en un producto de partida para la síntesis de compuestos, principalmente de sesquiterpenoides, diterpenos…, que posean posibles propiedades anti-microbianas, anti-virales e inmunomoduladoras (Ling et al., 2001).*

9. Derivados sintéticos del ácido acantoico.

Todos estos antecedentes han impulsado el desarrollo, mediante procesos de síntesis química, de diversas moléculas derivadas del ácido acantoico, con la finalidad de que éstas posean mayor actividad anti-inflamatoria y menor toxicidad que la molécula de la cual proceden. Estos compuestos, a pesar de ser isómeros estructurales del ácido acantoico, no se pueden obtener por modificaciones directas del mismo.

Los estudios realizados con dichos derivados han puesto de manifiesto que el carbono 4 (C4) posee una gran importancia en la capacidad anti-inflamatoria del ácido acantoico, siendo de especial relevancia la longitud del radical situado en dicha posición (Lee et al., 2005) y los derivados que presentan un residuo metil-éster en la misma (Lam et al., 2003).

Estos datos vienen reforzados por trabajos que identifican al ácido acantoico como un inhibidor de COX-2 (Suh et al., 2001), una enzima inducible que se expresa en diversos tipos celulares en respuesta a una gran variedad de factores pro-inflamatorios (Seibert and Masferrer, 1994), como LPS, IL-1, TNF-α; IFN-γ, etc. En el trabajo realizado por Suh y colaboradores se demuestra que el ácido acantoico inhibe COX-2 mediante la interacción de su grupo carboxilo, situado en C4, con los aminoácidos Arg120 y Tyr355 del centro activo de COX-2 (Suh et al., 2001). Estudios posteriores realizados con diterpenos obtenidos a partir del ácido acantoico,

demuestran que cuanto mayor es la longitud del radical situado en C4, mayor es la actividad inhibidora que presentan sobre COX-2 (Jung et al., 2007).

Teniendo en cuenta los criterios de baja citotoxicidad e inhibición de la inflamación junto con la importancia que parece tener el C4, se seleccionaron para la presente Tesis Doctoral cinco diterpenos (DTPs) que presentan diferentes modificaciones químicas en dicha posición (Figura VII).

9.1. Efectos de los DTPs sobre los receptores X hepáticos (LXRs).

Los receptores nucleares son una superfamilia de factores de transcripción dependientes de ligando, que regulan numerosos procesos implicados en la respuesta inmune. Entre estos receptores nucleares se encuentran los LXRs, una subfamilia compuesta por dos miembros: LXRα y LXRβ, muy similares entre sí, los cuales han sido descritos como factores de transcripción anti-inflamatorios, ya que son capaces de reprimir la expresión de genes pro-inflamatorios en el macrófago (Jakobsson et al., 2012).

Los LXRs pueden inhibir la activación de promotores mediada por otros factores de transcripción. Se trata de un mecanismo de acción dependiente de ligando y su ejemplo más característico es la capacidad de estos receptores para bloquear la expresión de genes pro-inflamatorios inducidos por factores de transcripción como AP-1 y NF-κB. Este proceso se produce una vez que AP-1 y NF-κB han sido activados y translocados desde el citoplasma al núcleo. Por tanto, se puede decir, que los LXRs constituyen uno de los mecanismos de señalización tardía para regular la respuesta inmune.

Estudios previos realizados con estos derivados sintéticos del ácido acantoico han demostrado que dichos compuestos, principalmente los DTPs 1, 3 y 5, actúan como ligandos agonistas de los receptores nucleares LXRα y LXRβ y además, son capaces de reprimir la expresión de una serie de genes inflamatorios como NOS-2, IL-6 y RANTES (Traves et al., 2007). Estas evidencias nos sugieren que quizás los efectos anti-inflamatorios de los DTPs podrían estar mediados por los LXRs.

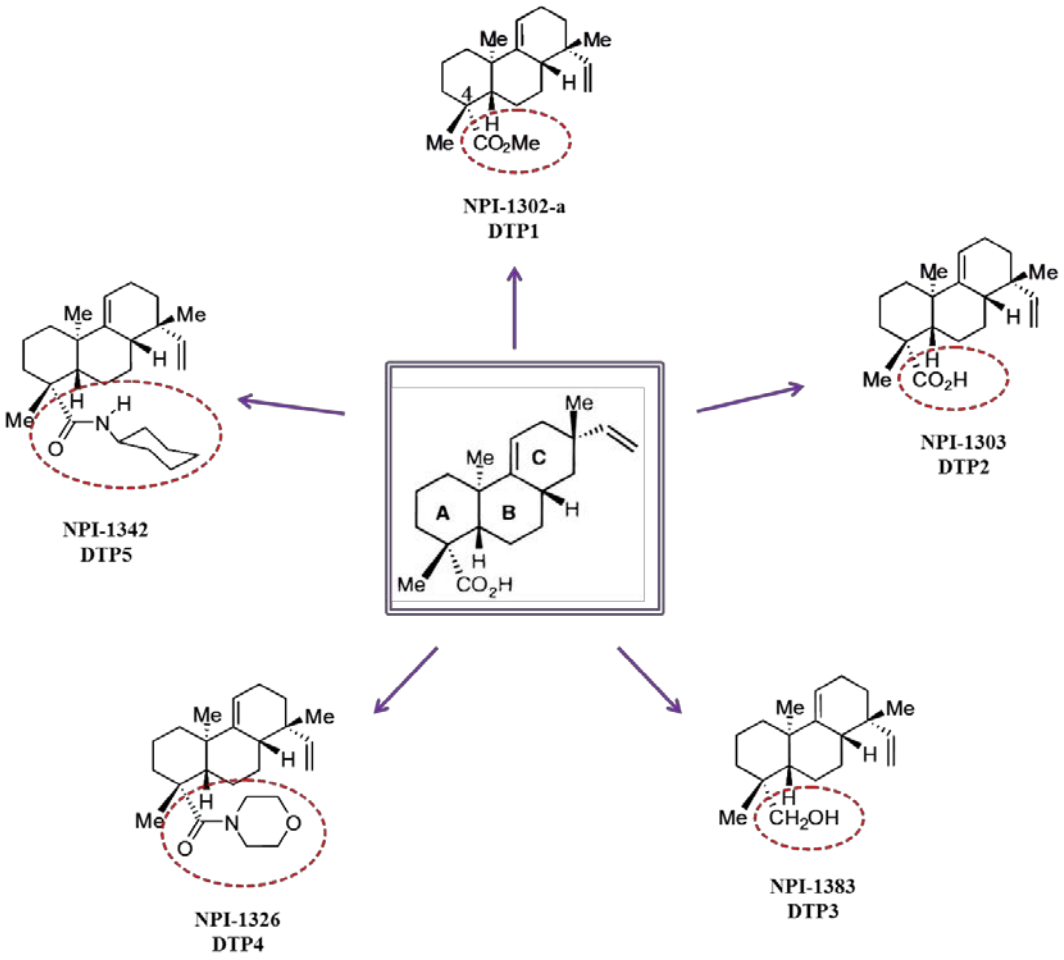

Figura VII. Derivados sintéticos del (-)ácido acantoico. *Diterpenos obtenidos, mediante modificaciones químicas, con variaciones en el residuo del carbono 4 (C4) del anillo A. El DTP2 conserva en C4 el residuo carboxilo del ácido acantoico. Esta molécula se ha empleado como referencia para determinar la actividad anti-inflamatoria del resto de los compuestos.*

OBJETIVOS

Tomando en consideración todos los antecedentes presentados en la Introducción, nos planteamos como hipótesis estudiar los mecanismos de acción por los que los derivados sintéticos del ácido acantoico median sus efectos anti-inflamatorios. Por tanto, los objetivos concretos propuestos para el desarrollo de la presente Tesis Doctoral fueron los siguientes:

1. Estudiar si el tratamiento con los diterpenos afecta a las principales vías de señalización tempranas implicadas en la respuesta inflamatoria.

2. Determinar si los análogos sintéticos del ácido acantoico muestran efectos anti-inflamatorios en diversos modelos *in vivo*.

3. Evaluar si los efectos anti-inflamatorios de los DTPs están medidados por LXRs.

MATERIALES Y MÉTODOS

1. MATERIALES.

1.1. Reactivos.

Los DTPs utilizados durante esta Tesis Doctoral fueron sintetizados por Nereus Pharmaceuticals, Inc., (San Diego, CA). Los ligandos específicos de los TLRs (LPS de *Escherichia coli*, pI:C y LTA) fueron suministrados por Invivogen (San Diego, CA). El inhibidor de PI3K, LY294002, y los inhibidores específicos para las isoformas de la región catalítica de la PI3K (p110α, p110β, p110γ) fueron adquiridos en Calbiochem (Darmstadt, Alemania), mientras que el inhibidor para la isoforma p110δ fue proporcionado por Selleckchem (Munich, Alemania).

Para la técnica de electroforesis se utilizaron reactivos de BioRad (Hercules, CA). Las membranas de Hybond^{TM}-PVDF empleadas en Western blot, así como los reactivos para la técnica de quimioluminiscencia ECL, fueron suministrados por Amersham (Buckinghamshire, Reino Unido).

Los anticuerpos primarios empleados se adquirieron en diversas casas comerciales (Tabla 1), siendo en su mayoría de Cell Signaling (Danvers, MA) y Santa Cruz Biotechnology (Dallas, Texas), aunque también se emplearon anticuerpos de Millipore, Amersham, R&D Systems (Minneapolis) y Sigma. Los anticuerpos secundarios conjugados con peroxidasa fueron proporcionados por Pierce (contra ratón y conejo) y Sigma (para cabra). El anticuerpo secundario utilizado para la detección de p-Akt Ser473 Alexa-Fluor 488 así como el 4',6-diamidino-2-fenilindol diclorohidrato (DAPI) fueron suministrados por Molecular Probes (Eugene, OR).

Los medios de cultivo celular se adquirieron en Gibco (Life Technologies; Carlsbad, CA), el suero fetal bovino (SFB) de Sigma y todo el material empleado en cultivo celular fue de las casas comerciales Falcon (Lincoln Park, NJ) o Corning (Nueva York). Para las transfecciones con plásmidos en células NIH3T3 se utilizó el reactivo FuGeneHD de Roche (Suiza) y para la transfección de macrófagos peritoneales con ARN de interferencia (siARN) se empleó Lipofectamina de Life Technologies.

La extracción de ARN se realizó con TRI Reagent® de Ambion (Life Technologies), mientras que para la RT-PCR se utilizó el kit Transcriptor First Strand cDNA Synthesis de Roche. Los cebadores empleados para la técnica de PCR cuantitativa fueron sintetizados por

Invitrogen® (Life Technologies) y el SYBR® Green utilizado fue suministrado por Applied Biosystems (Life Technologies).

Anticuerpo	Referencia	Casa comercial
Akt	9272	Cell Signaling
β-actina	A 5441	Sigma
COX-2	sc-1747	Santa Cruz
CXCL-1	AF-453-NA	R&D Systems
CXCL-10	500-P129	Peprotech
ERK	9102	Cell Signaling
IKKβ	2678	Cell Signaling
IκB-α	sc-371	Santa Cruz
IκB-β	sc-945	Santa Cruz
JNK	9252	Cell Signaling
NOS-2	sc-650	Santa Cruz
p38	9212	Cell Signaling
p85	06-195	Millipore
p-AKT Ser473	4060	Cell Signaling
p-AKT Thr308	sc-16646	Santa Cruz
p-ERK	9101	Cell Signaling
p-IKKα/β	2078	Cell Signaling
p-JNK	9251	Cell Signaling
p-p38	9211	Cell Signaling

Tabla 1. *Anticuerpos primarios empleados para Western blot e inmunofluorescencia.*

1.1. Animales de experimentación

Todos los animales utilizados en el desarrollo de esta Tesis Doctoral se mantuvieron y se trataron de acuerdo con los protocolos aprobados por el Comité Ético para la Investigación con Animales del Instituto de Investigaciones Biomédicas "Alberto Sols" en consonancia con las directrices europeas 2010/63/EU.

Se utilizaron ratones Balb/c, machos, de entre 8 y 10 semanas, libres de parásitos específicos, suministrados por Charles River y mantenidos en condiciones controladas de luz, presión y temperatura, permitiéndoles el acceso de agua y comida *ad libitum*.

Los ratones deficientes en MyD88 (MyD88$^{-/-}$ o MyD88 KO) y la línea control (MyD88$^{+/+}$ o WT), con un fondo genético C57BL/6J, fueron cedidos generosamente por Dr. Thomas Miethke (Institute for Medical Microbiology Immunology and Hygiene, Technical University of Munich, Alemania). Los ratones que carecen de LXRα y LXRβ (LXR DKO o LXRαβ$^{-/-}$) así como los correspondientes controles (LXRαβ$^{+/+}$ o WT), ambos con un fondo genético mixto C57Bl6/Sv129, fueron cedidos generosamente por el Dr. Antonio Castrillo (Universidad de Las Palmas de Gran Canarias, España) y se mantuvieron en las mismas condiciones que los animales Balb/c.

2. MÉTODOS.

2.1. Cultivos celulares.

Durante la realización de este trabajo se utilizaron líneas celulares y cultivos primarios de origen murino.

La manipulación y siembra de células se realizó bajo campana de flujo laminar Telstar modelo PV-100. Las células se mantuvieron en un incubador de células Heraeus con un 5% de CO_2 a saturación de humedad.

2.1.1. Cultivo de líneas celulares.

Se trabajó con la línea celular de fibroblastos de ratón NIH3T3. Las células se sembraron a $5x10^4$ cel/cm^2 en medio DMEM suplementado con 10% SFB, L-glutamina 2mM y antibióticos (50µg/ml de penicilina, estreptomicina y gentamicina). Previamente a las estimulaciones, las células NIH3T3 se lavaron con tampón fosfato salino (PBS) y se reemplazó el medio de cultivo por DMEM suplementado con un 2% de SFB, para sincronizar la división y metabolismo celular, al menos 6 h antes de cada experimento.

El cultivo y mantenimiento de la línea de fibroblastos murinos L929 se llevó a cabo con el fin de obtener medio enriquecido en M-CSF (factor estimulante de colonias de macrófagos), necesario para el cultivo y diferenciación de macrófagos obtenidos de médula ósea. Las células L929 se sembraron en DMEM complementado con 10% SFB y antibióticos (en la misma concentración indicada anteriormente). Una vez alcanzado el 80-90% de confluencia, se mantuvieron los fibroblastos en el mismo medio de cultivo durante 72-96 h, tras lo cual se recuperó dicho medio, se filtró (0,22 µm, Millipore) y se utilizó para la diferenciación de macrófagos derivados de médula ósea.

2.1.2. Cultivo de células primarias murinas.

<u>Aislamiento y cultivo de macrófagos peritoneales.</u>

Cuatro días antes de la extracción de los macrófagos se administró a los ratones 2,5 ml de caldo de tioglicolato (3% p/v) (Difco) mediante inyección intraperitoneal para estimular la migración de células de tipo macrofágico al foco de la inflamación. Pasado este tiempo se sacrificaron los animales por saturación del ambiente con CO_2. Se les retiró la piel de la cavidad abdominal y se inyectaron 10 ml de medio RPMI 1640 frio a cada animal. Tras aplicar un suave

masaje a la zona, se recuperó el medio de la cavidad abdominal y se centrifugó a 1200 rpm a 4 ºC durante 5 min. El precipitado obtenido, constituido mayoritariamente por macrófagos y linfocitos, se resuspendió en RPMI 1640 suplementado con 10% SFB y antibióticos. Las células se sembraron (10^6 cel/cm^2) y se mantuvieron durante 3 h a 37 ºC. Transcurrido ese periodo, se retiró el sobrenadante y se lavaron los platos con PBS frío con el fin de eliminar las células no adheridas a la placa (linfocitos) y obtener un cultivo únicamente de macrófagos. Al menos 6 h antes de estimular los macrófagos, el medio se sustituyó por RPMI 1640 con 2% SFB y antibióticos.

Obtención y cultivo de macrófagos de médula ósea.

Para obtener macrófagos derivados de precursores de médula ósea, se cortaron las patas traseras de ratones Balb/c machos (8-10 semanas) a la altura de la cadera y se les retiró toda la piel y el músculo, dejando los huesos limpios, para su posterior procesamiento.

Para procesarlas, se seleccionaron el fémur y la tibia de cada una de las extremidades. Se separaron de la rótula y se cortaron los extremos de ambos huesos. Con una jeringuilla de 10 ml y una aguja de 0,6 mm de diámetro se inyectó DMEM suplementado con 10% SFB a través de uno de los extremos. El proceso se repitió hasta que el hueso quedó totalmente blanco.

Una vez extraídas las células de médula ósea, se filtró el medio a través de un tamiz de nailon de 70 µm (BD Falcon) para eliminar posibles restos de tejidos. El resultado de la filtración se centrifugó a 1200 rpm durante 5 min, y las células se resuspendieron en DMEM con 10% SFB y antibióticos (50µg/ml de penicilina, estreptomicina y gentamicina). Posteriormente, las células se sembraron en botellas de cultivo de 150 cm^2 (Falcon) y se mantuvieron en estas condiciones durante 24 h para favorecer la adhesión de fibroblastos y otras células maduras.

Transcurrido este periodo de tiempo se recuperó el medio de cultivo, que contenía las células no adheridas, se centrifugó y el precipitado, formado por células inmaduras de médula ósea, se resuspendió en un medio enriquecido que favorece la diferenciación de estas células a macrófagos. Dicho medio está constituido por un 30% de medio procedente del cultivo de L929 y un 70% de DMEM con 10% SFB y antibióticos (a la concentración indicada anteriormente).

Las células se sembraron y mantuvieron en estas condiciones hasta que estuvieron completamente diferenciadas (8-10 días), adicionándoles medio de cultivo cada dos días.

16-24 h antes de realizar los experimentos, se sustituyó el medio de diferenciación por DMEM con un 10% SFB más antibióticos, para retirar del medio el M-CSF. Al igual que en los casos anteriores, antes de estimular las células se redujo la concentración de SFB al 2%.

2.2. Determinación de la síntesis de óxido nítrico.

La liberación de óxido nítrico (NO) se determinó por la acumulación de nitritos y nitratos (NO total) según el método de Griess (Green et al., 1982). Dicho método, se basa en la reacción de los nitritos con el ácido sulfanílico, originando una sal de diazonio que se une al naftiletilenodiamina (NEDA) (Sigma), dando un complejo diazo. Este complejo diazo genera una coloración rosa, más intensa según sea mayor la cantidad de nitritos existentes en el medio. Los nitritos se determinaron espectrofotométricamente por la adición al medio de cultivo de ácido sulfanílico (Panreac, España) 1 mM y NEDA 1 mM y se midió la absorbancia a 492 nm. Los valores obtenidos se interpolaron en la correspondiente curva patrón realizada con nitrito sódico, para determinar la concentración de nitritos presente en cada muestra.

Para evitar posibles interferencias con la coloración del complejo diazo, en aquellos experimentos en los que se llevó a cabo la determinación de la producción de nitritos, las células se incubaron en medios que no contenían rojo fenol.

2.3. Determinación de los niveles de citoquinas.

La secreción de diversas citoquinas en los cultivos de macrófagos se cuantificó mediante kits comerciales de ELISA (PeproTech). Las células se incubaron en presencia o ausencia de diferentes DTPs (10 µM) durante 30 min y a continuación se estimularon con LPS (250 ng/ml). Los sobrenadantes obtenidos tras 18 h de estimulación se recogieron y congelaron a -20 ºC hasta su utilización. Los resultados se expresaron como ng/ml de sobrenadante. Cada muestra se analizó por triplicado.

2.4. Análisis de viabilidad celular mediante citometría de flujo.

Para los experimentos de citometría de flujo las muestras se procesaron en un citómetro modelo Cytomics FC500 de Beckman-Coulter y los datos se analizaron con el programa informático CXP de la misma casa comercial.

Los macrófagos derivados de médula ósea se sembraron y mantuvieron como se ha descrito previamente y se estimularon con diferentes DTPs. Finalizado el tiempo de estimulación, el sobrenadante se recogió y se añadió a los tubos de citómetro. A continuación las

células adheridas a la placa de cultivo se levantaron con tripsina, su reacción se paró con 500 µl de SFB, y se agregaron a los tubos de citómetro. Seguidamente las muestras se centrifugaron a 1000 rpm durante 5 min a 4 ºC. El sobrenadante se aspiró y se adicionó a cada tubo 500 µl de PBS 1X con yoduro de propidio (IP) (Sigma) a una concentración final de 0,02 mg/ml. Se emplearon unas longitudes de onda de excitación 493 nm/emisión 630 nm para la detección de IP. La apoptosis se definió por la disminución en el tamaño celular y el aumento en la incorporación del colorante en el núcleo celular.

2.5. Preparación de extractos proteicos totales.

Las células se resuspendieron en un tampón de lisis (CHAPS 0,5%, Tris HCl 10 mM pH 7,5, $MgCl_2$ 1 mM, EGTA 1 mM, glicerol 10%, β-mercaptoetanol 5 mM) al que se añadieron extemporáneamente una combinación de inhibidores de proteasas (Protease Inhibitor Cocktail for use with mammalian and tissue extracts) (Sigma, 2 µl/ml) y fosfatasas (Phosphatase Inhibitor Cocktail 2 y 3) (Sigma, 1 µl/ml). Las muestras se mantuvieron 15 min en hielo y posteriormente se agitaron vigorosamente durante 30 min a 4 ºC. A continuación se centrifugaron a 13000 rpm durante 15 min y los sobrenadantes, que contenían las proteínas, se almacenaron a -20 ºC. Para la correcta extracción proteica, las muestras se mantuvieron a 4 ºC durante todo el proceso.

2.6. Determinación de la concentración proteica.

La determinación de la concentración proteica de los extractos se cuantificó en un lector de placas ATOM 340 ATC (SLT LabInstruments). Las medidas se realizaron según el método descrito por Bradford (Bradford, 1976), usando la albúmina de suero bovino como patrón. Este método se basa en la reacción entre los grupos sulfonados ácidos presentes en el azul de Coomasie, con grupos amino libres presentes en los aminoácidos básicos de las proteínas. Los cambios de absorbancia a 595 nm se normalizaron con el tampón de lisis, empleado como medida basal de absorbancia. Estas medidas de absorbancia son directamente proporcionales a la concentración de proteína presente.

2.7. Análisis de proteínas por Western blot.

2.7.1. Electroforesis y transferencia.

Las proteínas se separaron electroforéticamente en condiciones desnaturalizantes, utilizando geles SDS-poliacrilamida (acrilamida/bisacrilamida, 29:1) a distintos porcentajes (10-15%) según el peso molecular de la proteína diana (Laemmli, 1970). Para la desnaturalización de

las proteínas, se calentaron las muestras a 95 ºC durante 10 min en el tampón de carga Laemmli (Tris-HCl pH 6,8 60 mM, SDS 2%, glicerol 10%, β-mercaptoetanol 3% y azul de bromofenol 0,005%). Los geles se cargaron con cantidades iguales de proteína de cada muestra y se sometieron a corriente eléctrica en cubetas de electroforesis de BioRad a temperatura ambiente.

Finalizada la electroforesis, las proteínas se transfirieron en frío a membranas Hybond™-PVDF (Amersham) a 400 mA durante 90-120 min, en un tampón de transferencia constituido por Tris 25 mM, glicina 192 mM y metanol 20%, pH 8,3.

2.7.2. Inmunodetección.

Con el fin de saturar los sitios de unión inespecífica, las membranas se mantuvieron durante 1 h a temperatura ambiente en una solución de leche desnatada en polvo al 5% en PBS. Transcurrido ese tiempo, las membranas se incubaron con los anticuerpos específicos durante toda la noche a 4 ºC. Tras la incubación, las membranas se lavaron con T-PBS (PBS y Tween-20 0,1%) y se expusieron durante 1 h a temperatura ambiente con los correspondientes anticuerpos secundarios conjugados con peroxidasa. Finalmente y tras realizar los lavados correspondientes, las membranas se revelaron empleando reactivos ECL® (Amersham) en un analizador de imágenes acoplado a una cámara (Gel-Doc, BioRad). Se realizaron varias exposiciones de diferente duración para asegurar la linealidad de la intensidad de las bandas. La cuantificación de la intensidad de las bandas se realizó por densitometría utilizando el programa informático Image Gauge (FujiFilm).

Las membranas se sometieron a incubaciones sucesivas con diferentes anticuerpos tras ser tratadas con tampón PBS suplementado con SDS 2% y con β-mercaptoetanol (100 mM) durante 30 min a 60 ºC y en continua agitación. Como control de carga se empleó β-actina y las formas totales de las proteínas.

2.8. Inmunnoprecipitación de proteínas.

Las células se resuspendieron en tampón H frío (HEPES 10 mM pH 8, KCl 10 mM, EDTA 1 mM, EGTA 1 mM) al que se añadió extemporáneamente la combinación de inhibidores de proteasas y fosfatasas (Sigma 1 µl/ml) y Nonidet NP-40 0,5%. Tras incubarlas en hielo durante 15 min, las muestras se agitaron vigorosamente durante 10 s y se centrifugaron a 13000 rpm durante 15 min. El sobrenadante se almacenó a -20ºC. Todo el proceso se realizó a 4ºC.

A continuación se determinó la concentración proteica de cada una de las muestras, mediante el método descrito anteriormente, para partir de la misma cantidad de proteína al iniciar la inmunoprecipitación.

Para inmunoprecipitar la proteína de interés, las muestras se incubaron con el anticuerpo anti-p85 a una concentración saturante (5 µl) y se mantuvieron en agitación durante toda la noche a 4ºC. Tras la incubación de las muestras con el anticuerpo, se realizó una segunda fase en la que se añadieron proteínas A/G unidas a agarosa (Santa Cruz) y permanecieron en un orbital durante 4 h a 4ºC para favorecer las interacciones antígeno-anticuerpo. Previamente a este paso, el conjugado de agarosa se lavó tres veces con PBS mediante centrifugación a 12000 rpm durante 1 min.

Finalizado el proceso de incubación, las muestras se centrifugaron a 12000 rpm durante 10 min. El sobrenadante se transfirió a otro tubo para emplearlo en ensayos de Western blot y los precipitados se lavaron dos veces con PBS al que se añadió PMSF (1 µl/ml) y Tritón X-100 al 0,5%. A continuación, los precipitados de proteína se calentaron a 95 ºC durante 10 min en el tampón de carga Laemmli, para desnaturalizar las proteínas y romper las uniones con las proteínas A/G. Los geles se cargaron con cantidades iguales de proteína de cada muestra.

2.9. Ensayo quinasa *in vitro*.

Para determinar la actividad de PI3K, al inmunoprecipitado obtenido como se describe en el apartado anterior, se le añadió 25 µl de 1 mg/ml de L-α-fosfatidilinositol/L-α-fosfatidil-L-serina sonicado en HEPES 25 mM (pH 7,5) y EDTA 1 mM.

La reacción PI3 quinasa comenzó por adición de 100 nM [γ-^{32}P]ATP (10 µCi) y 300 µM ATP en 25 µl de HEPES 25 mM, pH 7,4, $MgCl_2$ 10 mM y EGTA 0,5 mM. Después de 15 min a temperatura ambiente, la reacción se detuvo al añadir 500 µl de $CHCl_3$-metanol (1:2), 125 µl de cloroformo y 125 µl HCl (10 mM). Las muestras se centrifugaron y la fase orgánica (fase inferior) se recuperó y lavó una vez con 480 µl de metanol, HCl 10 mM y EDTA 2 mM. Posteriormente, las muestras se secaron mediante vacío y se resuspendieron en cloroformo. Las muestras se cargaron en una placa de cromatografía en capa fina (Whatman, Clifton, NJ) y se revelaron con ácido acético-1-propanol (2N; 65:35 vol/vol), se secaron y se visualizó por autorradiografía (Diaz-Guerra et al., 1999).

2.10. Preparación de plásmidos y transfecciones celulares.

2.10.1. Transformación de bacterias competentes.

Para la amplificación de los plásmidos se utilizaron bacterias Subcloning Efficiency DH5α® Chemically Competent *E.coli* (Invitrogen). Las bacterias se descongelaron en hielo y se tomó una alícuota de 100 µl para cada una de las transformaciones. Se añadieron directamente 10 ng de ADN plasmídico a las bacterias y se mezclaron con agitación suave sin pipetear. Tras incubarlas en hielo durante 30 min se sometieron a un choque térmico en un baño a 37 ºC durante 1 min. Inmediatamente después los tubos se pusieron en hielo durante 5 min y a continuación se les añadió 1 ml de medio Luria Bertani (LB) sin antibiótico y se mezcló suavemente. Las muestras se incubaron en un baño a 37 ºC durante 1 h. Se tomaron 100 µl de las células transformadas y se sembraron en una placa de LB-agar con el antibiótico de selección, ampicilina. Las placas se incubaron durante toda la noche a 37 ºC para permitir el crecimiento de las colonias resistentes a ampicilina debido a la incorporación del plásmido.

2.10.2. Crecimiento de bacterias transformadas y purificación de plásmidos.

Transcurrido el tiempo necesario para el crecimiento de las colonias resistentes al antibiótico en las placas de agar, se seleccionó una única colonia, se inoculó con ella un tubo con 2 ml de LB con ampicilina 100 µg/ml y se mantuvo durante 2 h a 37 ºC en agitación. A continuación, se transfirió 1 ml de dicho cultivo a un matraz con 200 ml de LB-ampicilina y se incubó durante toda la noche a 37 ºC para permitir el crecimiento bacteriano. Tras 18-24 h, los cultivos se centrifugaron durante 5 min a 5000 rpm, se decantó el sobrenadante y a partir de los precipitados los plásmidos se purificaron con el kit Genopure Plasmid Maxi (Roche), siguiendo las instrucciones del fabricante. La concentración del ADN obtenido se cuantificó en un Nanodrop ND-1000 (Nanodrop Technologies) y las plásmidos se almacenaron a -20 ºC.

2.10.3. Transfecciones de células con ADN plasmídico.

Las células NIH3T3 se transfectaron transitoriamente con los plásmidos p110-WT, que codifica la subunidad catalítica, p110, de PI3K; y p110-KD que codifica para una isoforma inactiva de dicha subunidad, ya que contiene una mutación puntual (cambio de una arginina por una prolina en el aminoácido 916). Tanto la forma inactiva como la WT se clonaron en un vector pEF-Bos.

Para llevar a cabo las transfecciones con estos plásmidos se utilizó el reactivo de transfección FuGene HD (Roche), siguiendo las instrucciones del proveedor, a un ratio 8:2 (µl FuGene HD: µg ADN). Para la transfección se prepararon 2 µg de ADN en 100 µl de medio libre de suero y antibióticos, a los que se añadió 8 µl del reactivo de transfección FuGene HD; el complejo de transfección se incubó durante 15 min a temperatura ambiente. Transcurrido este periodo de tiempo, se adicionaron los 100 µl del complejo de transfección a cada uno de los pocillos, en los que previamente se había sustituido el medio de crecimiento por DMEM libre de antibióticos y suero.

18 h después de la transfección, las células se estimularon con DTP5, LY294002 o insulina durante 30 min. Una vez finalizados los estímulos, se analizó la fosforilación de Akt en Ser473 por inmunodetección, como marcador de la actividad de PI3K.

2.11. Silenciamiento génico mediante ARN de interferencia (siARN).

Los macrófagos peritoneales se transfectaron con distintos siARNs (Thermo Scientific Dharmacon®, Lafayette, CO) para las diferentes isoformas de la subunidad catalítica de la PI3K. Cada uno de los siARNs específicos para cada isoforma consta de un pool de cuatro de secuencias contra el gen de interés para garantizar el silenciamiento génico.

Para los experimentos se sembraron 2,5-3x10^6 células/ pocillo en una placa de 6 pocillos en medio RPMI al 10% SFB y antibióticos. Al día siguiente, se retiró dicho medio y se sustituyó por 1 ml de Opti-MEM I al que posteriormente se adicionó el complejo de transfección. La mezcla de transfección se preparó en tubos separados, por un lado se preparó 300 µl de Opti-MEM I junto con el siARN a una concentración final de 50 nM, y por otro lado se preparó 300 µl de Opti-MEM I junto con 10 µl de Lipofectamina 2000 (Invitrogen). Cada uno de los tubos se dejó atemperar durante 5 min, transcurridos los cuales se añadió la Lipofectamina sobre los siARNs y se dejó reposar durante 25 min a temperatura ambiente para favorecer la formación de los complejos de siARN con los liposomas. Pasado este periodo de tiempo, se añadieron los 600 µl del complejo de transfección al que las células fueron expuestas durante 18 h. A continuación, a cada uno de los pocillos se les añadió 1,6 ml de RPMI suplementado con el 20% de SFB y antibióticos, sin eliminar los complejos de transfección. Tras 48h de transfección, se sustituyó el medio por RPMI al 2% de SFB y al cabo de 6 h, las células se sometieron a los tratamientos indicados. Las células control se transfectaron del mismo modo, empleándose en este caso un siARN que no hibrida con ningún gen.

El tanto por ciento de silenciamiento se determinó por *qPCR*.

2.12. PCR cuantitativa (*qPCR*).

2.12.1. Aislamiento del ARN.

Las células ($5x10^6$) se lavaron con PBS frío y se procedió a la extracción del ARN utilizando el reactivo TRI Reagent® según las instrucciones del proveedor. Las muestras se transfirieron a tubos de polipropileno de 1,5 ml tratados con DEPC y se añadieron 200 µl de cloroformo a cada una de las muestras. A continuación se agitaron vigorosamente durante 30 s. Posteriormente se mantuvieron 15 min a temperatura ambiente y se centrifugaron durante 15 min a 13000 rpm a 4 ºC. La fase acuosa se transfirió a un nuevo tubo de 1,5 ml y se añadieron 500 µl de isopropanol. Las muestras se mantuvieron durante toda la noche a -20 ºC con el fin de favorecer la precipitación del ARN. Al día siguiente, las muestras se centrifugaron 15 min a 13000 rpm a 4 ºC y se decantó el sobrenadante con cuidado. El precipitado se lavó varias veces con etanol 70% y finalmente se resuspendió en agua ultrapura estéril. La concentración y pureza de los ARNs obtenidos se cuantificó utilizando un espectrofotómetro ND-1000 (NanoDrop Technologies). La pureza se determina por el valor de los ratios 260/280 y 260/230, indicativos de la existencia de impurezas de origen proteico y/o de compuestos orgánicos, respectivamente. Ambos ratios deben tener un valor en torno a 2 para garantizar la pureza del ARN. Los ARN se almacenaron a -80 ºC.

2.12.2. Retrotranscripción (RT).

Usando una enzima transcriptasa reversa, el ARN obtenido se retrotranscribió a cADN (ADN complementario). Este proceso se llevó a cabo utilizando el kit Transcriptor First Strand cDNA Synthesis (Roche). En todo momento se siguieron las recomendaciones del proveedor y la reacción se desarrolló en un termociclador MyIQ Real-Time PCR System (BioRad).

Se tomó 1 µg de cada uno de los ARNs purificados y se le añadió 2 µl de "*random hexamers*" (600 pmol/µl) o cebadores de secuencia aleatoria, llevando posteriormente cada muestra a un volumen final de 13 µl con agua estéril. Se incubaron los tubos durante 10 min a 65 ºC y posteriormente se mantuvieron a 4 ºC. A continuación se añadió a cada tubo 7 µl del cóctel de síntesis de cADN: 4 µl tampón RT 5x, 0,5 µl del inhibidor de RNasa (40 U/µl), 2 µl del cóctel de dNTPs (10 mM) y 0,5 µl de la enzima transcriptasa reversa (20 U/µl). Seguidamente los tubos se incubaron durante 10 min a 25 ºC, y posteriormente, durante 60 min a 50 ºC. Para detener la

reacción, se calentaron las muestras 5 min a 85 ºC y a continuación se enfriaron rápidamente en hielo. Como control negativo de la RT se empleó una muestra que contenía todos los reactivos del cóctel de reacción salvo el ARN.

Finalmente, para eliminar posibles trazas de ARN que pudieran contaminar el cADN, se les añadió 1 µl de RNasa H a cada una de las muestras y se mantuvieron a 37 ºC durante 20 min. Los cADNs se conservaron a -20 ºC hasta su utilización.

2.12.3. PCR cuantitativa (*qPCR*).

Para llevar a cabo los ensayos de PCR cuantitativa se tomaron 5 µl de cada uno de los cADNs obtenidos en la reacción de RT, se añadieron 10 µl del cóctel comercial *SYBR® Green PCR Master Mix* (Applied Biosystems) y 250 nM de cada uno de los cebadores "sentido" y "antisentido" para el gen de interés, llevando posteriormente cada muestra a un volumen final de 20 µl con agua estéril. La *qPCR* utiliza *SYBR®Green* como reportero, el cual es un agente intercalante fluorescente que se une al ADN de doble cadena (Bookout and Mangelsdorf, 2003). Para la normalización de los datos se empleó un gen correspondiente a una subunidad ribosómica cuya expresión no se ve modificada por los diversos tratamientos utilizados (36B4 o Arbp). En cada caso se realizaron duplicados tanto para los genes diana como para el gen empleado como control interno.

Las secuencias de los cebadores específicos usados en el presente trabajo (Tabla 2) se diseñaron utilizando el programa informático Primer Express 2.0 (Applied Biosystems) y fueron sintetizados por Invitrogen® (Life Technologies). Se corroboró la secuencia homóloga de hibridación de los cebadores para que fuesen únicas en el genoma murino mediante el uso de la herramienta informática BLAST (NCBI). Para cada gen evaluamos la curva de disociación para confirmar que nuestros cebadores eran realmente específicos de nuestro gen y amplificaban una única secuencia.

Gen	Sentido (5' a 3')	Antisentido (5' a 3')
COX-2	TGCTGTACAAGCAGTGGCAAAGGC	TCTCAATGAGTACCGCAAACGC
NOS-2	GAGCTGGGCTGTACAAACCTT	CATTGGAAGTGAAGCGTTTCG
36B4	AGATGCAGCAGATCCGCAT	GTTCTTGCCCATCAGCACC

Tabla 2. *Secuencia de los cebadores "sentido" y "antisentido" empleados en el presente trabajo.*

Los ensayos de PCR para las distintas isoformas de la subunidad catalítica, p110, de la PI3K se llevaron a cabo con sondas Taqman® (Life Technologies). Se tomaron 4 µl de cada uno de los cADNs a los que se añadió 1 µl de la sonda, 10 µl del cóctel comercial FastStart Universal Probe Master (Rox) (Roche), el cual contiene la enzima Taq ADN polimerasa, el buffer de reacción y los nucleótidos; y agua hasta llegar a 20 µl. En este caso el reactivo fluorescente es la sonda.

La reacción de *qPCR*, realizada con cebadores y con sondas Taqman, se desarrolló en un termociclador modelo MyIQ Real-Time PCR System (BioRad), empleándose como control negativo 5 µl de agua en lugar de cADN. El análisis de los resultados se realizó utilizando el programa informático IQ5 de la misma casa comercial. Se cuantificó la expresión relativa de cada una de las muestras frente al control, normalizando previamente con el gen utilizado como control interno, 36B4, mediante el método del ΔΔCt.

2.13. Inmunofluorescencia.

Los macrófagos peritoneales se sembraron en placas de 8 pocillos (Chamber Slides, Falcon) a una densidad celular de $1x10^5$ por pocillo en 300 µl de medio. Se realizaron los estímulos oportunos y a continuación las células se lavaron con PBS y se fijaron con paraformaldehído al 4% (pH 7,2) durante 15 min a temperatura ambiente. Tras un doble lavado con PBS, las células se permeabilizaron con metanol, previamente enfriado a -20 ºC, durante 10 min a temperatura ambiente. Seguidamente se lavaron de nuevo con PBS y después se incubaron con el anticuerpo primario durante toda la noche a 4 ºC (p-Akt Ser473, 1:500). Al día siguiente se lavaron los pocillos 3 veces con PBS y se incubaron las células con el anticuerpo secundario (anti-conejo Alexa-Fluor 488, 1:500) durante 2 h a temperatura ambiente. También se llevaron a cabo tinciones nucleares con el colorante DAPI (1:3000) durante 30 min. Finalmente se lavaron de nuevo todos los pocillos y se montaron las muestras con un gel de montaje especial para fluorescencia Prolong (Molecular Probes).

Las muestras se analizaron en un microscopio confocal modelo Espectral Leica TCS SP5 (Leica Microsystems). Las imágenes se adquirieron con el programa informático “Leica Application Suite Advanced Fluorescence Lite 1.81” de la misma casa comercial y se cuantificaron con el programa informático Image J.

2.14. Edema inducido en oreja de ratón por aplicación tópica del éster de forbol 12-o-tetradecanoil-forbol-13-acetato.

Para el desarrollo de este modelo de inflamación *in vivo* se siguió la técnica descrita por Recio (Recio et al., 1994). El proceso inflamatorio se inició mediante la aplicación de 10 µl del éster de forbol 12-O-tetradecanoil-forbol-13-acetato (TPA) (Sigma) (2 µg/oreja en dimetilsulfóxido (DMSO)), en cada superficie (interna y externa) de la oreja derecha de todos los ratones. Simultáneamente, se aplicaron en la misma oreja indometacina (Sigma), como agente anti-inflamatorio, o los DTPs analizados en este trabajo (500 ng/oreja), usando como vehículo DMSO. La oreja izquierda (control) de cada uno de los ratones recibió, además del TPA, el vehículo. Transcurridas 4 h, se procedió al sacrificio de los animales mediante dislocación cervical y a continuación, mediante un sacabocados, se obtuvieron secciones de 6 mm de diámetro de la porción central de las orejas. El edema producido en cada ratón se midió mediante la diferencia de peso entre la oreja tratada y la oreja control.

2.15. Estudios de letalidad inducida por inyección intraperitoneal de LPS/D-galactosamina.

El modelo de inducción de daño hepático por LPS/D-GalN es un modelo experimental bien establecido (Galanos et al., 1979). La D-GalN es un agente hepatotóxico que actúa únicamente sobre los hepatocitos produciendo la depleción de UTP y originando modificaciones en los nucleótidos de uracilo, lo que impide la biosíntesis de diversas macromoléculas (ARN, glicoproteínas de membrana, etc.). De este modo, la D-GalN aumenta hasta 100.000 veces la sensibilidad del hepatocito al LPS. En este modelo, las células de Kupffer se activan por LPS, secretando numerosas citoquinas como IL-1, IL-6 y TNF-α. Entre estas citoquinas inflamatorias, el TNF-α parece ser el principal responsable de la inducción del daño hepático, ya que induce la activación de NOS-2, elevándose de este modo las concentraciones de NO, responsable de la muerte celular de gran número de hepatocitos (Sass et al., 2001).

A ratones Balb/c de 8-10 semanas se les inyectó intraperitonealmente 0,5 ml del compuesto problema DTP1 o DTP5 (30 mg/kg), diluido en PBS. Los animales controles se trataron con una dilución que contenía el mismo volumen de DMSO, vehículo de nuestros compuestos. Después de 1 h se les administró, también intraperitonealmente, una combinación de LPS (2 µg/kg) y D-GalN (800 mg/kg) que les indujo un shock endotóxico. La mortalidad inducida por este tratamiento se analizó durante las 24 h siguientes a la administración de LPS/D-GalN.

2.16. Administración *in vivo* de DTP5 y determinación de la actividad mieloperoxidasa por bioluminiscencia.

Ratones Balb/c de 8-10 semanas fueron pre-tratados con el DTP5 (30 mg/kg) mediante inyección intraperitoneal (i.p.) y transcurrida 1 h se les administró 10 mg/kg zimosán (extracto del hongo *Saccharomyces cerevisiae*), también i.p., para inducir la inflamación. Justo antes de determinar la actividad mieloperoxidasa (MPO) por luminiscencia, se les inyectó luminol (5 mg en 200 µl). La bioluminiscencia se registró usando un IVIS Lumina (Caliper Life Science), según el método descrito previamente (Gross et al., 2009).

Una hora antes de la administración del zimosán, se realizó la primera medida de luminiscencia, a fin de cuantificar la autoluminiscencia del tejido. El luminol se administró a los ratones, justo antes de cada una de las medidas de emisión de fotones ya que el sustrato de la enzima se metaboliza en unos 50 min. A cada uno de los tiempos, se realizó una secuencia de medidas donde cada 5 min, durante un total de 45 min, el equipo (IVIS Lumina) adquirió una foto y determinó la luminiscencia dentro del área seleccionada. La medida de bioluminiscencia para un tiempo determinado, es el sumatorio de 9 datos de luminiscenia obtenidos tras la inyección i.p. de luminol. Los datos se analizaron con el programa informático Excell.

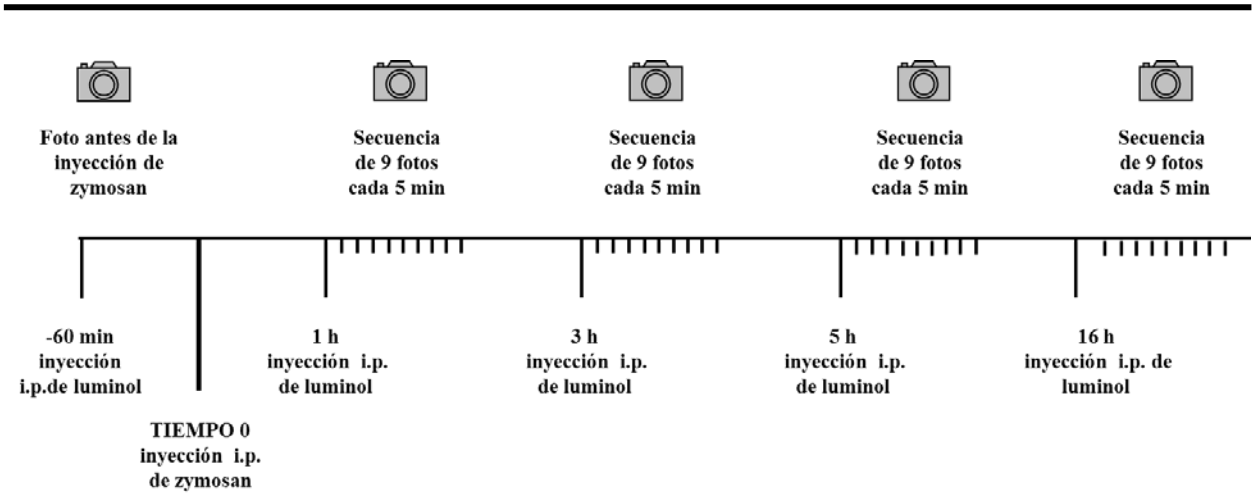

Figura A. *Protocolo de medida de la luminiscencia in vivo (IVIS Lumina).*

2.17. Estadística.

Los valores representados en las distintas gráficas expresan la media aritmética ± la desviación estándar (DE) de la misma. Para las comparaciones estadísticas se empleó la "*t de Student*" y se consideraron significativas las diferencias con un valor $p \leq 0,05$.

RESULTADOS

1. Efectos anti-inflamatorios de los DTPs.

En la presente Tesis Doctoral estudiamos la actividad anti-inflamatoria de derivados sintéticos del ácido acantoico para lo cual analizamos las principales vías de señalización implicadas en los procesos inflamatorios.

Para llevar a cabo dicho objetivo, se trabajó con los cinco DTPs expuestos anteriormente, a los que se les asignó un número para mayor comodidad.

NPI-1302-a: DTP1

NPI-1303: DTP2

NPI-1308: DTP3

NPI-1326: DTP4

NPI-1342: DTP5

Considerando datos previos de nuestro grupo, se estableció que la concentración óptima de los DTPs a la que se produce una inhibición de genes pro-inflamatorios era de 10 µM; y que el pre-tratamiento de los macrófagos con dichos compuestos durante 30 min era suficiente para actuar como agentes anti-inflamatorios (Traves et al., 2007).

1.1. Efecto de los DTPs sintéticos derivados del ácido acantoico sobre la expresión de NOS-2 y COX-2 en macrófagos activados con LPS.

Como una primera aproximación para determinar la capacidad anti-inflamatoria de los DTPs, se midió la expresión de las enzimas pro-inflamatorias NOS-2 y COX-2. Para ello, se pre-incubaron macrófagos peritoneales de ratones Balb/c durante 30 min con cada uno de los distintos DTPs y posteriormente se estimularon las células con LPS (250 ng/ml). Tras 18 h de tratamiento se analizó la expresión de las proteínas NOS-2 y COX-2 en extractos totales mediante Western blot. En la figura 1 se observa que todos los DTPs son capaces de inhibir la expresión tanto de NOS-2 como de COX-2, y en ambos casos, los DTPs 1, 3 y 5 parecen tener un efecto más pronunciado que los ejercidos por DTP2 y 4 (Figura 1).

En base a estos resultados, se seleccionaron los derivados sintéticos del ácido acantoico, 1, 3 y 5, para llevar a cabo el resto de experimentos realizados durante el desarrollo de esta Tesis Doctoral. Además, hay que tener en cuenta que uno de los factores limitantes durante el desarrollo de este proyecto ha sido la disponibilidad de los compuestos. En estas circunstancias y

dada la abundancia de los DTP1 y 5, y su estabilidad en disolución, la mayoría de los experimentos se hicieron con estos diterpenos, indicándose en todo momento aquellos que fueron realizados únicamente con uno de los compuestos o con ambos.

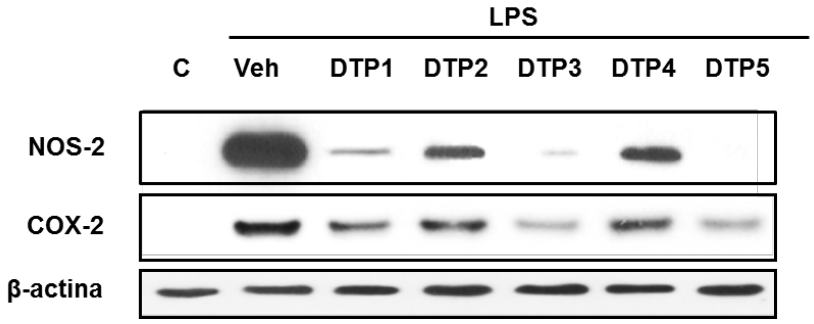

Figura 1. Efecto de los diterpenos sobre la expresión de NOS-2 y COX-2. *Macrófagos peritoneales procedentes de ratones Balb/c se pre-trataron durante 30 min con los diferentes DTPs (10 µM) y posteriormente se estimularon con 250 ng/ml de LPS. Tras 18 h de tratamiento se determinaron en extractos celulares y mediante Western blot, los niveles de expresión de NOS-2 y COX-2. Para normalizar la carga se utilizó β-actina. La figura muestra un experimento representativo de tres.*

1.2.Análisis de la citotoxicidad de los DTPs.

A continuación se analizó si los DTPs que se habían seleccionado, resultaban tóxicos, siendo capaces de inducir procesos apoptóticos en macrófagos; ya que cabía la posibilidad de que los efectos inhibitorios observados se debiesen a fenómenos de muerte celular derivados del tratamiento con dichos compuestos.

Para determinar los niveles de apoptosis celular se realizaron experimentos de citometría de flujo. Como control positivo de la inducción de apoptosis se empleó estaurosporina a una concentración de 200 ng/ml, basándonos en datos previos de nuestro grupo (Prieto et al., 2010).

Se comprobó que el tratamiento de macrófagos derivados de médula ósea durante 18 h con estaurosporina ocasionaba una apoptosis en estas células de aproximadamente un 35% respecto a la población celular total; sin embargo, ninguno de los DTPs analizados era capaz de inducir por sí mismo muerte celular (Figura 2).

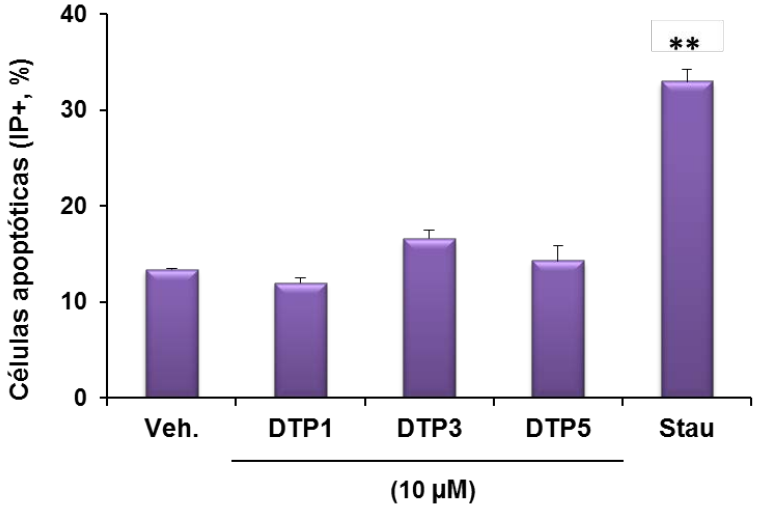

Figura 2. El tratamiento con los DTPs 1, 3 y 5 no induce apoptosis celular. *Macrófagos derivados de médula ósea se incubaron con los distintos diterpenos (10 µM). Tras 18 h de tratamiento se determinaron los niveles de apoptosis celular mediante marcaje con IP por citometría de flujo. Se empleó estaurosporina (200 ng/ml) como control positivo de muerte celular. El gráfico que se muestra representa la media ± DE de dos experimentos realizados por duplicado. **p≤0,01 vs. control, tratado con el vehículo (Veh). Stau: estaurosporina.*

1.3. Efecto de los DTPs sobre la expresión de citoquinas inflamatorias.

Las citoquinas son proteínas secretadas por células del sistema inmune en respuesta a diferentes antígenos y actúan mediando los procesos inflamatorios. Sin embargo, una producción excesiva de estos mediadores tiene consecuencias patológicas asociadas a enfermedades inflamatorias.

Basándonos en datos previos en los que se demuestran que los diterpenos fueron capaces de reducir la síntesis de citoquinas pro-inflamatorias (Chao et al., 2005), el siguiente abordaje experimental consistió en analizar si los DTPs 1 y 5 también eran capaces de inhibir la acumulación de citoquinas que se liberan al medio de cultivo en respuesta a estímulos pro-inflamatorios como el LPS (Lee and Kim, 2007). Para ello, los macrófagos peritoneales se pre-trataron con DTP1 o DTP5 durante 30 min y a continuación se estimularon con LPS durante 18 h, transcurridas las cuales se analizó la acumulación de diversas citoquinas (IL-1β, IL-6 e IL-12) y quimioquinas (CXCL-1 (KC), CXCL-10 (IP-10) y RANTES (CCL-5)) presentes en el medio de cultivo mediante kits de ELISA (Figura 3A). Estos datos se corroboraron mediante Western

blot al analizar los niveles de proteína intracelular de algunas de estas citoquinas y quimioquinas (Figura 3B).

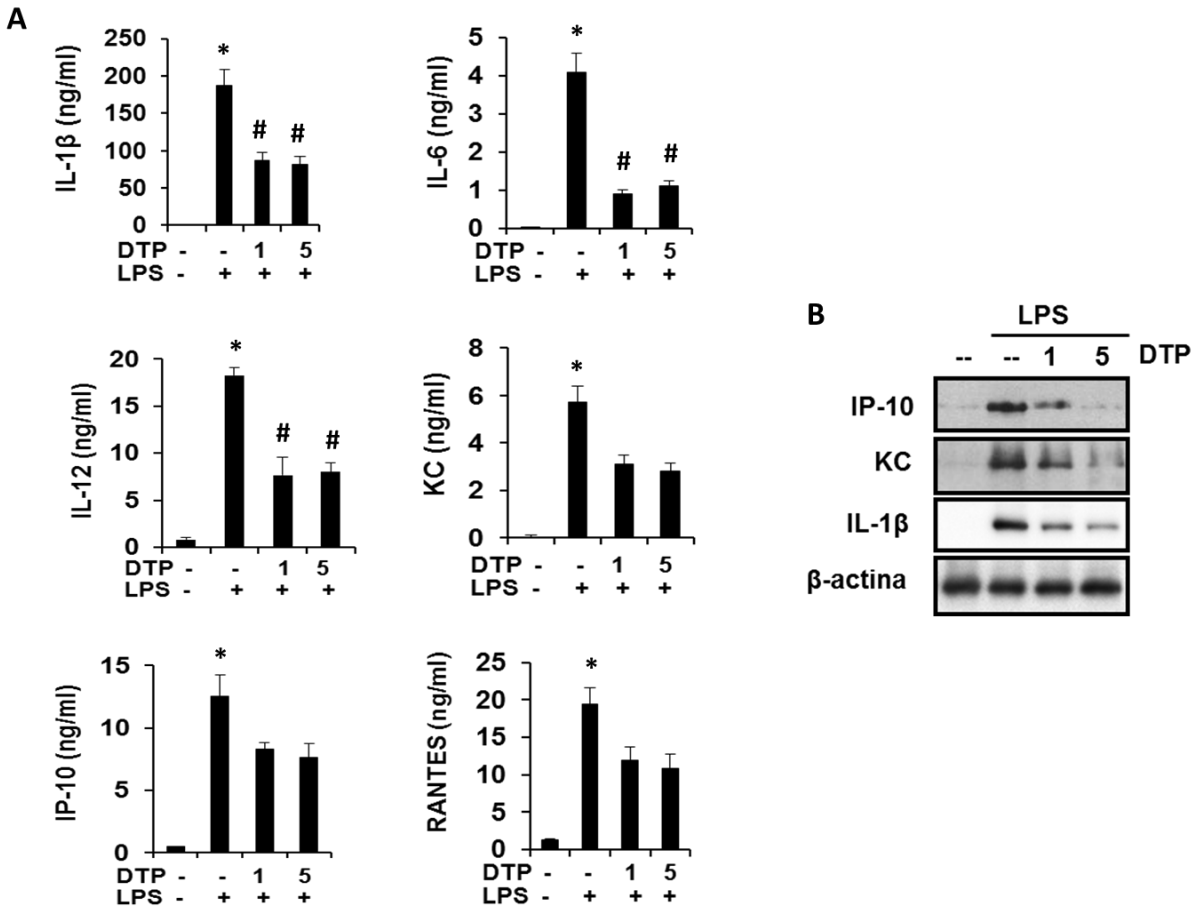

Figura 3. DTP1 y DTP5 inhiben las citoquinas y quimioquinas inducidas por LPS. *Macrófagos peritoneales se estimularon durante 18 h con LPS (250 ng/ml) en presencia o ausencia del DTP1 o 5 (10 µM, 30 min antes).* ***A)*** *Análisis de la acumulación en el medio de cultivo de IL-1β, IL-6, IL-12, IP-10, RANTES y KC, mediante kits de ELISA.* ***B)*** *Análisis de los niveles intracelulares de IP-10, KC e IL-1β mediante Western blot. Se empleó la β-actina como control de carga para normalizar los niveles proteicos. Los gráficos y el Western blot representan la media ± DE de tres experimentos independientes.*p≤0,05 respecto al control y #p≤0,05 respecto al tratamiento con el LPS.*

2. Efectos de los DTPs independientes de los receptores LXRs.

Estudios previos han demostrado la capacidad del ácido acantoico y sus derivados de inhibir la actividad de NOS-2 y COX-2 (Lee et al., 2005) (Suh et al., 2001), dos de las principales enzimas implicadas en la respuesta inflamatoria y responsables de la síntesis de NO y prostaglandinas (PGs), respectivamente.

Los derivados sintéticos del ácido acantoico, objeto de estudio en la presente Tesis Doctoral, han sido descritos, al igual que la molécula original, como agonistas de los receptores nucleares LXRs (Traves et al., 2007). Considerando que tanto LXRα como LXRβ son capaces de inhibir la expresión de genes pro-inflamatorios inducidos por LPS, tales como NOS-2, COX-2, IL-1, IL-6, etc, en macrófagos murinos (Myhre et al., 2008), nos planteamos estudiar si los posibles efectos anti-inflamatorios de los DTPs están mediados por los receptores nucleares LXRs o son independientes de los mismos.

Teniendo en cuenta los resultados obtenidos que demuestran que los DTPs 1, 3 y 5 presentan una mayor actividad anti-inflamatoria que la mediada por DTP2 y DTP4, se seleccionó el DTP5, como una primera aproximación, para llevar a cabo el planteamiento propuesto en el párrafo anterior.

2.1. Los derivados del ácido acantoico muestran efectos anti-inflamatorios en ausencia de los receptores LXRs.

Para determinar si los efectos anti-inflamatorios de los DTPs estaban mediados por los receptores LXRs, se utilizaron macrófagos peritoneales procedentes de animales de genotipo silvestre (wild type, WT) y de animales que carecen de LXRα y LXRβ (double knockout, DKO).

Como estímulo inflamatorio se seleccionó el LPS, ya que se trata de un modelo clásico bien conocido y uno de los estímulos más importantes para la inducción de genes inflamatorios como NOS-2 y COX-2. La regulación de ambos genes está controlada fundamentalmente por NF-κB ya que presentan en su promotor sitios de unión para este factor de transcripción. Para analizar el efecto de los DTPs sobre la expresión de genes inflamatorios clásicos, los macrófagos peritoneales se trataron con los DTPs durante 30 min antes de la adicción del estímulo pro-inflamatorio y permanecieron presentes en el medio de cultivo durante la duración del mismo. Como control se utilizó su vehículo, DMSO, que no presentaba efectos tóxicos a la concentración utilizada (0,5% v/v).

El tratamiento de los macrófagos, tanto WT como DKO LXR, con LPS durante 18 h indujo la expresión de NOS-2 y de COX-2 (Figura 4). En cambio, cuando las células se pre-trataban con los DTPs, se producía una disminución de la expresión de ambas enzimas, independientemente de la presencia o no de los LXRs ($p \leq 0,05$). Los resultados obtenidos con el DTP5 se corroboraron también con los DTPs 1 y 3. Así, nuestros datos indicaron que el efecto anti-inflamatorio de los DTPs frente a la respuesta inflamatoria inducida por LPS, tanto en macrófagos peritoneales de ratones WT como DKO de LXR, era independiente de los receptores nucleares.

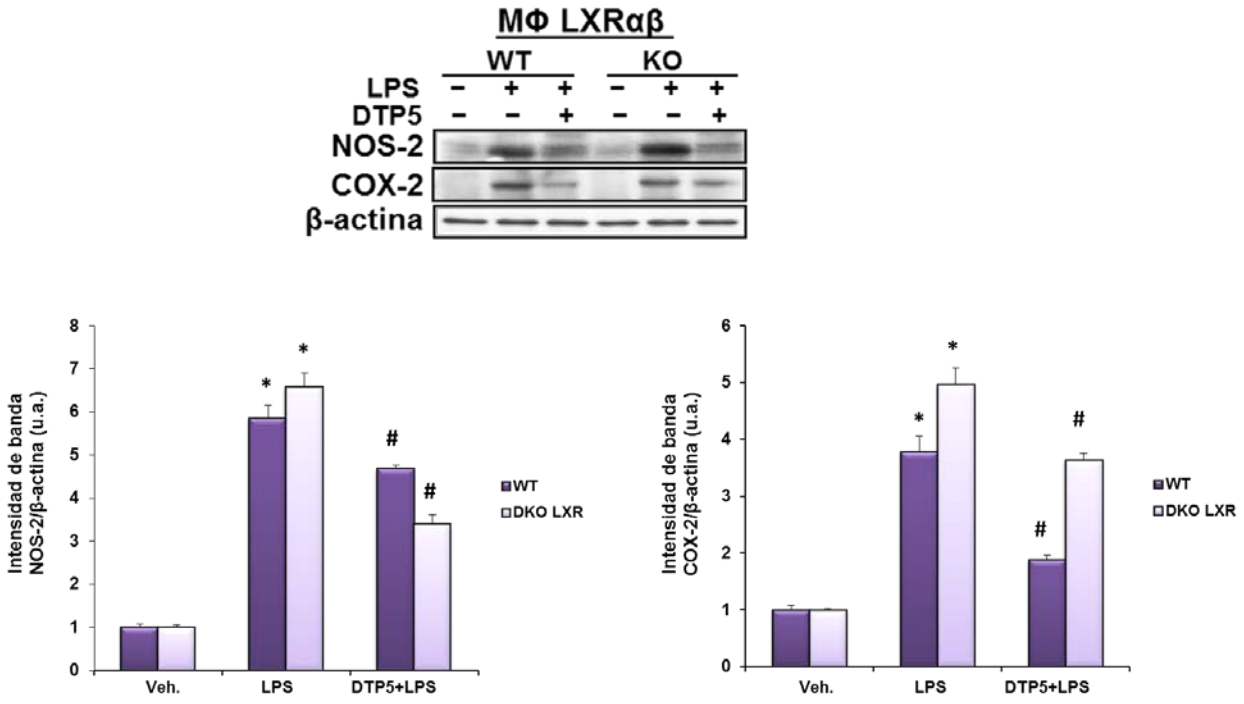

Figura 4. Inhibición de la expresión de las enzimas pro-inflamatorias NOS-2 y COX-2 en macrófagos peritoneales tratados con DTP5. *Las células se trataron con DTP5 (10 µM, 30 min) o el vehículo y a continuación con LPS (250 ng/ml) durante 18 h. Los niveles proteicos de NOS-2 y COX-2 se analizaron en extractos totales mediante Western blot. Los niveles de expresión se cuantificaron y normalizaron utilizando β-actina como control de carga. Los gráficos representan la media ± DE de tres experimentos independientes.*p≤0,05 vs. controles tratados con el vehículo y #p≤0,05 vs. LPS.*

Como se ha indicado anteriormente, uno de los mecanismos de acción dependiente de ligando de los receptores nucleares consiste en inhibir la activación de promotores mediada por otros factores de transcripción. Uno de los ejemplos más característicos es la capacidad de bloquear la expresión de genes pro-inflamatorios inducidos por factores de transcripción como NF-κB (Glass and Ogawa, 2006), para lo cual se requiere que NF-κB se transloque previamente al núcleo. Es decir, que se trata de un proceso totalmente nuclear que no implica la inhibición de la degradación de las proteínas IκBs.

En base a esto se decidió analizar la expresión de la proteína inhibitoria IκBα tras el tratamiento con el DTP5. Para ello, los macrófagos WT y DKO LXR se estimularon con DTP5 y con LPS (Figura 5) como agente inflamatorio. El LPS indujo una degradación de la proteína IκBα dependiente del tiempo de estímulo; sin embargo, cuando las células se trataron con DTP5 30 min antes de la adición del LPS, se observó una atenuación en la degradación de la proteína IκBα tanto en macrófagos peritoneales procedentes de animales WT como de DKO LXR. Como control, se trataron las células con el ligando farmacológico de los LXRs, T1317 (0,5 µM), demostrándose que dicho ligando no fue capaz de producir una disminución de la degradación de IκBα inducida por el LPS. Por lo tanto, estos resultados demuestran que el DTP5 presenta un efecto anti-inflamatorio independiente de su función como ligando agonista de LXR.

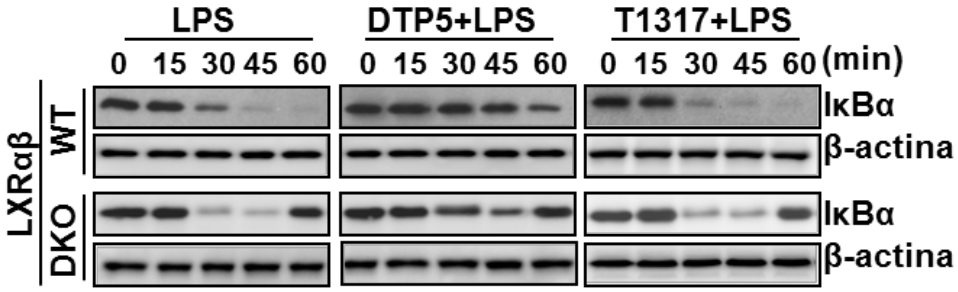

Figura 5. DTP5 inhibe la degradación de IκBα en macrófagos WT y deficientes en LXRα/β. *Macrófagos peritoneales procedentes de ratones WT y DKO LXR se trataron con LPS (250 ng/ml) durante los tiempos indicados en presencia de DTP5 (10 µM) o DMSO, adicionados al medio 30 min antes del estímulo inflamatorio. El ligando de los receptores LXR, T1317 (0,5 µM), se utilizó como control. El tratamiento con DTP5 redujo la degradación de IκBα inducida tras el tratamiento con LPS, independientemente de la presencia de LXR. Además, la activación de LXR con T1317 no modificó la degradación de IκBα promovida por el LPS. Los niveles de carga de proteína se normalizaron utilizando β-actina. Se muestra un experimento representativo de tres.*

3. Papel de los terpenos en la señalización temprana de los procesos inflamatorios.

La activación de los TLRs es esencial para activar al sistema inmune innato y erradicar al organismo invasor. La señalización de los TLRs puede ser llevada a cabo a través de la vía dependiente de MyD88 o independiente de MyD88, en función del TLR que haya sido activado. Para evaluar el efecto del DTP5 en la respuesta inflamatoria mediada por los TLRs, se utilizaron los siguientes ligandos: LPS (ligando de TLR4), que es capaz de señalizar a través de la vía dependiente e independiente de MyD88; LTA (agonista de TLR2), que señaliza a través de la vía MyD88 dependiente, y pI:C (ligando de TLR3), capaz de desencadenar una señalización a través de la vía dependiente de TRIF.

3.1. El pre-tratamiento con DTP5 inhibe la activación de genes pro-inflamatorios clásicos tras la estimulación con diferentes ligandos de TLRs.

Para evaluar los efectos del DTP5 sobre la expresión de NOS-2 y COX-2 inducida por diferentes ligandos de TLRs, se trataron macrófagos peritoneales de ratones Balb/c durante 30 min con este DTP (10 µM) y a continuación se estimularon con LPS (250 ng/ml), pI:C (25 µg/ml) o LTA (5 µg/ml) durante 18 h. Se evaluaron los niveles de expresión de NOS-2 y COX-2 mediante Western blot y se observó que tanto el LPS como el pI:C y el LTA eran capaces de inducir la expresión de ambas enzimas; mientras que el DTP5 era capaz de prevenir dicho efecto en respuesta a todos los estímulos empleados (Figura 6). Este experimento también se realizó con macrófagos derivados de médula ósea, obteniéndose resultados similares.

Estos datos nos indican que el derivado sintético 5 del ácido acantoico es capaz de atenuar la respuesta desencadenada por diferentes ligandos de los TLRs.

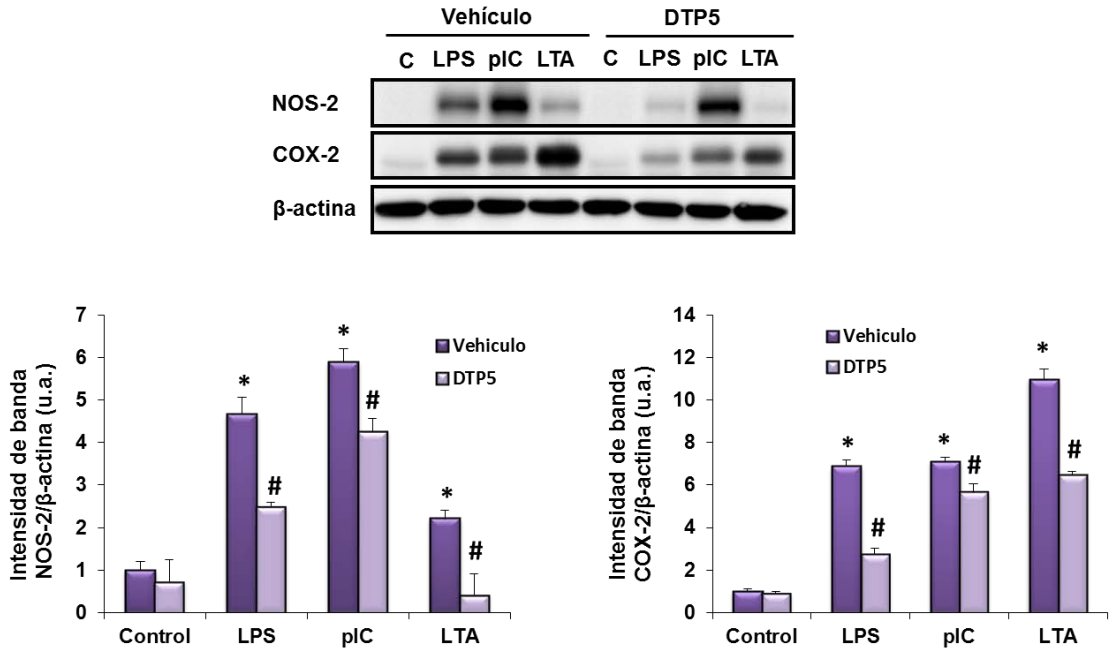

Figura 6. Efecto del DTP5 en la expresión de NOS-2 y COX-2 inducida por diferentes ligandos de los TLRs. *Macrófagos peritoneales se trataron durante 30 min con 10μM de DTP5 y se activaron posteriormente con LPS (250 ng/ml), pI:C (25μg/ml) o LTA (5 μg/ml). Tras 18 h de tratamiento se analizaron los niveles de NOS-2 y COX-2 mediante Western blot. Se empleó β-actina como control de carga para normalizar los resultados. Los gráficos representan la media ± DE de tres experimentos independientes.*p≤0,05 respecto al control estimulado con el vehículo y #p≤0,05 respecto al tratamiento con los distintos ligandos de los TLRs.*

La NOS-2 es una enzima inducible responsable de la síntesis de NO en grandes cantidades, el cual es fácilmente oxidado en condiciones fisiológicas, dando lugar a la formación de nitritos (NO_2) y nitratos (NO_3). La producción total de NO puede determinarse, por tanto, midiendo la acumulación de estos metabolitos (NOx) en el medio de cultivo según el método de Griess (Green et al., 1982).

Por este motivo se decidió analizar la acumulación de NOx en el medio de cultivo, ya que constituye una aproximación que permite medir de forma indirecta la actividad de NOS-2. Para ello, se pre-incubaron macrófagos peritoneales durante 30 min con DTP5 y posteriormente se estimularon las células con LPS, pI:C o LTA. Tras 18 h de tratamiento se midieron los niveles de NOx acumulados en el medio de cultivo. Los resultados obtenidos permitieron comprobar que el DTP5 inhibía la producción de NOx mediada por NOS-2 (Figura 7A). Por tanto, la reducción de

NOx observada tras el tratamiento con el DTP5 se corresponde con la inhibición de dicha enzima mostrada en la figura 6.

Para determinar si los efectos inhibitorios de los DTPs sobre la expresión de NOS-2 y COX-2 eran debidos a un mecanismo transcripcional o post-traduccional, se completaron los estudios de proteína con ensayos de *qPCR*, que nos permitieron analizar el papel de los derivados sintéticos del ácido acantoico sobre la activación de la transcripción de estos genes diana. De este modo se corroboró que los DTPs 1 y 5 son capaces de inhibir la expresión génica de NOS-2 y COX-2 inducida por LPS (Figura 7B).

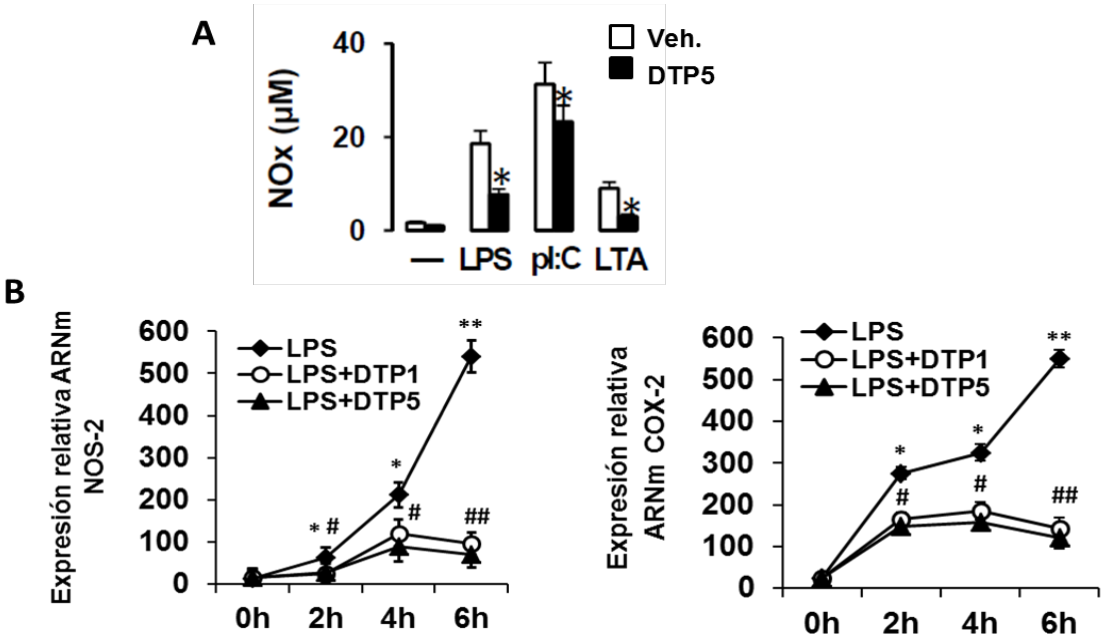

Figura 7. Inhibición de la producción de NOx y de la expresión génica inducida por estímulos inflamatorios. A) *Macrófagos peritoneales de ratones Balb/c se trataron con diferentes ligandos de los TLRs: LPS (250 ng/ml), pI:C (25µg/ml) o LTA (5 µg/ml); en presencia de DTP5 (10µM) o de su vehículo, adicionado 30 min. Tras 18 h de tratamiento se determinaron los niveles de NOx acumulados en el medio de cultivo según el método de Griess. Los resultados muestran un experimento representativo de tres. *p≤0,05 respecto al tratamiento con los distintos ligandos de los TLRs.* ***B)*** *Macrófagos peritoneales de ratones Balb/c se pre-trataron con diferentes DTPs (10µM) o su vehículo durante 30 min y se estimularon con LPS (250 ng/ml) a los tiempos indicados. Los niveles de expresión a nivel de ARNm de COX-2 y NOS-2 fueron cuantificados mediante qPCR, utilizando 36B4 como gen de referencia. Se calcularon los valores de expresión relativa mediante el método ΔΔCt. Los resultados muestran la media± DE de tres experimentos. .*p≤0,05 y **p≤0,01 respecto al control no tratado con DTPs y, #p≤0,05 y ##p≤0,01 respecto a su correspondiente valor en ausencia de DTPs.*

3.2. El derivado sintético DTP5 inhibe la vía de activación del factor de transcripción NF-κB y de las MAPKs.

Uno de los principales reguladores de la transcripción de NOS-2 y COX-2, es el factor de transcripción NF-κB. Según los resultados obtenidos en los que se observa que el DTP5 disminuye la degradación de IκB, junto con los datos de estudios previos sobre los efectos anti-inflamatorios del ácido acantoico, se decidió analizar la vía de activación de NF-κB con el objetivo de determinar las posibles dianas de acción de los compuestos problema.

Mediante la técnica de Western blot se observó que los niveles de degradación de IκBα e IκBβ se veían reducidos en las células pre-incubadas con el DTP5. Como la degradación de las proteínas inhibidoras IκBs está mediada por la fosforilación y posterior ubiquitinación de las mismas, se decidió estudiar también el complejo IKK, responsable de la fosforilación, y en consecuencia, de la degradación de las IκBs (Figura 8).

Para llevar a cabo dicho estudio se emplearon macrófagos peritoneales y macrófagos derivados de médula ósea tratados con DTP5 durante 30 min y estimulados posteriormente con diferentes ligandos de los TLRs (Figura 8A con LPS, B con pI:C y C con LTA) durante los tiempos indicados. Se comprobó que la degradación de IκBβ observada a los 30 min de estimulación con LPS o pI:C (en el caso de LTA, a los 15 min) se correspondió con un aumento en el grado de fosforilación de IKK. Sin embargo, cuando los macrófagos se pre-trataron con el DTP5, la atenuación de la degradación de IκBs se relacionó con una menor fosforilación de IKK.

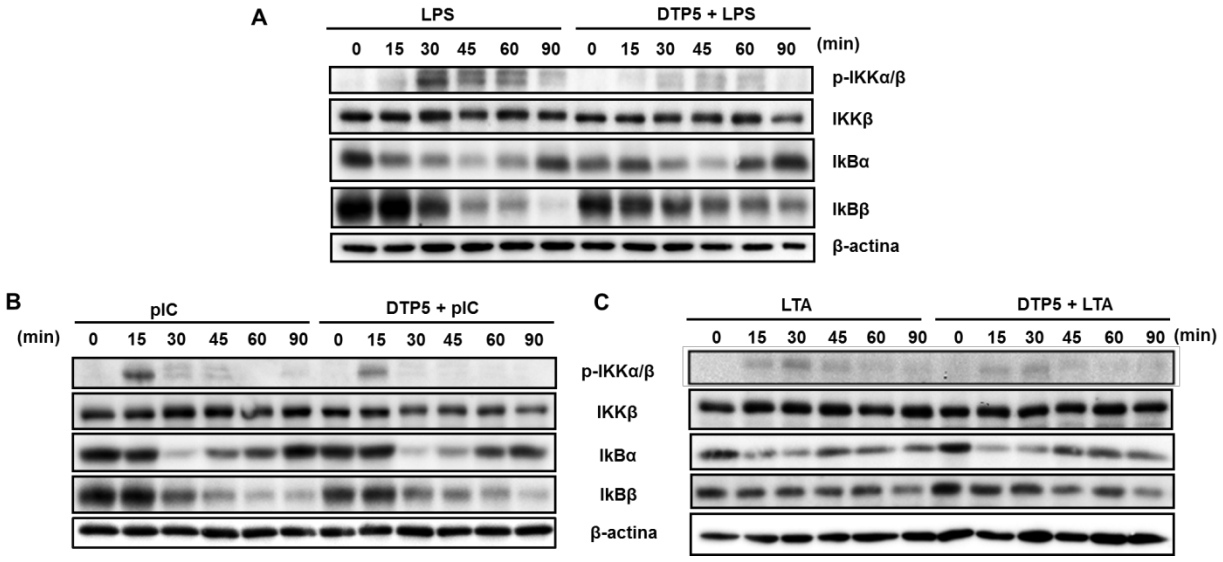

Figura 8. DTP5 inhibe la vía de activación de NF-κB en macrófagos estimulados con diferentes ligandos de los TLRs. *La degradación de las proteínas IκBs así como el grado de fosforilación de IKK se determinó en extractos celulares de macrófagos peritoneales mediante Western blot. Las células se activaron con 250 ng/ml de LPS (**A**), 25 µg/ml de pI:C (**B**) o 5 µg/ml de LTA (**C**) durante los tiempos indicados, en presencia o ausencia de DTP5 (10 µM, 30min). La figura muestra un ejemplo representativo de tres.*

Además, se llevaron a cabo otros experimentos donde se analizó la vía de las MAPKs, ya que se trata de una ruta de transducción de señales de células eucariotas que es activada tras la unión de diversos ligandos a sus correspondientes TLRs, y que culmina con la activación de factores de transcripción, como AP-1, el cual media la expresión de genes pro-inflamatorios (Kaminska, 2005).

Por tanto, teniendo en cuenta estos antecedentes, se decidió estudiar la vía de señalización de las MAPKs, a fin de analizar si dicha ruta se encuentra regulada por la acción de nuestros derivados sintéticos del ácido acantoico, constituyendo otro de los posibles mecanismos de acción de estos compuestos.

Tras un pre-tratamiento de los macrófagos peritoneales o macrófagos derivados de médula ósea con DTP5, éstos se estimularon con diferentes ligandos de los TLRs durante los tiempos indicados (Figura 9). Los niveles de fosforilación de las MAPKs se cuantificaron mediante Western blots.

Nuestros resultados indicaron que el tratamiento con LPS (Figura 9A), pI:C (Figura 9B) o LTA (Figura 9C) estaba induciendo la fosforilación y consecuente activación de ERK, p38 y JNK a partir de los 15-30 min de exposición a los estímulos inflamatorios. Por el contrario, se observó que las células que recibieron el pre-tratamiento con el DTP5 presentaron una disminución en cuanto al grado de fosforilación de ERK y p38, sin afectar a la vía de JNK (Figura 9).

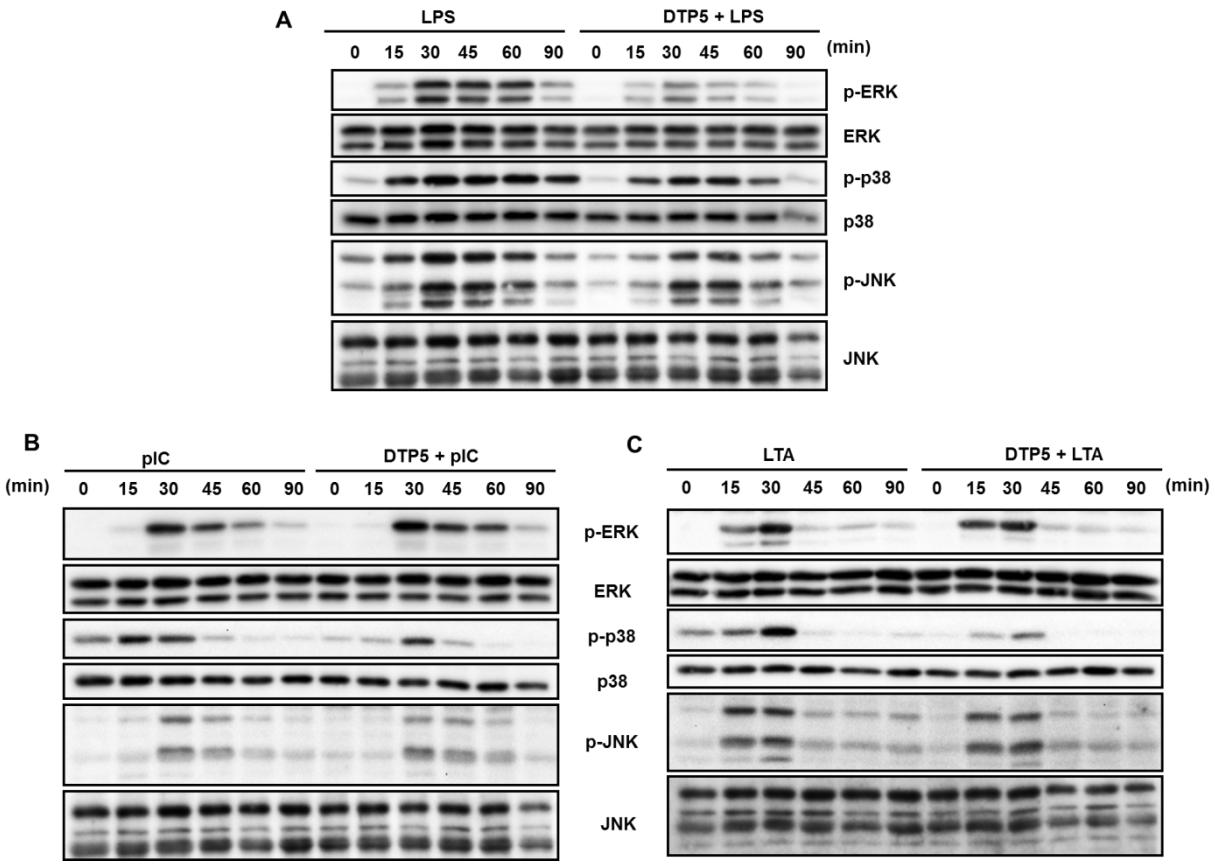

Figura 9. Implicación de la vía de las MAPKs en los efectos inhibitorios de la inflamación del DTP5. *Los macrófagos peritoneales se trataron con 250 ng/ml de LPS (**A**), 25µg/ml de pI:C (**B**) o 5µg/ml de LTA (**C**) durante los tiempos indicados en presencia o ausencia de un pre-tratamiento con DTP5 (10 µM, 30 min). Los niveles de expresión y fosforilación de ERK, p38 y JNK se analizaron en extractos proteicos totales mediante Western blot, utilizando como control de carga la forma total de cada una de las MAPKs. La figura muestra unos geles representativos de tres experimentos independientes.*

3.3. Efectos de los DTPs 1 y 5 en macrófagos peritoneales procedentes de ratones deficientes en MyD88.

Como se ha visto que los DTPs son capaces de inhibir la expresión de genes pro-inflamatorios clásicos inducida, tanto a través de la vía dependiente como independiente de MyD88, por acción de diferentes ligandos de los TLRs; decidimos analizar si al tratar los macrófagos con nuestros compuestos, éstos presentan unos efectos más exacerbados en los macrófagos WT que en los KO de MyD88 (MyD88$^{-/-}$).

Para confirmar si el efecto de los DTPs está mediado por MyD88 se realizaron experimentos, utilizando ratones deficientes en dicha proteína adaptadora y empleando el LPS como estímulo pro-inflamatorio, ya que es capaz de desencadenar una respuesta inflamatoria a través de la vía dependiente e independiente de MyD88.

Para llevar a cabo este abordaje experimental, se obtuvieron macrófagos peritoneales de animales WT y KO MyD88. Dichas células se pre-trataron con DTP1 o DTP5 durante 30 min y a continuación se estimularon con LPS durante 18 h, tal y como se indica en la figura 10. A continuación se determinaron los niveles de la quimioquina inflamatoria IP-10, inducida por el LPS, mediante un kit de ELISA.

La producción de la quimioquina IP-10, regulada principalmente por la vía independiente de MyD88, fue similar tanto en macrófagos peritoneales de animales WT como MyD88$^{-/-}$ tras el tratamiento con LPS. Se detectó 10,6 ng/ml ± DE de dicha quimioquina en el medio de cultivo de células WT y 13,2 ng/ml ± DE en el caso de los animales KO MyD88. En base a estos valores, considerados como el 100% de producción de IP-10 en cada uno de los grupos, se calculó el porcentaje de inhibición que presentaban los DTPs, obteniéndose una inhibición en los animales WT de casi el 40% con el pre-tratamiento con DTP1 y, aproximadamente del 50% cuando se empleó el DTP5. En el caso de animales KO MyD88 se obtuvo una inhibición de los niveles de IP-10 del 60% tras ser pre-tratados con uno u otro de los DTPs.

Por otro lado, se llevó a cabo otro experimento en paralelo, en el que los macrófagos se estimularon con pI:C, el cual señaliza únicamente a través de la vía independiente de MyD88, por lo que era de esperar que la respuesta tanto en macrófagos WT como MyD88$^{-/-}$ fuese similar tras el tratamiento con los distintos DTPs (Figura 10). En este caso, los valores de IP-10 inducida por pI:C, en base a los cuales se calculó la inhibición que presentaban los DTPs fueron 14,7 ng/ml ± DE en el caso de los macrófagos WT estimulados sólo con pI:C, y 18,4 ng/ml ± DE para

los macrófagos MyD88$^{-/-}$. En ambos grupos de animales se obtuvo una inhibición de aproximadamente el 40% tras el pre-tratamiento con ambos DTPs.

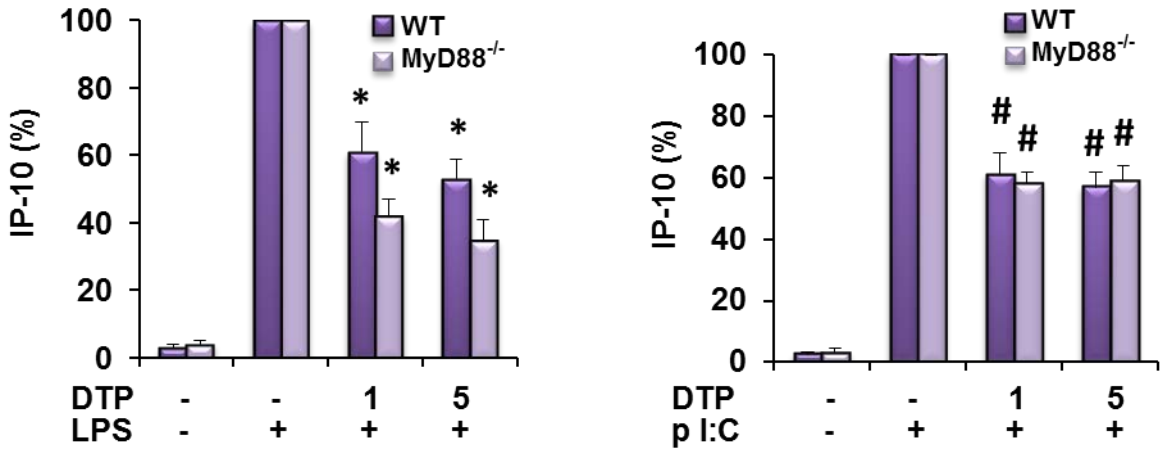

Figura 10. Efecto de los DTPs 1 y 5 sobre la producción de IP-10 inducida por LPS y pI:C en macrófagos peritoneales de ratones MyD88$^{-/-}$. *Macrófagos peritoneales de ratones WT y MyD88$^{-/-}$ se estimularon con LPS (250 ng/ml) o pI:C (25µg/ml) en presencia o ausencia del pre-tratamiento con DTP1 o 5 (10 µM) durante 30 min. La producción de IP-10 se cuantificó mediante un kit de ELISA. El gráfico representa el tanto por ciento de acumulación de IP-10 en el medio de cultivo. La cantidad de IP-10 correspondiente al tratamiento con LPS o pI:C, se consideró el 100% de producción. Se muestra la media ± DE de tres experimentos independientes. *p≤0,05 vs. LPS y #p≤ vs. pI:C.*

4. El tratamiento con los derivados sintéticos del ácido acantoico activa la vía de PI3K/Akt.

La vía de señalización de PI3K-Akt juega un papel fundamental a nivel celular regulando, entre otros procesos, la respuesta inmune. Actúa como un regulador negativo de la activación de las MAPKs y de la vía de NF-κB, ya que induce la expresión de IκB y reprime la expresión de NOS-2 (Diaz-Guerra et al., 1999) (Fukao and Koyasu, 2003) (Guha and Mackman, 2002).

Tomando esto como referencia, se decidió analizar si la disminución en la fosforilación de las MAPKs p38 y ERK, así como la menor inducción de NOS-2 y COX-2 observada en los macrófagos pre-tratados con los DTPs, podría deberse a una activación de la vía de PI3K/Akt.

4.1. Activación de Akt por acción de los DTPs.

Para la completa activación de Akt, ésta tiene que ser fosforilada en Thr308 y Ser473. Sin embargo, para que Akt sea fosforilada en Ser473 previamente ha tenido que haber incorporado un grupo fosfato en treonina 308; por este motivo se analizó la fosforilación en Ser473 para determinar el efecto de los DTPs sobre dicha proteína.

Para comprobar si los DTPs eran capaces de modular la vía de Akt en macrófagos primarios, estas células se estimularon con diferentes DTPs: 1, 3 y 5, y el nivel de fosforilación se cuantificó y analizó mediante Western blot (Figura 11A). Se observó que el tratamiento de los macrófagos con estos DTPs indujo la fosforilación de la proteína Akt frente a los niveles basales del control tratado con el vehículo.

A su vez se llevó a cabo otro experimento en el que los macrófagos peritoneales se trataron con DTP5 durante 10, 20 y 30 min, observándose una rápida fosforilación de Akt a partir de los 10 min de tratamiento (Figura 11B).

Estos resultados indican que los DTPs son capaces de activar la vía de PI3K/Akt mediante la fosforilación de Akt.

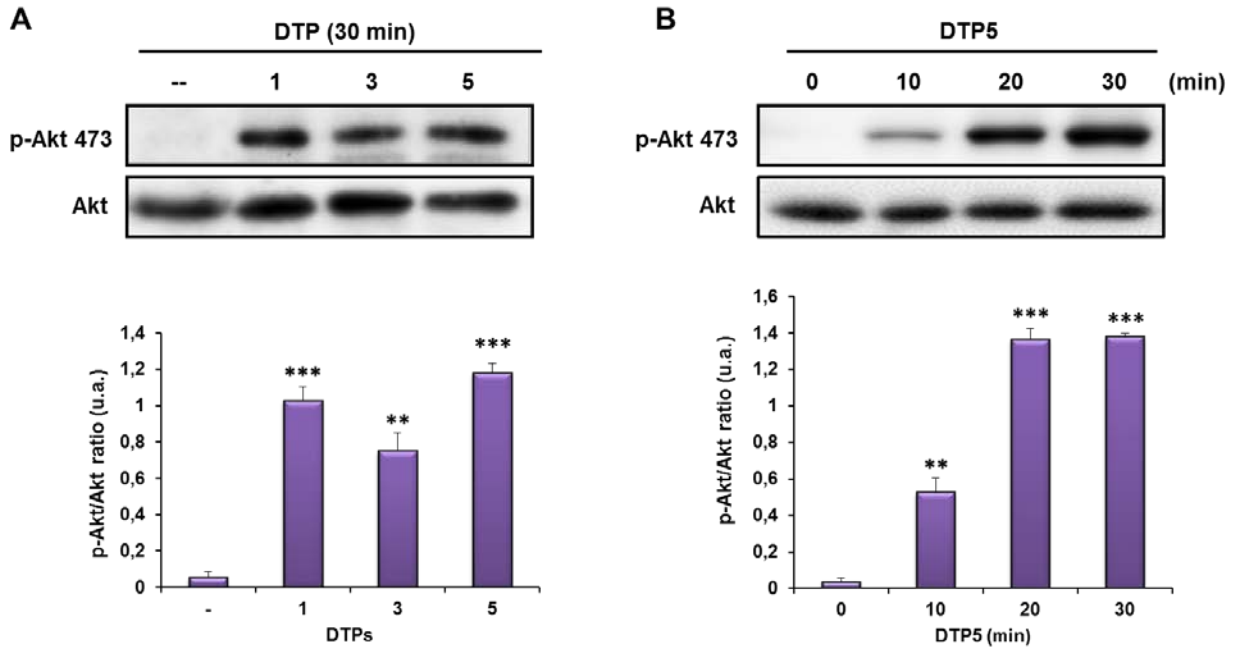

Figura 11. Activación de la vía de Akt mediada por los DTPs en macrófagos peritoneales. A) *Los macrófagos peritoneales se estimularon con diferentes DTPs (1, 3 y 5; 10 µM) durante 30 min. El grado de fosforilación de Akt en Ser473 se analizó en extractos proteicos totales y se calculó el ratio entre la cantidad de proteína fosforilada y total en cada uno de los puntos (se muestra la cuantificación en la parte inferior).* ***B)*** *Los macrófagos peritoneales y los macrófagos derivados de médula ósea se estimularon con DTP5 durante los tiempos indicados; los niveles de fosforilación en Ser473 de Akt se cuantificaron y determinaron mediante Western blot, empleándose la forma total de dicha proteína como control de carga. Tanto en* ***A*** *como en* ***B*** *se muestra un gel representativo de los cuatro que se realizaron independientemente. Las gráficas representan la media ± DE de p-Akt tras normalizar con Akt. **p≤0,01; ***p≤0,001 vs. control.*

En paralelo se realizó otro experimento en el que los macrófagos peritoneales de ratones Balb/c se estimularon con LPS, pI:C o LTA durante 30 min en presencia del DTP5 o de su vehículo. Estos resultados corroboraron los datos del experimento anterior, ya que el DTP5 era capaz de inducir la fosforilación de Akt por sí mismo, aumentado los niveles de Akt fosforilado hasta 8 veces más que el control sin estimular. Además, dicho efecto persistía incluso después de la estimulación con diversos ligandos de los TLRs: LPS (TLR4), pI:C (TLR3) y LTA (TLR2) (Figura 12).

En base a estos resultados se determinó que el DTP5 era capaz de activar de forma significativa a la proteína Akt frente a diversos estímulos pro-inflamatorios, siendo el caso más

evidente el del tratamiento con LPS, en el que los niveles de Akt fosforilado en Ser473 tras el pre-tratamiento con el DTP5 se duplicaban con respecto al tratamiento con LPS en ausencia de nuestro compuesto (Figura 12).

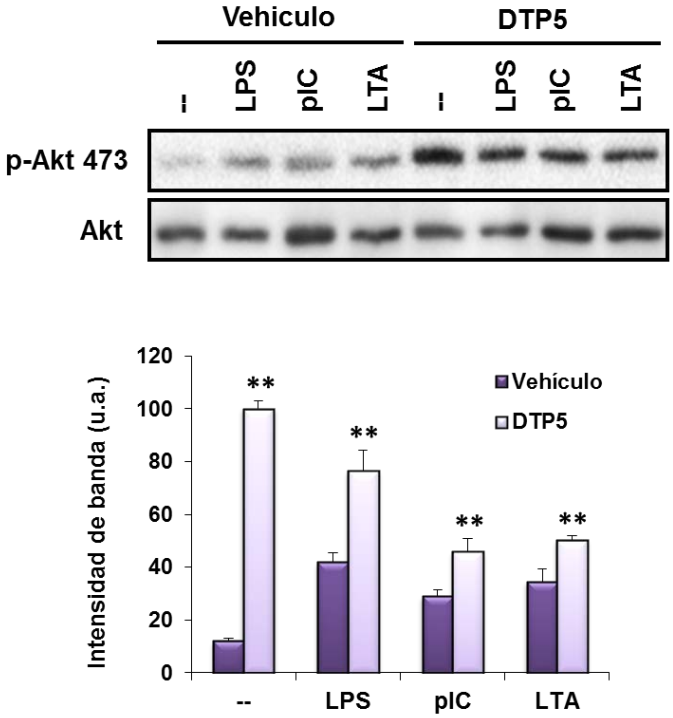

Figura 12. Papel del DTP5 en la activación de Akt frente a diversos ligandos de los TLRs en macrófagos peritoneales. *Las células se pre-trataron con DTP5 (10 µM) o su vehículo durante 30 min. A continuación se indujo la respuesta inflamatoria con LPS (250 ng/ml), pI:C (25µg/ml) o LTA (5µg/ml) durante 30 min. Los niveles de fosforilación de Akt se determinaron mediante Western blot. El gráfico representa la media ± DE de dos experimentos independientes realizados por duplicado. **p≤0,01 respecto al correspondiente valor en ausencia de DTP5.*

Para confirmar estos datos, las células se trataron de la misma forma que en el apartado anterior y se analizaron los niveles de Akt fosforilado en Ser473 por inmunofluorescencia (Figura 13). Se muestra un ejemplo representativo de las imágenes obtenidas en la figura 13A. Nuestros resultados mostraron que en la mayoría de las células control Akt no se encuentra fosforilado, sin embargo, cuando las células se estimularon con LPS, los niveles de fluorescencia de la proteína Akt activada aumentaban hasta 4 veces con respecto a las células control (Figura 13B). El pre-tratamiento de los macrófagos peritoneales con DTP5 durante 30 min era capaz de

aumentar los valores de Akt fosforilado hasta 10 veces con respecto a las células tratadas con el vehículo.

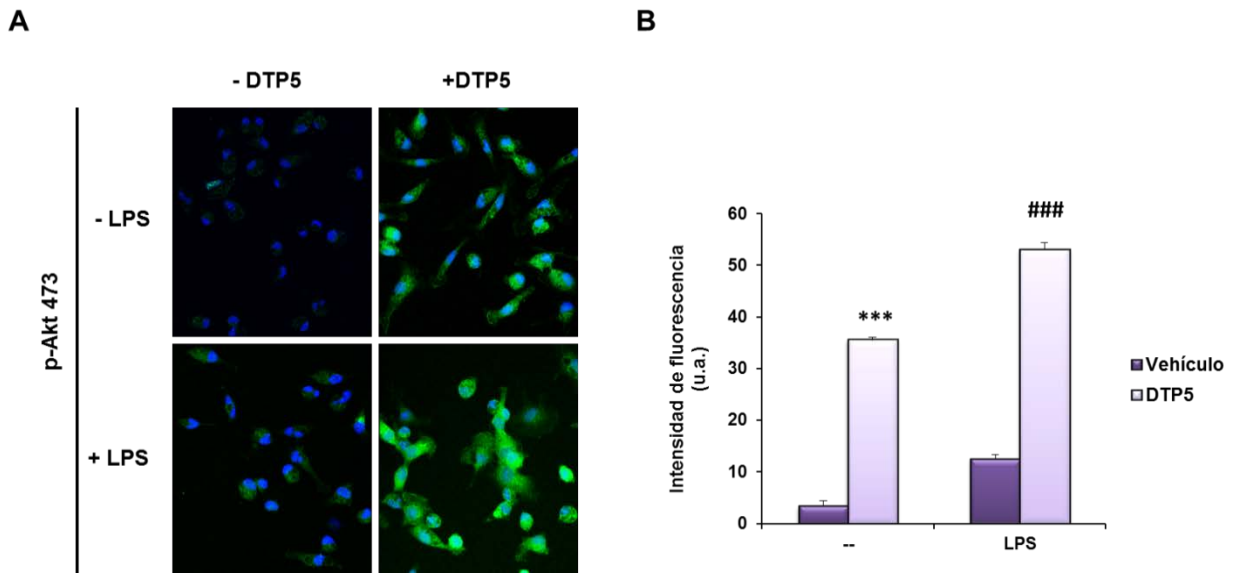

Figura 13. Activación de Akt mediada por DTP5 en macrófagos peritoneales. *Macrófagos peritoneales se trataron con DTP5 (10 µM) o su vehículo durante 30 min y a continuación se estimularon con LPS (250 ng/ml) durante media hora. La activación de Akt se analizó mediante microscopía confocal.* ***A)*** *Se muestra un ejemplo representativo de las imágenes obtenidas.* ***B)*** *La intensidad de fluorescencia se determinó utilizando el programa Image J. El gráfico representa la media ± DE de cuatro experimentos independientes. ***p≤0,001, ###p≤0,001 respecto al correspondiente valor obtenido en ausencia de DTP5.*

4.2. Efectos del tratamiento con DTP5 sobre la enzima PI3K.

Tras analizar los efectos del DTP5 sobre Akt, decidimos estudiar si dicho compuesto es capaz de inducir la activación de la enzima PI3K.

Por este motivo, nos centramos en estudiar la actividad PI3K en respuesta al tratamiento con DTP5. Para ello, se utilizaron macrófagos peritoneales tratados con DTP5 durante 5, 10 y 15 min; como control positivo que induce la activación de PI3K se empleó la insulina y como control negativo, el inhibidor de la PI3K, LY294002, durante los tiempos indicados en la figura 14A. Una vez realizados los tratamientos, se inmunoprecipitó la enzima con un anticuerpo de la

subunidad reguladora, p85, y se realizó un ensayo *in vitro* de actividad de la PI3K, analizándose la capacidad de esta enzima de convertir el PIP2 en PIP3 (Figura 14A). En todos los casos, con independencia de la duración del estímulo, se observó que la pre-incubación de las células con DTP5 aumentaba los niveles de PIP3, por tanto, podemos concluir que dicho compuesto es capaz de inducir la activación de PI3K.

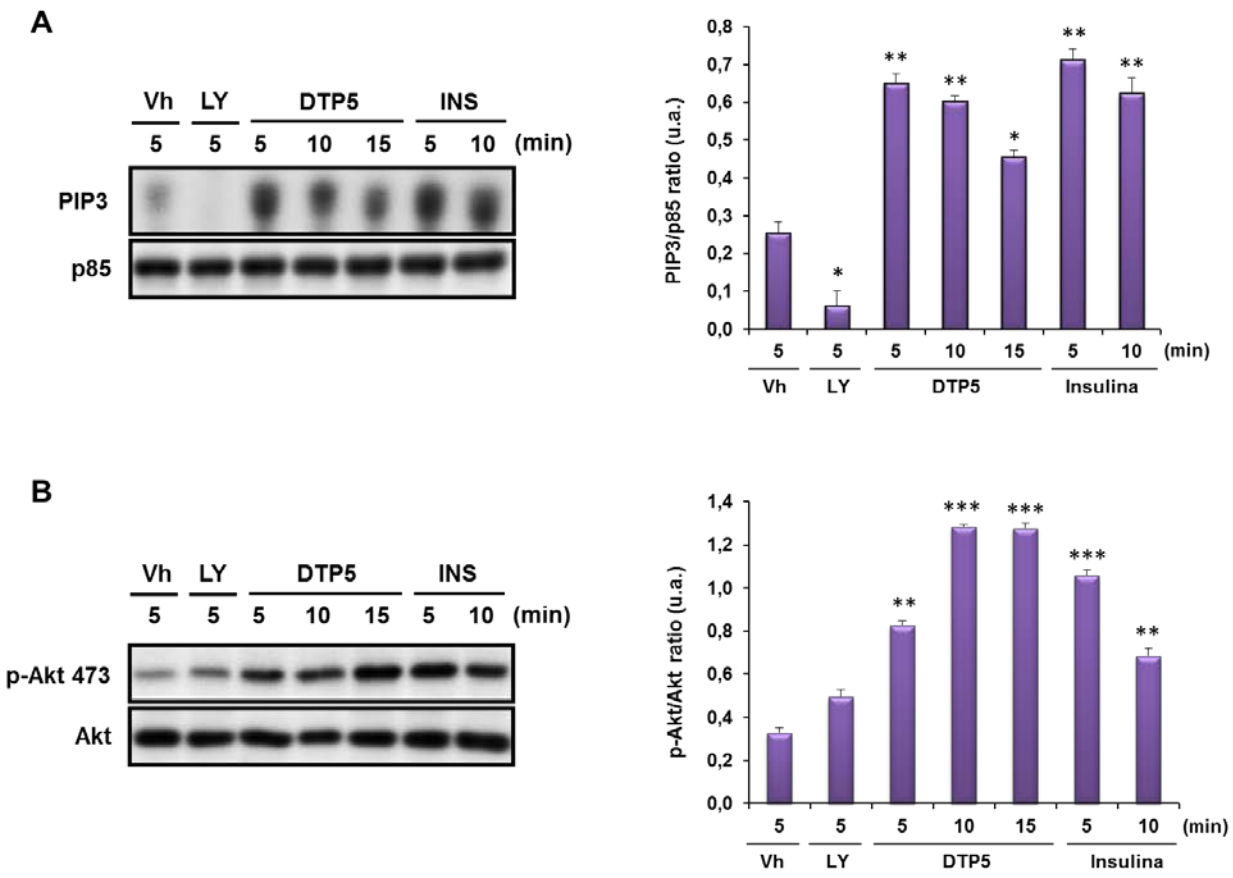

Figura 14. Activación de la PI3K mediada por DTP5. *Los macrófagos se pre-trataron con 10 µM del DTP5, 50 nM de insulina, la cual se empleó como control positivo, ya que induce la activación de PI3K, y 10 µM de LY294002, inhibidor de la PI3K, durante los tiempos indicados.* ***A)*** *La actividad quinasa de la PI3K se analizó inmunoprecipitando la enzima y usando PIP2 como sustrato. El efecto del DTP5 sobre la activación de PI3K se determinó midiendo la cantidad de PIP3 generado. La subunidad p85 se usó como normalizador de carga.* ***B)*** *El sobrenadante de dichos inmunoprecipitados se empleó para analizar los niveles de p-Akt. Se utilizó la forma total de la enzima como control de carga. El análisis densitométrico se muestra a la derecha de cada uno de los paneles. La imagen refleja un resultado representativo de dos experimentos. *p≤0,05; **p≤0,01;***p≤0,001 respecto al control tratado con el vehículo. Vh: Vehículo. INS: Insulina.*

Además, se analizó mediante Western blot el sobrenadante obtenido tras la inmunoprecipitación para determinar los niveles de Akt fosforilado y se observó un aumento de la fosforilación de este mediador tras los distintos tratamientos con el DTP5, que llegaron a ser incluso cuatro veces superiores en relación a los niveles basales de las células control, estimuladas solamente con el vehículo (Figura 14B). Datos que están en total consonancia con los resultados que demuestran un aumento de la actividad de PI3K inducida por nuestro compuesto.

Como la activación de PI3K induce la fosforilación de PDK1, que a su vez fosforila a Akt en el residuo treonina 308, permitiendo que mTORC2 fosforile a Akt en serina 473; se decidió analizar si el DTP5 era capaz de inducir la fosforilación en ambos residuos de Akt (Figura 15).

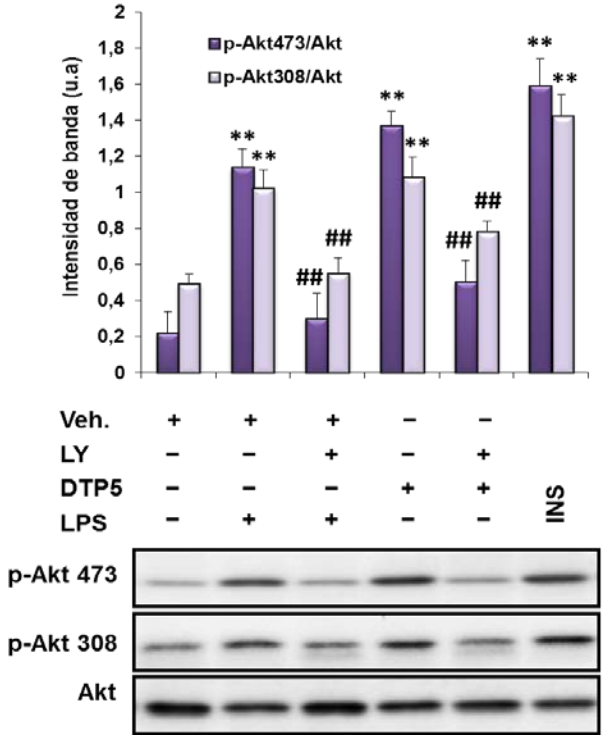

Figura 15. Fosforilación de Akt en Thr308 y Ser473 tras el tratamiento con DTP5 en macrófagos peritoneales. *Los macrófagos peritoneales se estimularon con DTP5 (10 µM) o LPS (250 ng/ml) durante 30 min. El inhibidor farmacológico LY294002 se utilizó como control (10 µM, 30 min antes). Tanto los niveles de expresión como el grado de fosforilación de Akt en Thr308 y Ser473 se analizaron en extractos proteicos totales y se calculó el ratio entre la cantidad de proteína fosforilada y total en cada uno de los puntos. Se muestra un gel representativo en la parte inferior. La figura representa la media ± DE de dos experimentos independientes. **p≤0,01 respecto al correspondiente valor de la condición control tratada con el vehículo; ##p≤0,01 respecto al correspondiente valor en ausencia de LY294002. INS: Insulina.*

Para ello los macrófagos peritoneales y macrófagos derivados de médula ósea se trataron con el DTP5 (10 μM) o con LPS (250 ng/ml) durante 30 min en presencia o en ausencia del inhibidor LY294002, el cual se adicionó al medio de cultivo 30 min antes del tratamiento con el DTP5 o con LPS. El objetivo de tratar las células con el LY294002 era determinar si el efecto sobre la fosforilación de Akt inducida por nuestro compuesto como consecuencia de la activación de PI3K, se revertía. Como control positivo se empleó la insulina (50 nM) durante 30 min. En la figura 15 se observa que el DTP5 es capaz de inducir la fosforilación de Akt en ambos residuos, resultado que fue corroborado mediante el uso del inhibidor farmacológico LY294002, ya que fue capaz de revertir el efecto del DTP5 sobre Akt.

4.3. Implicación de la vía de PI3K en la inhibición de la vía de NF-κB y MAPKs mediada por DTP5.

Para evaluar la posible implicación de la vía de PI3K/Akt en los efectos observados por el tratamiento con DTP5, en las rutas de NF-κB y MAPKs, se analizó si el carácter anti-inflamatorio de este compuesto se mantenía en los macrófagos peritoneales en presencia de LY294002 (Figura 16).

En primer lugar se analizó los niveles de Akt fosforilado en Ser473, para comprobar que tanto el DTP como el LY funcionaron en estos experimentos. Como se muestra en la figura 16, se observa una inducción de la fosforilación de Akt debido al tratamiento con nuestro compuesto; sin embargo cuando las células se pre-trataron con el inhibidor de la PI3K, este efecto no se aprecia.

El análisis de la vía de NF-κB, mostró que el nivel de fosforilación de la quinasa IKK, disminuía en presencia del DTP5, al igual que ocurría con la activación de las MAPKs p38 y ERK, datos que corroboran los resultados obtenidos hasta el momento. Sin embargo, en presencia del LY294002 dicho efecto se revertía, recuperándose prácticamente en todos los casos los niveles de fosforilación basales, tanto de IKK como de las MAPKs, obtenidos en respuesta al estímulo inflamatorio (LPS). Mientras que los niveles de p-JNK no se vieron alterados ni por la presencia del DTP5 ni del inhibidor.

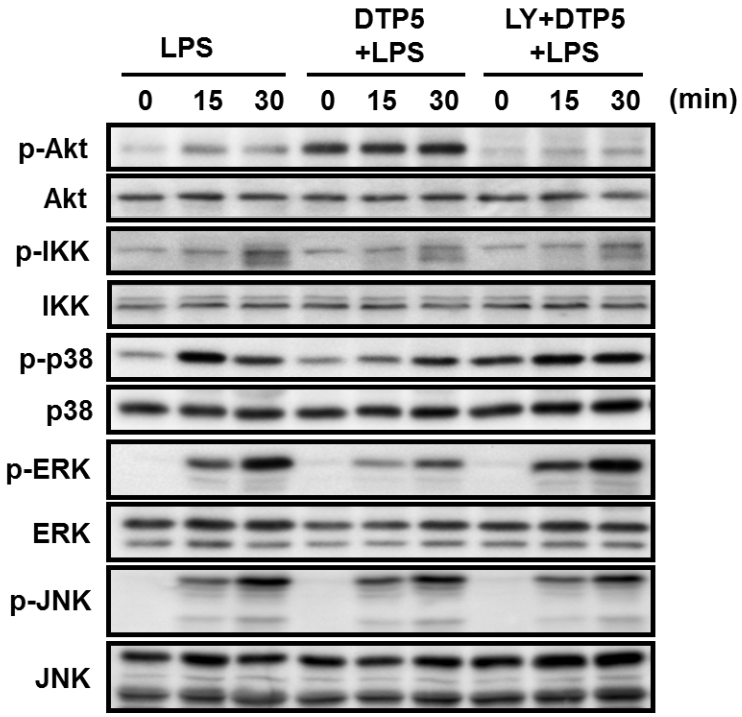

Figura 16. El inhibidor LY294002 revierte la fosforilación de Akt y la inhibición de NF-κB y MAPKs mediada por DTP5. *Los macrófagos se pre-trataron con DTP5 (10 µM) o su vehículo durante 30 min y seguidamente se estimularon con LPS (250 ng/ml) en presencia o en ausencia de LY294002 (10 µM), adicionado 30 min antes del pre-tratamiento con el DTP5 o DMSO (vehículo). Los niveles de fosforilación de Akt en Ser473, IKK y de las distintas MAPKs se analizaron en extractos proteicos totales y como control de carga se empleó la correspondiente forma total de cada una de las proteínas. Se muestra un gel representativo de tres experimentos.*

Estos datos señalan que el efecto anti-inflamatorio observado en los macrófagos tras el tratamiento con el DTP5 depende, al menos en parte, de la activación de la vía de PI3K/Akt.

Para confirmar el efecto del DTP5 sobre la activación de PI3K se llevaron a cabo experimentos de sobreexpresión. Para ello, se realizaron transfecciones transitorias en la línea celular NIH3T3, en la que previamente habíamos comprobado que nuestro compuesto actuaba de manera similar que en los macrófagos peritoneales, en cuanto a la activación de la vía de PI3K/Akt se refiere, induciendo igualmente la fosforilación de Akt.

Las transfecciones se hicieron con dos plásmidos, uno de los cuales codifica para la forma WT de la subunidad catalítica p110 (p110-WT) y otro que codifica para una forma inactiva de la quinasa, ya que contiene una mutación puntual de la subunidad p110 (p110-KD) que conlleva al cambio de una arginina por una prolina en el aminoácido 916. Posteriormente las

células fueron expuestas a diversos estímulos. Se utilizó insulina (50 nM durante 30 min) como control positivo de la activación de PI3K. Por otro lado, se trataron con DTP5 (10 µM) durante 30 min, en presencia o en ausencia del inhibidor de PI3K (LY294002, 10 µM), el cual se adicionó media hora antes de que comenzara el tratamiento con DTP5, para determinar la posible existencia de un efecto directo sobre la activación de la vía PI3K/Akt (Figura 17).

Nuestros resultados indican que, tras la transfección con el plásmido p110-WT, el tratamiento con DTP5 produce un aumento significativo de los niveles de fosforilación de Akt en Ser473, efecto que es revertido cuando las células son pre-tratadas con el inhibidor LY294002. Por el contrario, cuando se transfectan con el plásmido que codifica para la forma inactiva de la PI3K, la ausencia de actividad de p110 disminuye la fosforilación de Akt dependiente de DTP5.

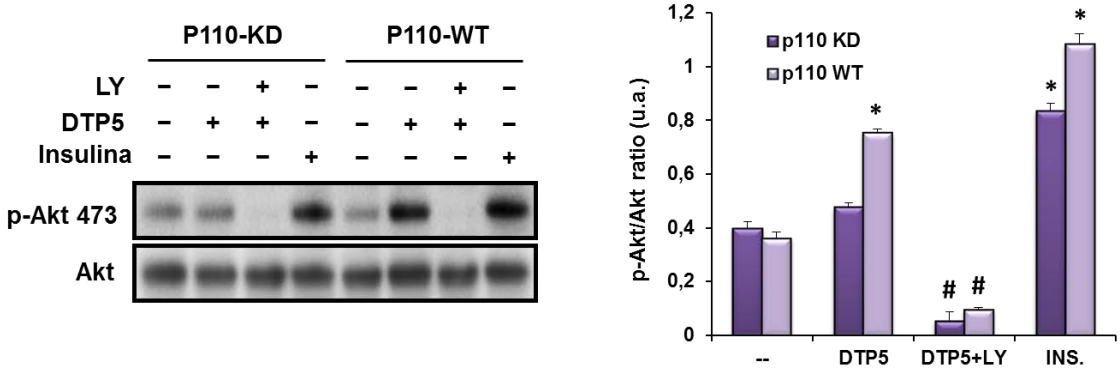

Figura 17. Efecto del DTP5 sobre la activación de PI3K. *Las células NIH3T3 se transfectaron con los vectores p110-WT y p110-KD, para garantizar la sobreexpresión de la subunidad p110 o de una forma inactiva de la misma. A continuación las células se trataron con LY294002 (10 µM, 30 min) en los casos indicados y se estimularon con DTP5 (10 µM) durante media hora. La insulina (50 nM, 30 min) se utilizó como control positivo. A continuación como medida indirecta de la activación de PI3K, se determinaron los niveles de fosforilación de Akt en Ser473 mediante Western blot en extractos proteicos totales (se muestra un gel representativo en la parte izquierda) y se cuantificaron empleando la forma total de la proteína como control de carga. El gráfico muestra la media ± DE de dos experimentos independientes. *p≤0,05 respecto a cada uno de sus controles tratados con el vehículo; #p≤0,05 respecto al correspondiente valor en presencia del DTP5. INS:Insulina.*

4.4. Efecto del DTP1 sobre las distintas isoformas de la subunidad catalítica de la PI3K.

Inhibición farmacológica.

Una vez comprobado que los DTPs modulan la vía de PI3K/Akt mediante una activación directa de la quinasa PI3K, decidimos analizar si el DTP1 activa de manera específica a algunas de las cuatro isoformas de clase I de PI3K, para lo cual los macrófagos se trataron durante una hora con diferentes concentraciones de inhibidores específicos para cada una de las distintas subunidades catalíticas, realizando una curva dosis-respuesta para determinar la concentración adecuada (Delgado-Martin et al., 2011). Para la elección de una dosis frente a otra se analizaron los niveles de fosforilación de Akt (Figura 18).

Los inhibidores que más afectaron a la fosforilación de Akt mediada por el DTP1 fueron los específicos para las isoformas γ y δ, lo que coincidiría con los datos bibliográficos que las describen como las más abundantes en células del sistema inmune (Kok et al., 2009), por lo que se escogieron los inhibidores de estas dos isoformas para analizar la implicación de p110γ y p110δ en la vía de activación de NF-κB. En el caso del inhibidor para la isoforma γ se decidió utilizar la concentración de 5 μM, ya que concentraciones superiores a dichos valores afectaron a la expresión basal de la proteína Akt; mientras que la concentración empleada para el inhbidor de la isoforma δ fue de 1 μM.

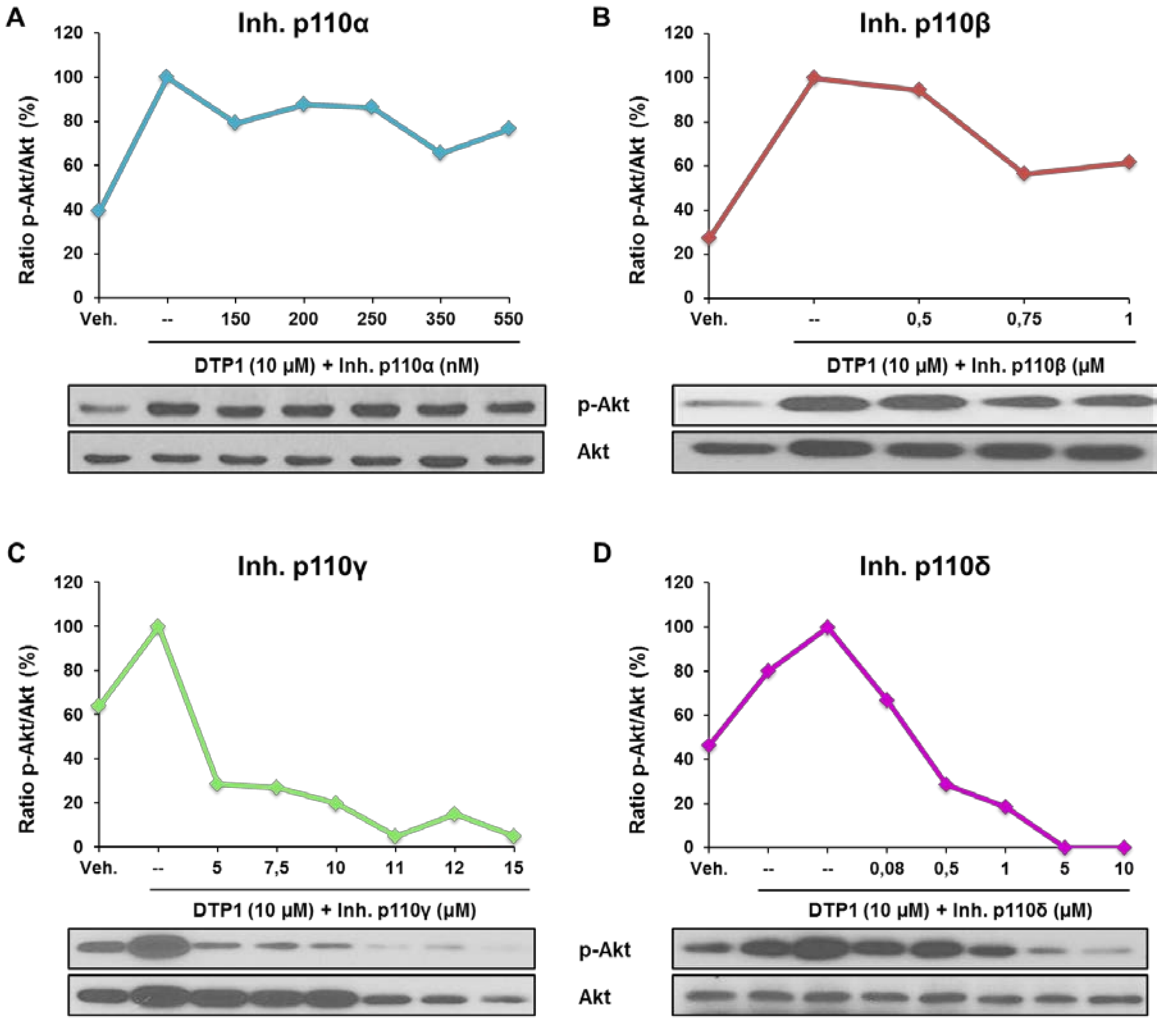

Figura 18. Curvas dosis-respuesta de los inhibidores específicos para cada una de las isoformas de la subunidad catalítica de la PI3K. *Se determinó la concentración de inhibidor, para cada una de las isoformas, mediante el análisis de la fosforilación de Akt inducida por el DTP1 (10 μM). La concentración del inhibidor para la isoforma α (**A**) seleccionada fue la más alta de las testadas, 550 nM, ya que en ninguna de las concentracones probadas la fosforilación de Akt se vio altamente comprometida en comparación con el resto de inhibidores. En el caso de p110β (**B**) y p110γ (**C**) la concentración empleada fue de 1 μM y 5 μM respectivamente, ya que concentraciones superiores a dichos valores afectaron a la expresión de la proteína Akt. Por último, la concentración de uso para el inhbidor de la isoforma δ fue de 1 μM (**D**).*

Al analizar la vía de NF-κB observamos que el DTP1 era capaz de inhibir la fosforilación de IKK inducida por el LPS. Sin embargo, cuando se trataron los macrófagos con el inhibidor para la isoforma p110δ, la disminución de los niveles de p-IKK inducida por el DTP se revirtió al menos parcialmente; al igual que ocurre con la degradación de la proteína IκBα (Figura 19). Esto nos podría estar indicando que parte de la acción del DTP1 estaría mediada por la PI3K. Obtuvimos resultados similares al emplear el inhibidor de p110γ.

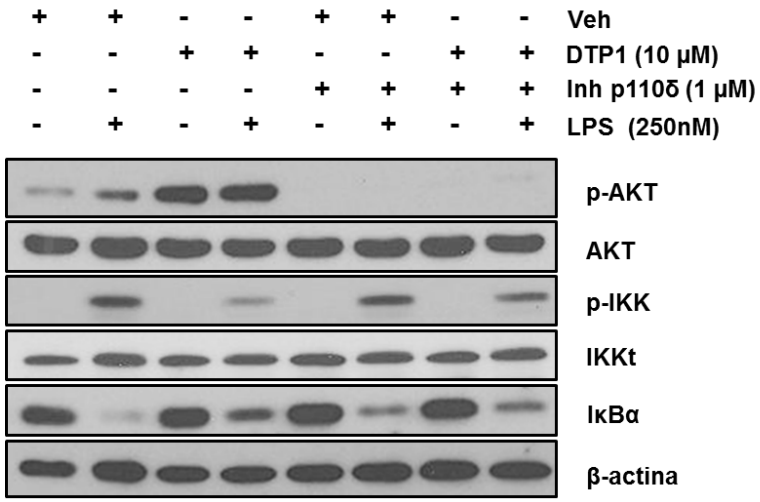

Figura 19. Papel de la isoforma p110δ en los efectos que ejerce DTP1 en la vía de NF-κB. *Macrófagos peritoneales se trataron con el inhibidor de p110δ durante 1 h antes de ser estimulados con LPS (250 ng/ml, 30 min) en presencia del DTP1 (10 μM, 30 min antes del LPS) o su vehículo. La degradación de la proteína IκBα, así como los niveles de fosforilación de IKK, se determinaron mediante Western blot empleando extractos proteicos totales. La β-actina se utilizó como normalizador de carga. La figura muestra un ejemplo representativo de cuatro experimentos realizados de forma independiente.*

Inhibición génica.

Debido a que los inhibidores farmacológicos pueden presentar problemas de especificidad, se llevaron a cabo transfecciones con ARN de interferencia (siARN), específicos para cada una de las isoformas, modulando así la expresión génica de cada una de las subunidades catalíticas de la PI3K.

La eficiencia del silenciamiento se comprobó mediante *qPCR* (Figura 20), para lo cual, los macrófagos peritoneales se transfectaron con 50 nM de cada uno de los siARNs y 48 horas

después, se analizaron los niveles de expresión de cada una de las isoformas a nivel de ARNm. Las células control fueron transfectadas del mismo modo, empleándose en este caso un siARN que no hibrida con ningún gen (siARNC-).

Posteriormente, se confirmó, mediante Western blot, el efecto del DTP1 sobre la fosforilación de Akt tras la inhibición génica de las isoformas de la p110 (Figura 20). Una de las principales moléculas efectoras de la vía de PI3K es Akt, cuya fosforilación puede ocurrir incluso en ausencia de una de las isoformas (datos obtenidos por nuestro grupo). Para evitar este paso limitante, se realizaron cotransfecciones con tres de los cuatro siARNs de los que disponemos, de modo que se expresaría predominantemente una de las isoformas, sobre la que el DTP1 ejercería su acción. Transcurridas 48 h de la transfección, los macrófagos peritoneales se trataron con el DTP1 durante 30 min.

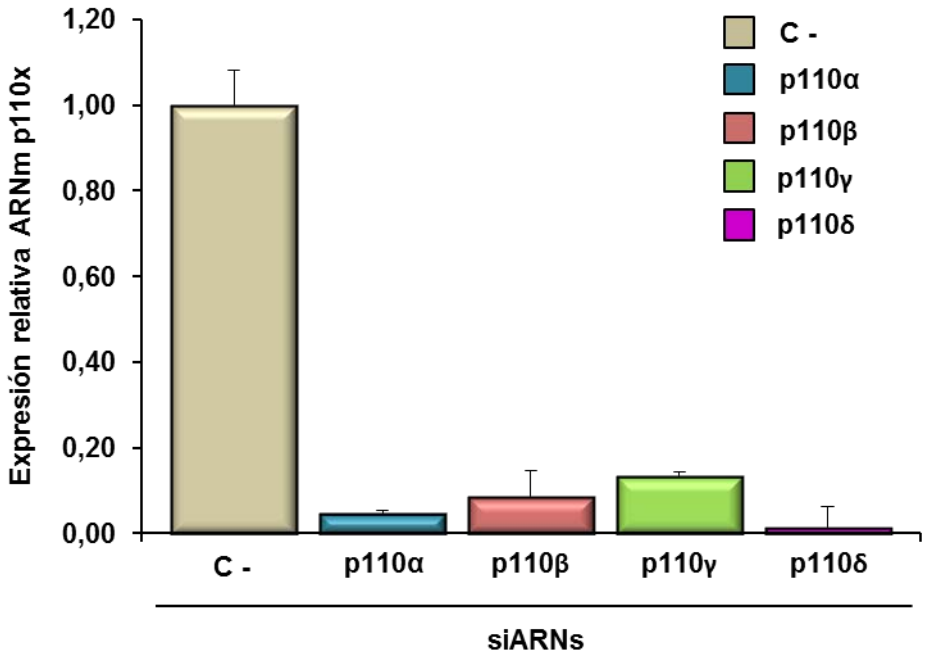

Figura 20. Silenciamiento de las isoformas p110 mediante siARNs en macrófagos peritoneales. *Los macrófagos peritoneales se transfectaron con 50 nM de cada uno de los siARNs para las distintas isoformas de la subunidad p110. Tras 48 h de transfección se analizaron los niveles de expresión a nivel de ARNm de cada una de las subunidades (α, β, γ y δ) mediante qPCR, utilizando 36B4 como gen de referencia. Se calcularon los valores de expresión relativa mediante el método del ΔΔCt. Los resultados muestran la media ± DE de cuatro experimentos independientes. No se consideraron como significativos cambios de expresión relativa inferiores a 2.*

Como se observa en la figura 21, la fosforilación de Akt inducida por el DTP1 en macrófagos que mayoritariamente expresaban la isoforma γ o δ, fue de un 76 y 68% respectivamente. Sin embargo, los niveles de p-Akt debidos al efecto de DTP1 sobre p110α o p110β fueron de un 50%. Estos datos, junto con los obtenidos con el empleo de inhibidores farmacológicos, indican que nuestro compuesto podría inducir la fosforilación de Akt mediante la activación de las isoformas γ y δ.

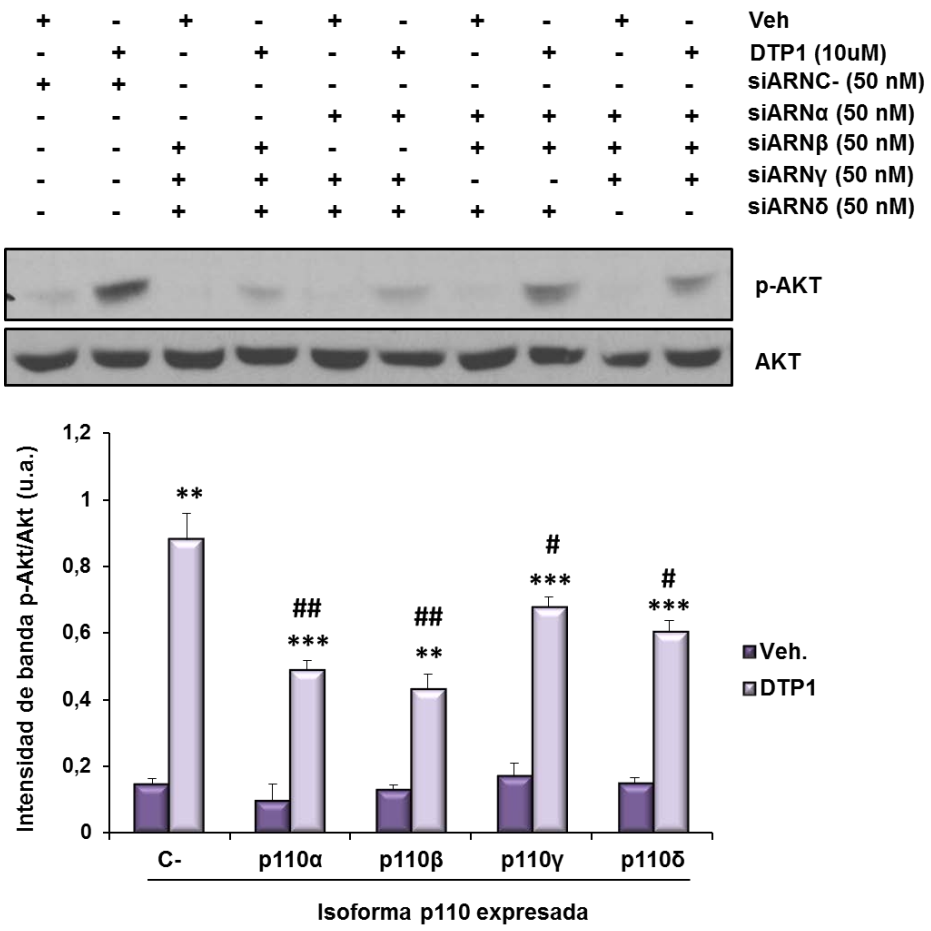

Figura 21. Efecto del DTP1 en macrófagos peritoneales transfectados con siARNs específicos para las distintas isoformas de p110. *Macrófagos peritoneales se transfectaron con distintas combinaciones de los siARNs (50 nM cada uno), de modo que solo se dejase sin inhibir una de las isoformas. Tras 48 h de transfección, los macrófagos se trataron con el DTP1 (10 μM) o su vehículo, durante 30 min. Los niveles proteicos de Akt fosforilado en Ser473 se analizaron en extractos proteicos totales mediante Western blot. Se empleó la forma total de la proteína como control de carga. El análisis densitométrico se muestra en la parte inferior. El gráfico representa la media ± DE de dos experimentos independientes. **p≤0,01; ***p≤0,001 respecto a su correspondiente valor en ausencia del DTP1. #p≤0,05; ##p≤0,01 respecto al control estimulado con DTP1.*

5. Los DTPs 1 y 5 presentan actividad anti-inflamatoria *in vivo*.

Los datos obtenidos hasta el momento demuestran que los DTPs empleados en la presente Tesis Doctoral presentan una actividad anti-inflamatoria, al menos en estudios realizados *in vitro*. Sin embargo, para considerar estas moléculas como compuestos de interés desde el punto de vista farmacológico, resulta necesario comprobar si dichos efectos se reproducen en modelos experimentales *in vivo*.

5.1. Efectos del DTP1 y DTP5 sobre la inducción de edema de oreja.

Uno de los modelos experimentales empleados para determinar si los DTPs 1 y 5 presentaban efectos anti-inflamatorios *in vivo* fue la inducción de edema en oreja de ratón por aplicación tópica del éster de forbol TPA, también conocido como forbol-12-miristato-13-acetato (PMA). El TPA es capaz de promover la activación de la proteína quinasa C (PKC), implicada en una gran variedad de funciones como es la síntesis de proteínas inflamatorias (De Young et al., 1989).

El edema inducido se midió por la diferencia de peso entre secciones idénticas de la oreja tratada con el DTP frente a la oreja control. En la figura 22 se observa que la inducción del edema en presencia de DTP1 y DTP5, se encuentra significativamente atenuada, ya que éste se redujo en un 30 y 50% aproximadamente, en relación al edema provocado en las orejas controles, a las cuales se aplicó únicamente el TPA junto con el vehículo (100% de inflamación). De hecho, la inhibición de la formación del edema mediada por el DTP5 fue incluso mayor que la producida por la indometacina, utilizada como control por su efecto anti-inflamatorio.

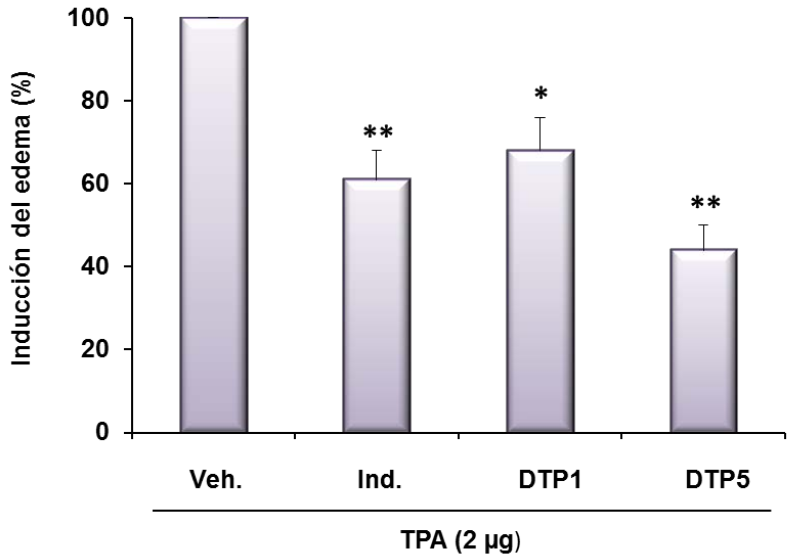

Figura 22. Los DTPs 1 y 5 son capaces de inhibir el edema inducido por TPA en oreja de ratón. *A ratones machos C57BL/6 se les aplicó tópicamente 2 µg/oreja de TPA disueltos en 20 µl de DMSO, aplicándose 10 µl a cada lado de la oreja del ratón. Junto con el TPA se les administró los compuestos ensayados (500 ng/oreja) o el vehículo. La indometacina se empleó como control de la inhibición (0,5 µg en 20 µl) en una de las orejas mientras que en la otra se aplicó el vehículo. Tras 4 h los animales fueron sacrificados y se midió la diferencia de peso entre secciones iguales de ambas orejas. *p≤0,05, **p≤0,01 respecto al tratamiento con el vehículo (=100). Ind: Indometacina.*

5.2. Efecto protector de los derivados sintéticos del ácido acantoico, DTP 1 y 5, sobre el fallo hepático inducido por LPS/D-GalN.

A continuación se empleó un modelo de daño hepático agudo, en el que intervienen numerosos mediadores inflamatorios, entre los que destaca el TNF-α, que induce una apoptosis masiva de los hepatocitos que conlleva a la muerte del animal (Gong et al., 2013).

En este ensayo, a los ratones se les aplicó intraperitonealmente 30 mg/kg del DTP1 o DTP5. Transcurrida una hora, se les inyectó una combinación de LPS (a una dosis no letal, 2 µg/kg) y D-GalN (800 mg/kg) y se analizaron los niveles de supervivencia de los animales durante las 24 h siguientes a la inyección con LPS/D-GalN. Se comprobó que el pre-tratamiento con ambos DTPs protegía de manera significativa frente a la letalidad inducida por el LPS/D-GalN, aumentando hasta 3 veces el tiempo de supervivencia de los ratones con respecto a los animales control, los cuales fueron pre-tratados con el vehículo (Figura 23).

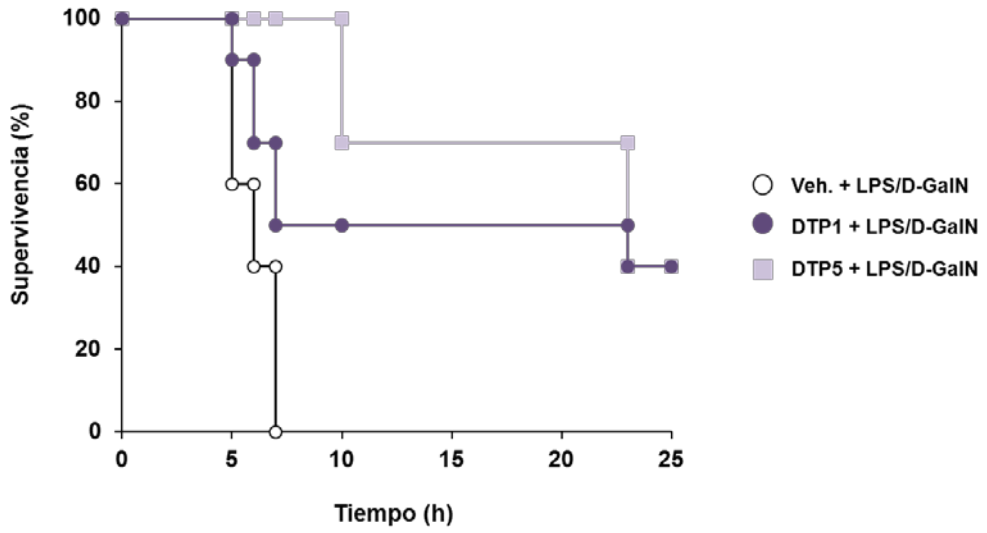

Figura 23. DTP1 y DTP5 protegen contra la letalidad inducida por LPS/D-GalN. *Para evaluar el efecto de estos diterpenos sobre un modelo de daño hepático agudo inducido por LPS/D-GalN, los ratones se trataron intraperitonealmente con DTP1 o DTP5 (30 mg/kg) una hora antes de la inyección con LPS/D-GalN (2 µg/kg y 800 mg/kg, respectivamente). Los resultados se representan en una curva de Kaplan-Meier, indicando el tiempo de supervivencia de los distintos grupos de animales (n=10).*

5.3. Determinación de los niveles de TNF-α en plasma de ratones tratados con los DTPs 1 y 5.

El TNF-α constituye el principal mediador en la respuesta inflamatoria aguda frente a bacterias Gram negativas y otros patógenos infecciosos. El principal productor de TNF-α es el macrófago activado, siendo el LPS el estímulo más potente que induce su producción. Entre las principales funciones del TNF-α se encuentra la de reclutar y activar neutrófilos y monocitos a las zonas de infección con el objetivo de eliminar a los agentes patógenos.

Por este motivo se decidió analizar los niveles de TNF-α en el plasma de ratones a los que se les inyectó LPS (1 mg/kg), habiendo sido tratados previamente con el vehículo o los DTPs a las concentraciones indicadas. A la hora de haber sido tratados con LPS se determinaron los niveles de TNF-α en el plasma de dichos ratones mediante un kit de ELISA. Se observó una inhibición dosis-dependiente, con resultados similares al pre-tratar tanto con el DTP1 como con el DTP5, llegándose a reducir a la mitad la producción de dicha citoquina (Figura 24).

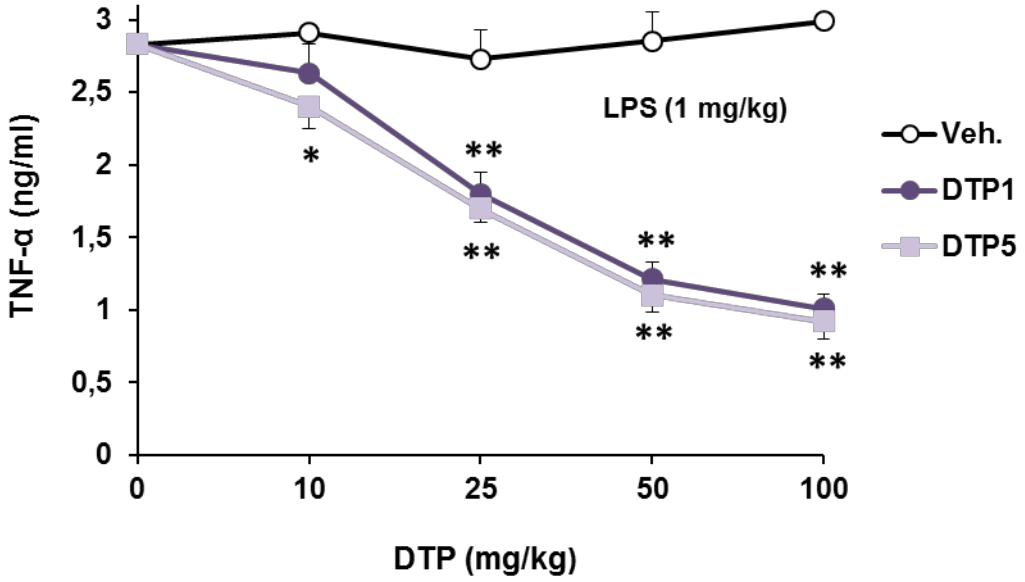

Figura 24. DTP1 y 5 inhiben la síntesis de TNF-α. *A los animales se les inyectó intraperitonealmente dos de nuestros diterpenos a las concentraciones indicadas. Transcurrida media hora se les administró del mismo modo LPS (1 mg/kg) y al cabo de una hora se analizaron los niveles de TNF-α en plasma mediante kit de ELISA. Los resultados muestran la media ± DE de los niveles de TNF-α obtenidos en un grupo de animales. *p≤0,05; **p≤0,01 respecto a la condición control correspondiente.*

5.4. Efectos de los DTPs sobre la actividad MPO medida por bioluminiscencia.

La enzima MPO es el principal componente de los lisosomas de los neutrófilos. La actividad MPO se utiliza como marcador indirecto de la cantidad de neutrófilos infiltrados en inflamación aguda (Gross et al., 2009) y por tanto del grado de inflamación inducido. Basándonos en estas premisas, nos propusimos estudiar la posible implicación de los DTPs en la actividad MPO en el modelo de inflamación aguda inducida por la inyección intraperitoneal de zimosán en ratones.

Para ello, se trataron los animales intraperitonealmente con el DTP5 (30mg/kg) y una hora después se les indujo la inflamación con el agente inflamatorio, zimosán (10 mg/kg). La actividad MPO se determinó *in vivo* a las 1, 3, 5 y 16 horas de la inyección intraperitoneal con zimosán. La actividad se determinó mediante bioluminiscencia después de la administración de luminol (5 mg en 200 µl), el cual genera luz al ser oxidado como consecuencia de la actividad MPO (Figura 25).

Como se muestra en la figura 25A, transcurrida una hora de la inyección intraperitoneal con zimosán, la actividad MPO era significativamente menor en los ratones pre-tratados con el DTP5 con respecto a los animales que recibieron el vehículo. Este cambio era mucho más significativo a las 3 y 5 horas de tratamiento con zimosán, observándose alrededor de un 45% menos de actividad MPO que en los ratones control. Sin embargo, a las 16 h de tratamiento la actividad MPO en ambos grupos de estudio era muy similar y con niveles reducidos respecto a los tiempos anteriores.

En la figura 25B, se muestran las fotografías representativas correspondientes a la actividad MPO después de inducir la inflamación con zimosán a las 1, 3, 5 y 16 horas. Se observa que en todos los casos los ratones control presentaban una luminiscencia mucho mayor que los ratones tratados con el DTP5, siendo esta diferencia estadísticamente significativa, excepto a las 16 h de tratamiento.

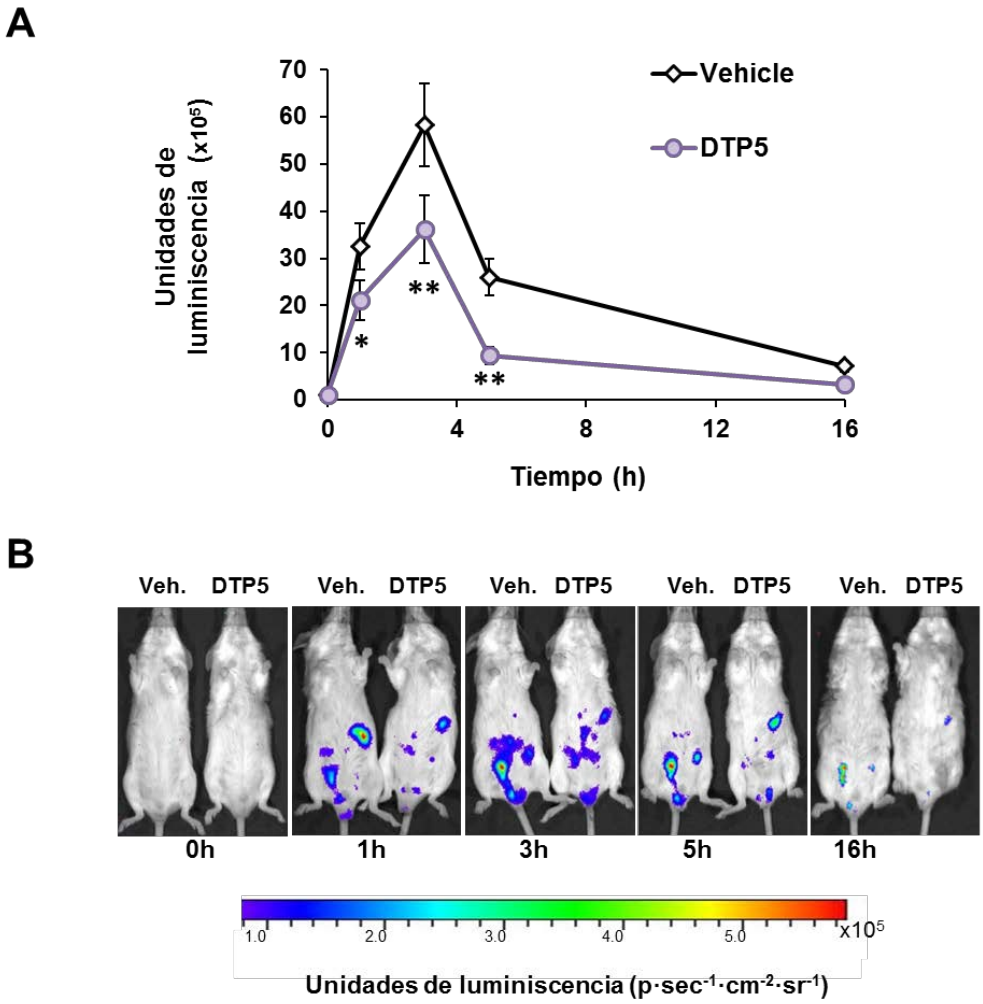

Figura 25. Disminución, por acción del DTP5, de la actividad MPO inducida tras la inyección intraperitoneal de zimosán. A) *Cuantificación de la luminiscencia in vivo en el peritoneo de ratones Balb/c tratados durante 1 h con el DTP5 (30mg/kg) o su vehículo antes de la inyección con zimosán (10 mg/kg). Las medidas se tomaron transcurridas 1, 3, 5 y 16 h tras el tratamiento con zimosán.*

B) *Imágenes representativas de bioluminiscencia. Éstas se tomaron cada 5 minutos después de la administración de luminol y durante un periodo de 45 min. Una hora antes de la administración del zimosán, se realizó la primera medida de luminiscencia con la finalidad de cuantificar la autoluminiscencia del tejido. *p≤0,05; **p≤0,01 respecto al correspondiente valor de los ratones tratados con el vehículo.*

DISCUSIÓN

La respuesta inflamatoria es un importante mecanismo de defensa que tiene lugar en el organismo frente a daños de tipo traumático, infeccioso, isquémico, tóxico o autoinmune. Se trata de un tipo de respuesta beneficiosa frente al daño producido por agentes externos, que a su vez está relacionada con el mantenimiento de la homeostasis tisular (Giron et al., 2010). La respuesta inflamatoria es un mecanismo altamente regulado y una vez finalizado el proceso inflamatorio, es necesario el inicio de la denominada resolución de la inflamación, que se desencadena unas horas después de que haya comenzado la respuesta inflamatoria. En el proceso de resolución, los agentes patógenos, restos celulares e incluso células inflamatorias implicadas en el proceso inflamatorio tienen que ser eliminados para que tenga lugar la reparación de las funciones tisulares y se recupere así la homeostasis celular. Si se rompe el equilibrio entre ambos procesos, puede dar lugar a la aparición de infecciones a nivel sistémico y al desarrollo de diversas patologías como son la aterosclerosis, la artritis reumatoide, asma, Alzheimer o cáncer, las cuales se han descrito que tienen lugar en un contexto altamente inflamatorio. De hecho, las infecciones y la inflamación descontrolada han sido y son una de las principales causas de muerte en el ser humano (Ulevitch et al., 2004).

Por este motivo, la regulación de los procesos inflamatorios se convierte en una de las principales dianas en el desarrollo de agentes terapéuticos para el tratamiento de enfermedades inflamatorias, por lo que resulta fundamental entender con profundidad cuáles son los mecanismos moleculares y celulares que gobiernan la activación y regulación del sistema inmune. Datos recientes obtenidos en relación al sistema inmune innato sobre la existencia de ligandos específicos para receptores de este sistema inmune, como son los TLRs, y el esclarecimiento de las vías de señalización activadas por dichos receptores, han proporcionado nuevas dianas para el desarrollo de fármacos destinados al tratamiento de diversas patologías relacionadas con procesos inflamatorios (Ulevitch, 2004).

Una de las principales fuentes para obtener nuevos compuestos terapéuticos capaces de inhibir o regular la respuesta inflamatoria son los productos naturales. De hecho, la mayoría de los fármacos utilizados hoy en día, tienen como componentes esenciales elementos derivados de moléculas de origen vegetal, como es el caso de los analgésicos codeína y morfina; la artemisinina, empleada contra la malaria; o el taxol, utilizado como anticancerígeno (Balunas and Kinghorn, 2005). En la actualidad, los remedios tradicionales están siendo intensamente examinados en busca de los metabolitos responsables de sus propiedades farmacológicas. La finalidad principal de estos análisis es dilucidar sus mecanismos de acción y determinar si estos

compuestos pueden o no, ser empleados como agentes terapéuticos en el tratamiento de numerosas enfermedades prevalentes en la sociedad.

En base a esto, durante el desarrollo de esta Tesis Doctoral, se han analizado los efectos de varias moléculas sintéticas derivadas del ácido acantoico, sobre las vías de señalización tempranas implicadas en la respuesta inflamatoria. Desde que Kopp y Ghosh describieron en 1994 al salicilato sódico y su derivado semi-sintético, la aspirina, como los primeros compuestos derivados de plantas capaces de inhibir NF-κB (Kopp and Ghosh, 1994), multitud de terpenos han sido testados para evaluar su capacidad inhibitoria sobre dicho factor de transcripción. El ácido acantoico es un diterpeno tricíclico, de tipo pimarano, que fue aislado de un extracto de la raíz de *Acanthopanax koreanum* y ha sido descrito en los últimos años como un potente anti-inflamatorio, ya que es capaz de inhibir la síntesis de citoquinas inflamatorias y la expresión de genes inflamatorios clásicos como NOS-2 y COX-2 (Suh et al., 2001) (Suh et al., 2004) (Cai et al., 2003) (Kang et al., 1996). Teniendo en cuenta estos datos, decidimos analizar las características de las moléculas derivadas del mismo, con el objetivo de determinar sus efectos en la respuesta inflamatoria.

Las moléculas estudiadas se obtuvieron por modificaciones químicas del grupo carboxilo del C4 del anillo A de la estructura del ácido acantoico. Trabajos previos realizados con análogos sintéticos de dicha molécula, en los que el grupo carboxilo ha sido sustituido por otros grupos químicos, proporcionan a cada uno de los distintos análogos diferentes propiedades anti-inflamatorias (Lam et al., 2003) (Lee et al., 2005) (Chao et al., 2005).

La importancia de los macrófagos en el desarrollo de la respuesta inflamatoria lo convierte en el sistema idóneo para llevar a cabo el estudio de los compuestos derivados del ácido acantoico. Por ello, la mayoría de los experimentos han sido realizados empleando cultivos primarios de macrófagos peritoneales y macrófagos derivados de precursores de médula ósea.

En primer lugar estudiamos la actividad anti-inflamatoria de los DTPs, midiendo los niveles de expresión de NOS-2 y COX-2, genes característicos de la respuesta inducida por LPS, uno de los modelos más útiles y recurrentes debido a su capacidad para activar la vía de señalización de los TLRs. Los resultados obtenidos demuestran que los cinco DTPs son capaces, en mayor o menor medida, de inhibir la expresión de ambas enzimas y por tanto de ejercer efectos anti-inflamatorios, datos que corroboran los estudios realizados por otros autores con diferentes diterpenos (Giron et al., 2010) (Diaz-Viciedo et al., 2008) (Giron et al., 2008). Además, es importante destacar que los efectos anti-inflamatorios observados no son

consecuencia de la citotoxicidad que pudieran presentar los DTPs, ya que, por sí mismos son incapaces de inducir muerte celular a la concentración empleada (10 µM). Nuestros resultados de citotoxicidad se soportan además por trabajos previos realizados en células mononucleares humanas de sangre periférica con diversos análogos del ácido acantoico, en los que también se demuestran su baja toxicidad (Lam et al., 2003) (Chao et al., 2005). Un efecto similar se había obtenido en monocitos y macrófagos humanos por Kang y colaboradores, donde el ácido acantoico no parecía tener efectos directos sobre la viabilidad celular (Kang et al., 1996). Por el contrario, trabajos realizados recientemente utilizando células HL-60 (células promielocíticas de leucemia humana) ponen de manifiesto que el ácido acantoico presenta efectos citotóxicos, lo que se traduce en una disminución de la proliferación y en un aumento de la apoptosis (Kim et al., 2012). Cabe destacar que, en esta publicación, las concentraciones del ácido acantoico empleadas (50-200 µM) están muy por encima de la usada en nuestro trabajo. Todo ello parece indicar que los efectos mediados por el ácido acantoico dependen del tipo celular y de la concentración empleada.

Además, cuando los macrófagos se activan en respuesta a patógenos, producen citoquinas pro-inflamatorias, como la IL-1β y la IL-6, que son fundamentales en la fase de iniciación y mantenimiento del proceso inflamatorio (Nathan, 2002). En el presente trabajo demostramos que los derivados 1 y 5 presentan mayor actividad anti-inflamatoria que el ácido acantoico en cuanto a la producción de citoquinas pro-inflamatorias se refiere, ya que son capaces de inhibir todas y cada una de las quimioquinas y citoquinas testadas. En este sentido, estudios previos realizados con el ácido acantoico indicaron que éste solo fue capaz de suprimir la síntesis de algunas citoquinas, como la IL-1 (Kang et al., 1996), mientras que la producción de otras, como la IL-6, no se vio alterada (Kang et al., 1998); lo que demuestra que sus efectos anti-inflamatorios son dependientes del tipo de citoquina (Ling et al., 2001).

A pesar de que han sido muchos los estudios que han descrito a los terpenos, incluyendo diterpenos, triterpenos y sesquiterpenos, como compuestos con actividad anti-inflamatoria tanto *in vitro* como *in vivo*, los mecanismos precisos de acción no han sido completamente caracterizados. En este sentido, datos obtenidos por nuestro grupo han descrito que los análogos empleados durante esta Tesis Doctoral, pueden actuar como potentes activadores de los receptores nucleares LXRαβ (Traves et al., 2007), los cuales regulan negativamente la respuesta inflamatoria mediante un proceso conocido como transrepresión (Pascual-Garcia and Valledor, 2012). Sin embargo, nuestros resultados demuestran que estos DTPs mantienen su actividad anti-

inflamatoria en macrófagos obtenidos de ratones que carecen de LXRαβ, poniendo de manifiesto que el efecto inhibitorio de estos compuestos es llevado a cabo por un mecanismo independiente de estos receptores nucleares.

Con el objetivo de determinar posibles mecanismos de acción de los DTPs, empleamos distintos ligandos de la vía de los TLRs con la finalidad de independizar esta ruta y estudiar sus niveles jerárquicos de señalización. Hasta la fecha, los estudios realizados que demuestran la capacidad anti-inflamatoria de los compuestos usados en la presente Tesis Doctoral así como de diversas moléculas obtenidas de productos naturales, han sido llevados a cabo empleando el LPS como agente inductor de la respuesta inflamatoria (Traves et al., 2007) (Lam et al., 2003) (Kim et al., 2010) (Hueso-Falcon et al., 2011) (Diaz-Viciedo et al., 2008) (Chao et al., 2005). En este sentido nosotros empleamos pI:C como ligando específico para TLR3, que señaliza a través de la vía independiente de MyD88; LTA, como agonista de TLR2, que desencadena una respuesta mediante la vía dependiente de MyD88; y el LPS, ligando de TLR4 e integrador de ambas vías de señalización, para determinar si nuestros compuestos son capaces de ejercer sus efectos anti-inflamatorios con independencia de la vía de TLR activada tras la unión de su ligando.

Al analizar la vía de los TLRs, la cual culmina con la activación de NF-κB y de las MAPKs, observamos una inhibición en la vía de activación de NF-κB y de la fosforilación de las MAPKs p38 y ERK, frente a todos los estímulos usados. Estos resultados están en consonancia con un estudio previo en el que diterpenos con estructura de kaurano, además de la vía de NF-κB, también inhibieron estas MAPKs (Castrillo et al., 2001). Además, estos datos nos estarían indicando, por un lado, que los DTPs son capaces de regular negativamente la respuesta inflamatoria desencadenada tanto a través de la vía dependiente como independiente de MyD88, disminuyendo la expresión de citoquinas, quimioquinas y mediadores inflamatorios, y por otro lado estarían apoyando la hipótesis inicial de un mecanismo de acción independiente de los LXRs. Para que los LXRs repriman la expresión de genes inflamatorios, es necesario que NF-κB haya sido translocado desde el citoplasma al núcleo, por lo que se trata de un proceso totalmente nuclear que no afecta a la degradación de las proteínas IκBs. Sin embargo, los efectos anti-inflamatorios de los DTPs observados hasta el momento demuestran que su acción se produce a muy corto plazo, inhibiendo la degradación de las proteínas inhibitorias mediante una disminución de la fosforilación del complejo IKK.

Para evaluar más específicamente la acción de los DTPs sobre la vía de señalización MyD88 dependiente y la vía dependiente de TRIF, empleamos macrófagos obtenidos a partir de

ratones que carecen de MyD88. Resultó muy interesante comprobar que la ausencia de MyD88 no afectó a las acciones inhibitorias de los DTPs. Estos datos corroboran los obtenidos con distintos ligandos de los TLRs y sugieren la existencia de una diana común a las diferentes vías de señalización analizadas, independientemente de MyD88 o TRIF, a través de la cual los DTPs podrían ejercer sus efectos anti-inflamatorios.

Estudios recientes han demostrado que la PI3K contribuye a la regulación de las fases iniciales de la respuesta inmune frente a diversos patógenos de origen microbiano (Fukao and Koyasu, 2003) (Hazeki et al., 2007) (Ruse and Knaus, 2006) (Fruman and Bismuth, 2009), por lo que nos planteamos estudiar si los efectos de los DTPs estarían mediados también por la activación de la vía PI3K/Akt. En esta línea, en un estudio realizado con monocitos humanos activados, se observa que la activación de PI3K/Akt limita la expresión de mediadores inflamatorios inducidos por la endotoxina (Guha and Mackman, 2002), así como la vía de las MAPKs y NF-κB. En células dendríticas y en macrófagos, la activación de la vía de PI3K/Akt limita la producción de citoquinas y quimioquinas inducida por LPS, así como la expresión de NOS-2, tanto a través de la vía dependiente de MyD88 como de TRIF (van Dop et al., 2010) (Aksoy et al., 2005); por lo que los DTPs podrían estar activando dicha vía de señalización. Sin embargo, existe una gran controversia en cuanto al papel de la vía PI3K/Akt en inflamación (Troutman et al., 2012), pues existen trabajos que la describen como inhibidora de la respuesta inflamatoria (Guha and Mackman, 2002) (Schabbauer et al., 2004) (Luyendyk et al., 2008) y otros que, por el contrario, la proponen como necesaria para la inflamación inducida por diversos estímulos (Ojaniemi et al., 2003). Todo ello parece indicar que el efecto de dicha vía de señalización en la regulación de la respuesta inflamatoria es dependiente del contexto celular y del agonista empleado (Diaz-Guerra et al., 1999) (Strassheim et al., 2004) (Li et al., 2003) (Ruse and Knaus, 2006).

Los resultados obtenidos indican que los DTPs son capaces de inducir por sí mismos la activación de Akt, detectándose niveles más elevados de fosforilación de esta proteína tras el tratamiento. Por otra parte, la fosforilación de Akt inducida por los diferentes ligandos de los TLRs en macrófagos murinos, se ve incrementada por el tratamiento con los DTPs. Estos resultados sugieren que los DTPs podrían mejorar significativamente la activación de la vía PI3K/Akt independientemente del estímulo inflamatorio empleado (LPS, pI:C o LTA), potenciando el papel de esta vía en la regulación de la respuesta inmune innata. La implicación de la vía de señalización PI3K/Akt en los efectos mediados por los DTPs se corroboró mediante

el uso del inhibidor farmacológico de PI3K, LY294002, en cuya presencia se revirtió el efecto anti-inflamatorio mediado por nuestros compuestos, recuperándose en parte los niveles de fosforilación de IKK, p38 y ERK. Nuestros resultados están en perfecta consonancia con el mecanismo de acción propuesto recientemente por Su y colaboradores en la línea celular RAW264.7, según el cual la vía de PI3K/Akt tiene un importante papel en la regulación de la respuesta inflamatoria (Su et al., 2013).

El papel de la PI3K en ciertas vías de señalización, se determina mediante el empleo de inhibidores farmacológicos como el LY294002; sin embargo, hay que tener en cuenta que existen varias restricciones, ya que este compuesto es capaz de inhibir también otras quinasas como la caseína quinasa 2 (Hazeki et al., 2007) y no contribuye a una comprensión de las funciones de las isoformas individuales. En ocasiones se han obtenido resultados contradictorios al emplear inhibidores de amplio espectro de la PI3K, ya que hay trabajos que describen que la wortmanina (otro inhibidor de PI3K) induce la producción de citoquinas inflamatorias mediada por los TLRs; mientras que el LY294002 inhibe dicha respuesta (Hazeki et al., 2006). Para analizar la vía PI3K/Akt de manera más específica, lo ideal sería emplear mutantes de la PI3K, sin embargo, los plásmidos que contienen estos mutantes son difíciles de transfectar en células hematopoyéticas (Hazeki et al., 2007). Considerando ambas limitaciones, por un lado decidimos emplear inhibidores farmacológicos específicos para cada una de las isoformas de la PI3K de clase I, que puede contribuir a aclarar algunas de las inconsistencias observadas; y por otro realizamos transfecciones en la línea celular de fibroblastos murinos NIH3T3.

Las transfecciones llevadas a cabo en las células NIH3T3 con un plásmido que codifica para una forma inactiva de la PI3K, constituye una interesante aproximación que debe ser cuidadosamente verificada ya que el contexto intracelular de estas células podría ser distinto al de los macrófagos. Estos datos, junto con el análisis de la actividad PI3K realizado en macrófagos, parecen indicar que los DTPs ejercen su efecto sobre la actividad quinasa de la PI3K.

Los resultados obtenidos al emplear inhibidores específicos de las subunidades catalíticas de la PI3K, demuestran que los DTPs inducen la fosforilación de Akt a través de una activación de las isoformas p110γ y p110δ principalmente, que poseen un importante papel en la señalización y función de células del sistema inmune (Foster et al., 2012). No obstante, los estudios farmacológicos siempre se enfrentan al problema de la especificidad, por lo que decidimos emplear siARNs para cada una de las isoformas de la PI3K, que corroboraron los

resultados obtenidos con los inhibidores farmacológicos. Nuestros resultados muestran que la fosforilación de Akt mediada por el DPT1 no se ve alterada por la ausencia de p110α. Estos datos concuerdan con un estudio publicado por Tsukamoto y colaboradores en la línea celular macrofágica RAW264.7 con shARN, en el que se indica que la p110α no está implicada en la señalización de los TLRs (Tsukamoto et al., 2008).

En cuanto a los resultados *in vivo*, estudios previos realizados con modelos animales han demostrado que el ácido acantoico, además de conservar su actividad anti-inflamatoria, presenta bajos niveles de citotoxicidad *in vivo* (Nan et al., 2008, Wu et al., 2010). Estos datos, junto con los que proponen que estos compuestos son capaces de inhibir varias citoquinas pro-inflamatorias simultáneamente, nos llevaron a probar los DTPs en varios modelos experimentales *in vivo*, con el fin de determinar si estas moléculas podrían tener un posible uso terapéutico.

A partir de los datos obtenidos en los ensayos *in vitro*, que demuestran una mayor efectividad anti-inflamatoria de los DTPs 1, 3 y 5, y teniendo en cuenta la mayor disponibilidad de los compuestos 1 y 5, se seleccionaron estos dos DTPs para el desarrollo de los experimentos *in vivo*. De esta forma, hemos comprobado que los DTPs 1 y 5 conservan, en todos los modelos animales evaluados, los efectos anti-inflamatorios observados anteriormente en los sistemas celulares. Estos compuestos presentan efectos protectores frente al daño hepático inducido por inyección intraperitoneal de una combinación de LPS y D-GalN. En este caso, ambos DTPs, administrados también intraperitonealmente, prolongan el periodo de supervivencia de los animales. Otros autores también han descrito que el ácido acantoico protege a los ratones de la toxicidad hepática inducida por LPS/D-GalN (Nan et al., 2008). En este estudio las concentraciones empleadas del compuesto fueron de 100 y 200 mg/kg, hasta 3 y 6 veces superiores a la usada en nuestro trabajo (30 mg/kg), asimismo, hay diferencias en el tipo de administración, ya que el ácido acantoico se suministró de manera oral. Todo ello parece indicar que un modo de administración es más efectivo frente otro, lo que podría justificar la menor cantidad empleada de nuestros compuestos en esta Tesis; o bien, que los DTPs son más eficaces que la molécula de la cual proceden.

Además, los niveles de TNF-α en plasma aparecen notablemente reducidos en aquellos animales que recibieron los DTPs como pre-tratamiento.

El edema en oreja inducido por TPA se vio reducido al tratar a los ratones con nuestros compuestos, hasta niveles equivalentes a los obtenidos con la indometacina, empleada como

control. La aplicación, tanto de TPA como de los DTPs, se realizó por vía tópica, ya que con ella se pueden conseguir concentraciones mayores del producto en el lugar de la inflamación (Carlson et al., 1985), frente a otros modos de administración. La inflamación en el modelo del TPA parece estar relacionada con los procesos de liberación y metabolismo del ácido araquidónico, y puede ocurrir simultáneamente a la interacción del TPA con el receptor de la proteína kinasa C (Just et al., 1998) (Rabanal et al., 2005) (Sanchez-Mateo et al., 2006). Los inhibidores de la ciclooxigenasa (como la indometacina), así como los corticoides, son efectivos en este modelo (Carlson et al., 1985) (De Young et al., 1989), lo que nos sugiere que los DTPs estudiados, mediante la interferencia con mediadores inflamatorios, podrían ser capaces de inhibir el edema inducido por TPA.

También analizamos si el tratamiento con los DTPs afecta a la actividad MPO, enzima principal de los gránulos azurófilos presentes en el citoplasma de los neutrófilos, que se emplea como marcador indirecto de la cantidad de neutrófilos infiltrados en inflamación aguda (Gross et al., 2009) y por tanto del grado de inflamación inducido. Igualmente, en nuestro abordaje experimental, observamos que los ratones que recibieron el pre-tratamiento con DTP5, mostraron una menor actividad MPO. Los datos obtenidos en los diferentes modelos experimentales *in vivo* coinciden con resultados previos, los cuales emplearon diversas moléculas de origen terpenoide y cuyos efectos anti-inflamatorios fueron analizados en diversos modelos murinos (de las Heras and Hortelano, 2009) (de las Heras et al., 2003). Hay que tener en cuenta que la actividad MPO no es el único marcador de neutrófilos activados, las especies reactivas de oxígeno derivadas de neutrófilos son también necesarias para la eliminación del agente que desencadena la respuesta inflamatoria. Por tanto, sería interesante estudiar en el futuro si estos DTPs poseen una capacidad antioxidante, y si ésta es mayor que la presentada por el ácido acantoico, capaz de inhibir la producción de especies reactivas de oxígeno, como el anión superóxido o el peróxido de hidrógeno, en monocitos y macrófagos humanos (Kang et al., 1996).

- **Modelo propuesto.**

Basándonos en los resultados obtenidos a lo largo de esta Tesis Doctoral, proponemos un modelo del posible mecanismo anti-inflamatorio de los DTPs en macrófagos (Esquema I), en el que se muestra las posibles dianas moleculares sobre las que nuestros compuestos ejercen su acción.

En resumen, nuestros datos demuestran que los DTPs aquí estudiados tendrían un efecto inhibitorio de la respuesta inflamatoria, ya que son capaces de regular negativamente las vías de las MAPKs (p38 y ERK) y de NF-κB (IKK), disminuyendo la expresión de NOS-2 y COX-2, así como la liberación de quimioquinas y citoquinas pro-inflamatorias. Estos efectos pueden ser debidos, al menos en parte, a un aumento de la actividad PI3K (p110γ y p110δ), y, por lo tanto, de la fosforilación de Akt. Akt, además inhibe GSK-3β, que es requerido para la expresión de varios genes inflamatorios regulados por NF-κB (Steinbrecher et al., 2005).

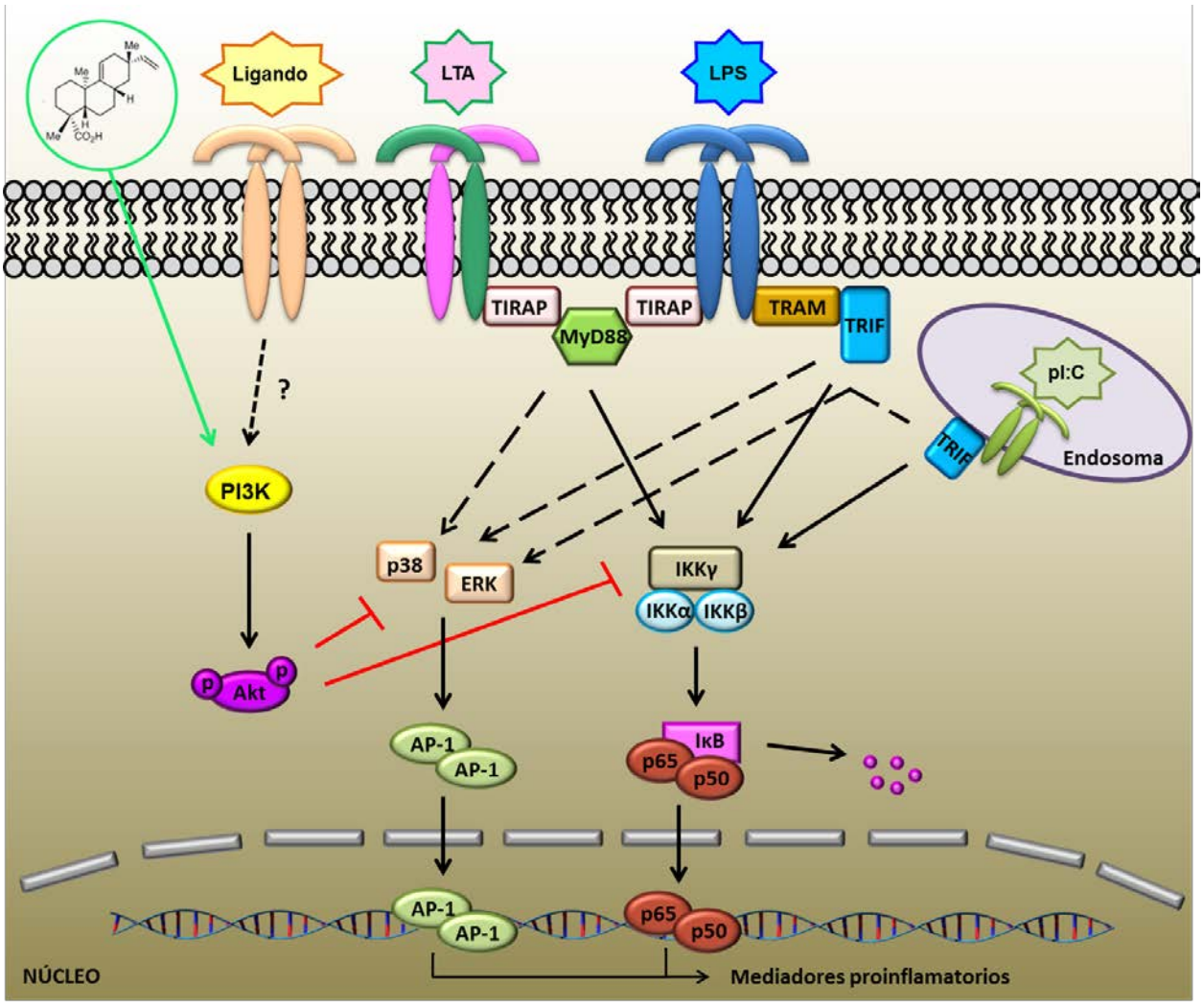

Esquema I. *Mecanismo propuesto para la acción anti-inflamatoria mediada por los DTPs.*

Por lo tanto, nuestros resultados apoyarían la idea de que la PI3K actúa como regulador negativo, al menos en macrófagos, de la respuesta inflamatoria desencadenada por los TLRs (Hazeki et al., 2007) (Park et al., 1997) (Guha and Mackman, 2002) (Aksoy et al., 2005). Sin embargo, son necesarios más estudios para esclarecer la molécula que sirve de enlace entre la vía de los TLRs y la vía de PI3K, ya que ésta podría ser una posible diana de acción de los DTPs. Actualmente no se conoce con exactitud los mecanismos por los cuales la PI3K es activada a través de los TLRs, ya que hay trabajos que proponen una interacción directa entre la PI3K y el receptor (Sarkar et al., 2004) y otros que exponen que esta interacción se produce a través de proteínas adaptadoras, como MyD88 (Rhee et al., 2006) o TRIF (Aksoy et al., 2005). En este sentido, es necesario profundizar en el mecanismo molecular y las vías de señalización por las que los DTPs estarían ejerciendo su acción.

Un aspecto fundamental del presente trabajo es que los efectos anti-inflamatorios de los DTPs observados en los estudios *in vitro*, se reproducen en modelos *in vivo*.

En la actualidad, el desarrollo de agentes terapéuticos para el tratamiento de enfermedades inflamatorias es uno de los principales objetivos en investigación. Para ello es fundamental conocer las vías de señalización implicadas en el desarrollo de estas enfermedades. En la enfermedad de Alzheimer la inhibición de la vía de los inositoles fosfato podría ser la responsable de la activación de GSK-3β, una de las proteínas responsables de la hiper-fosforilación de la proteína tau y formación de ovillos neurofibrilares (Lee et al., 2008). Akt inhibe a GSK-3β mediante fosforilación, por lo que ha sido señalada como posible diana para el tratamiento de esta enfermedad neurodegenerativa. En este sentido, los DTPs podrían jugar un papel importante en la enfermedad de Alzheimer, ya que son capaces de promover la activación de la vía PI3K/Akt, y por consiguiente de inhibir a GSK-3β.

En definitiva, los datos aportados en la presente Tesis Doctoral demuestran la habilidad de nuestros compuestos para activar la PI3K, lo que ofrece nuevas posibilidades para el desarrollo clínico de moléculas anti-inflamatorias con un gran potencial terapéutico para el tratamiento de diversas patologías, ya que son capaces de actuar sobre las vías de PI3K/Akt, NF-κB y MAPKs.

CONCLUSIONES

Las principales conclusiones que se derivan de los resultados obtenidos en la presente Tesis Doctoral son los siguientes:

- Todos los derivados sintéticos presentan efectos anti-inflamatorios *in vitro*, siendo los compuestos DTP1, DTP3 y DTP5 los que presentan mayor actividad. Además, la capacidad de estos DTPs para inhibir la respuesta inflamatoria no se debe a efectos citotóxicos.

- Los DTPs son capaces de inhibir, en macrófagos, la respuesta inflamatoria inducida por diferentes ligandos de los TLRs. Esta acción anti-inflamatoria observada se produce a muy corto plazo a través de los siguientes mecanismos:

    - Inhibición de la vía de NF-κB, mediante una disminución de la fosforilación del complejo IKK.
    - Inhibición de la activación de las MAPKs p38 y ERK.
    - Activación de la vía PI3K/Akt.

- La vía de PI3K/Akt parece ser la diana más importante de acción de los DTPs, ya que su activación (a través de las isoformas p110γ y p110δ) conlleva a una inhibición de NF-κB y de las MAPKs durante la señalización temprana de la respuesta inflamatoria.

- Los efectos anti-inflamatorios de los DTPs reduce el grado de inflamación sufrida por los ratones en distintos modelos experimentales:

    - Reducción del edema inducido por la aplicación tópica de TPA.
    - Protección frente a la letalidad inducida por LPS/D-GalN, aumentando la supervivencia de los animales.
    - Disminución de la actividad MPO, indicativa del grado de inflamación así como del número de neutrófilos reclutados, en un modelo de inflamación inducida con zimosán.

BIBLIOGRAFÍA

ABREU, M. T. & ARDITI, M. 2004. Innate immunity and toll-like receptors: clinical implications of basic science research. *J Pediatr,* 144**,** 421-9.

AKIRA, S. & TAKEDA, K. 2004. Toll-like receptor signalling. *Nat Rev Immunol,* 4**,** 499-511.

AKIRA, S., TAKEDA, K. & KAISHO, T. 2001. Toll-like receptors: critical proteins linking innate and acquired immunity. *Nat Immunol,* 2**,** 675-80.

AKSOY, E., VANDEN BERGHE, W., DETIENNE, S., AMRAOUI, Z., FITZGERALD, K. A., HAEGEMAN, G., GOLDMAN, M. & WILLEMS, F. 2005. Inhibition of phosphoinositide 3-kinase enhances TRIF-dependent NF-kappa B activation and IFN-beta synthesis downstream of Toll-like receptor 3 and 4. *Eur J Immunol,* 35**,** 2200-9.

ALESSI, D. R., JAMES, S. R., DOWNES, C. P., HOLMES, A. B., GAFFNEY, P. R., REESE, C. B. & COHEN, P. 1997. Characterization of a 3-phosphoinositide-dependent protein kinase which phosphorylates and activates protein kinase Balpha. *Curr Biol,* 7**,** 261-9.

BALUNAS, M. J. & KINGHORN, A. D. 2005. Drug discovery from medicinal plants. *Life Sci,* 78**,** 431-41.

BOOKOUT, A. L. & MANGELSDORF, D. J. 2003. Quantitative real-time PCR protocol for analysis of nuclear receptor signaling pathways. *Nucl Recept Signal,* 1**,** e012.

BOSCA, L., ZEINI, M., TRAVES, P. G. & HORTELANO, S. 2005. Nitric oxide and cell viability in inflammatory cells: a role for NO in macrophage function and fate. *Toxicology,* 208**,** 249-58.

BRADFORD, M. M. 1976. A rapid and sensitive method for the quantitation of microgram quantities of protein utilizing the principle of protein-dye binding. *Anal Biochem,* 72**,** 248-54.

BROOM, O. J., WIDJAYA, B., TROELSEN, J., OLSEN, J. & NIELSEN, O. H. 2009. Mitogen activated protein kinases: a role in inflammatory bowel disease? *Clin Exp Immunol,* 158**,** 272-80.

CAI, X. F., LEE, I. S., SHEN, G., DAT, N. T., LEE, J. J. & KIM, Y. H. 2004. Triterpenoids from Acanthopanax koreanum root and their inhibitory activities on NFAT transcription. *Arch Pharm Res,* 27**,** 825-8.

CAI, X. F., SHEN, G., DAT, N. T., KANG, O. H., KIM, J. A., LEE, Y. M., LEE, J. J. & KIM, Y. H. 2003. Inhibitory effect of TNF-alpha and IL-8 secretion by pimarane-type diterpenoids from Acanthopanax koreanum. *Chem Pharm Bull (Tokyo),* 51**,** 605-7.

CARLSON, R. P., O'NEILL-DAVIS, L., CHANG, J. & LEWIS, A. J. 1985. Modulation of mouse ear edema by cyclooxygenase and lipoxygenase inhibitors and other pharmacologic agents. *Agents Actions,* 17**,** 197-204.

CASTRILLO, A., DE LAS HERAS, B., HORTELANO, S., RODRIGUEZ, B., VILLAR, A. & BOSCA, L. 2001. Inhibition of the nuclear factor kappa B (NF-kappa B) pathway by tetracyclic kaurene diterpenes in macrophages. Specific

effects on NF-kappa B-inducing kinase activity and on the coordinate activation of ERK and p38 MAPK. *J Biol Chem,* 276**,** 15854-60.

COHEN, P. 2009. Targeting protein kinases for the development of anti-inflammatory drugs. *Curr Opin Cell Biol,* 21**,** 317-24.

CHAO, T. H., LAM, T., VONG, B. G., TRAVES, P. G., HORTELANO, S., CHOWDHURY, C., BAHJAT, F. R., LLOYD, G. K., MOLDAWER, L. L., BOSCA, L., PALLADINO, M. A. & THEODORAKIS, E. A. 2005. A new family of synthetic diterpenes that regulates cytokine synthesis by inhibiting IkappaBalpha phosphorylation. *Chembiochem,* 6**,** 133-44.

CHEN, Z., GIBSON, T. B., ROBINSON, F., SILVESTRO, L., PEARSON, G., XU, B., WRIGHT, A., VANDERBILT, C. & COBB, M. H. 2001. MAP kinases. *Chem Rev,* 101**,** 2449-76.

DE LAS HERAS, B. & HORTELANO, S. 2009. Molecular basis of the anti-inflammatory effects of terpenoids. *Inflamm Allergy Drug Targets,* 8**,** 28-39.

DE LAS HERAS, B., RODRIGUEZ, B., BOSCA, L. & VILLAR, A. M. 2003. Terpenoids: sources, structure elucidation and therapeutic potential in inflammation. *Curr Top Med Chem,* 3**,** 171-85.

DE YOUNG, L. M., KHEIFETS, J. B., BALLARON, S. J. & YOUNG, J. M. 1989. Edema and cell infiltration in the phorbol ester-treated mouse ear are temporally separate and can be differentially modulated by pharmacologic agents. *Agents Actions,* 26**,** 335-41.

DELGADO-MARTIN, C., ESCRIBANO, C., PABLOS, J. L., RIOL-BLANCO, L. & RODRIGUEZ-FERNANDEZ, J. L. 2011. Chemokine CXCL12 uses CXCR4 and a signaling core formed by bifunctional Akt, extracellular signal-regulated kinase (ERK)1/2, and mammalian target of rapamycin complex 1 (mTORC1) proteins to control chemotaxis and survival simultaneously in mature dendritic cells. *J Biol Chem,* 286**,** 37222-36.

DIAZ-GUERRA, M. J., CASTRILLO, A., MARTIN-SANZ, P. & BOSCA, L. 1999. Negative regulation by phosphatidylinositol 3-kinase of inducible nitric oxide synthase expression in macrophages. *J Immunol,* 162**,** 6184-90.

DIAZ-VICIEDO, R., HORTELANO, S., GIRON, N., MASSO, J. M., RODRIGUEZ, B., VILLAR, A. & DE LAS HERAS, B. 2008. Modulation of inflammatory responses by diterpene acids from Helianthus annuus L. *Biochem Biophys Res Commun,* 369**,** 761-6.

DONG, L. Q. & LIU, F. 2005. PDK2: the missing piece in the receptor tyrosine kinase signaling pathway puzzle. *Am J Physiol Endocrinol Metab,* 289**,** E187-96.

DURONIO, V. 2008. The life of a cell: apoptosis regulation by the PI3K/PKB pathway. *Biochem J,* 415**,** 333-44.

FOSTER, J. G., BLUNT, M. D., CARTER, E. & WARD, S. G. 2012. Inhibition of PI3K signaling spurs new therapeutic opportunities in inflammatory/autoimmune diseases and hematological malignancies. *Pharmacol Rev,* 64**,** 1027-54.

FRUMAN, D. A. & BISMUTH, G. 2009. Fine tuning the immune response with PI3K. *Immunol Rev,* 228**,** 253-72.

FUKAO, T. & KOYASU, S. 2003. PI3K and negative regulation of TLR signaling. *Trends Immunol,* 24**,** 358-63.

GALANOS, C., FREUDENBERG, M. A. & REUTTER, W. 1979. Galactosamine-induced sensitization to the lethal effects of endotoxin. *Proc Natl Acad Sci U S A,* 76**,** 5939-43.

GHOSH, S. & KARIN, M. 2002. Missing pieces in the NF-kappaB puzzle. *Cell,* 109 Suppl**,** S81-96.

GHOSH, S., MAY, M. J. & KOPP, E. B. 1998. NF-kappa B and Rel proteins: evolutionarily conserved mediators of immune responses. *Annu Rev Immunol,* 16**,** 225-60.

GIRON, N., PEREZ-SACAU, E., LOPEZ-FONTAL, R., AMARO-LUIS, J. M., HORTELANO, S., ESTEVEZ-BRAUN, A. & DE LAS HERAS, B. 2010. Evaluation of labdane derivatives as potential anti-inflammatory agents. *Eur J Med Chem,* 45**,** 3155-61.

GIRON, N., TRAVES, P. G., RODRIGUEZ, B., LOPEZ-FONTAL, R., BOSCA, L., HORTELANO, S. & DE LAS HERAS, B. 2008. Suppression of inflammatory responses by labdane-type diterpenoids. *Toxicol Appl Pharmacol,* 228**,** 179-89.

GLASS, C. K. & OGAWA, S. 2006. Combinatorial roles of nuclear receptors in inflammation and immunity. *Nat Rev Immunol,* 6**,** 44-55.

GONG, X., ZHANG, L., JIANG, R., WANG, C. D., YIN, X. R. & WAN, J. Y. 2013. Hepatoprotective effects of syringin on fulminant hepatic failure induced by D-galactosamine and lipopolysaccharide in mice. *J Appl Toxicol*.

GORDON, S. & TAYLOR, P. R. 2005. Monocyte and macrophage heterogeneity. *Nat Rev Immunol,* 5**,** 953-64.

GREEN, L. C., WAGNER, D. A., GLOGOWSKI, J., SKIPPER, P. L., WISHNOK, J. S. & TANNENBAUM, S. R. 1982. Analysis of nitrate, nitrite, and [15N]nitrate in biological fluids. *Anal Biochem,* 126**,** 131-8.

GROSS, S., GAMMON, S. T., MOSS, B. L., RAUCH, D., HARDING, J., HEINECKE, J. W., RATNER, L. & PIWNICA-WORMS, D. 2009. Bioluminescence imaging of myeloperoxidase activity in vivo. *Nat Med,* 15**,** 455-61.

GUHA, M. & MACKMAN, N. 2002. The phosphatidylinositol 3-kinase-Akt pathway limits lipopolysaccharide activation of signaling pathways and expression of inflammatory mediators in human monocytic cells. *J Biol Chem,* 277**,** 32124-32.

HAHN, D.-R. K., C. J., AND KIM, J. H. 1985. A study on the chemical constituents of Acanthopanax koreanum Nakai and its pharmacological activities. *Yakhak Hoechi,* 29**,** 357-361.

HAN, S. B., PARK, S. K., AHN, H. J., YOON, Y. D., KIM, Y. H., LEE, J. J., LEE, K. H., MOON, J. S., KIM, H. C. & KIM, H. M. 2003. Characterization of B cell membrane receptors of polysaccharide isolated from the root of Acanthopanax koreanum. *Int Immunopharmacol,* 3**,** 683-91.

HASHIMOTO, C., HUDSON, K. L. & ANDERSON, K. V. 1988. The Toll gene of Drosophila, required for dorsal-ventral embryonic polarity, appears to encode a transmembrane protein. *Cell,* 52**,** 269-79.

HAZEKI, K., KINOSHITA, S., MATSUMURA, T., NIGORIKAWA, K., KUBO, H. & HAZEKI, O. 2006. Opposite effects of wortmannin and 2-(4-morpholinyl)-8-phenyl-1(4H)-benzopyran-4-one hydrochloride on toll-like receptor-mediated nitric oxide production: negative regulation of nuclear factor-{kappa}B by phosphoinositide 3-kinase. *Mol Pharmacol,* 69**,** 1717-24.

HAZEKI, K., NIGORIKAWA, K. & HAZEKI, O. 2007. Role of phosphoinositide 3-kinase in innate immunity. *Biol Pharm Bull,* 30**,** 1617-23.

HUANG, G., SHI, L. Z. & CHI, H. 2009. Regulation of JNK and p38 MAPK in the immune system: signal integration, propagation and termination. *Cytokine,* 48**,** 161-9.

HUESO-FALCON, I., CUADRADO, I., CIDRE, F., AMARO-LUIS, J. M., RAVELO, A. G., ESTEVEZ-BRAUN, A., DE LAS HERAS, B. & HORTELANO, S. 2011. Synthesis and anti-inflammatory activity of ent-kaurene derivatives. *Eur J Med Chem,* 46**,** 1291-305.

JAKOBSSON, T., TREUTER, E., GUSTAFSSON, J. A. & STEFFENSEN, K. R. 2012. Liver X receptor biology and pharmacology: new pathways, challenges and opportunities. *Trends Pharmacol Sci,* 33**,** 394-404.

JIN, M. S. & LEE, J. O. 2008. Structures of the toll-like receptor family and its ligand complexes. *Immunity,* 29**,** 182-91.

JUNG, H. J., SHIM, J. S., SUH, Y. G., KIM, Y. M., ONO, M. & KWON, H. J. 2007. Potent inhibition of in vivo angiogenesis and tumor growth by a novel cyclooxygenase-2 inhibitor, enoic acanthoic acid. *Cancer Sci,* 98**,** 1943-8.

JUST, M. J., RECIO, M. C., GINER, R. M., CUELLAR, M. J., MANEZ, S., BILIA, A. R. & RIOS, J. L. 1998. Anti-inflammatory activity of unusual lupane saponins from Bupleurum fruticescens. *Planta Med,* 64**,** 404-7.

KAMINSKA, B. 2005. MAPK signalling pathways as molecular targets for anti-inflammatory therapy--from molecular mechanisms to therapeutic benefits. *Biochim Biophys Acta,* 1754**,** 253-62.

KANG, H. S., KIM, Y. H., LEE, C. S., LEE, J. J., CHOI, I. & PYUN, K. H. 1996. Suppression of interleukin-1 and tumor necrosis factor-alpha production by acanthoic acid, (-)-pimara-9(11),15-dien-19-oic acid, and it antifibrotic effects in vivo. *Cell Immunol,* 170**,** 212-21.

KANG, H. S., SONG, H. K., LEE, J. J., PYUN, K. H. & CHOI, I. 1998. Effects of acanthoic acid on TNF-alpha gene expression and haptoglobin synthesis. *Mediators Inflamm,* 7**,** 257-9.

KAWAI, T. & AKIRA, S. 2006. TLR signaling. *Cell Death Differ,* 13**,** 816-25.

KAWAI, T. & AKIRA, S. 2007a. Signaling to NF-kappaB by Toll-like receptors. *Trends Mol Med,* 13**,** 460-9.

KAWAI, T. & AKIRA, S. 2007b. TLR signaling. *Semin Immunol,* 19**,** 24-32.

KAWAI, T. & AKIRA, S. 2011. Toll-like receptors and their crosstalk with other innate receptors in infection and immunity. *Immunity,* 34**,** 637-50.

KIM, J. A., KIM, D. K., JIN, T., KANG, O. H., CHOI, Y. A., CHOI, S. C., KIM, T. H., NAH, Y. H., CHOI, S. J., KIM, Y. H., BAE, K. H. & LEE, Y. M. 2004. Acanthoic acid inhibits IL-8 production via MAPKs and NF-kappaB in a TNF-alpha-stimulated human intestinal epithelial cell line. *Clin Chim Acta,* 342**,** 193-202.

KIM, J. A., YANG, S. Y., KOO, J. E., KOH, Y. S. & KIM, Y. H. 2010. Lupane-type triterpenoids from the steamed leaves of Acanthopanax koreanum and their inhibitory effects on the LPS-stimulated pro-inflammatory cytokine production in bone marrow-derived dendritic cells. *Bioorg Med Chem Lett,* 20**,** 6703-7.

KIM, J. A., YANG, S. Y., SONG, S. B. & KIM, Y. H. 2011. Effects of impressic acid from Acanthopanax koreanum on NF-kappaB and PPARgamma activities. *Arch Pharm Res,* 34**,** 1347-51.

KIM, K. N., HAM, Y. M., MOON, J. Y., KIM, M. J., JUNG, Y. H., JEON, Y. J., LEE, N. H., KANG, N., YANG, H. M., KIM, D. & HYUN, C. G. 2012. Acanthoic acid induces cell apoptosis through activation of the p38 MAPK pathway in HL-60 human promyelocytic leukaemia. *Food Chem,* 135**,** 2112-7.

KIM, Y. H., CHUNG, B. S., AND SANKAWA, U. 1988. Pimaradiene diterpenes from Acanthopanax koreanum. *Journal of Natural Products,* 51**,** 1080-1083.

KINGHAM, E. & WELHAM, M. 2009. Distinct roles for isoforms of the catalytic subunit of class-IA PI3K in the regulation of behaviour of murine embryonic stem cells. *J Cell Sci,* 122**,** 2311-21.

KOK, K., GEERING, B. & VANHAESEBROECK, B. 2009. Regulation of phosphoinositide 3-kinase expression in health and disease. *Trends Biochem Sci,* 34**,** 115-27.

KOPP, E. & GHOSH, S. 1994. Inhibition of NF-kappa B by sodium salicylate and aspirin. *Science,* 265**,** 956-9.

KRISHNA, M. & NARANG, H. 2008. The complexity of mitogen-activated protein kinases (MAPKs) made simple. *Cell Mol Life Sci,* 65**,** 3525-44.

KUMAR, H., KAWAI, T. & AKIRA, S. 2009. Toll-like receptors and innate immunity. *Biochem Biophys Res Commun,* 388**,** 621-5.

KUMAR, H., KAWAI, T. & AKIRA, S. 2011. Pathogen recognition by the innate immune system. *Int Rev Immunol,* 30**,** 16-34.

LAEMMLI, U. K. 1970. Cleavage of structural proteins during the assembly of the head of bacteriophage T4. *Nature,* 227**,** 680-5.

LAM, K. S. 2007. New aspects of natural products in drug discovery. *Trends Microbiol,* 15**,** 279-89.

LAM, T., LING, T., CHOWDHURY, C., CHAO, T. H., BAHJAT, F. R., LLOYD, G. K., MOLDAWER, L. L., PALLADINO, M. A. & THEODORAKIS, E. A. 2003. Synthesis of a novel family of diterpenes and their evaluation as anti-inflammatory agents. *Bioorg Med Chem Lett,* 13**,** 3217-21.

LEE, K. O., MIN, K. H. & SUH, Y. G. 2005. Synthesis of C4-modified acanthoic acid analogs and their biological evaluation as nitric oxide inhibitors. *Arch Pharm Res,* 28**,** 648-51.

LEE, K. Y., KOH, S. H., NOH, M. Y., KIM, S. H. & LEE, Y. J. 2008. Phosphatidylinositol-3-kinase activation blocks amyloid beta-induced neurotoxicity. *Toxicology,* 243**,** 43-50.

LEE, M. S. & KIM, Y. J. 2007. Signaling pathways downstream of pattern-recognition receptors and their cross talk. *Annu Rev Biochem,* 76**,** 447-80.

LEMAITRE, B., NICOLAS, E., MICHAUT, L., REICHHART, J. M. & HOFFMANN, J. A. 1996. The dorsoventral regulatory gene cassette spatzle/Toll/cactus controls the potent antifungal response in Drosophila adults. *Cell,* 86**,** 973-83.

LEMAITRE, B., NICOLAS, E., MICHAUT, L., REICHHART, J. M. & HOFFMANN, J. A. 2012. Pillars article: the dorsoventral regulatory gene cassette spatzle/Toll/cactus controls the potent antifungal response in Drosophila adults. Cell. 1996. 86: 973-983. *J Immunol,* 188**,** 5210-20.

LI, X., TUPPER, J. C., BANNERMAN, D. D., WINN, R. K., RHODES, C. J. & HARLAN, J. M. 2003. Phosphoinositide 3 kinase mediates Toll-like receptor 4-induced activation of NF-kappa B in endothelial cells. *Infect Immun,* 71**,** 4414-20.

LIM, K. H. & STAUDT, L. M. 2013. Toll-like receptor signaling. *Cold Spring Harb Perspect Biol,* 5**,** a011247.

LING, T., CHOWDHURY, C., KRAMER, B. A., VONG, B. G., PALLADINO, M. A. & THEODORAKIS, E. A. 2001. Enantioselective synthesis of the antiinflammatory agent (-)-acanthoic acid. *J Org Chem,* 66**,** 8843-53.

LING, T., KRAMER, B. A., PALLADINO, M. A. & THEODORAKIS, E. A. 2000. Stereoselective synthesis of (-)-acanthoic acid. *Org Lett,* 2**,** 2073-6.

LU, Y. C., YEH, W. C. & OHASHI, P. S. 2008. LPS/TLR4 signal transduction pathway. *Cytokine,* 42**,** 145-51.

LUYENDYK, J. P., SCHABBAUER, G. A., TENCATI, M., HOLSCHER, T., PAWLINSKI, R. & MACKMAN, N. 2008. Genetic analysis of the role of the PI3K-Akt pathway in lipopolysaccharide-induced cytokine and tissue factor gene expression in monocytes/macrophages. *J Immunol,* 180**,** 4218-26.

MEDZHITOV, R. & JANEWAY, C. A., JR. 1997. Innate immunity: the virtues of a nonclonal system of recognition. *Cell,* 91**,** 295-8.

MORISATO, D. & ANDERSON, K. V. 1995. Signaling pathways that establish the dorsal-ventral pattern of the Drosophila embryo. *Annu Rev Genet,* 29**,** 371-99.

MURRAY, P. J. & WYNN, T. A. 2011. Protective and pathogenic functions of macrophage subsets. *Nat Rev Immunol,* 11**,** 723-37.

MYHRE, A. E., AGREN, J., DAHLE, M. K., TAMBURSTUEN, M. V., LYNGSTADAAS, S. P., COLLINS, A. J., FOSTER, S. J., THIEMERMANN, C., AASEN, A. O. & WANG, J. E. 2008. Liver X receptor is a key regulator of cytokine release in human monocytes. *Shock,* 29**,** 468-74.

NAN, J. X., JIN, X. J., LIAN, L. H., CAI, X. F., JIANG, Y. Z., JIN, H. R. & LEE, J. J. 2008. A diterpenoid acanthoic acid from Acanthopanax koreanum protects against D-galactosamine/lipopolysaccharide-induced fulminant hepatic failure in mice. *Biol Pharm Bull,* 31**,** 738-42.

NAPETSCHNIG, J. & WU, H. 2013. Molecular basis of NF-kappaB signaling. *Annu Rev Biophys,* 42**,** 443-68.

NATHAN, C. 2002. Points of control in inflammation. *Nature,* 420**,** 846-52.

OJANIEMI, M., GLUMOFF, V., HARJU, K., LILJEROOS, M., VUORI, K. & HALLMAN, M. 2003. Phosphatidylinositol 3-kinase is involved in Toll-like receptor 4-mediated cytokine expression in mouse macrophages. *Eur J Immunol,* 33**,** 597-605.

PARK, E. J., ZHAO, Y. Z., KIM, Y. H., LEE, J. J. & SOHN, D. H. 2004. Acanthoic acid from Acanthopanax koreanum protects against liver injury induced by tert-butyl hydroperoxide or carbon tetrachloride in vitro and in vivo. *Planta Med,* 70**,** 321-7.

PARK, Y. C., LEE, C. H., KANG, H. S., CHUNG, H. T. & KIM, H. D. 1997. Wortmannin, a specific inhibitor of phosphatidylinositol-3-kinase, enhances LPS-induced NO production from murine peritoneal macrophages. *Biochem Biophys Res Commun,* 240**,** 692-6.

PASARE, C. & MEDZHITOV, R. 2004. Toll-like receptors: linking innate and adaptive immunity. *Microbes Infect,* 6**,** 1382-7.

PASCUAL-GARCIA, M. & VALLEDOR, A. F. 2012. Biological roles of liver X receptors in immune cells. *Arch Immunol Ther Exp (Warsz),* 60**,** 235-49.

PHUONG, N. T., LEE, K. A., JEONG, S. J., FU, C. X., CHOI, J. K., KIM, Y. H. & KANG, J. S. 2006. Capillary electrophoretic method for the determination of diterpenoid isomers in Acanthopanax species. *J Pharm Biomed Anal,* 40**,** 56-61.

PIMIENTA, G. & PASCUAL, J. 2007. Canonical and alternative MAPK signaling. *Cell Cycle,* 6**,** 2628-32.

POLAK, R. & BUITENHUIS, M. 2012. The PI3K/PKB signaling module as key regulator of hematopoiesis: implications for therapeutic strategies in leukemia. *Blood,* 119**,** 911-23.

PRIETO, P., CUENCA, J., TRAVES, P. G., FERNANDEZ-VELASCO, M., MARTIN-SANZ, P. & BOSCA, L. 2010. Lipoxin A4 impairment of apoptotic signaling in macrophages: implication of the PI3K/Akt and the ERK/Nrf-2 defense pathways. *Cell Death Differ,* 17**,** 1179-88.

QIAN, C. & CAO, X. 2013. Regulation of Toll-like receptor signaling pathways in innate immune responses. *Ann N Y Acad Sci,* 1283**,** 67-74.

RABANAL, R. M., BONKANKA, C. X., HERNANDEZ-PEREZ, M. & SANCHEZ-MATEO, C. C. 2005. Analgesic and topical anti-inflammatory activity of Hypericum canariense L. and Hypericum glandulosum Ait. *J Ethnopharmacol,* 96**,** 591-6.

RECIO, M. C., GINER, R. M., MANEZ, S. & RIOS, J. L. 1994. Structural considerations on the iridoids as anti-inflammatory agents. *Planta Med,* 60**,** 232-4.

RHEE, S. H., KIM, H., MOYER, M. P. & POTHOULAKIS, C. 2006. Role of MyD88 in phosphatidylinositol 3-kinase activation by flagellin/toll-like receptor 5 engagement in colonic epithelial cells. *J Biol Chem,* 281**,** 18560-8.

RUSE, M. & KNAUS, U. G. 2006. New players in TLR-mediated innate immunity: PI3K and small Rho GTPases. *Immunol Res,* 34**,** 33-48.

SANCHEZ-MATEO, C. C., BONKANKA, C. X., HERNANDEZ-PEREZ, M. & RABANAL, R. M. 2006. Evaluation of the analgesic and topical anti-inflammatory effects of Hypericum reflexum L. fil. *J Ethnopharmacol,* 107**,** 1-6.

SARBASSOV, D. D., GUERTIN, D. A., ALI, S. M. & SABATINI, D. M. 2005. Phosphorylation and regulation of Akt/PKB by the rictor-mTOR complex. *Science,* 307**,** 1098-101.

SARKAR, S. N., PETERS, K. L., ELCO, C. P., SAKAMOTO, S., PAL, S. & SEN, G. C. 2004. Novel roles of TLR3 tyrosine phosphorylation and PI3 kinase in double-stranded RNA signaling. *Nat Struct Mol Biol,* 11**,** 1060-7.

SASS, G., KOERBER, K., BANG, R., GUEHRING, H. & TIEGS, G. 2001. Inducible nitric oxide synthase is critical for immune-mediated liver injury in mice. *J Clin Invest,* 107**,** 439-47.

SCHABBAUER, G., TENCATI, M., PEDERSEN, B., PAWLINSKI, R. & MACKMAN, N. 2004. PI3K-Akt pathway suppresses coagulation and inflammation in endotoxemic mice. *Arterioscler Thromb Vasc Biol,* 24**,** 1963-9.

SEIBERT, K. & MASFERRER, J. L. 1994. Role of inducible cyclooxygenase (COX-2) in inflammation. *Receptor,* 4**,** 17-23.

SEN, R. & BALTIMORE, D. 1986. Inducibility of kappa immunoglobulin enhancer-binding protein Nf-kappa B by a posttranslational mechanism. *Cell,* 47**,** 921-8.

SIOMEK, A. 2012. NF-kappaB signaling pathway and free radical impact. *Acta Biochim Pol,* 59**,** 323-31.

STEINBRECHER, K. A., WILSON, W., 3RD, COGSWELL, P. C. & BALDWIN, A. S. 2005. Glycogen synthase kinase 3beta functions to specify gene-specific, NF-kappaB-dependent transcription. *Mol Cell Biol,* 25**,** 8444-55.

STOUT, R. D. & SUTTLES, J. 2004. Functional plasticity of macrophages: reversible adaptation to changing microenvironments. *J Leukoc Biol,* 76**,** 509-13.

STRASSHEIM, D., ASEHNOUNE, K., PARK, J. S., KIM, J. Y., HE, Q., RICHTER, D., KUHN, K., MITRA, S. & ABRAHAM, E. 2004. Phosphoinositide 3-kinase and Akt occupy central roles in inflammatory responses of Toll-like receptor 2-stimulated neutrophils. *J Immunol,* 172**,** 5727-33.

SU, N. Y., PENG, T. C., TSAI, P. S. & HUANG, C. J. 2013. Phosphoinositide 3-kinase/Akt pathway is involved in mediating the anti-inflammation effects of magnesium sulfate. *J Surg Res*.

SUH, Y. G., KIM, Y. H., PARK, M. H., CHOI, Y. H., LEE, H. K., MOON, J. Y., MIN, K. H., SHIN, D. Y., JUNG, J. K., PARK, O. H., JEON, R. O., PARK, H. S. & KANG, S. A. 2001. Pimarane cyclooxygenase 2 (COX-2) inhibitor and its structure-activity relationship. *Bioorg Med Chem Lett,* 11**,** 559-62.

SUH, Y. G., LEE, K. O., MOON, S. H., SEO, S. Y., LEE, Y. S., KIM, S. H., PAEK, S. M., KIM, Y. H., JEONG, J. M., LEE, S. J. & KIM, S. G. 2004. Synthesis and anti-inflammatory effects of novel pimarane diterpenoid analogs. *Bioorg Med Chem Lett,* 14**,** 3487-90.

TAKEDA, K. & AKIRA, S. 2004. TLR signaling pathways. *Semin Immunol,* 16**,** 3-9.

TAYLOR, P. R. & GORDON, S. 2003. Monocyte heterogeneity and innate immunity. *Immunity,* 19**,** 2-4.

TRAVES, P. G., HORTELANO, S., ZEINI, M., CHAO, T. H., LAM, T., NEUTEBOOM, S. T., THEODORAKIS, E. A., PALLADINO, M. A., CASTRILLO, A. & BOSCA, L. 2007. Selective activation of liver X receptors by acanthoic acid-related diterpenes. *Mol Pharmacol,* 71**,** 1545-53.

TROUTMAN, T. D., BAZAN, J. F. & PASARE, C. 2012. Toll-like receptors, signaling adapters and regulation of the pro-inflammatory response by PI3K. *Cell Cycle,* 11**,** 3559-67.

TSUKAMOTO, K., HAZEKI, K., HOSHI, M., NIGORIKAWA, K., INOUE, N., SASAKI, T. & HAZEKI, O. 2008. Critical roles of the p110 beta subtype of phosphoinositide 3-kinase in lipopolysaccharide-induced Akt activation and negative regulation of nitrite production in RAW 264.7 cells. *J Immunol,* 180**,** 2054-61.

TURVEY, S. E. & BROIDE, D. H. 2010. Innate immunity. *J Allergy Clin Immunol,* 125**,** S24-32.

ULEVITCH, R. J. 2004. Therapeutics targeting the innate immune system. *Nat Rev Immunol,* 4**,** 512-20.

ULEVITCH, R. J., MATHISON, J. C. & DA SILVA CORREIA, J. 2004. Innate immune responses during infection. *Vaccine,* 22 Suppl 1**,** S25-30.

VAN DOP, W. A., MARENGO, S., TE VELDE, A. A., CIRAOLO, E., FRANCO, I., TEN KATE, F. J., BOECKXSTAENS, G. E., HARDWICK, J. C., HOMMES, D. W., HIRSCH, E. & VAN DEN BRINK, G. R. 2010. The absence of functional PI3Kgamma prevents leukocyte recruitment and ameliorates DSS-induced colitis in mice. *Immunol Lett,* 131**,** 33-9.

VERMA, I. M., STEVENSON, J. K., SCHWARZ, E. M., VAN ANTWERP, D. & MIYAMOTO, S. 1995. Rel/NF-kappa B/I kappa B family: intimate tales of association and dissociation. *Genes Dev,* 9**,** 2723-35.

WAGNER, K. H. & ELMADFA, I. 2003. Biological relevance of terpenoids. Overview focusing on mono-, di- and tetraterpenes. *Ann Nutr Metab,* 47**,** 95-106.

WELLS, J. M., LOONEN, L. M. & KARCZEWSKI, J. M. 2010. The role of innate signaling in the homeostasis of tolerance and immunity in the intestine. *Int J Med Microbiol,* 300**,** 41-8.

WU, Y. L., JIANG, Y. Z., JIN, X. J., LIAN, L. H., PIAO, J. Y., WAN, Y., JIN, H. R., JOON LEE, J. & NAN, J. X. 2010. Acanthoic acid, a diterpene in Acanthopanax koreanum, protects acetaminophen-induced hepatic toxicity in mice. *Phytomedicine,* 17**,** 475-9.

ZHU, J., LUO, C., WANG, P., HE, Q., ZHOU, J. & PENG, H. 2013. Saikosaponin A mediates the inflammatory response by inhibiting the MAPK and NF-kappaB pathways in LPS-stimulated RAW 264.7 cells. *Exp Ther Med,* 5**,** 1345-1350.

ANEXOS

Los resultados presentados en esta Tesis Doctoral están plasmados en un artículo en preparación, del que María Pimentel Santillana es co-autora, titulado:

Anti-inflammatory actions of acanthoic acid-related diterpenes involve activation of the PI3kinase/AKT pathway and inhibition of the IKK/NF-κB pathway.

Se adjunta dicho artículo.

Además, se han publicado los siguientes artículos en los que el doctorando ha participado:

The specificity protein factor Sp1 mediates transcriptional regulation of P2X7 receptors in the nervous system. García-Huerta P, Díaz-Hernandez M, Delicado EG, Pimentel-Santillana M, Miras-Portugal MT, Gómez-Villafuertes R. J Biol Chem. 2012 Dec 28;287(53):44628-44.

Relevance of the MEK/ERK signaling pathway in the metabolism of activated macrophages: a metabolomic approach. Través PG, de Atauri P, Marín S, Pimentel-Santillana M, Rodríguez-Prados JC, Marín de Mas I, Selivanov VA, Martín-Sanz P, Boscá L, Cascante M. J Immunol. 2012 Feb 1;188(3):1402-10.

Selective impairment of P2Y signaling by prostaglandin E2 in macrophages: implications for Ca2+-dependent responses. Través PG, Pimentel-Santillana M, Carrasquero LM, Pérez-Sen R, Delicado EG, Luque A, Izquierdo M, Martín-Sanz P, Miras-Portugal MT, Boscá L. J Immunol. 2013 Apr 15;190(8):4226-35.

Anti-inflammatory actions of acanthoic acid-related diterpenes involve activation of the PI3kinase/Akt pathway and inhibition of the IKK/NF-κB pathway.

Paqui G. Través*[1], María Pimentel-Santillana*[1], Daniel Rico[2], Thanh Lam[4], Nuria Rodriguez[5], Thomas Miethke[5], Antonio Castrillo[1], Michael A. Palladino[3], and Lisardo Boscá[1].

*P.G.T. and M.P.-S. contributed equally to this work

[1]Instituto de Investigaciones Biomédicas Alberto Sols (Centro Mixto CSIC-UAM). Arturo Duperier 4, 28029 Madrid, Spain.[2]Structural Biology and BioComputing Programme, National Cancer Research Center (CNIO), Melchor Fernández Almagro 3, 28029 Madrid, Spain. [3]Nereus Pharmaceuticals, Inc. 10480 Wateridge Circle, San Diego, CA 92121, USA..[5]Institute for Medical Microbiology Immunology and Hygiene, Technical University of Munich. Trogerstrasse 30, 81675 Munich, Germany.

Running Title: ***Acanthoic-related diterpenes target PI3K***

Key words: diterpene, acanthoic acid, TLRs, NF-κB, PI3K, Akt and inflammation.

Address for correspondence:

Lisardo Boscá
Instituto de Investigaciones Biomédicas Alberto Sols (CSIC-UAM)
Arturo Duperier 4
28029 Madrid. Spain
Phone +34914972747 FAX +34914972748
e-mail: lbosca@iib.uam.es

Summary

The effect of acanthoic acid-related positional derivatives on the response of macrophages to pro-inflammatory challenge was investigated. These pimarane diterpenes (DTP1, DTP3 and DTP5) are known activators of the LXRαβ nuclear receptors, but we show here that they also exert a rapid and potent activation of the PI3K/Akt pathway. Together, both effects result in an important attenuation of the global transcriptional response to LPS in macrophages. PI3K/Akt activation leads to inhibition of the LPS-dependent stimulation of IKK/NF-κB and p38 and ERK MAPKs. Macrophages from LXRαβ-deficient mice exhibited a similar inhibition of these pathways than the corresponding wild type cells. Inhibition of PI3K or Akt suppressed the effect of these DTPs on IKK/NF-κB and MAPKs signaling. Furthermore, the PI3K activation induced by DTPs decreased the IKK/NF-κB and p38 activities after triggering of TLR2 (MyD88-dependent) and TLR3 (TRIF-dependent). Studies in macrophages from IRF3- and MyD88-deficient mice indicated that DTPs act both in MyD88- and TRIF-dependent pathways suggesting the presence of "shared" signaling pathways upon TLR2, TLR3 and TLR4 engagement. *In vivo* administration of DTPs to mice exerted anti-inflammatory actions on the TPA-induced ear edema, reduced the release of TNF-α by whole blood cell preparations, improved animal survival in a model of D-galactosamine/LPS-dependent lethality and inhibited zymosan-induced myeloperoxidase release. Taken together, these data show a multi-target anti-inflammatory mechanism by these DTPs including an unusual selective activation of the PI3K/Akt pathway.

Introduction

The study of the ability of natural and chemically modified terpenes and polyphenols to impair the inflammatory response has been accomplished in the past years and, in some cases, the molecular mechanisms underlying their actions have been assessed (1, 2). The view emerging from these studies points to NF-κB as a common target in the action of these compounds, which might explain their anti-inflammatory and immunomodulatory effects, at the time that allows establishing some of the cell-specific actions. The NF-κB pathway acts as an integrator pathway covering the information from different extracellular stimuli and plays a major role in the control of the expression of inflammatory genes, immune responses, apoptosis and cell growth (3). Most of the studies on natural products, in particular of terpenes, have focused on this pathway. Indeed, several targets have been identified, ranging from the inhibition of upstream kinase NIK, IKK activation and p65 phosphorylation, to the up-regulation of the inhibitory proteins IκBα and Bcl-3. Moreover, recent works have reported the activation by terpenes of nuclear receptors, such as LXRs. These receptors antagonize NF-κB activation by ligand-dependent transrepression (2, 4-6).

Diterpenes have been recognized as anti-inflammatory drugs for years, and their biosynthesis is well known since most of these molecules are precursors of various plant hormones, such as gibberellins (7). In this regard, acanthoic acid has been described as an anti-inflammatory molecule that inhibits TNF-α production and exerts antifibrotic effects *in vivo* in models of experimental silicosis (8) and protective effects against fulminant hepatic failure in mice (9). In addition to NF-κB, other targets have been described in the mechanism of action of terpenes. The sesquiterpene partenolide promotes apoptosis both in a NF-κB dependent and independent manner as assessed in Jurkat T cells with inactive NF-κB (10). Triterpenoids from oleanolic acid protect cells from stress by interacting with Keap1 to increase the transcriptional activity of Nrf2 (11). Sesquiterpene lactones target the SERCA pump, modify the iron metabolism and induce proteasomal degradation of HDAC-1 by inhibiting DNMT1 (12).

Toll-like receptors (TLRs) exert essential functions in the activation of innate immunity as sensors of microbial infection (13, 14). Signaling downstream from TLRs involves the recruitment of distinct TIR-domain-containing adapter molecules including the myeloid differentiation factor 88 (MyD88) and the TIR domain-containing adapter-inducing IFNβ (TRIF). Most TLRs signal through MyD88-dependent signaling pathway, whereas TLR3, the receptor recognizing double-stranded (ds) RNA, is coupled to TRIF. TLR4, receptor for bacterial lipopolysaccharide (LPS), is the only receptor that engages both MyD88- and TRIF-dependent pathways. MyD88- and TRIF-dependent pathways results in the activation of transcription factor NF-κB. However, only TRIF-dependent pathway led to the activation of IRF3 (15).

Phosphatidylinositol (PI) 3-kinases play an important role in cellular functions regulating immune responses, including cell migration, phagocytosis and apoptosis (16). Recent studies provided evidence that PI3K regulates MyD88- and TRIF-dependent events (17, 18). PI3K converts PIP_2 into

PIP_3 that act as second messenger to activate downstream protein kinases including Akt (19). Indeed, PI3K activation in the macrophage contributes to the negative regulation of the NF-κB pathway, decreasing the inflammatory response (20-25).

In this work we have investigated the effect of diterpenes (DTPs) structurally related to acanthoic acid on macrophage activation and systemic inflammation. The synthesis and characterization of acanthoic acid related diterpenes is well documented (26-29). Preliminary studies showed that these DTPs activated LXRαβ and inhibited TNF-α release without noticeable effects on apoptosis (30, 31). Our data extend these previous studies and show that, in addition to the effects on LXRs, DTPs exert a potent activation of PI3K in macrophages. Moreover, the inhibition of this enzyme impairs the anti-inflammatory effects of DTPs on the IKK/NF-κB pathway and on the p38 and ERK MAPKs, even in the absence of LXRαβ. *In vivo* studies with oral or systemic administration of these DTPs confirmed the potential therapeutic role and safe profile of these molecules as anti-inflammatory drugs.

Materials and Methods

Chemicals. Reagents were obtained from Sigma-Aldrich (St. Louis, MO), Roche (Mannheim, Germany), Amersham-GE Healthcare (UK), Merck (Darmstadt, Germany), Bio-Rad (Hercules, CA), R&D Systems (Minneapolis, MN) and Promega (Madison, WI). DTPs were synthesized in the laboratory of Prof. E. Theodorakis (UCSD). Antibodies were from Santa Cruz Biotech. (Santa Cruz, CA), Cell Signaling (Danvers, MA), Abcam (Cambridge, UK), PeproTech (London, UK), Sigma-Aldrich, Millipore (Billerica, MA) and R&D Systems. TLRs ligands (LPS from *E. coli*, LTA and poly I:C) were from Invivogen (San Diego, CA). Inhibitors LY294002, MG-132 and Akt inhibitor II were purchased from Calbiochem (San Diego, CA). Tissue culture serum and media were from BioWhittaker (Walkersville, MD). Tissue culture dishes were from Falcon (Lincoln Park, NJ).

Animals and peritoneal macrophage isolation. Mice were housed and bred in our pathogen-free facility. C57BL/6 and BALB/c mice were used for macrophage isolation. LXRαβ$^{+/+}$ (WT) and LXRαβ$^{-/-}$ (DKO) mice (mixed Sv129/C57BL/6 background) were maintained on standard chow under pathogen-free conditions (31). MyD88$^{+/+}$ (WT) and MyD88$^{-/-}$ (KO), IRF3$^{+/+}$ (WT) and IRF3$^{-/-}$ (KO) were previously described (32, 33). Experimental procedures were approved by the Institutional Committee for Research Ethics in accordance with Spanish and EU guidelines. Animals were used aged 8-12 weeks as follows: Four days prior to the assay, mice were intraperitoneally (i.p.) injected 2.5 ml of thioglycollate broth. Elicited peritoneal macrophages were prepared from mice killed by cervical dislocation (4-8 animals per condition), as previously described (31, 34).

Cell death detection. Cells were collected and washed in cold PBS. After centrifugation at 4ºC for 5 min at 1,000***g*** cells were resuspended in annexin V-binding buffer (10 mM HEPES; pH 7.4, 140 mM NaCl and 2.5 mM $CaCl_2$), following a previous protocol (35).

Determination of NO synthesis. NO release was measured as the accumulation of nitrite and nitrate in the incubation medium (phenol-red free). Nitrate was reduced to nitrite with nitrate reductase and was determined spectrophotometrically with Griess reagent (35).

Cytokine and Chemokine assays. Cytokine production by cultured macrophages and its accumulation in the incubation medium was quantified by the Bio-Plex cytokine assay following the supplier's instructions (Bio-Rad). Serum TNF-α was measured by Cytoset ELISA kits (Biosource International, Camarillo, CA). Levels of CXCL-1 and CXCL-10 were measured with ELISA kits from R&D Systems according to the manufacturer's instructions.

Quantitative Real-Time PCR (qRT-PCR). 1 μg of total RNA, extracted with TRIzol reagent (Invitrogen) according to the manufacturer's instructions, was reverse transcribed using Transcriptor First Strand cDNA Synthesis Kit for RT-PCR following the indications of the manufacturer (Roche). qRT-PCR was conducted with SYBR Green (Applied Biosystems) on a MyiQ Real-Time PCR System (Bio-Rad). PCR thermocycling parameters were 95°C for 10 min, 40 cycles of 95°C for 15 s, and 60°C for 1 min. All samples were analyzed for 36B4 expression in parallel. Each sample was run in duplicate and was normalized to 36B4. The replicates were then averaged, and fold induction (FI) or relative

quantity (RQ) was determined in a ΔΔCt based fold-change calculations. Primer sequences are available on request (36).

Preparation of total protein cell extracts. Cells (5×10^6) were homogenized in a buffer containing 10 mM Tris-HCl (pH 7.5), 1 mM $MgCl_2$, 1 mM EGTA, 10% glycerol, 0.5% CHAPS, 1 mM β-mercaptoethanol, 0.1 mM PMSF and a protease and phosphatase inhibitor cocktail (Sigma-Aldrich). The extracts were vortexed for 30 min at 4ºC and after centrifuging for 15 min at 13,000***g*** the supernatants were stored at -20ºC. Protein levels were determined using Bradford reagent (Bio-Rad).

Preparation of cytosolic and nuclear extracts. Cells (5×10^6) were washed with PBS and collected by centrifugation. Cell pellets were homogenized with 100 µl of buffer A (10 mM Hepes; pH 7.9, 1 mM EDTA, 1 mM EGTA, 100 mM KCl). After 10 min at 4°C, Nonidet P-40 was added to reach a 0.5% concentration. The tubes were gently vortexed for 30 s, and nuclei were collected by centrifugation at 13,000***g*** for 15 min (4, 37). The supernatants were stored at -20°C (cytosolic extracts); the pellets were resuspended in 50 µl of buffer A supplemented with 20% glycerol and 0.4 M KCl and gently shaken for 30 min at 4°C. Nuclear protein extracts were obtained by centrifugation at 13,000***g*** for 15 min, and the supernatants were stored at -80°C. Protein content was assayed using the Bio-Rad protein reagent. All cell fractionation steps were carried out at 4°C. All buffers contained protease and phosphatase inhibitor cocktail (Sigma-Aldrich).

Characterization of proteins by immunoblot. Protein extracts were boiled in loading buffer (250 mM Tris-HCl; pH 6.8, 2% SDS, 10% glycerol, 2% β-mercaptoethanol) and size-separated by 10-15% SDS-PAGE. The gels were blotted onto a Hybond-P membrane (Amersham) and incubated with anti-NOS-2, anti-COX-2, anti-IκBα, anti-IκBβ and anti-phospho-Akt (Thr308) (Santa Cruz Biotech.), anti-phospho-IKKαβ, anti-IKKβ, anti-phospho-Akt (Ser473) and anti-Akt (Cell Signaling), anti-CXCL-1 (R&D Systems), anti-CXCL-10 (PeproTech), anti-p85 (Millipore) and anti-β-actin (Sigma). The levels of phosphorylated and total p38, JNK and ERKs p44/p42 were determined by Western blot using total extracts and specific commercial Abs (Cell Signaling). In experiments using anti-phospho-S32-IκBα (Cell Signaling), the blot incubation solution contained 100 ng/ml purified-IκBα (Ser32) (Santa Cruz Biotech.). The blots were submitted to sequential reprobing with Abs after treatment with 100 mM β-mercaptoethanol and 2% SDS in Tris-buffered saline and heated at 60ºC for 30 min. The blots were revealed by ECL Advance (Amersham). Different exposure times of the blots were acquired with a Caged Coupling Device camera in a luminescent image analyzer (Molecular Imager, Bio-Rad) ensuring that bands were not saturated. Quantification of the images was performed by using Quantity One software (Bio-Rad).

EMSAs. The sequence 5'-TGCTAGGGGGATTTTCCCTCTCTCTGT-3', corresponding to the consensus NF-κB binding site (nucleotides -978 to -952) of the murine NOS-2 promoter (4) was used. Oligonucleotides were annealed with their complementary sequence by incubation for 5 min at 85°C in 10 mM Tris-HCl (pH 8.0), 50 mM NaCl, 10 mM $MgCl_2$, 1 mM DTT. Aliquots of 50 ng of these

annealed oligonucleotides were end-labeled with Klenow enzyme fragment in the presence of 50 µCi of [α-^{32}P]dCTP and the other unlabeled dNTPs in a final volume of 50 µl. A total of 5×10^4 dpm of the DNA probe was used for each binding assay of nuclear extracts as follows. 3 µg of nuclear protein were incubated for 15 min at 4°C with the DNA and 2 µg of poly dI:dC, 5% glycerol, 1 mM EDTA, 100 mM KCl, 5 mM $MgCl_2$, 1 mM DTT, 10 mM Tris-HCl (pH 7.8) in a final volume of 20 µl. The DNA-protein complexes were separated on native 6% polyacrylamide gels in 0.5% Tris-borate-EDTA buffer (4). Supershift assays were carried out after incubation of the nuclear extracts with 2 µg of Abs (anti-p50, anti-c-Rel, anti-p65) (Santa Cruz Biotech.) for 1 h at 4°C, followed by EMSAs (not shown).

Measurement of IKKβ activity. Cells (10^7) were homogenized in buffer A and centrifuged at 13,000***g*** for 15 min. The supernatant (1 ml) was pre-cleared, and IKKβ was immunoprecipitated with 1 µg of anti-IKKβ (38). After extensive washing of the immunoprecipitate with buffer A, the pellet was resuspended in kinase buffer (modified buffer A containing 0.1 mM EDTA, 5 mM $MgCl_2$ and 10 nM okadaic acid). Kinase activity was assayed in 100 µl of kinase buffer containing 100 ng of immunoprecipitate, 50 µM [γ-^{32}P]ATP (0.5 µCi) and 100 ng of purified IκBα(Ser32) as substrate. Aliquots of the reaction mixture were stopped at various times in 1 ml of ice-cold buffer A supplemented with 5 mM EDTA. The same protocol was used when the activity of IKKβ was followed by Western blotting using anti-phospho-S32-IκBα, except for the use of 1 mM MgATP instead of [γ-^{32}P]ATP. The linearity of the kinase reaction was confirmed over a period of 30 min. *In vitro* IKKβ activity was measured by homogeneous time-resolved fluorescence (HTRF) assay, using cloned and expressed IKKβ and biotinylated-IκBα (aminoacids 28 to 40) as substrate. Fluorescence (excitation at 330 nm and emission at 615 and 665 nm) was recorded after addition of europium cryptate phospho-Ab recognizing the S32/S36 phosphorylation peptide and streptavidin-XL665. Inhibition of IKKβ by staurosporine was used as control.

Proteomics of IKKβ. Bacterially expressed and purified IKKβ was treated with DTPs and submitted to digestion with trypsin and V8 proteases, followed by MALDI-TOFF peptide analysis. Treatment with the cyclopentenone prostaglandin 15-deoxy-$\Delta^{12,14}$-PGJ_2 which alkylates C187 was used as control (39, 40).

Confocal microscopy. Peritoneal macrophages ($1x10^5$) were grown on coverslips and incubated with the indicated stimuli. After washing the covers with PBS, cells were fixed with paraformaldehyde (4%; pH 7.2) for 15 min at RT and washed again. The macrophages were permeabilized with cold methanol for 10 min at RT. After incubation with anti-phospho-S473Akt overnight at 4ºC, cells were washed with PBS followed by incubation with anti-rabbit secondary Ab for 2 h at RT. Nuclei were revealed by staining with DAPI. Cells were analyzed using an Espectral Leica TCS SP5 confocal microscope.

Transient transfections. NIH3T3 transfections were performed using FuGene HD transfection reagent (Roche), with a FuGene:DNA ratio of 8:2 and following the indications of the manufacturer (Roche). 24-48 h after transfection, cells were treated with the indicated stimuli. Transfection experiments were

performed using vectors encoding p110 Wild type (p110WT) and p110 Kinase Deficient (p110KD)(22). Phosphorylation of Akt was analyzed by immunoblot as a marker of PI3-kinase activity.

Measurement of PI3-kinase activity. PI3-kinase activity was measured in the immunoprecipitates by *in vitro* phosphorylation of PI as previously described (22).

LPS-induced D-GalN-dependent lethality studies. Male C57BL/6 mice aged 8 to 10 weeks old were induced an endotoxic shock. The lethal injury was produced by i.p. injection of LPS (2 μg/kg) in combination with D-GalN (800 mg/kg). The DTPs (30 mg/kg) were administered by i.p. injection (0.5 ml) 1 h prior to the challenge with D-GalN/LPS. DMSO was given to the control animals. The lethality was monitored until 25 h after the administration of D-GalN/LPS.

12-O-Tetradecanoylphorbol acetate (TPA)-induced mouse ear edema and myeloperoxidase (MPO) activity assay. 2 μg of TPA dissolved in 20 μl of DMSO, was applied to both surfaces of the right ear of each mouse. The left ear (control) received the vehicle (DMSO). The DTPs were administered topically (500 ng per ear in 20 μl of DMSO) simultaneously with TPA application. The reference drug, indomethacin, was administered at the same doses. After 4 h, the animals were killed by cervical dislocation and a 6 mm diameter disc from each ear was removed with a metal punch and weighed. Ear edema was calculated by subtracting the weight of the left ear (vehicle) from the right ear (treatment) (41). Ear sections were homogenized in 750 μl of saline. After centrifugation at 10,000***g*** for 15 min at 4ºC, MPO activity was measured in supernatants, as described before (41).

In vivo administration of DTP and ex vivo whole blood assay. C57BL/6 mice were starved overnight and administrated orally with 25 mg/kg of DTP1 and DTP5 prepared in 40% Solutol HS15 (BASF, Ludwigshafen, Germany). 90 min later, whole blood was collected into heparinized tubes through cardiac puncture, pooled (n=4) and mixed 1:3 with pre-warmed complete RPMI 1640 medium. 0.9 ml/well of the diluted whole blood was dispensed into 24-well tissue culture plate and stimulated with LPS (10 and 100 ng/ml) diluted in RPMI-1640 basal medium. The 24-well plate was then incubated for 4 h with occasional mixing. Finally, samples were transferred to 1.5 ml tubes and centrifuged at 14,000***g*** for 30 s at RT. Supernatants were assayed for TNF-α levels by the Cytoset ELISA kits.

Bioluminescence imaging of myeloperoxidase (MPO) activity in vivo. MPO activity was measured in the whole animal as described previously (Gross et al, 2009). Briefly, BALB/c mice were pretreated with the DTP5 (30 mg/kg) and after 1 h was administered the zymosan (10 mg/kg) by i.p. injection. At the times indicated, luminol (5 mg in 200 μl) was i.p. injected and the bioluminescence (BLI) was recorded in an IVIS Lumina (Caliper Life Sciences).

Microarray analysis. RNA samples were labeled and hybridized in Agilent 4x44K 1-colour microarrays following the manufacturer protocol and two independent experiments. The slides were scanned and images were converted to raw signal txt files using Feature Extraction software (Agilent). Data preprocessing and normalization was performed using *codelink* and *limma* and Bioconductor

packages (42). Differential expression was analyzed using *limma* paired *T-test* (43) as implemented in Pomelo II (44). Gene set enrichment analysis was done with FatiScan method in Babelomics v3 (45).

Statistical analysis. Unless otherwise stated, data are expressed as mean ± standard deviation (SD). To compare means between two independent samples Mann-Whitney rank sum test was used. The results were considered significant at $P<0.05$. Data were analyzed by SPSS for Windows statistical package version 9.0.1.

Results

Acanthoic acid-related DTPs inhibit the expression of genes mediating inflammation in peritoneal macrophages. We analyzed the effect of DTP1, one of the five acanthoic acid C-4 derivatives assayed in this work (Fig. 1A), on LPS transcriptional response on macrophages. Cells were incubated for 30 min with DTP1 or DMSO (as control) and then activated with LPS for up to 4 h. The profound impact of LPS on macrophage gene expression has been well characterized and even modeled by systems biology approaches (i.e.,(46)). Accordingly, we identified a high number of significant Differentially Expressed Genes (DEGs; 5075 genes, FDR≤0.05) between control and LPS-stimulated cells (Fig. 1B). Co-treatment with DTP1 and LPS resulted in *ca.* 50% reduction of the number of significant DEGs (2456 genes, using the same FDR threshold) indicating that DTP1 partially inactivates the pro-inflammatory transcription induced by LPS. Not only less DEGs are observed after DTP1 treatment, but also a general attenuation of LPS-induced fold changes was observed. As shown in Fig. 1B (*right*), most of the genes assayed with the expression microarrays presented a less marked up or down-regulation after LPS in DTP1 pretreated samples. To characterize the biological role of the genes affected by DTP1, functional enrichment of KEGG pathways analysis was performed using FatiScan (45). The significant results (FDR≤0.05) are shown in Fig. 1C. Most of the pathways were enriched in DTP1 down-regulated genes and were directly related with inflammation and immunity (*Cytokine-cytokine receptor interaction, Leukocyte transendothelial migration*) or related signaling pathways (*Toll-like receptor, MAPK, JAK-STAT*). A clustering of the gene expression of members of the geneset *Toll-like receptor signaling pathway* is shown in Supp. Fig. 1 and qRT-PCR of selected genes showed similar results between DTP1 and DTP5 treatment (not shown). As DTP1 transrepresses a high number of inflammation-related genes, this effect was compared with that described for activated GR, LXR and PPARγ using published genesets (47). The target genes of all three activated nuclear receptors (LXR, PPARγ and GR) resulted significantly enriched in the DTP1 down-regulated genes (Supp. Fig. 2). In summary, the DTP1 transrepression profile overlaps with the one of LXR ligand GW3965, but it also seems to transrepress LXR-independent LPS-induced genes, as the ones repressed exclusively by the GR ligand dexamethasone. This implies that DTP1, a LXR ligand (31), additionally represses the inflammatory response by LXR-independent mechanisms.

We then designed a set of experiments to confirm that the decreased transcriptional response to LPS was accompanied by an observable anti-inflammatory effect independently of LXR activation induced by DTPs. Cells were incubated for 30 min with each of the five DTPs (Fig.1A) and then activated with LPS for up to 18 h. As Fig. 1D shows, there was a reduction in the accumulation of nitrate plus nitrite (NOx) in the culture medium (a marker of inflammatory response) after the treatment with all five DTPs. This effect was dose dependent: DTPs 1, 3 and 5 exhibited an inhibition higher than 60% at 10 μM, whereas DTP2 and DTP4 inhibited less than 30% and 40%, respectively, of NO synthesis. As previously reported, DTP1, DTP3 and DTP5 have the capacity to activate the LXRs, nuclear receptors that counteract NF-κB-dependent responses (31). Interestingly, this inhibitory effect of DTPs,

although diminishes compared with WT cells, persisted when DTP1, DTP3 and DTP5 were assayed in macrophages from LXRαβ-DKO mice (Fig. 1D, *right*). The time-course of NOS-2 and COX-2 mRNA upon activation with LPS was analyzed, showing an inhibitory effect by these DTPs (Fig 1F), as well as a reduction in the corresponding protein levels (Fig. 1E). In agreement with this anti-inflammatory activity of DTP1 and DTP5, the accumulation in the culture medium of IL-1β, CXCL-1, CXCL-10, IFNγ, IL-6, RANTES, IL-12 and the anti-inflammatory cytokine IL-10 were decreased in the presence of the DTPs (Fig. 1G). The intracellular protein levels of some of these cytokines and chemokines were measured at 18 h after stimulation (Fig. 1H). Similar results were obtained when the mRNA levels of these factors were measured by qRT-PCR (data not shown). These results suggest that DTP1 and DTP5 are interfering with early signaling events after LPS challenge, independently of the effects on LXR activation (31). These DTPs did not affect cell viability and partially attenuated the LPS-dependent apoptosis, probably because of the decrease in NO synthesis (data not shown).

DTP1 and DTP5 exert in vivo anti-inflammatory activity. To evaluate the potential anti-inflammatory action of DTP1 and DTP5 the model of ear edema was used. As Fig. 2A shows, the myeloperoxidase activity due to infiltrated neutrophils, induced by topical application of TPA to the ear, was significantly attenuated when animals received the DTPs. The edema was determined by weighing identical ear sections and this parameter was significantly reduced in animals treated with DTPs (indomethacin was used as control). In addition to this, an *ex vivo* whole blood assay demonstrated that TNF-α production by whole blood cells obtained from animals treated orally with DTP1 and DTP5 at 25 mg/kg was inhibited by 75% and 54% at 10 and 100 ng/ml LPS stimulation, respectively (Fig. 2B). The anti-inflammatory activity was also evaluated using the D-GalN-sensitized LPS-dependent toxicity. As Fig. 2C shows, both DTP1 and DTP5 exerted a significant protection against the lethality induced by an acute dose of D-GalN/LPS, extending three folds the survival time of the mice with respect to the controls treated with vehicle. In agreement to the survival mediated by the DTPs a dose-dependent inhibition of TNF-α levels in plasma (1h after LPS) was also observed when animals were i.p. injected with DTPs and 30 min later received i.p. LPS (1 mg/kg) (Fig. 2D). In the same line, MPO activity was measured *in vivo* by bioluminescence recording after i.p. injection of DTP5 (30 mg/kg) followed 1 h later by zymosan (10 mg/kg) administration (Fig. 2E). A 29% inhibition of luminescence was observed in animals treated with DTP5.

DTPs inhibit the IKK/NF-κB and MAPKs activation in response to different pro-inflammatory stimuli. To study the effect of these DTPs on IKK activation, the enzyme was immunoprecipitated from cells pretreated for 30 min with the indicated DTPs and then challenged for 10 min with LPS. The IKK activity was determined *in vitro* using purified IκBα as substrate and measuring the phospho-S32-IκBα levels with specific antibodies. Fig. 3A shows a decreased activation of IKK in cells pretreated with DTP1, 3 and 5. Fig. 3B shows the IKK activity at 10 and 20 min after LPS activation

in cells treated with DTP5 and following the incorporation of [^{32}P]phosphate into IκBα. To evaluate the possibility that DTPs might inhibit directly IKK through the formation of adducts (2, 4, 48, 49), purified IKKβ was incubated with DTP1 and analyzed by proteomics, without noticeable changes in the composition of the peptides (see methodology; data not shown). Alkylation of C187 by 15-deoxy-$\Delta^{12,14}$-PGJ_2 was used as control (39); furthermore, *in vitro* addition of DTP1 or DTP5 to immunoprecipitated IKK from LPS-treated cells did not affect the activity (not shown). Moreover, direct effects of the DTPs on the activity of the kinase were evaluated by using purified IKKβ and adding the DTPs to the *in vitro* HTRF assay. As Fig. 3C shows, the activity remained unaffected by the DTPs when assayed up to 100 μM. As expected, treatment with staurosporine, which was used as positive control, inhibited IKK with an EC_{50} value below 0.5 μM. As Fig. 3D shows, the activation of NF-κB, evaluated by EMSAs, was significantly impaired when cells were incubated with DTP5, and similar results were obtained with DTP1 (data not shown). Fig. 3E shows the time-dependent changes in IKK phosphorylation that were lesser in the presence of DTP5, and the levels of IκBα and IκBβ that showed a delayed degradation (IκBβ), and a more rapid resynthesis (IκBα). Under the same conditions, the LPS-dependent activation of the MAP kinases ERK and p38 was inhibited by DTP5 whereas JNK activation was unaffected (Fig. 3F). Fig. 3G shows an inhibitory effect of DTP5 on NOS-2 and COX-2 protein levels in both LXRαβ wild type and deficient mice although, as expected, this effect is partially reduced in LXRαβ-DKO mice (especially in COX-2 expression). Furthermore, DTP5 impaired IκBα degradation in LPS-treated cells, regardless the presence of LXR. Nevertheless, pharmacological activation of LXR with T1317 was not able to modify the IκBα degradation induced by treatment with LPS. Taken together, these data pointed to the IKK/NF-κB pathway and MAPKs as the main targets in the LXR-independent mechanism of action of DTP5. Similar results were obtained with DTP1.

In addition to LPS, the response of macrophages to the TLR3 ligand, poly I:C and to the TLR2 ligand, LTA was analyzed. As Fig. 4A shows, LPS, poly I:C and LTA promoted the expression of NOS-2 and COX-2, an effect that was attenuated in the presence of DTP5. Moreover, the accumulation of nitrate plus nitrite in the culture medium induced by these stimuli was also inhibited by DTP5. The TLR3 uses a MyD88-independent pathway, but activates IRF3 through the TRIF-dependent pathway. When the experiment was repeated in macrophages from IRF3-deficient mice, the absence of IRF3 did not affect the inhibitory effect of DTP5 (not shown). Fig. 4B shows the time course of the IκBα and IL-6 mRNA levels after activation with LPS, LTA and poly I:C in the absence or presence of DTP5, reflecting a decrease in the mRNA levels of both genes. Fig. 4C, shows the *in vivo* phosphorylation of IκBα in S32, analyzed after proteasome inhibition with MG132 to avoid IκBα degradation. The inhibitory effect of DTP5 is observed both on LPS and poly I:C-induced activation of IKK. When macrophages from MyD88-deficient mice were used, the inhibition of CXCL-10 by DTP1 and DTP5 was similar in LPS and poly I:C-stimulated macrophages, regardless the presence of MyD88 (Fig. 4D). Taken together, these results suggest that these DTPs are acting both through the MyD88

dependent and independent (TRIF-dependent) pathways. Moreover, activation with poly I:C or LTA of DTP5-pretreated macrophages showed a decreased IKK activity (IKK phosphorylation and IκBα/IκBβ degradation-recovery; Fig. 5A) and an inhibition of p38 phosphorylation on MAPKs activity (Fig. 5B), but without noticeable effects on ERK and JNK activation.

DTPs activate the PI3K/Akt pathway in macrophages. We aimed to identify the molecular target that is mediating the effects of DTP1 and DTP5 on NF-κB inhibition, and in view of the above results we reasoned that one likely candidate was the PI3K/Akt pathway (22, 50). As Fig. 6A shows, DTP1, 3 and 5 promote a time dependent phosphorylation of Akt in Ser473. This S473-Akt phosphorylation was visualized by confocal microscopy (Fig. 6B), and the effect persisted upon activation with LPS, poly I:C or LTA (Fig. 6C). This Akt phosphorylation was connected to an activation of PI3K, as deduced by the determination of the PIP2-dependent kinase in cell extracts immunoprecipitated with anti-p85 (Fig. 6D). In addition to Ser473-Akt phosphorylation, Thr308-Akt was also phosphorylated in response to DTP5 (Fig. 6E). A positive control (50 nM insulin treatment; C+) was included in the blot. Inhibition of PI3K with LY294002 suppressed PI3K activity and Akt phosphorylation. Using macrophages from LXRαβ-DKO to avoid the inhibitory effects on NF-κB by the nuclear receptors, inhibition of Akt suppressed the effect of DTP5 decreasing NOS-2, COX-2, CXCL-1 and CXCL-10 levels (Fig. 6F), and similar results were observed after inhibition of PI3K with LY294002 (not shown). In the same line, the effects of DTP5 on the inhibition of IKK, ERK and p38 phosphorylation were attenuated when cells were treated with LY294002 (Fig. 6G). Using NIH3T3 cells transiently expressing a p110WT or p110 kinase deficient (KD) construct, the absence of p110 activity decreased significantly the DTP5-dependent phosphorylation of Akt (Fig. 6H).

Discussion

Few studies have been achieved to evaluate and molecularly characterize the anti-inflammatory effects of acanthoic acid, a pimarane diterpene isolated from the root bark of *Acanthopanax koreanum* Nakai, which has been used in traditional Korean medicine for the treatment of rheumatism (8, 26, 29). Previous works using series of synthetic analogues of this molecule showed the main structural motifs essential for the anti-inflammatory effect of these DTPs (8, 26). In a previous study we described that some of these DTPs were potent activators of LXRαβ, which might explain in part their anti-inflammatory effects (31); however, these DTPs still retained their anti-inflammatory activity when assayed in macrophages from LXRαβ-deficient mice. In the present study, we have analyzed the activity of five acanthoic acid related analogues. We found that the chemical modifications introduced in the structure of this diterpene, mainly positional substitution and modification of the R-groups at C4 of the ring A, render molecules with different quantitative effects on the expression of typical pro-inflammatory genes, such as NOS-2 and COX-2. Most of the studies

in this report have been performed with DTP1 and DTP5 since these molecules exhibited higher effects in cellular models of inflammation (effects that were present even in the absence of LXRαβ), at the time that were chemically more stable.

The data reported in this work show that, at least in macrophages, DTPs negatively regulate inflammatory responses triggered by different TLRs, both *in vitro* and *in vivo,* decreasing the expression of cytokines, chemokines and inflammatory mediators such as nitric oxide. These DTPs significantly inhibit the IKK/NF-κB pathway and ERK/p38 MAP kinases activated in response to LPS. These results are consistent with previous studies in which diterpenes with kaurene structure, in addition to the NF-κB pathway, also inhibited these MAPKs (4). LPS activates TLR4 that is the only receptor able to signal through both MyD88-dependent and TRIF-dependent pathways (12-14). Similar results were obtained when macrophages were triggered with LTA, a TLR2 ligand (MyD88-dependent) or poly I:C, a ligand for TLR3 (TRIF-dependent) but without noticeable effects on ERK activation. Interestingly, the absence of MyD88 (using CXCL-10 as target) or IRF3 did not affect the inhibitory actions of DTPs upon challenge with LPS or poly I:C. These data suggest the presence of a "shared" target for DTPs common to the different signaling pathways analyzed but independent of MyD88 or TRIF. Moreover, these inhibitory effects persisted when the compounds were assayed in macrophages from LXRαβ-deficient mice pointing to a nuclear receptor-independent mechanism. In this regard, the EMSAs demonstrated that DTPs reduced the NF-κB translocation to the nucleus in contrast to the transrepression effects described for LXRs inhibition of NF-κB activity.

When the inhibition of the NF-κB early signaling was investigated we were unable to observe direct effects of the DTPs on the activity of the IKK complex despite that IKKβ phosphorylation was abrogated; moreover, proteomic analysis of IKKβ treated with DTPs showed the absence of any chemical modification in the protein (not shown), which suggests that the DTPs target is located upstream IKK activation. Recent reports show that PI3K contributes to the fine tuning of the initial phases of the innate immune response to diverse microbial pathogens (50-52). In DC and macrophages, activation of PI3K/Akt pathway was found to limit LPS induced production of cytokines and chemokines and expression of NOS-2 through both MyD88-dependent and independent pathways (19-22). In this study we have shown that DTPs 'per se' induce a persistent Akt phosphorylation at the two major sites, Thr308 and Ser473. We confirmed that this Akt activation was dependent on PI3K activity as far as was suppressed by PI3K pharmacological inhibitors. Moreover, the phosphorylation of Akt in Ser473 was blocked by the expression of a kinase deficient isoform of p110. In the same way, the involvement of DTPs-dependent activation of PI3K/Akt in the negative regulation of LPS-induced IKK, p38 and ERK (p42/p44) phosphorylation was confirmed by the suppression of the DTPs effects after PI3K or Akt inhibition (LY294002 or Akt inhibitor II, respectively). Fig.7 shows a schematic representation of the molecular targets sensing the effect of these DTPs.

In vivo studies with these DTPs showed a significant anti-inflammatory action in all the models assayed: The synthesis of TNF-α by whole blood cells collected from animals administered orally with the DTPs was inhibited, systemic (i.p.) administration delayed significantly the rate of animal death in a model of D-GalN/LPS-induced hepatotoxicity and the TNF-α levels in plasm. The development of TPA-induced edema was also prevented to similar levels as those elicited by indomethacin. Taken together, these data contribute to better understand the mechanisms of action of the acanthoic acid derivatives in innate inflammatory responses. In summary, our results have demonstrated that DTPs negatively regulates IKK/NF-κB and MAPKs (p38 and ERK) pathways by increasing PI3K activity and consequently, Akt phosphorylation. The ability of our compounds to activate PI3K opens new prospects in the search for anti-inflammatory molecules and point to the possible use of these acanthoic acid-related diterpenes as anti-inflammatory drugs with potential therapeutic activity in different inflammatory pathologies targeting simultaneously the PI3K/Akt and the LXRαβ pathways.

Acknowledgements. This work was supported by grants SAF 2002/00783 from MCYT and 08.3/0008/01 from CAM and RECAVA (FISS), plus NIH grant R44AI49014 awarded to MAP. We thank to S. Akira and T. Taniguchi for MyD88$^{-/-}$ and IRF3$^{-/-}$ mice, respectively.

Legends to Figures.

Figure 1. ***Effect of acanthoic acid-related DTPs on inflammatory-mediators expression***. Chemical structure of the five acanthoic acid C-4 derivatives that were synthesized (A). Transcriptional response to LPS measured by gene expression microarrays is affected by the DTP1 (B). Peritoneal macrophages were pretreated with 10 μM DTP1 or DMSO (as vehicle) and then activated with 250ng/ml of LPS for 4h. The number of significant Differential Expressed Genes (DEGs, False Discovey Rate (FDR) ≤ 0.05) obtained after LPS+DTP1 is about half the number of DEGs after LPS+vehicle (B, left). The global fold-changes (indicated in the heat map as log2) of LPS up- and down-regulated genes were dramatically affected (B, right). Functional analysis of KEGG pathways with FatiScan resulted in 13 significantly enriched (FDR ≤ 0.05) pathways: three of them were enriched in genes up-regulated (red) and the other ten were enriched in genes down-regulated (blue) by DTP1 (C). Peritoneal macrophages from wild type (WT) and LXRαβ-DKO mice were pretreated for 30 min with the indicated DTPs and then activated with 250 ng/ml of LPS. After 18 h of incubation the accumulation of NOx in the culture medium (D) and the mRNA (up to 6 h) and protein levels of NOS-2 and COX-2 (F, E) were determined. Panel G shows the accumulation (18 h) in the culture medium of IL-1β, CXCL-1 (KC), CXCL-10 (IP-10), IFN-γ, IL-6, RANTES, IL-10 and IL-12. The intracellular levels of IL-1β, CXCL-1, CXCL-10 were also determined at 18 h (H). NOx concentration was expressed as percentage; 100%= 15.4 and 21.2 nmol/mg of protein for LXRαβ WT and DKO macrophages, respectively. Results shows a representative experiment out of 3 (*panels* E, H), the mean (n=4, *panels* D, F) and the mean±SD (n=4, *panel* G). *P<0.01 *vs.* the LPS condition.

Figure 2. ***DTP1 and DTP5 inhibit TPA-induced ear edema and delay D-GalN/LPS lethality***. Male C57BL/6 mice received topically the indicated DTPs (0.5 μg in 20 μl DMSO) or indomethacin (0.5 μg in 20 μl) and TPA (2 μg in 20 μl) in one ear and vehicle in the other. After 4 h, animals were sacrificed and the myeloperoxidase (MPO) activity and the weight of identical sections of ear tissues were determined (A). Pooled whole blood samples from C57BL/6J mice-treated orally for 90 min with 25 mg/kg DTP 1 and DTP5 prepared in 40% Solutol HS15 (vehicle control) were stimulated with LPS at 10 ng/ml and 100 ng/ml *ex vivo* for 4 h, and TNF-α levels were measured by ELISA (B). To evaluate the effect on LPS/D-GalN lethality, mice were i.p. injected with 30 mg/kg body weight of the indicated DTPs and 1 h later were i.p. conditioned with D-GalN and LPS. Results show the Kaplan-Meier representation of the survival time of the groups (n=7) (C). In a similar way, animals received i.p. the indicated concentrations of DTP1 and DTP5, followed 1 h later by i.p. administration of LPS. The TNF-α plasma levels were measured at 1 h after LPS challenge (D). The *in vivo* effect of DTP5 (30 mg/kg; 1h prior to zymosan administration) on MPO activity was measured in the whole animal after administration of zymosan (10 mg/kg) and measuring the bioluminescence after challenge with

luminol (5 mg in 200 µl) using an IVIS Lumina (E). Results show the mean±SD (n=5). *P<0.05, **P<0.01 *vs*. the corresponding control.

Figure 3. ***Acanthoic acid-related DTPs inhibit early signaling leading to NF-κB activation, but not IKK activity directly.*** Unless otherwise indicated, LXRαβ WT macrophages were pre-treated for 30 min with 10 µM of the indicated DTPs and then activated for 10 min with 250 ng/ml of LPS. The activity of IKK was assayed after immunoprecipitation of the enzyme and using purified-IκBα as substrate followed by immunoblot analysis using Abs against P-S32-IκBα (A). The mean of the band ratios from 3 experiments was indicated after normalization *vs.* the first lane (A). A time course of IKK activation by LPS in cells treated with DTP5 was determined, following the incorporation of [^{32}P] from [γ-^{32}P]ATP into purified-IκBα (B). The direct effect of DTPs on purified IKKβ activity was determined by homogeneous time-resolved fluorescence (HTRF) assays, using biotinylated IκBα (28-40 aa) as substrate and inhibition by staurosporine as a control (C). The effect of DTP5 on the LPS-activation of NF-κB was determined by EMSAs (D) and the effects on the phosphorylation state and levels of IKK, IκBα, IκBβ (E) and ERK, p38 and JNK MAPKs were determined by immunoblot (F). The levels of NOS-2 and COX-2 at 18h of treatment with LPS in the absence or presence of DTP5, and the time-course of IκBα changes were determined in macrophages from LXRαβ WT and DKO mice (G); T1317 was used as control for maximal activation of LXRαβ. Results show a representative experiment out of 3.

Figure 4. ***The inhibition of IKK activation by DTP1 and DTP5 is independent of MyD88 signaling.*** Macrophages were treated for 30 min with 10 µM of DTPs and activated with LPS (250 ng/ml), LTA (5 µg/ml) or poly I:C (25 µg/ml). The protein levels of NOS-2 and COX-2 and the accumulation of NOx in the culture medium were determined at 18 h (A). The time course of the mRNA levels of IκBα and IL-6 were determined by qRT-PCR and normalized as percentage *vs.* the maximal value in the absence of DTP for each gene (B). The levels of IκBα phosphorylated in S32 were determined by immunoblot in cells treated with 10 µM MG132 to inhibit proteosomal degradation (C). The accumulation in the medium of CXCL-10 was determined in macrophages from wild type or MyD88 deficient mice stimulated with LPS or poly I:C and expressed as percentage *vs.* the corresponding value with LPS or poly I:C alone (values were 14 and 10.6 ng/ml for WT and MyD88 KO treated with LPS; 19.2 and 15.9 ng/ml for WT and MyD88 KO treated with poly I:C, respectively; *panel* D). The blots show a representative experiment out of 4 (*panels* A,C), and the mean (B; n=4) or the mean±SD (D; n=3). *P<0.01 *vs.* the condition without DTP.

Figure 5. ***Effect of DTP5 on IKK and MAPKs activities in macrophages treated with poly I:C or LTA.*** Cells were treated as described in Fig. 4 with poly I:C (25 µg/ml) or LTA (5 µg/ml) and cell

extracts were prepared at the indicated times to determine IKK phosphorylation and IκBα/IκBβ levels (A) and MAPKs phosphorylation levels. Results show a representative blot out of 4.

Figure 6. ***DTPs activate the PI3K/Akt pathway in peritoneal macrophages***. Cells were treated with the indicated DTPs (10 μM) for 30 min and the levels of S473-Akt were determined (A, *left*). The time course of S473-Akt phosphorylation induced by DTP5 was analyzed (A, *right*). Panel B show the visualization of Akt phosphorylation by confocal microscopy. Macrophages treated with DTP5 for 30 min were activated with LPS, poly I:C or LTA for 30 min and the levels of phosphorylated S473-Akt were determined (C). Cells incubated with LY294002 (10 μM), DTP5 or insulin (50 nM) were homogenized and immunoprecipitated with anti-p85 Ab. PIP2 kinase activity was determined in vitro and visualized by TLC. Samples of the extracts were used to determine p85 and P-S473-Akt/Akt levels (D). The T308-Akt and S473-Akt phosphorylation were determined in cells incubated with LPS, DTP5 and LY294002, as described in *panel* C (E). The effect of Akt inhibition (Akt inhibitor II, 10 μM) on the protein levels of NOS-2, COX-2, CXCL-1 and CXCL-10 determined at 18h, was analyzed in cells treated with DTP5 and LPS, using LXRαβ DKO macrophages (F). Panel G shows the effect of LY294002 on the time course of Akt, IKK and MAPKs phosphorylation in macrophages treated with DTP5 and LPS. NIH3T3 cells were transfected with a p110 kinase deficient (KD) or wild type plasmids and the effect on P-S473-Akt levels were determined after incubation with LY and DTP5. Insulin was used as a positive control. Results show a representative experiment out of 3.

Figure 7. Schematic model of DTPs mechanism of action: PI3K/Akt and LXRs are the main targets mediating NF-κB/MAPKs inhibition. As early event, DTPs activate PI3K. The phosphorylated lipid products generated by PI3K act as second messengers to activate Akt, that becomes phosphorylated at two major sites Thr308 and Ser473. Akt negatively regulates activation of NF-κB and MAPKs. At the same time, DTPs activate LXRαβ (31) impairing NF-κB transactivation (53).

Supplemental figures

Supplemental figure 1. ***Functional KEGG analysis of LPS vs. DTP1+LPS shows association between down-regulated genes and inflammation-related pathways.*** Ranked list metric of TLR signaling pathway. LPSR and DTP1+LPSR are biological replicates of LPS and DTP1+LPS, respectively. Some genes were confirmed by qRT-PCR using DTP5 instead of DTP1.

Supplemental figure 2. ***Transrepression profile by activated nuclear receptors and DTP1***. The transrepression activity of DTP1 was compared with that of activated GR, LXR and PPARγ using GSEA and the genesets defined by Ogawa et al. (47). Target genes of GR, LXR and PPARγ resulted to be significantly enriched in the down-regulated part of the list, with an important overlapping in transrepressed genes (A). Genesets representation of target genes specific for each nuclear receptor

after GSEA analysis (B). Genesets enrichment after activation of LXR, GR and PPARγ (C,D,E). For DTP1-specific genesets see supplemental Fig. 1.

****

Abbreviations

COX-2, Cyclooxygenase-2; DEG, Differentially Expressed Gen, D-Gal, D-Galactosamine; DKO, double *knockout;* DMSO, dimethyl sulfoxide; DTP, diterpene; EMSA, Electrophoretic Mobility Shift Assay; ERK, extracellular signal regulated-kinase; FDR, False Discovery Rates; GSEA, Gene Set Enrichment Analysis; HTRF, Homogeneous Time-Resolved Fluorescence; IFNγ, Interferon γ; IKK, IκB kinase; IL-1β/6/10/12, Interleukin-1β/6/10/12; Ind., Indomethacin; i.p., intraperitoneal; IP-10/CXCL10, Chemokine (C-X-C motif) ligand 10; IRF3, *Interferon regulatory factor 3;* JNK, c-Jun N-terminal kinase; KC/CXCL1, Chemokine (C-X-C motif) ligand 1; KD, kinase deficient; LPS, Lipopolysaccharide; KO, *knockout*; LTA, Lipoteichoic Acid; LXR, liver X *receptor*; MAPK, Mitogen-Activated Protein Kinase; MPO, myeloperoxidase; MyD88, Myeloid Differentiation factor 88; NF-κB, *nuclear factor kappa B*; NIK, NF-κB inducing kinase; NO, nitric oxide; NOS-2, Nitric Oxide Synthase-2; NRF2, NF-E2- (nuclear factor erythroid-derived 2) related factor-2; PIP2, phosphatidylinositol 4,5-bisphosphate; PI3K, Phosphatidylinositol 3-Kinase; polyI·C, polyriboinosinic:polyribocytidylic acid; PVDF, Polyvinylidene Fluoride; qRT-PCR, Quantitative Real-Time (RT) Polymerase *Chain Reaction* (PCR); RT, room temperature; SDS-PAGE, Sodium Dodecyl Sulphate Polyacrylamide gel electophoresis; TIR, Toll/Interleukin-1 receptor; TLC, *thin layer chromatography;* TLRs, Toll-Like Receptors; TNF-α, Tumor Necrosis Factor-α; TPA, tetradecanoylphorbol acetate; TRIF, TIR domain-containing adapter-inducing IFNβ; WT, wild-type.

1. Bremner, P., and M. Heinrich. 2002. Natural products as targeted modulators of the nuclear factor- k B pathway. *J.Pharm.Pharmacol.* 54:453-472.
2. de las Heras, B., B. Rodriguez, L. Bosca, and A. M. Villar. 2003. Terpenoids: sources, structure elucidation and therapeutic potential in inflammation. *Curr.Top.Med.Chem.* 3:171-185.
3. Wang, C. Y., M. W. Mayo, R. G. Korneluk, D. V. Goeddel, and A. S. Baldwin, Jr. 1998. NF- k B antiapoptosis: induction of TRAF1 and TRAF2 and c-IAP1 and c-IAP2 to suppress caspase-8 activation. *Science* 281:1680-1683.
4. Castrillo, A., B. de las Heras, S. Hortelano, B. Rodriguez, A. Villar, and L. Bosca. 2001. Inhibition of the nuclear factor k B (NF- k B) pathway by tetracyclic kaurene diterpenes in macrophages. Specific effects on NF- k B-inducing kinase activity and on the coordinate activation of ERK and p38 MAPK. *J.Biol.Chem.* 276:15854-15860.
5. de las Heras, B., S. Hortelano, N. Giron, P. Bermejo, B. Rodriguez, and L. Bosca. 2007. Kaurane diterpenes protect against apoptosis and inhibition of phagocytosis in activated macrophages. *Br J Pharmacol* 152:249-255.
6. de las Heras, B., A. Navarro, M. J. Diaz-Guerra, P. Bermejo, A. Castrillo, L. Bosca, and A. Villar. 1999. Inhibition of NOS-2 expression in macrophages through the inactivation of NF- k B by andalusol. *Br.J.Pharmacol.* 128:605-612.
7. Helliwell, C. A., A. Poole, W. J. Peacock, and E. S. Dennis. 1999. Arabidopsis ent-kaurene oxidase catalyzes three steps of gibberellin biosynthesis. *Plant Physiol* 119:507-510.
8. Kang, H. S., Y. H. Kim, C. S. Lee, J. J. Lee, I. Choi, and K. H. Pyun. 1996. Suppression of interleukin-1 and tumor necrosis factor-à production by acanthoic acid, (-)-pimara-9(11),15-dien-19-oic acid, and it antifibrotic effects in vivo. *Cell Immunol.* 170:212-221.
9. Nan, J. X., X. J. Jin, L. H. Lian, X. F. Cai, Y. Z. Jiang, H. R. Jin, and J. J. Lee. 2008. A diterpenoid acanthoic acid from Acanthopanax koreanum protects against D-galactosamine/lipopolysaccharide-induced fulminant hepatic failure in mice. *Biol Pharm Bull* 31:738-742.
10. Pozarowski, P., D. H. Halicka, and Z. Darzynkiewicz. 2003. Cell cycle effects and caspase-dependent and independent death of HL-60 and Jurkat cells treated with the inhibitor of NF- k B parthenolide. *Cell Cycle* 2:377-383.
11. Liby, K. T., M. M. Yore, and M. B. Sporn. 2007. Triterpenoids and rexinoids as multifunctional agents for the prevention and treatment of cancer. *Nat Rev Cancer* 7:357-369.
12. Ghantous, A., H. Gali-Muhtasib, H. Vuorela, N. A. Saliba, and N. Darwiche. What made sesquiterpene lactones reach cancer clinical trials? *Drug Discov Today* 15:668-678.
13. Garantziotis, S., J. W. Hollingsworth, A. K. Zaas, and D. A. Schwartz. 2008. The effect of toll-like receptors and toll-like receptor genetics in human disease. *Annu Rev Med* 59:343-359.
14. Trinchieri, G., and A. Sher. 2007. Cooperation of Toll-like receptor signals in innate immune defence. *Nat Rev Immunol* 7:179-190.
15. O'Neill, L. A., and A. G. Bowie. 2007. The family of five: TIR-domain-containing adaptors in Toll-like receptor signalling. *Nat Rev Immunol* 7:353-364.
16. Katso, R., K. Okkenhaug, K. Ahmadi, S. White, J. Timms, and M. D. Waterfield. 2001. Cellular function of phosphoinositide 3-kinases: implications for development, homeostasis, and cancer. *Annu Rev Cell Dev Biol* 17:615-675.

17. Arbibe, L., J. P. Mira, N. Teusch, L. Kline, M. Guha, N. Mackman, P. J. Godowski, R. J. Ulevitch, and U. G. Knaus. 2000. Toll-like receptor 2-mediated NF-kappa B activation requires a Rac1-dependent pathway. *Nat Immunol* 1:533-540.
18. Sarkar, S. N., K. L. Peters, C. P. Elco, S. Sakamoto, S. Pal, and G. C. Sen. 2004. Novel roles of TLR3 tyrosine phosphorylation and PI3 kinase in double-stranded RNA signaling. *Nat Struct Mol Biol* 11:1060-1067.
19. Franke, T. F., S. I. Yang, T. O. Chan, K. Datta, A. Kazlauskas, D. K. Morrison, D. R. Kaplan, and P. N. Tsichlis. 1995. The protein kinase encoded by the Akt proto-oncogene is a target of the PDGF-activated phosphatidylinositol 3-kinase. *Cell* 81:727-736.
20. Aksoy, E., W. Vanden Berghe, S. Detienne, Z. Amraoui, K. A. Fitzgerald, G. Haegeman, M. Goldman, and F. Willems. 2005. Inhibition of phosphoinositide 3-kinase enhances TRIF-dependent NF-kappa B activation and IFN-beta synthesis downstream of Toll-like receptor 3 and 4. *Eur J Immunol* 35:2200-2209.
21. van Dop, W. A., S. Marengo, A. A. te Velde, E. Ciraolo, I. Franco, F. J. ten Kate, G. E. Boeckxstaens, J. C. Hardwick, D. W. Hommes, E. Hirsch, and G. R. van den Brink. The absence of functional PI3Kgamma prevents leukocyte recruitment and ameliorates DSS-induced colitis in mice. *Immunol Lett* 131:33-39.
22. Diaz-Guerra, M. J., A. Castrillo, P. Martin-Sanz, and L. Bosca. 1999. Negative regulation by phosphatidylinositol 3-kinase of inducible nitric oxide synthase expression in macrophages. *J Immunol* 162:6184-6190.
23. Guha, M., and N. Mackman. 2002. The phosphatidylinositol 3-kinase-Akt pathway limits lipopolysaccharide activation of signaling pathways and expression of inflammatory mediators in human monocytic cells. *J Biol Chem* 277:32124-32132.
24. Chaurasia, B., J. Mauer, L. Koch, J. Goldau, A. S. Kock, and J. C. Bruning. Phosphoinositide-dependent kinase 1 provides negative feedback inhibition to Toll-like receptor-mediated NF-kappaB activation in macrophages. *Mol Cell Biol* 30:4354-4366.
25. Medina, E. A., I. R. Morris, and M. T. Berton. Phosphatidylinositol 3-kinase activation attenuates the TLR2-mediated macrophage proinflammatory cytokine response to Francisella tularensis live vaccine strain. *J Immunol* 185:7562-7572.
26. Kim, J. A., D. K. Kim, T. Jin, O. H. Kang, Y. A. Choi, S. C. Choi, T. H. Kim, Y. H. Nah, S. J. Choi, Y. H. Kim, K. H. Bae, and Y. M. Lee. 2004. Acanthoic acid inhibits IL-8 production via MAPKs and NF- k B in a TNF-à-stimulated human intestinal epithelial cell line. *Clin.Chim.Acta* 342:193-202.
27. Kim, Y. H., B. S. Chung, and U. Sankawa. 1988. Pimaradiene diterpenes from Acanthopanax koreanum. *J.Nat.Prod.* 51 1080-1083.
28. Lam, T., T. Ling, C. Chowdhury, T. H. Chao, F. R. Bahjat, G. K. Lloyd, L. L. Moldawer, M. A. Palladino, and E. A. Theodorakis. 2003. Synthesis of a novel family of diterpenes and their evaluation as anti-inflammatory agents. *Bioorg.Med.Chem.Lett.* 13:3217-3221.
29. Park, E. J., Y. Z. Zhao, Y. H. Kim, J. J. Lee, and D. H. Sohn. 2004. Acanthoic acid from Acanthopanax koreanum protects against liver injury induced by tert-butyl hydroperoxide or carbon tetrachloride in vitro and in vivo. *Planta Med.* 70:321-327.
30. Chao, T. H., T. Lam, B. G. Vong, P. G. Traves, S. Hortelano, C. Chowdhury, F. R. Bahjat, G. K. Lloyd, L. L. Moldawer, L. Bosca, M. A. Palladino, and E. A. Theodorakis. 2005. A new family of synthetic diterpenes that regulates cytokine synthesis by inhibiting I k Bà phosphorylation. *Chembiochem.* 6:133-144.

31. Traves, P. G., S. Hortelano, M. Zeini, T. H. Chao, T. Lam, S. T. Neuteboom, E. A. Theodorakis, M. A. Palladino, A. Castrillo, and L. Bosca. 2007. Selective activation of liver X receptors by acanthoic acid-related diterpenes. *Mol Pharmacol* 71:1545-1553.
32. Adachi, O., T. Kawai, K. Takeda, M. Matsumoto, H. Tsutsui, M. Sakagami, K. Nakanishi, and S. Akira. 1998. Targeted disruption of the MyD88 gene results in loss of IL-1- and IL-18-mediated function. *Immunity* 9:143-150.
33. Sato, M., H. Suemori, N. Hata, M. Asagiri, K. Ogasawara, K. Nakao, T. Nakaya, M. Katsuki, S. Noguchi, N. Tanaka, and T. Taniguchi. 2000. Distinct and essential roles of transcription factors IRF-3 and IRF-7 in response to viruses for IFN-alpha/beta gene induction. *Immunity* 13:539-548.
34. Velasco, M., M. J. Diaz-Guerra, P. Diaz-Achirica, D. Andreu, L. Rivas, and L. Bosca. 1997. Macrophage triggering with cecropin A and melittin-derived peptides induces type II nitric oxide synthase expression. *J Immunol* 158:4437-4443.
35. Hortelano, S., P. G. Traves, M. Zeini, A. M. Alvarez, and L. Bosca. 2003. Sustained nitric oxide delivery delays nitric oxide-dependent apoptosis in macrophages: contribution to the physiological function of activated macrophages. *J Immunol* 171:6059-6064.
36. Rodriguez-Prados, J. C., P. G. Traves, J. Cuenca, D. Rico, J. Aragones, P. Martin-Sanz, M. Cascante, and L. Bosca. 2010. Substrate fate in activated macrophages: a comparison between innate, classic, and alternative activation. *J Immunol* 185:605-614.
37. Castrillo, A., P. G. Traves, P. Martin-Sanz, S. Parkinson, P. J. Parker, and L. Bosca. 2003. Potentiation of protein kinase C zeta activity by 15-deoxy-delta(12,14)-prostaglandin J(2) induces an imbalance between mitogen-activated protein kinases and NF-kappa B that promotes apoptosis in macrophages. *Mol Cell Biol* 23:1196-1208.
38. Castrillo, A., D. J. Pennington, F. Otto, P. J. Parker, M. J. Owen, and L. Bosca. 2001. Protein kinase Cî is required for macrophage activation and defense against bacterial infection. *J.Exp.Med.* 194:1231-1242.
39. Rossi, A., P. Kapahi, G. Natoli, T. Takahashi, Y. Chen, M. Karin, and M. G. Santoro. 2000. Anti-inflammatory cyclopentenone prostaglandins are direct inhibitors of I k B kinase. *Nature* 403:103-108.
40. Oliva, J. L., D. Perez-Sala, A. Castrillo, N. Martinez, F. J. Canada, L. Bosca, and J. M. Rojas. 2003. The cyclopentenone 15-deoxy- D 12,14-prostaglandin J2 binds to and activates H-Ras. *Proc.Natl.Acad.Sci.U.S.A* 100:4772-4777.
41. Navarro, A., H. B. de Las, and A. M. Villar. 1997. Andalusol, a diterpenoid with anti-inflammatory activity from Siderits foetens Clemen. *Z.Naturforsch.[C.]* 52:844-849.
42. Gentleman, R. C., V. J. Carey, D. M. Bates, B. Bolstad, M. Dettling, S. Dudoit, B. Ellis, L. Gautier, Y. Ge, J. Gentry, K. Hornik, T. Hothorn, W. Huber, S. Iacus, R. Irizarry, F. Leisch, C. Li, M. Maechler, A. J. Rossini, G. Sawitzki, C. Smith, G. Smyth, L. Tierney, J. Y. Yang, and J. Zhang. 2004. Bioconductor: open software development for computational biology and bioinformatics. *Genome Biol* 5:R80.
43. Smyth, G. K. 2005. Limma: linear models for microarray data. In: 'Bioinformatics and Computational Biology Solutions using R and Bioconductor'. R. Gentleman, V. Carey, S. Dudoit, R. Irizarry, W. Huber (eds), Springer, New York, pages 397-420.
44. Morrissey, E. R., and R. Diaz-Uriarte. 2009. Pomelo II: finding differentially expressed genes. *Nucleic Acids Res* 37:W581-586.
45. Al-Shahrour, F., P. Minguez, J. Tarraga, D. Montaner, E. Alloza, J. M. Vaquerizas, L. Conde, C. Blaschke, J. Vera, and J. Dopazo. 2006. BABELOMICS: a systems biology

perspective in the functional annotation of genome-scale experiments. *Nucleic Acids Res* 34:W472-476.

46. Tegner, J., R. Nilsson, V. B. Bajic, J. Bjorkegren, and T. Ravasi. 2006. Systems biology of innate immunity. *Cell Immunol* 244:105-109.
47. Ogawa, S., J. Lozach, C. Benner, G. Pascual, R. K. Tangirala, S. Westin, A. Hoffmann, S. Subramaniam, M. David, M. G. Rosenfeld, and C. K. Glass. 2005. Molecular determinants of crosstalk between nuclear receptors and toll-like receptors. *Cell* 122:707-721.
48. Russo, M. P., B. L. Bennett, A. M. Manning, D. A. Brenner, and C. Jobin. 2002. Differential requirement for NF- k B-inducing kinase in the induction of NF- k B by IL-1á, TNF-à, and Fas. *Am.J.Physiol Cell Physiol* 283:C347-C357.
49. Castrillo, A., M. Mojena, S. Hortelano, and L. Bosca. 2001. Peroxisome proliferator-activated receptor- g -independent inhibition of macrophage activation by the non-thiazolidinedione agonist L-796,449. Comparison with the effects of 15-deoxy- D (12,14)-prostaglandin J(2). *J.Biol.Chem.* 276:34082-34088.
50. Fukao, T., and S. Koyasu. 2003. PI3K and negative regulation of TLR signaling. *Trends Immunol* 24:358-363.
51. Hazeki, K., K. Nigorikawa, and O. Hazeki. 2007. Role of phosphoinositide 3-kinase in innate immunity. *Biol Pharm Bull* 30:1617-1623.
52. Ruse, M., and U. G. Knaus. 2006. New players in TLR-mediated innate immunity: PI3K and small Rho GTPases. *Immunol Res* 34:33-48.
53. Glass, C. K., and S. Ogawa. 2006. Combinatorial roles of nuclear receptors in inflammation and immunity. *Nat Rev Immunol* 6:44-55.

Neurobiology:

The Specificity Protein Factor Sp1 Mediates Transcriptional Regulation of P2X7 Receptors in the Nervous System

Paula García-Huerta, Miguel Díaz-Hernandez, Esmerilda G. Delicado, María Pimentel-Santillana, Mª Teresa Miras-Portugal and Rosa Gómez-Villafuertes

J. Biol. Chem. 2012, 287:44628-44644.
doi: 10.1074/jbc.M112.390971 originally published online November 8, 2012

THE JOURNAL OF BIOLOGICAL CHEMISTRY VOL. 287, NO. 53, pp. 44628–44644, December 28, 2012

The Specificity Protein Factor Sp1 Mediates Transcriptional Regulation of P2X7 Receptors in the Nervous System*

Received for publication, June 12, 2012, and in revised form, November 7, 2012 Published, JBC Papers in Press, November 8, 2012, DOI 10.1074/jbc.M112.390971

Paula García-Huerta[‡§¶1], Miguel Díaz-Hernandez[‡§¶], Esmerilda G. Delicado[‡§¶], María Pimentel-Santillana[‖], Mª Teresa Miras-Portugal[‡§¶], and Rosa Gómez-Villafuertes[‡§¶2]

From the [‡]Departamento de Bioquímica y Biología Molecular and [§]Instituto Universitario de Investigación en Neuroquímica, Universidad Complutense de Madrid, 28040 Madrid, Spain, [¶]Instituto de Investigación Sanitaria del Hospital Clínico San Carlos, 28040 Madrid, Spain, and [‖]Instituto de Investigaciones Biomédicas Alberto Sols, Consejo Superior de Investigaciones Científicas-Universidad Autonoma de Madrid, 28029 Madrid, Spain

Background: Purinergic P2X7 receptors regulate proliferation, differentiation, and cell death in both the CNS and non-CNS tissues.
Results: Sp1 factor activates the *P2rx7* promoter. This regulation is abolished by SP1 binding sites mutation, Sp1 knockdown, and mithramycin A treatment.
Conclusion: Sp1 regulates the expression of P2X7 receptor.
Significance: Learning how P2X7 expression is controlled is crucial for understanding P2X7-mediated brain processes in health and disease.

P2X7 receptors are involved not only in physiological functions but also in pathological brain processes. Although an increasing number of findings indicate that altered receptor expression has a causative role in neurodegenerative diseases and cancer, little is known about how expression of *P2rx7* gene is controlled. Here we reported the first molecular and functional evidence that Specificity protein 1 (Sp1) transcription factor plays a pivotal role in the transcriptional regulation of P2X7 receptor. We delimited a minimal region in the murine *P2rx7* promoter containing four SP1 sites, two of them being highly conserved in mammals. The functionality of these SP1 sites was confirmed by site-directed mutagenesis and Sp1 overexpression/down-regulation in neuroblastoma cells. Inhibition of Sp1-mediated transcriptional activation by mithramycin A reduced endogenous P2X7 receptor levels in primary cultures of cortical neurons and astrocytes. Using *P2rx7*-EGFP transgenic mice that express enhanced green fluorescent protein under the control of *P2rx7* promoter, we found a high correlation between reporter expression and Sp1 levels in the brain, demonstrating that Sp1 is a key element in the transcriptional regulation of P2X7 receptor in the nervous system. Finally, we found that Sp1 mediates P2X7 receptor up-regulation in neuroblastoma cells cultured in the absence of serum, a condition that enhances chromatin accessibility and facilitates the exposure of SP1 binding sites.

Purinergic P2X7 receptor belongs to the family of ATP-gated cation channels that mediate a non-selective cation conductance when activated by an appropriate ligand. Currently, seven different P2X subunits (P2X1-P2X7) and various splice variants have been molecularly identified in mammals, with P2X7 receptor being the most divergent member of this family in terms of molecular structure, pharmacology, and function (1). The P2X7 receptor forms trimeric complexes of identical subunits in the plasma membrane and is unable to oligomerize with other P2X receptors (2). Although its structure is basically similar to other P2X receptor subunits, having two transmembrane domains and a large extracellular loop, the intracellular carboxyl terminal domain of P2X7 receptor is much longer (239 amino acids) (3). Within the P2X family, the P2X7 receptor has a distinguished role in the central nervous system (CNS) for its implication in several biological tasks such as learning and memory, circadian rhythms, mood, and motivation (4). In the last years the knowledge about the role of P2X7 receptors in the CNS, in terms of intracellular pathways coupled to its activation, has been noticeably improved. Thus, P2X7 receptors induce calcium/calmodulin-dependent protein kinase II phosphorylation in cerebellar granule neurons (5) and are also coupled to GSK-3 inhibition and neuroprotection in the same neuronal model (6). Moreover, calcium/calmodulin-dependent kinase II signaling cascade mediates P2X7 receptor-dependent inhibition of axonal growth and branching in hippocampal neurons and neuroblastoma cells (7, 8). P2X7 receptors seem to be involved not only in physiological functions but also in a variety of pathological brain processes, where the functional expression level of P2X7 receptor seems to be crucial. This has been highlighted by an increasing number of findings that aberrant or altered receptor expression and function have a causative role in neurodegenerative diseases, mood disorders, and neuropathic pain (4, 9–12). In addition, P2X7 receptor is highly expressed in a variety of human neuroblastoma cells from either primary tumors or cell lines, and its activation increases the proliferation and growth of the tumors (13, 14). Altogether, these evidences point to P2X7 receptor as an appealing target

* This work was supported by the Ministry of Science and Innovation (BFU2008-02699 and BFU2011-24743), the Spanish Ion Channel Initiative (CSD2008-00005), and the Marcelino Botín Foundation.
⌘ *Author's Choice*—Final version full access.
[1] Supported by a fellowship from Spanish Education Ministry.
[2] Supported by Spanish Ion Channel Initiative. To whom correspondence should be addressed: Departamento de Bioquímica y Biología Molecular, Facultad de Veterinaria, Universidad Complutense de Madrid, Avda. Puerta de Hierro s/n, 28040 Madrid, Spain. Tel.: 34-913943890; Fax: 34-913943909; E-mail: marosa@vet.ucm.es.

for pharmacological intervention; however, little is known about the transcriptional regulation of P2X7 receptor expression in the CNS.

The gene encoding P2X7 subunit was initially cloned from a rat brain cDNA library (15) and afterward was identified in many other mammalian and non-mammalian species including human and mouse (16, 17). There are more than 815 single nucleotide polymorphisms (SNPs)[3] that have been described in the human *P2RX7* gene, but only a few of them have been functionally characterized to cause either loss or gain of receptor function (18–26). Interestingly, five SNPs have been identified upstream of exon 1 of P2RX7 gene, although none of them has been associated with a specific ATP response phenotype at the moment (27). First studies reported P2X7 promoter activity within a 2-kb DNA segment of the 5′ of the gene (28). Afterward, the active promoter of the human *P2RX7* gene was located in the −158/+32-nucleotide region surrounding the transcription start site, although the transcription factors involved in the promoter activity were unknown (29). To further characterize the molecular mechanisms underlying transcriptional regulation of P2X7 receptor, we cloned and functionally identified the active promoter of the murine *P2rx7* gene. We found that *P2rx7* gene promoter region lacks TATA and CAAT boxes and contains seven putative motifs for the Specificity protein 1 (Sp1) family of transcription factors, with at least two of them fully functional and conserved between species. Using interference and overexpression experiments, we demonstrate that Sp1 up-regulates endogenous P2X7 mRNA and protein levels in neuroblastoma Neuro-2a (N2a) cells. Mithramycin A, an inhibitor of Sp1-mediated transcriptional activation, decreases *P2rx7* gene expression in N2a neuroblastoma cells, primary cultures of mouse cortical neurons and astrocytes, and macrophages. Moreover, using *P2rx7*-EGFP transgenic mice that express enhanced green fluorescent protein (EGFP) under the control of *P2rx7* promoter, we observed that most cells expressing P2X7 receptors in the brain of newborn mice also contain high amounts of Sp1 factor. We also described that Sp1 mediates up-regulation of P2X7 receptor expression under serum deprivation, a condition that has been previously reported to enhance open chromatin accessibility, facilitating exposure of SP1 binding sites.

EXPERIMENTAL PROCEDURES

Antibodies and Chemicals—Antibodies used in the study were Sp1 (Merck, catalog #07-645), P2X7 receptor intracellular epitope (Alomone Laboratories, catalog #PR-004), GAPDH (Ambion, catalog #AM4300), NeuN (Chemicon International, catalog #MAB377), GFAP (Santa Cruz Biotechnology, catalog #sc-9065), and Iba1 (Wako, catalog #019-19741). Horseradish peroxidase-conjugated secondary antibodies were from Dako. Cy3™-conjugated donkey anti-rabbit IgG was from Jackson ImmunoResearch. Penicillin, streptomycin, kanamycin, amphotericin, and Glutamax® were from Invitrogen. All other chemicals were from Sigma.

[3] The abbreviations used are: SNPs, single nucleotide polymorphisms; EGFP, EGF protein; N2a, Neuro-2a cells; Q-PCR, quantitative real time-PCR; Sp1, Specificity protein 1, TSS, transcription start site; ANOVA, analysis of variance.

Genomic Cloning of the Mouse P2rx7 Gene and Construction of Several Deletion Reporter Plasmids—A PCR-based technique was used to clone a 3450-kb fragment of the mouse *P2rx7* gene 5′-flanking region ranging from −3212 bp upstream to +220 bp downstream of the transcription start site (TSS). Sense and antisense oligonucleotides (5′-TGTTACGGCTGCATAGTCTGTCCT-3′ and 5′-GGATCCGGGTGACTTTGTTTGTCT-3′, respectively) were chosen from genomic sequence of the mouse *P2rx7* gene. The putative TSS designated as +1 was obtained from the mRNA sequences available in GenBank™ corresponding to the transcript variants 1, 2, 3, and 4 (accession nos. NM_011027, NM_001038845, NM_001038839, and NM_001038887, respectively). The 3450-kb genomic fragment was isolated by PCR amplification from mouse genomic DNA using PfuUltra™ Hotstart DNA polymerase (Stratagene). Genomic DNA (extracted from neuroblastoma N2a) was obtained with DNeasy Blood & Tissue (Qiagen) following the manufacturer's instructions. Afterward, genomic fragment was adenylated and cloned in the pGEM-T® Easy vector (Promega) and subjected to double-strand DNA sequencing. A set of truncated constructs was then generated by sequential deletions of the 5′ end by PCR (Fig. 2*A*). Different forward primers bearing a XhoI site and several antisense oligonucleotides bearing a HindIII site at the 5′ end were used for direct cloning into pGL4.23 firefly luciferase reporter vector (Promega). Deletion plasmids were confirmed by sequencing and restriction enzyme digestion. Primer nucleotide sequences are listed in Table 1.

Site-directed Mutagenesis—To assess whether SP1c and SP1d binding sites were responsible for the transcriptional activation of *P2rx7* promoter, mutation of SP1c and SP1d sites was performed by PCR site-directed mutagenesis using pP2X7-F2 and pP2X7-F3 as a template, respectively. PCR was followed by DpnI digestion (QuikChange XL, Stratagene). The designed primers (SP1c-mut forward (fw) 5′-GGAGGCTAGCGGGGCTTGGTCATCTGCCAGCC-3′, SP1c-mut reverse (rv) 5′-GGCTGGCAGATGACCAAGCCCCGCTAGCCTCC-3′, SP1d-mut fw 5′-GTTGCCAGGACCCGCAACCGCTGCAGTCACTGG-3′ and SP1d-mut rv 5′-CCAGTGACTGCAGCGGTTGCGGGTCCTGGCAAC-3′) replace two nucleotides of each SP1 binding site (mutated nucleotides underlined).

Animals, Cell Culture, and Transfection—All animal procedures were carried out at the Universidad Complutense de Madrid in accordance with European and Spanish regulations (86/609/CEE; RD1201/2005) following the guidelines of the International Council for the Laboratory Animal Science. Male or female C57B1/6J mice were used at different development stages (E18 mouse embryos for neuronal cultures and P0-P1 postnatal day old pups for astrocyte cultures). *P2rx7*-EGFP reporter mice that express EGFP immediately downstream of the *P2rx7* promoter were obtained from United States National Institutes of Health Mutant Mouse Regional Resource Centers (stock 011959-UCD) (30) and were granted by Dr. M. Nedergaard (University of Rochester Medical School, Rochester, NY).

Primary cultures of cortical neurons and astrocytes were prepared as previously described (31). Briefly, the cortex was dissected and dissociated using the Papain Dissociation System (Worthington Biochemical, Lakewood, NJ). For neuronal cultures, cells were plated at a density of 200,000 cells/cm^2 on

TABLE 1
Oligonucleotide primers used to obtain luciferase reporter plasmids
fw, forward; rv, reverse.

Fragment name	Oligonucleotides used to amplified each fragment	Fragment size
		bp
A	fw, 5'-GGTTTGGAAATCAGGCAGCTAG-3' rv, 5'-CGATTGAAGCTTGGTGACTTTGTTTGTCT-3'	2332
B	fw, 5'-GTGCTGGCTAGAGAGGGCTACA-3' rv, 5'-CGATTGAAGCTTGGTGACTTTGTTTGTCT-3'	1795
C	fw, 5'-GTGGTCCCTCGCAACTATAGTC-3' rv, 5'-CGATTGAAGCTTGGTGACTTTGTTTGTCT-3'	1256
D	fw, 5'-GATAATCTCTGTGGGGTGCGGT-3' rv, 5'-CGATTGAAGCTTGGTGACTTTGTTTGTCT-3'	670
E	fw, 5'-GATAATCTCTGTGGGGTGCGGT-3' rv, 5'-CATTAAGCTTGTTGCCTGTTTGAGACCTGTTC-3'	150
F	fw, 5'-GCAGCTCGAGCATCTAGGCCCTTGTCTGAG- 3' rv, 5'-CGATTGAAGCTTGGTGACTTTGTTTGTCT-3'	468
G	fw, 5'-CGCCCTCGAGGCAGTCACTGGAGGAACTGGAAG-3' rv, 5'-CGATTGAAGCTTGGTGACTTTGTTTGTCT-3'	203
F1	fw, 5'-GCAGCTCGAGCATCTAGGCCCTTGTCTGAG-3' rv, 5'-TTAAAAGCTTCCCTCCCCACCCCCTTTCCTTG-3'	110
F2	fw, 5'-AGGACTCGAGGTGGGGAGGGGGAATTTTAAAAATG-3' rv, 5'-CAAGAAGCTTGTCCTACAGGCCTGGCTGGCAG-3'	107
F3	fw, 5'-GCCACTCGAGCCTGTAGGACTTGGTTCTTG-3' rv, 5'-TTCTAAGCTTGAACGGTTAACTTCCAGTTC-3'	100

6-well plates coated with 10 μg/ml poly-L-lysine (Biochrom AG) and 3 μg/ml laminin. After plating, neurons were cultured for 24 h in Neurobasal medium supplemented with 1% B-27 (both from Invitrogen), 0.5 mM glutamine, 1 mM pyruvate, 100 units/ml penicillin, and 100 μg/ml streptomycin. For astrocyte cultures, cells were plated onto culture flasks (~100,000 cells/cm^2) and grown until confluence in DMEM supplemented with 10% fetal bovine serum (FBS) (EuroClone), 50 units/ml penicillin, 50 μg/ml streptomycin, 100 μg/ml kanamycin, and 2.5 μg/ml amphotericin. Afterward, astrocytes were trypsinized and plated on 6-well plates coated with poly-L-lysine at a density of 40,000 cells/cm^2. Microglial contamination of primary cultures of neurons and astrocytes was checked by Western blot using antibodies that recognize marker proteins for neurons, astrocytes, and microglial cells (NeuN, GFAP and Iba1, respectively). Macrophage cell line RAW264.7 and neuroblastoma cell line N2a were grown in DMEM supplemented with 10% FBS, Glutamax®, 100 units/ml penicillin, and 100 μg/ml streptomycin. Elicited peritoneal macrophages were obtained as previously described (32). Briefly, 60 h before the assay, 10-week-old mice were intraperitoneal injected with 2.5 ml of 3% thioglycolate broth. Afterward, mice were killed by cervical dislocation and injected intraperitoneally with 10 ml of sterile RPMI 1640 medium. The peritoneal fluid was carefully aspirated, avoiding hemorrhage, and kept at 4 °C to prevent the adhesion of the macrophages to the plastic. Spleens of the same animals were also harvested for immunohistochemical studies. Cells were washed twice with ice-cold PBS and seeded at 30,000 cells/cm^2 in RPMI 1640 medium supplemented with 10% of heat-inactivated FBS and antibiotics. After incubation for 3 h at 37 °C in a 5% CO_2 atmosphere, non-adherent cells were removed by extensive washing with PBS. All cell cultures were grown at 37 °C in humidified atmosphere containing 5% CO_2.

When appropriate, mithramycin A, a selective inhibitor of Sp1-mediated transcriptional activation, was assayed. Cells were treated 24 h after plating with 300 nM mithramycin A for 24–48 h and then lysed for either RNA or protein extraction. The stock solution of mithramycin A was prepared in methanol (vehicle) to a concentration of 1 mM. Control cells were treated with the same concentration of vehicle solution (final dilution factor higher than 1:3000). For serum withdrawal experiments, N2a cells were seeded on 6-well plates at a density of 75,000 cels/cm^2 for 24 h. Afterward, complete medium was changed to DMEM without serum, and cells remained 24, 48, or 72 h depending on each experiment. Transient transfections of plasmid DNAs were carried out using Lipofectamine™ 2000 (Invitrogen) following the manufacturer's instructions.

Luciferase Reporter Assay—Cell lines were plated on 24-well plates coated with poly-L-lysine the day before transfection (cells reached ~80% confluence the day of transfection). A mixture of 0.64 μg of pGL4.23-based constructs, and 0.16 μg of *Renilla* luciferase vector pGL4.74[hRluc/TK] were cotransfected into cells. The final DNA concentration in all experiments was preserved by the addition of empty expression vector when necessary. Cells were harvested after 24–48 h and assayed for luciferase activity. Firefly luciferase and *Renilla* luciferase activities were measured sequentially using the Dual-Luciferase Reporter Assay System (Promega). The firefly luciferase activity was normalized according to *Renilla* and expressed as relative luciferase units to reflect the promoter activity.

Sp1 Overexpression and Small Hairpin (shRNA) Transfection Experiments—The mouse Sp1 cDNA was amplified from the commercial plasmid pENTR223.1 (Source BioScience, Nottingham, UK) by using the oligonucleotides forward (5′-CTAGCTCGAGATGAGCGACCAAGATCACTC-3′) and reverse (5′-CTAGGAATTCTTAGAAACCATTGCCACTGA-3′). The amplified fragment was digested with XhoI and EcoRI enzymes and subcloned into the corresponding sites of pIRES-EGFP vector (Clontech Laboratories) for expression in mammalian cells. The ligation product was confirmed by sequencing. N2a cells and astrocytes were transiently transfected with 4 μg of DNA. After 6 h, the medium was removed, and cells were further incubated for the indicated time periods in culture medium. The parallel expression of EGFP from this vector allowed the identification of transfected cells by green fluorescence.

Sp1 knockdown was achieved by RNA interference using a vector-based shRNA approach (pRFP-C-RS vector, OriGene). The shRNA target sequences used were: shSP1.1 (5′-CCTTGCTACCTGTCAACAGCGTTTCTGCA-3′) and shSP1.2 (5′-AGGACAGACTCAGTATGTGACCAATGTAC-3′). To specifically rule out the potential nonspecific effect induced by expression of the shRNAs, control cells were transfected with a scrambled negative control non-effective shRNA (5′-GCACTACCAGAGCTAACTCAGATAGTACT-3′) (OriGene). N2a cells were transiently transfected with 4 μg of DNA. After 6 h the medium was removed, and cells were further incubated for the indicated time periods in culture medium. The concomitant expression of RFP from these vectors allowed transfected cells to be identified by red fluorescence.

Quantitative Real Time-PCR (Q-PCR)—Total RNA was extracted from cultured cells using RNeasy® plus mini kit (Qiagen) following the manufacturer's instructions. After digestion with TURBO DNase (Ambion), total RNA was quantified and reverse-transcribed using M-MLV reverse transcriptase, 6 μg of random primers, and 350 μM dNTPs (Invitrogen). Q-PCRs were performed using gene-specific primers and Taqman MGB probes for mouse P2X7, Sp1, and GAPDH (all from Applied Biosystems). Fast thermal cycling was performed using a StepOnePlus® Real-Time System (Applied Biosystems) as follows: denaturation, 1 cycle of 95 °C for 20 s followed by 40 cycles each of 95 °C for 1 s and 60 °C for 20 s. The results were normalized as indicated by parallel amplification of GAPDH.

Western Blot—Cells were lysed and homogenized for 1 h at 4 °C in lysis buffer containing 50 mM Tris/HCl, 150 mM NaCl, 1% Nonidet P40, and Complete™ Protease Inhibitor Mixture Tablets (Roche Diagnostics), pH 7.4. Separation of the proteins (50 μg of total protein/well) was performed on 8% SDS-PAGE gels. Proteins were transferred to nitrocellulose transfer membrane (PROTRAN®, Whatman GmbH), saturated for 1 h at room temperature with 5% nonfat dried milk in 0.1% TBS/Tween, and incubated overnight at 4 °C with the following commercial primary antibodies: anti-Sp1 (1:1000, 95–105 kDa) (33), anti-P2X7 receptor (1:1000, 75 kDa) (8), anti-GAPDH (1:5000, 37 kDa) (34), anti-NeuN (1:1000, 46, 48, and 66 kDa) (10), anti-GFAP (1:200, 50 kDa) (34), and anti-Iba1 (1:1000, 17 kDa) (10). Proteins were visualized by chemiluminescence using the ECL Chemiluminescence (Amersham Biosciences GE Healthcare), and quantified using ImageJ free software (National Institutes of Health).

Immunocytochemical and Immunohistochemical Studies—Cells cultured on coverslips placed in 35-mm dishes (250,000 cells per well) were washed with PBS and fixed with 4% paraformaldehyde for 15 min. After washing with PBS, cells were permeabilized with 0.1% Triton X-100 and blocked with 5% goat serum and 10% FBS for 1 h at room temperature. After washing with 3% BSA in PBS, cells were incubated for 1 h with primary antibodies against either P2X7 receptor (1:200), Sp1 (1:200), or CD11 (1:200). Afterward, cells were washed with PBS and incubated for 1 h with Cy3™ secondary antibody. Nuclei were counterstained with DAPI (Invitrogen). Coverslips were mounted on glass slides using FluoroSave™ Reagent (Calbiochem). For immunohistochemical studies, brains from P0 postnatal-day-old pups and spleens from 10-week-old mice were harvested and fixed in 4% paraformaldehyde for 48 h at 4 °C and cryoprotected in sucrose before sectioning. Sections were pretreated with Sudan black B, 1% BSA, and 1% Triton X-100 in PBS followed by incubation with the primary antibody anti-Sp1 when indicated. Sections were washed again and incubated with secondary antibody coupled to Cy3™ when necessary. Sections were also treated with DAPI and then coverslipped with FluoroSave™ reagent. Confocal images were acquired with a TCS SPE microscope from Leica Microsystems (Wetzlar, Germany).

Statistical Analysis—Data were analyzed using one way ANOVA with the post hoc Newman-Keuls test or, for two-group comparisons, Student's *t* test (Graph Pad Prism 5, Graph Pad Software Inc., San Diego, CA). Data are expressed as the mean ± S.E. Differences were considered significant at $p \leq 0.05$.

RESULTS

P2rx7 Gene Promoter Lacks TATA/CAAT Boxes and Has Multiple Sp1 Motifs—The murine *P2rx7* gene codifies for at least 5 transcript variants named 1, 2, 3, 4, and *k* (35). To characterize the minimal *P2rx7* promoter region involved in the regulation of *P2rx7* gene expression, we cloned a 2334-bp fragment of the 5′-flanking region of the gene from mouse genomic DNA. This fragment corresponds to positions −2114 to +220 bp relative to the TSS. The putative TSS was designated as +1 and was obtained from the mRNA sequences available in GenBank™ corresponding to the transcript variants 1, 2, 3, and 4 (accession nos. NM_011027, NM_001038845, NM_001038839, and NM_001038887, respectively). A computer-based transcription binding site search using the Genomatix MatInspector software reveals that this 5′-proximal regulatory region lacks TATA and CAAT boxes and contains seven putative motifs for the Sp1 family of transcription factors (Fig. 1*A*). All of these sites have a very high similarity with the theoretical matrix (score >0.85) and are located in both strands: forward strand (sites −1457/−1441, −281/-265, −155/−139, −150/−134, and −79/−63 bp) and reverse strand (−1/+16 and +131/+147 bp) (Table 2). Interestingly, most putative SP1 sites were located close to the TSS, suggesting the implication of Sp1 family of transcription factors as potential key regulators for *P2rx7* gene expression. Methylation degree of CpG islands contained within the SP1 consensus elements may interfere with the binding of Sp1 to DNA, modulating the Sp1-dependent transcription of genes (36). Using CpGPlot software, the presence of CpG islands at the 5′-proximal regulatory region of the murine *P2rx7* gene was analyzed based on two basic parameters: a CG percentage higher than 50% and a ratio of observed-to-expected higher than 0.6 (Fig. 1*B*). Bioinformatics analysis showed that murine *P2rx7* promoter lacks CpG islands, discarding that methylation of SP1 sites located into the promoter region could be interfering Sp1 binding to DNA.

In addition, the 5′-flanking sequence of *P2rx7* promoter contains other putative regulatory elements including four motifs for AP1 (activator protein 1), one CREB (c-AMP-responsive element-binding proteins) binding element, one E-box binding site, one HIF (hypoxia-inducible factor) motif, three STAT (signal transducer and activator of transcription) binding elements,

A

```
-2114                                                                                                  5′- AGGTTTGGAAATCA
                                                  YY1F                                  TCF/LEF1
-2100 GGCAGCTAGCCCTCTAGTTCTACCCACTAGACTTTACTGCTCTAATGGAAGCCCTTTGGCCTACTATTTGTTACATTCATCTTTGGTGTGTGTGTGTG
-2000 TGTGTGTGTAGCTTGCGTGACCACCTGTGCATATTTGTGCACAGTTTTAATGGAGTCAGTTCTCTCCAAGTATTCGGGTCCTGGGGACCGAACTCAGGTC
                                  CREB
-1900 ATCAGGCTTGATGGCACCTTCGTCATCTCACTGGTCCCATTTATTGAAGGTTACTGTACTCCTCCGAGTTTTGAAAGAGTAGCGACAAAGGTCAGGGCAG
-1800 AGTTAAGAGAAAGCGGTAAGAGTGTGCTGGCTAGGGGCTGGCGAGATGGCTCAGTGGTTAAGAGCGCCGTCTGCTTTTCCAAAGGTCCCGAGTTCAAATC
                E-box
-1700 CGAGCAACCACATGGTGGCTCACAACTATCCGTAACGAGATCTGATGCCCTCTTCTGGAGTATCTGAGGACAGCTATAGTGTACTTACATATAATAAATA
-1600 AATAAATGTTCAAAAAAAAAAAGTGTGCTGGCTAGAGAGGGCTACAGAGGGAAGCCCTTACCCCTCCGGGGCCTCCCGAGTAAACAGAGAGGGTTGGGAG
                                  SP1
-1500 ACGCATCTAGCATCACTGCCTTCTAGTCCCTTGAACTGGAGCCAACAGGGGCAGGGGCCTTTGATGTAGATCATAAGGAGGAGAAAGTACAAATTAAGTTA
-1400 GGCTGGAAACATGTAAGTCTGCCTGGCCCATAATGCAGCAGGCAAGACAGCAGTAGGTTGGGATGCTTGCGGGGAGATGGTTCTTTCTCCCTAGGGAGGG
                                                  STAT                                  STAT                HIFF
-1300 ATAACGCCTGAGTGACTGTTGCTTCCTTTCTCTAACGTCTAACATCCCACTTGTGCCTGGAAGATTCCAGGTCTCAGAGAAGCAGCAGCCATAGCCACGT
-1200 TAGGACAGAGCCTCAGACACCAGGCTCTGCAGGTGCCTCATTTGAGGACGATCGGGTCTTTATCACCCAGGACCACCGATCCACTGTGTAAACCGTGTGG
-1100 GAAAGGCCTGCTTTATACATCCTGCTTTCCTACAGCCTGTCGGAGCAGGGTTTCAGCCCTGGTGTGGTCCCTCGCAACTATAGTCCCAGAATTTGTGAGC
                                                                  AP1
-1000 TGGAGGTGTGGGAAAGATGAAGGCTTAAGGGTCAGTCTCAGCCTCACAGTAAGTTACAGAGAAGTCTGAGTTACACGAGACCCTGTCTCAAAACAAAACA
                                                                                                  STAT
 -900 AATAGAGAATAAAACAACAAAACCGCACAGCAAAAAAAAAAAAAAAAAAAAAAAAAAAAAATCAACCAAACAAGATTTCCTCTCAACTCCACCTTCCTCA
                                                                                                  TCF/LEF1
 -800 GAATTCTACAATGAGGCTACCTCTTCTACTATTTGGAGATAGCATTGGTCCTCTCTCATGAGGTGTCTCCATGGTCAGGAGGGATACTGGATGCAGCTTT
 -700 GTTCTTGGTGGTCTAGGACTGACTGGACCATGAGATGACCTCCCGGGTCCCGAGCAGGATGAAGTGTAGATGGAGGAGAGAGTGAGACAAGCGTGGATAT
                                  YY1F                                                            YY1F
 -600 AATCTTCCCATCCCACAATGAATCTGATCTGGCAGCCATCTTTGGCAGACCAGAGTATCCCGTGGAGCAGCGGAGGACAAAGATGCCATTCAGTCATCGG
                TCF/LEF1                TCF/LEF1
 -500 GTGCACCTGTACATGTGGACTGAACAAAGGGTTGTCCGGAAAACAAAGGGATAATCTCTGTGGGGTGCGGTGGGGCTCACCTATAATCCCAGCACTCGGG
                                  AP1             AP1
 -400 AGGTGGAGGCAGGAGGATCAGAAGTTCATAGCTAGCCTTGAGTGAGTAACAAATCTAAGGTCAGCCTGGCTGCTTGAGAACAGGTCTCAAACAGGCAACA
                SP1                                                               AP1
 -300 AAAGAAATGGATGGGTCTGAGTGGGGGTGGGGGGGCTTGAGGCAGTGGTCGCATCTAGGCCCTTGTCTGAGTCACACTGGGTCTTACAACATTTGAAGGA
                                  SP1                 SP1                 YY1F
 -200 CTGCCCTTTTCTCTCAAATGAAATGAGTTCCAAAAGAGCACAAGGAAAGGGGGTGGGGAGGGGGAATTTTAAAAATGCCCATCTTCTGAACACGATCTTT
                SP1
 -100 GTGCGGGCGTCTGGGGGAGGCTAGCGGGGCGGGGTCATCTGCCAGCCAGGCCTGTAGGACTTGGTTCTTGTTTATTCCACTCACATTCAGGGCAGTTGCC
   +1 SP1
      AGGACCCGCCCCCGCTGCAGTCACTGGAGGAACTGGAAGTTAACCGTTCCTGCTGAGAAATCGGTGTGTTTCCTTTGGCTGCTCCTAGGTGAGGGTTTGC
                                  SP1
+100 TGTGGTCTAGCCTGGGAAGTAGGTCTAGCCCAAGTCCAGCCTGAACAGAGCGAGCCTGTCGCCATGCCGGCTTGCTGCAGCTGGAACGATGTCTTGCAGT
                TCF/LEF1
+200 ATGAGACAAACAAAGTCACC-3′
```

B

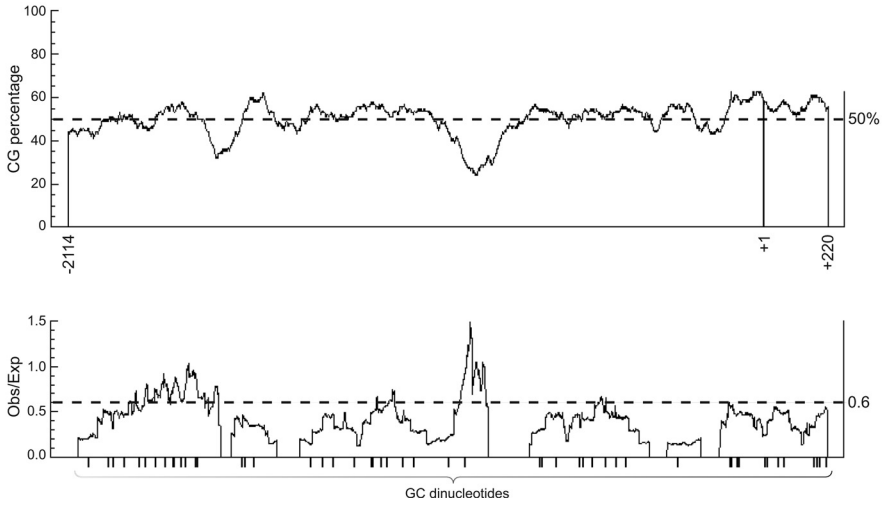

TABLE 2

Main putative transcription factor binding sites found in the *P2rx7* promoter region

Start/End pos., starting/ending position of the consensus binding site in the sequence (relative to +1 TTS); Str., strand sense; Matrix sim., matrix (groups of functionally similar transcription factors) similarity factor (0–1); Core sim., core consensus sequence (4 highest conserved positions) similarity factor (0–1); AP1, activator protein 1; CREB, cAMP-responsive element-binding proteins; E-box, E-box binding factors; HIFF, hypoxia-inducible factor, bHLH/PAS protein family; SP1/GC, stimulating protein 1/GC box elements; STAT, signal transducer and activator of transcription; TCF/LEF1, involved in the Wnt signal transduction pathway; YY1F, activator/repressor binding to transcription initiation site.

Family	Factor	Start pos.	End pos.	Str.	Core sim.	Matrix sim.	Sequence
AP1	AP1	−937	−925	(+)	1.000	0.874	gtctGAGTtacac
	AP1	−365	−353	(+)	1.000	0.878	ccttGAGTgagta
	AP1	−361	−349	(+)	1.000	0.904	gagtGAGTaacaa
	AP1	−236	−224	(+)	1.000	0.968	gtctgAGTCacac
CREB	CREB	−1887	−1867	(−)	1.000	0.918	ccagtgagaTGACgaaggtgc
E-box	c-Myc/Max	−1696	−1684	(+)	0.860	0.931	caaccaCATGgtg
HIFF	HIFF	−1210	−1194	(−)	1.000	0.953	tgtcctaaCGTGgctat
SP1/GC	SP1	−1457	−1441	(+)	1.000	0.919	aacagGGGCaggggcct
	GC box	−281	−265	(+)	0.872	0.912	agtgggGGTGgggggc
	GC box	−155	−139	(+)	0.872	0.904	aaagggGGTGgggaggg
	SP1	−150	−134	(+)	0.877	0.890	gggtgGGGAgggggaat
	SP1	−79	−63	(+)	1.000	0.998	tagcgGGGCggggtcat
	SP1	−1	+16	(−)	1.000	0.973	agcggGGGCgggtcctg
	SP2	+131	+147	(−)	1.000	0.854	tgttcaggctGGACttg
STAT	STAT3	−1253	−1235	(−)	1.000	0.977	aatcTTCCaggcacaagtg
	STAT3	−1240	−1222	(+)	1.000	0.964	aagaTTCCaggtctcagag
	STAT6	−811	−793	(+)	1.000	0.954	caccTTCCtcagaattcta
TCF/LEF1	TCF/LEF1	−2052	−2036	(−)	1.000	0.879	agtaggcCAAAgggctt
	TCF/LEF1	−709	−693	(−)	1.000	0.890	ccaagaaCAAAgctgca
	TCF/LEF1	−483	−467	(+)	1.000	0.908	gactgaaCAAAgggttg
	TCF/LEF1	−464	−448	(+)	1.000	0.962	cggaaaaCAAAgggata
	TCF/LEF1	+204	+220	(+)	1.000	0.873	agacaaaCAAAgtcacc
YY1F	YY2F	−2068	−2048	(−)	1.000	0.872	ggcttCCATtagagcagtaaa
	YY1F	−570	−550	(+)	1000	0.875	ggcagCCATctttggcagacc
	REX1	−520	−500	(+)	1.000	0.874	agatgCCATtcagtcatcggg
	YY1F	−127	−107	(+)	1.000	0.960	aatgcCCATcttctgaacacc

five TCF/LEF1 (involved in Wnt signal transduction pathway) binding sites, and four YY1F (activator/repressor binding to transcription initiation site) motifs (Fig. 1*A* and Table 2).

Functional Analysis of P2rx7 Gene Promoter—To study the transcriptional activity of the *P2rx7* promoter fragment, sequential deletions of the 5′-flanking region from −2114 to +220 bp of the *P2rx7* proximal promoter were amplified by PCR and subcloned into pGL4.23. This reporter vector contains a minimal promoter and a multiple cloning site upstream of the luciferase reporter gene exhibiting very low basal luciferase expression. A schematic representation of the promoter fragments cloned into pGL4.23 with the location of TSS is shown in Fig. 2*A*. The *P2rx7* promoter constructs were cotransfected into N2a cells with pGL4.74[hRluc/TK] plasmid (a transfection efficiency control), and their basal transcription activities were assessed 24 h after transfection.

Compared with empty vector, pP2X7-A exhibited a significant luciferase activity in N2a cells (1.53 ± 0.12) (Fig. 2*B*, *bar A*). Plasmid pP2X7-B containing the region from −1577 to +220 bp displayed higher promoter activity than pP2X7-A (2.04 ± 0.33) (Fig. 2*B*, *bar B*). Plasmid pP2X7-C, containing 1258 bp from −1038 to +220 bp had a strong effect on the promoter activity, reflected by a significant increase in luciferase activity to 3.45 ± 0.26 (Fig. 2*B*, *bar C*). Plasmids pP2X7-D (−451 to +220 bp) and pP2X7-F (−249 to +220 bp) displayed a luciferase activity similar to pP2X7-C (2.97 ± 0.19 and 2.98 ± 0.24, respectively) (Fig. 2*B*, *bars D* and *F*). Deletion of 3′-522 bp or 5′-468 bp from the D fragment to generate pP2X7-E (−451 to −302 bp) or pP2X7-G (+17 to +220 bp), respectively, drastically reduced the luciferase activity to empty vector values (0.87 ± 0.09 and 0.97 ± 0.09, respectively) (Fig. 2*B*, *bars E* and *G*). Taken together, these data suggest that the sequence from −249 to +17 bp, containing the TSS, includes the sequence of nucleotides necessary for basal transcription of the *P2rx7* gene.

As previously shown, a transcription factor binding site search revealed that the 2334-bp 5′-flanking region of the *P2rx7* gene contains seven putative SP1 binding sites, four of which are included into the −249/+17 bp sequence (Fig. 3*A*, Table 2). To examine functional SP1 regulatory elements in the promoter region of the *P2rx7* gene, three more deletion plasmids were constructed, and luciferase assays were performed. The first plasmid pP2X7-F1 (−249 to −139 bp) encloses the first two putative SP1 binding sites (SP1a and SP1b), the second plasmid pP2X7-F2 (-148 to −41 bp) includes the second and third putative SP1 motifs (SP1b and SP1c), and the plasmid pP2X7-F3 (−50 to +49 bp) contains the TSS and the fourth putative SP1 binding site (SP1d) (Fig. 3*B*). The pP2X7-F1 construct behaved as the empty vector (2.13 ± 0.27), whereas pP2X7-F3 plasmid displayed similar luciferase activity compared with whole F fragment (3.55 ± 0.39 and 2.98 ± 0.24, respectively) (Fig. 3*C*, *bars F*, *F1*, and *F3*). Interestingly, pP2X7-F2 containing SP1b and SP1c exerted a significant up-

FIGURE 1. **Sequence features of the 5′-flanking region of the mouse *P2rx7* gene promoter.** *A*, shown is *in silico* analysis of the putative transcription factor binding sites. A 2334-bp fragment of the 5′-flanking region of the *P2rx7* gene was isolated from mouse genomic DNA. Nucleotide numbering is relative to the first nucleotide (adenine +1) of the TSS, which is indicated in a *gray background*. The sequence lacks TATA and CAAT boxes. The positions of putative transcription factor binding motives identified using the Genomatix MatInspector software tool are *boxed*. *B*, shown is a schematic representation of the *P2rx7* promoter comprising the region −2114 to +220 bp. CG sites are depicted by *black bars*. CG content is shown as percentage of the total number of G+C (*top*) and by methylation-susceptible CG pairs, represented by the observed *versus* expected index (*Obs/Exp*; *bottom*).

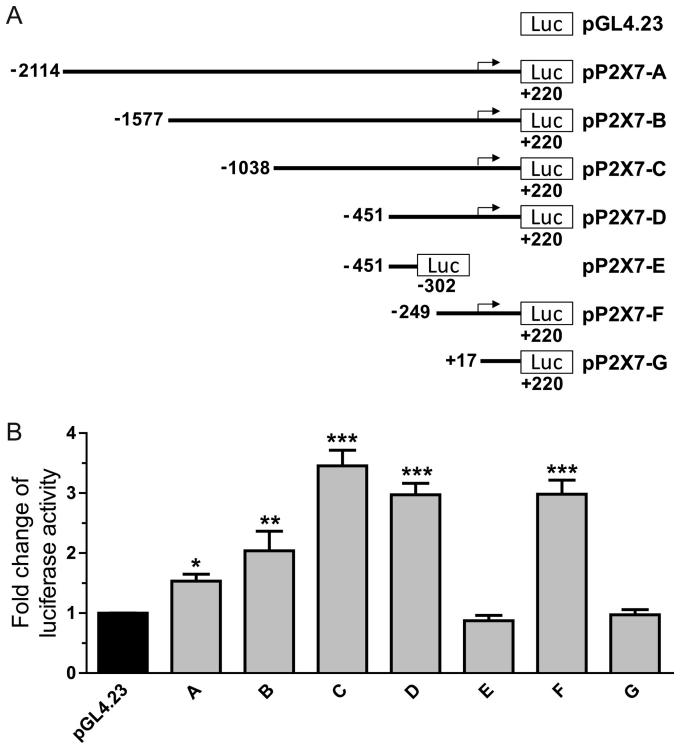

FIGURE 2. **Deletion analysis of the mouse *P2rx7* gene promoter.** *A*, shown is a schematic diagram of the P2X7 promoter constructs consisting of a 5′-flanking region with serial deletions cloned into the pGL4.23 luciferase reporter vector. The *arrow* shows the direction of transcription. *Numbers* represent the end points of each construct. *B*, plasmid constructs were cotransfected with *Renilla* luciferase vector pGL4.74[hRluc/TK] into N2a cells. 24 h after transfection, cells were harvested, and luciferase activity was measured. *Renilla* luciferase activity was used to normalize the transfection efficiency. The values represent the mean ± S.E. of at least three independent experiments in triplicate. *, $p < 0.05$; **, $p < 0.01$; ***, $p < 0.001$ (ANOVA with the post hoc Newman-Keuls test).

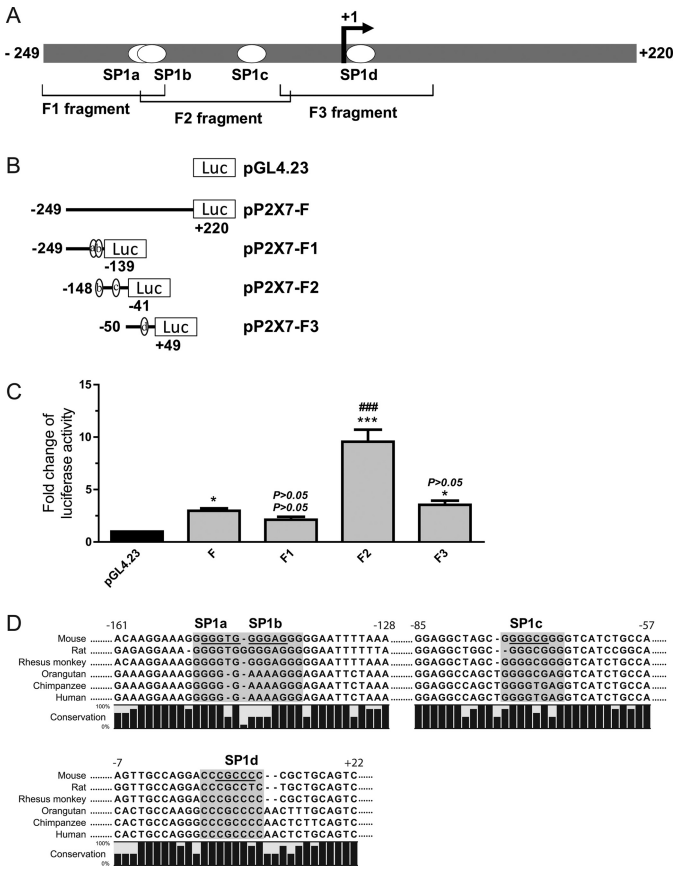

FIGURE 3. **Functional analyses of putative SP1 elements in the mouse *P2rx7* gene promoter.** *A*, shown is a schematic representation of the F fragment (−249 to +220) cloned into the pGL4.23 reporter vector containing the four SP1 binding sites located close to the TSS (+1). F fragment was divided in three subfragments named F1 (−249 to −139), F2 (−148 to −41), and F3 (−50 to +49) as indicated. *B*, deletion constructs of the whole F fragment were obtained by PCR and cloned into pGL4.23. *Numbers* represent the end points of each construct. *White ellipses* represent SP1 sites location. *C*, plasmid constructs were cotransfected with pGL4.74[hRluc/TK] vector into N2a cells. 24 h after transfection, luciferase activity was measured. *Renilla* luciferase activity was used to normalize the transfection efficiency. The values represent the mean ± S.E. of at least four independent experiments in triplicate. *, $p < 0.05$; ***, $p < 0.001$ *versus* empty vector; ###, $p < 0.001$ *versus* F fragment (ANOVA with the *post hoc* Newman-Keuls test). *D*, shown is sequence alignment of the SP1 binding sites located along the mouse *P2rx7* gene promoter across different mammalian species. Sequences were obtained from NCBI-GenBank™ and Ensembl databases. Numbers refer to the mouse sequence and ranges from −161 to +22 bp. Alignments of the putative regulatory sites are shown in a *gray background*. *Black bars* indicate the percentage of conservation with the mouse sequence. Putative core sequences for the binding of Sp1 are *underlined*.

regulation in the *P2rx7* promoter activity, inducing an increase in luciferase activity of 9.56 ± 1.16 (Fig. 3*C*, *bar F2*). This result suggests that SP1c could be the most potent motif in the regulation of *P2rx7* gene transcription.

SP1 Binding Sites Are Functional and Highly Conserved among Different Species—To evaluate the importance of each putative SP1 regulatory site contained into the −249/+17 bp sequence, the upstream sequence of P2X7 receptor genes from several mammalian species were compared. To perform the alignments, the same SP1-containing regions than those we were studying in mouse were selected. As shown in Fig. 3*D*, SP1a and SP1b putative sites are well conserved in mouse, rat, and macaque (rhesus monkey) but disappeared in human and other non-human hominids such as orangutan and chimpanzee. On the contrary, SP1c and SP1d putative sites show a high degree of homology between species. SP1c site is perfectly conserved between mouse, rat, macaque, and orangutan. We notice that the putative SP1c site shows a C/T substitution in chimpanzee and human; however, this nucleotide modification produces a GT-box that also behaves as a putative SP1 binding site (37, 38). The SP1d putative site, located in the region surrounding TSS (+1), is highly conserved between species. These results showed that SP1c and SP1d binding sites and their relative distances are conserved, suggesting an important regulatory role of Sp1 factors in the expression of P2X7 receptor in mammals.

To confirm the involvement of SP1c and SP1d binding sites in the regulation of *P2rx7* promoter, we performed reporter luciferase experiments in N2a cells with pP2X7-F2 and pP2X7-F3 promoter constructs bearing a double point mutation at each of the two SP1 cores (Fig. 4*A*). The mutations completely blocked the promoter activity observed in non-mutated constructs, indicating that both SP1 sites are actively regulating *P2rx7* gene expression (Fig. 4*B*). To explore whether the regulation of *P2rx7* gene expression by Sp1 is limited to neuronal cells, we performed analogous experiments in immune cells that express high levels of P2X7 receptors (39). Thus the macrophage RAW264.7 cell line was transfected with pP2X7-F2 or

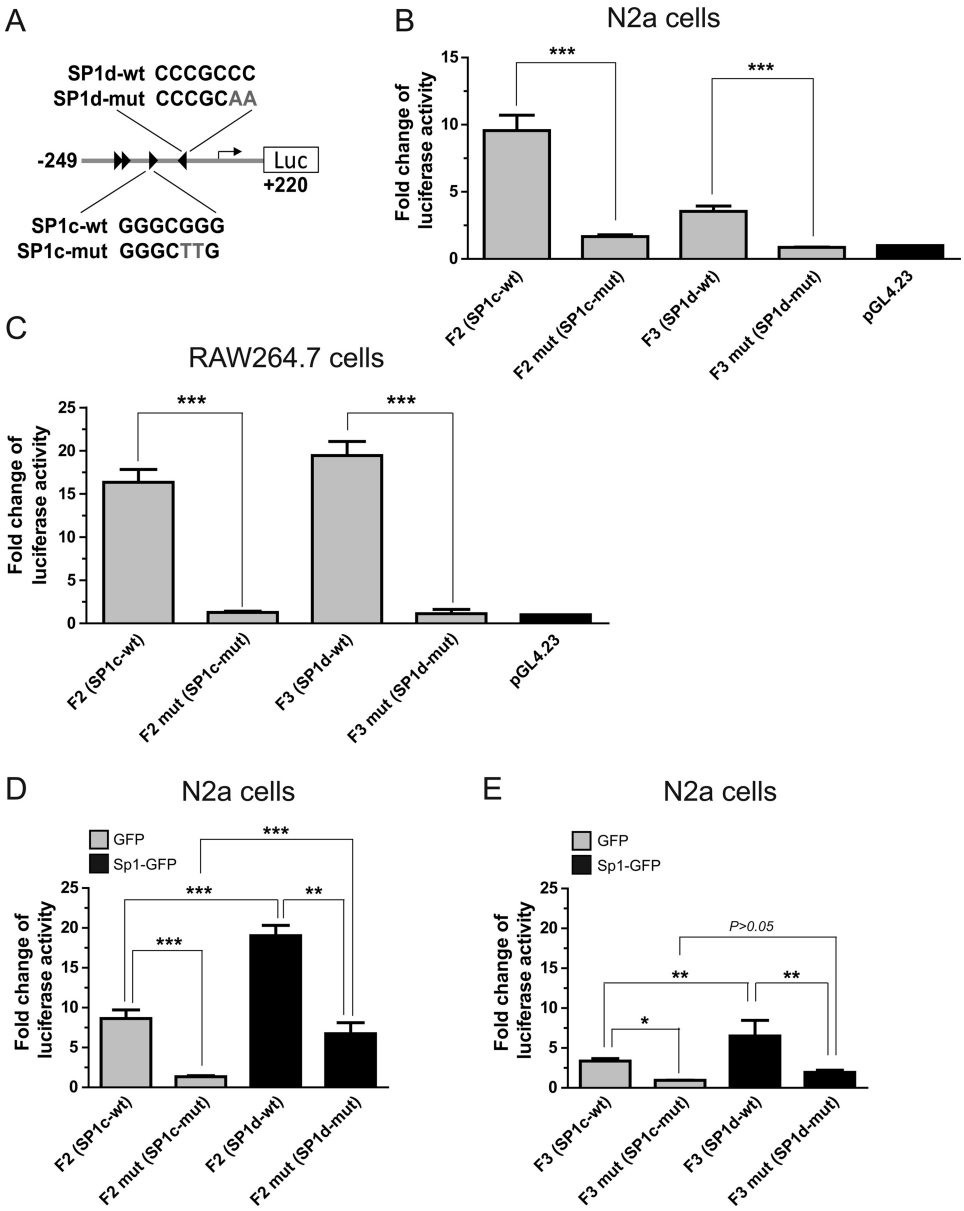

FIGURE 4. **SP1c and SP1d binding sites are directly involved in the transcriptional activation of *P2rx7* promoter by Sp1 protein.** *A*, shown is a schematic representation of the F fragment (−249 to +220) cloned into the pGL4.23 reporter vector containing four SP1 binding sites located close to the TSS (+1). The position and orientation of SP1 sites are indicated by *arrowheads*. The sequences of SP1c and SP1d sites are depicted as well as the double point mutations (in *gray*) performed to eliminate Sp1-dependent regulation. In N2a cells (*B*) and RAW264.7 cells (*C*) mutation of SP1c and SP1d sites inhibits activation of basal transcription exerted by pP2X7-F2 and pP2X7-F3 constructs, respectively. Reporter activity is shown for pP2X7-F2 (*F2*), mutated pP2X7-F2 containing the mutation of SP1c site (*F2 mut*), pP2X7-F3 (*F3*), mutated pP2X7-F3 containing the mutation of SP1d site (*F3 mut*), and empty vector (*pGL4.23*). *D*, overexpression of Sp1 protein increases promoter activity induced by pP2X7-F2 construct. The pP2X7-F2 plasmid (*F2*) containing SP1c site was cotransfected with Sp1 expression plasmid (*Sp1-GFP*) or empty vector (GFP) into N2a cells. Mutation of SP1c binding site (*F2 mut*) reduces promoter activity even in presence when Sp1 is overexpressed. *E*, shown is overexpression of Sp1 protein increases promoter activity induced by pP2X7-F3 construct. The pP2X7-F3 plasmid (*F3*)-containing SP1d site was cotransfected with Sp1 plasmid (*Sp1-GFP*) or empty vector (*GFP*) into N2a cells. Mutation of SP1d binding site (*F3 mut*) inhibits promoter activity. The values represent the mean ± S.E. of at least three independent experiments in triplicate. $*p < 0.05$, $**p < 0.01$, $***p < 0.001$ (ANOVA with the *post hoc* Newman-Keuls test).

pP2X7-F3 promoter constructs, and luciferase assays were performed. Interestingly, both pP2X7-F2 and pP2X7-F3 promoter constructs behaved equally potent, inducing an increase in luciferase activity of 16.34 ± 1.50 and 19.45 ± 1.63, respectively. Moreover, mutation of Sp1 cores completely blocked the promoter activity observed in non-mutated constructs (Fig. 4*C*). Altogether these results demonstrate that the regulation of P2X7 expression by Sp1 is not tissue-restricted.

To verify that both SP1c and SP1d are functional binding sites, the *P2rx7* promoter activity was studied in cells overexpressing Sp1 protein. Either Sp1 expression plasmid (Sp1-GFP) or empty vector (GFP) was cotransfected with pP2X7-F2, pP2X7-F3, or empty pGL4.23 into N2a cells. Cells were harvested 48 h after transfection, and luciferase activity was measured. As shown in Fig. 4*D*, pP2X7-F2 luciferase activity was noticeably enhanced in cells transfected with Sp1 vector by 2-fold. This increase was significantly reduced when SP1c site was mutated. We notice that SP1c mutation did not completely reverse the transcriptional activity of F2 construct when Sp1 protein was overexpressed, probably due to Sp1 binding to the

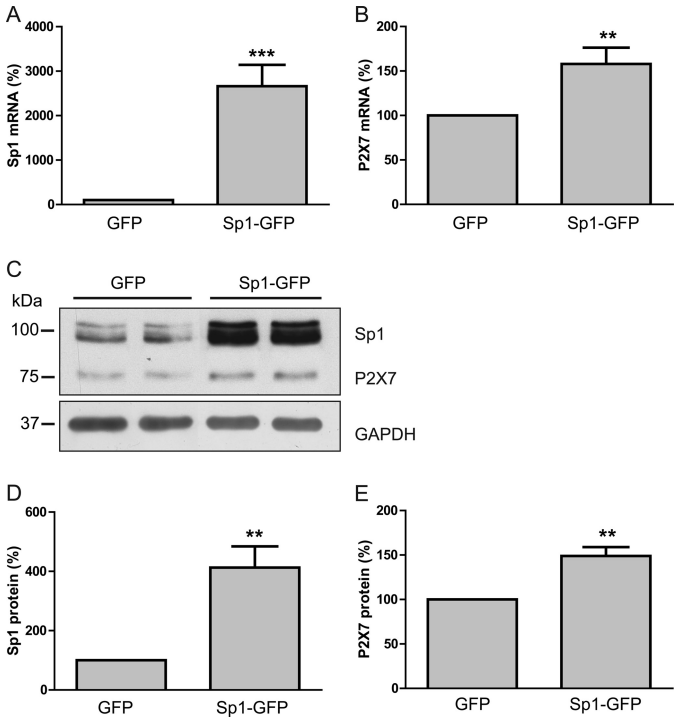

FIGURE 5. **Facilitation of endogenous P2X7 receptor expression by Sp1 overexpression.** N2a cells were transfected with Sp1 expression plasmid (*Sp1-GFP*) or empty vector (*GFP*) and analyzed 48 h later for Sp1 (*A*) and P2X7 (*B*) mRNA levels by Q-PCR. *C*, SDS-PAGE was performed to analyze cell lysates from Sp1-transfected N2a cells. Both Sp1 and P2X7 proteins were detected at a size of around 95–105 and 75 kDa, respectively. GAPDH was used as internal loading control. Densitometric analysis was performed using Image J software (*D* and *E*). The values represent the mean ± S.E. of three independent experiments in triplicate. *, $p < 0.05$; **, $p < 0.01$; ***, $p < 0.001$ (Student's *t* test).

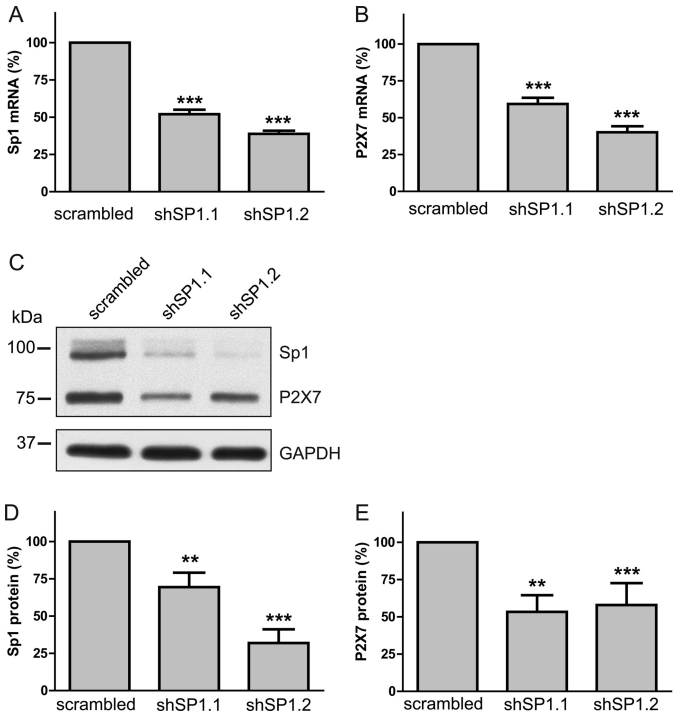

FIGURE 6. **Down-regulation of endogenous P2X7 receptor expression by Sp1 interference.** Endogenous Sp1 expression was knocked down in N2a cells using two specific shRNA (*shSP1.1* and *shSP1.2*) and analyzed 48 h later for Sp1 (*A*) and P2X7 (*B*) mRNA level by Q-PCR. Scrambled shRNA was used as negative control. *C*, silencing of Sp1 reduces both Sp1 and P2X7 proteins expression. SDS-PAGE was performed to analyze cell lysates from N2a cells transfected with shSP1.1, shSP1.2, or scrambled for 72 h. GAPDH was used as internal loading control. Densitometric analysis was performed using Image J software (*D* and *E*). The values represent the mean ± S.E. of three independent experiments in duplicate or triplicate. **, $p < 0.01$; ***, $p < 0.001$ (Student's *t* test).

SP1b motif, which is also included in F2 fragment (Fig. 3*B*). Sp1 overexpression was also able to increase 2-fold the transcriptional activity of pP2X7-F3 (Fig. 4*E*), although in this case the increment in luciferase activity was completely abolished by SP1d site mutation even in the presence of an excess of Sp1 protein. These data clearly demonstrate that overexpression of Sp1 significantly up-regulates *P2rx7* gene promoter activity by its binding to SP1 sites.

Sp1 Is Crucial for the Basal Transcription of Endogenous P2X7 Receptor—In transient transfection experiments using luciferase reporter plasmids, the proximal promoter region of *P2rx7* gene is not packaged into a chromatin-like structure, leading to high accessibility to different nuclear factors. Therefore, it is essential to study the promoter activity in its native chromatin context. To investigate whether Sp1 plays a relevant role in the transcriptional regulation of endogenous *P2rx7* gene, N2a cells were transiently transfected with Sp1 expression plasmid (Sp1-GFP) or empty vector (GFP), and both mRNA and protein levels were quantified 48 h and 72 h after transfection, respectively. Q-PCR studies revealed that the endogenous levels of both Sp1 and P2X7 transcripts were significantly increased in Sp1 over-expressing cells (Fig. 5, *A* and *B*). Moreover, Western blot analysis also demonstrated that Sp1 overexpression markedly enhanced the protein levels of both Sp1 (Fig. 5, *C* and *D*) and P2X7 receptor (Fig. 5, *C* and *E*) in N2a cells.

To further assess the relevance of Sp1 in *P2rx7* transcription, endogenous Sp1 expression was knocked down in murine N2a cells using two specific shRNA (shSP1.1 and shSP1.2). N2a cells were transiently transfected with shRNAs or scrambled vector, and both mRNA and protein levels were quantified 48 and 72 h after transfection, respectively. As expected, Sp1 interference significantly reduced both the transcript and the protein levels of Sp1 (Fig. 6*A*, *C*, and *D*) and P2X7 receptor (Fig. 6, *B*, *C*, and *E*) in N2a cells. Taken together, these data are consistent with the results obtained from the luciferase assays, corroborating that Sp1 factor plays an important role in the transcriptional regulation of endogenous P2X7 receptor.

Sp1 Up-regulates P2rx7 Gene Expression in Primary Cultures of Mouse Cortical Neurons and Astrocytes—To determine whether SP1 binding elements contained in the *P2rx7* promoter functionally regulate P2X7 receptor expression not only in a cell line but also in primary cultures from mouse brain, cortical neurons and astrocytes were treated with mithramycin A, an antibiotic reported to block the binding of Sp1 to GC-rich regions in the DNA (40). First, we confirmed that the level of contaminant microglia in cultures of neurons and astrocytes was almost undetectable by Western blot techniques (data not shown). The treatment with 300 nM mithramycin A for 24 h markedly reduced the endogenous levels of P2X7 mRNA in both astrocytes (Fig. 7*A*) and neurons (Fig. 7*B*). P2X7 protein levels were also significantly reduced in astrocytes and neurons

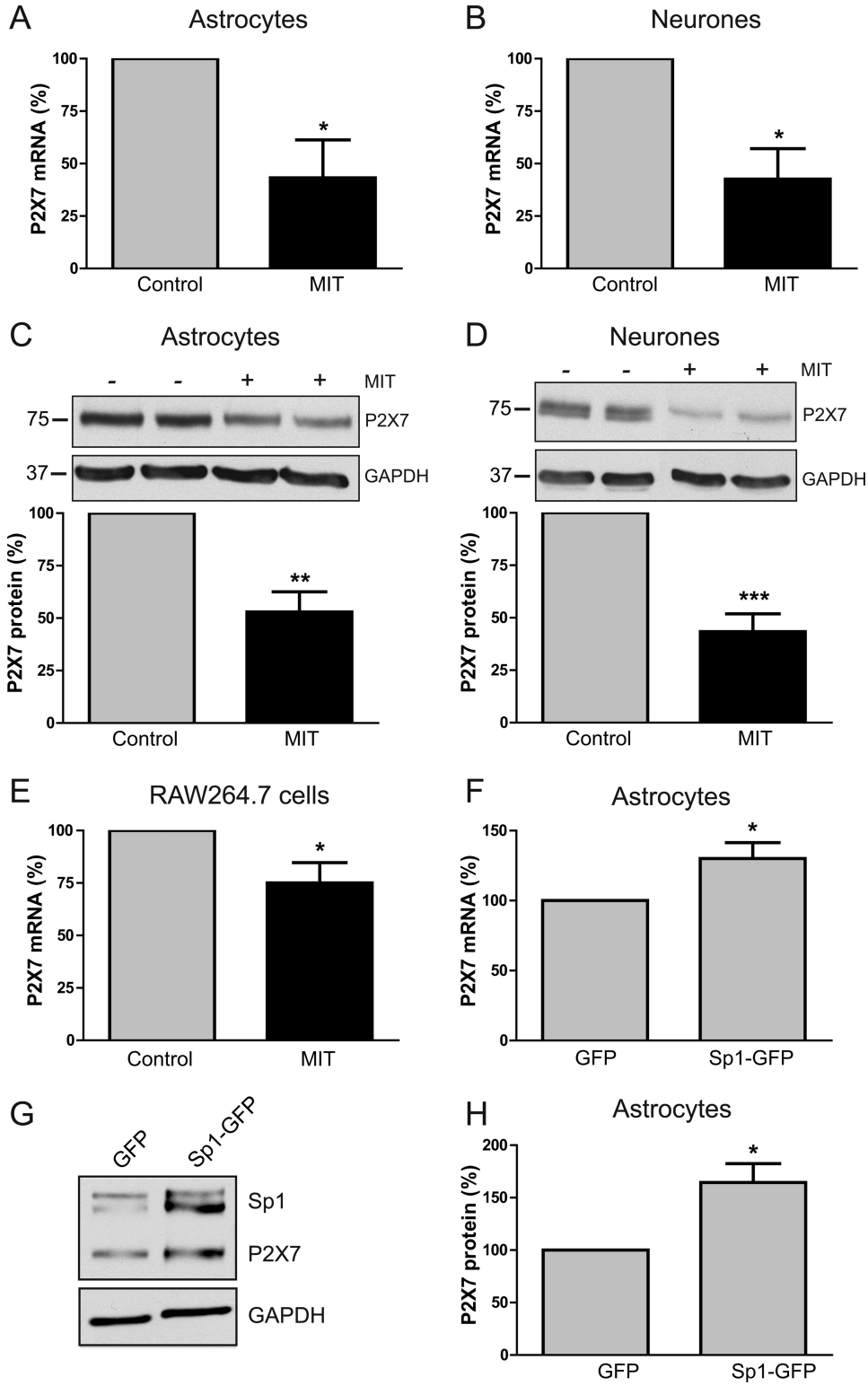

FIGURE 7. **Sp1-dependent regulation of P2X7 expression in primary cultures of cortical astrocytes and neurons.** Primary cultures of cortical astrocytes (*A*) and neurons (*B*) were treated with 300 nM mithramycin A (*MIT*) or vehicle (control) for 24 h. Total RNA was extracted and analyzed for P2X7 mRNA levels by Q-PCR. SDS-PAGE was performed to analyze cell lysates from primary cultures of cortical astrocytes (*C*) and neurons (*D*) treated with 300 nM mithramycin A or vehicle for 48 h. GAPDH was used as internal loading control. *E*, after 24 h of treatment with mithramycin A or vehicle, total RNA from RAW264.7 cells was extracted and analyzed for P2X7 mRNA expression by Q-PCR. *F*, cortical astrocytes were transfected with Sp1 expression plasmid (*Sp1-GFP*) or empty vector (*GFP*) and analyzed 48 h later for P2X7 mRNA level by Q-PCR. *G*, SDS-PAGE was performed to analyze cell lysates from Sp1-transfected astrocytes using anti-P2X7 antibodies. The ratio of P2X7 to GAPDH protein level was calculated by densitometric analysis (*H*). The values represent the mean ± S.E. of three independent experiments in duplicate or triplicate. *, $p < 0.05$; **, $p < 0.01$; ***, $p < 0.001$ (Student's *t* test).

treated with mithramycin A for 48 h (Fig. 7, *C* and *D*). When analogous assay was performed in the macrophage RAW264.7 cell line, mithramycin A was also able to reduce the endogenous levels of P2X7 mRNA, corroborating that the regulation of *P2rx7* gene expression by Sp1 is not limited to neural cells (Fig. 7*E*). Next, cortical astrocytes were transiently transfected with Sp1 expression plasmid (Sp1-GFP) or empty vector (GFP), and both mRNA and protein levels were quantified 48 and 72 h after transfection, respectively. Overexpression of Sp1 enhanced transcript (Fig. 7*F*) and protein levels (Fig. 7, *G* and *H*) of endogenous P2X7 receptor, indicating that Sp1 is also able to regulate endogenous P2X7 receptor expression in primary cultures from mouse brain.

Distribution of P2X7 Receptor and Sp1 Factor in the Postnatal Murine Brain—To determine whether Sp1 is also able to regulate P2rx7 gene expression *in vivo*, we sought to analyze the distribution of Sp1 and P2X7 receptor in the brain of newborn (P0) mice. To perform this study we used *P2rx7*-EGFP transgenic mice that express EGFP under the control of *P2rx7* promoter (30). First, to validate the reliability of the *P2rx7*-EGFP reporter mice, we analyzed the expression of EGFP in immune tissues/cells, which natively express high levels of P2X7 receptors (39). As expected, both peritoneal macrophages (Fig. 8*A*) and spleen (Fig. 8, *B* and *C*) express high levels of EGFP in 10-week-old mice, indicating the consistency of the reporter mice model. CD11 was used as protein marker of macrophages. Regarding the distribution of Sp1 and P2X7 receptor in the mouse brain, we found the EGFP fluorescence signal in a small population of cortical cells, mostly located in the upper layers of the cerebral cortex (Fig. 9, *A* and *E*). Immunohistochemical studies using antibodies against Sp1 protein showed that basal levels of Sp1 were widely expressed in the cortex, although some cells showed a higher Sp1 expression compared with the neighboring ones (Fig. 9, *B* and *F*). We notice that 76.09 ± 6.74% ($n = 68$ cells) EGFP-positive cells also showed a strong Sp1-positive immunostaining (Fig. 9, *A*–*H*). To confirm this observation, other brain regions enriched in EGFP-positive cells were analyzed, and we found a strong EGFP fluorescence signal at the pons of newborn mice (Fig. 9*J*). Interestingly, 62.81 ± 9.45% ($n = 143$ cells) of EGFP-positive cells colocalized with Sp1-positive cells in this brain region (Fig. 9, *J*–*L*). Thus we confirmed that cells expressing P2X7 receptor also contain a high amount of Sp1 factor.

Sp1 Mediates Up-regulation of P2X7 Receptor Expression under Serum Deprivation—Previous studies reported that serum deprivation of a human hepatocarcinoma cell line enhances open chromatin accessibility and helps to expose SP1 binding sites (41). Moreover, it is well known that Sp1 is an autoregulated gene (42–44). To examine the effects of serum deprivation in Sp1 and P2X7 expression, N2a cells were cultured in the absence of FBS, and both mRNA and protein levels were quantified. After 24 h serum starvation a significant up-regulation of both Sp1 and P2X7 transcripts was observed, being even more evident after 48 h (Fig. 10, *A* and *B*). Treatment of N2a cells with 300 nM mithramycin for 48 h resulted in the reduction of both Sp1 and P2X7 mRNA levels in control conditions (cells cultured in 10% FBS) and also in cells cultured in the absence of serum (Fig. 10, *A* and *B*). When protein levels

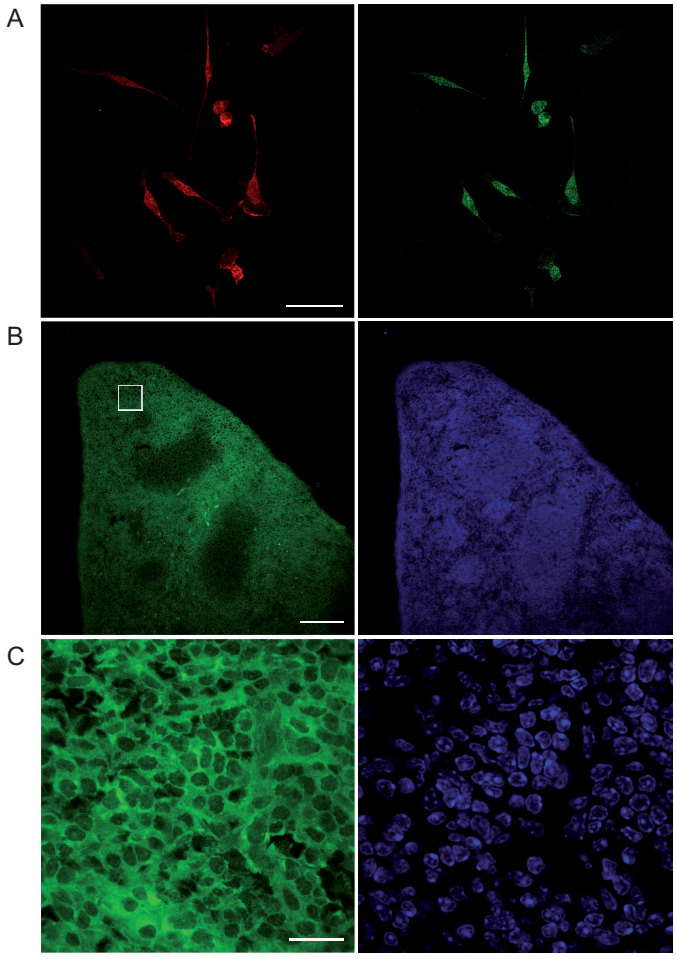

FIGURE 8. **Expression of P2X7 receptors in macrophages and spleen from adult *P2rx7*-EGFP mice.** *A*, representative photomicrographs show the macrophage marker CD11 (*red*) and native EGFP immunofluorescence (*green*) in elicited peritoneal macrophages from 10-week-old P2rx7-EGFP mice. *Scale bar* = 50 μm. *B*, photomicrographs show native EGFP immunofluorescence (*green*) in spleen from 10-week-old *P2rx7*-EGFP mice. Nuclei are counterstained with DAPI (*blue*). *Scale bar* = 300 μm. The *square* in *panel B* is shown at higher magnification in *C*. *Scale bar* = 15 μm.

were quantified, both Western blot and immunocytochemical experiments demonstrated that serum withdrawal produced a rapid and transient increase in Sp1 protein after 24 h serum removal (Fig. 10, *C*, *E*, and *F*), whereas the expression P2X7 receptor was gradually increased during 48–72 h of serum withdrawal (Fig. 10, *D*, *G*, and *H*). These results indicate that serum deprivation facilitates the up-regulation of *Sp1* gene exerted by Sp1 factor and, consequently, an increase in the endogenous levels of P2X7 receptor takes place.

DISCUSSION

Purinergic receptors have been shown to be widely distributed throughout the nervous system, being present in both neurons and glial cells (45). It is well known that activation of P2X receptors by ATP is implicated in fast excitatory neurotransmission, presynaptic regulation of neurotransmitter release, cell proliferation, axonal growth and development, and also in disease and cytotoxicity (6, 7, 46–50). Within the P2X family, the P2X7 receptor has a distinguished role in the central nervous system for its implication in both normal behavior and

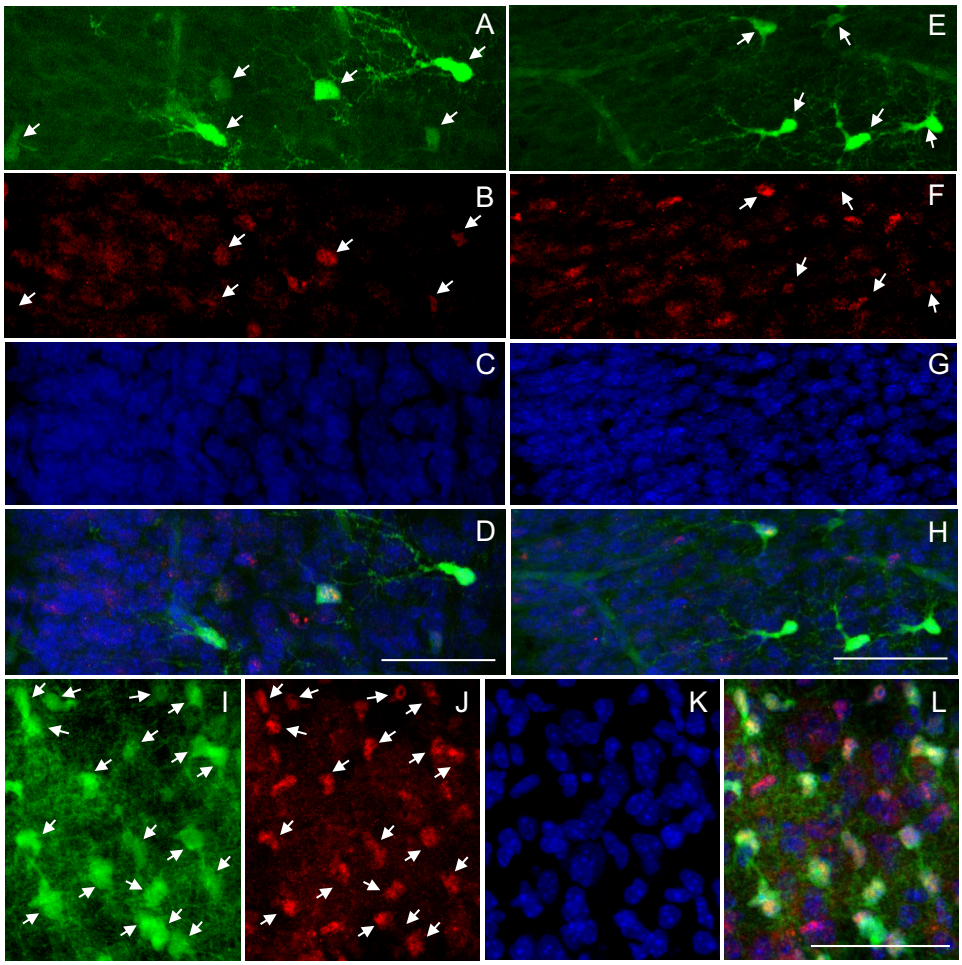

FIGURE 9. ***In vivo* colocalization of P2X7 receptor and Sp1 factor in the brain from neonatal *P2rx7*-EGFP mice.** Representative photomicrographs show native EGFP immunofluorescence (*A* and *E*, *green*) and Sp1 immunostaining (*B* and *F*, *red*) in different cortical subfields from P2rx7-EGFP mice. *Arrows* mark the position of EGFP-positive cells. Nuclei are counterstained with DAPI (*C* and *G*, *blue*). Merge images are shown (*D* and *H*). Photomicrographs show native EGFP immunofluorescence (*I*, *green*) and Sp1 immunostaining (*J*, *red*) in pons, a brain region with a high P2X7 receptor expression in neonatal *P2rx7*-EGFP mice. *Arrows* indicate EGFP-positive cells. Nuclei are counterstained with DAPI (*K*, *blue*). A merge image is shown (*L*). *Scale bars* = 50 μm.

pathological brain functions including neurodegenerative diseases and neuropsychiatric disorders (4). Moreover, high P2X7 expression in most human neuroblastoma so far investigated seems to be related with malignant cell growth and progression (13, 14, 51). All these evidences point to P2X7 receptor as a relevant pharmacological target for the treatment of both neurodegenerative disorders and cancer, thus it seems necessary to understand the mechanisms involved in the regulation of P2X7 receptor expression.

This study reports for the first time that Sp1 is a key factor necessary for the basal expression of P2X7 receptor in the nervous system. Previous studies located the active promoter of the human *P2RX7* gene in the −158/+32-nucleotide region surrounding the transcription start site, although the transcription factors involved in the promoter activity were unknown (28, 29). To characterize the molecular mechanisms that control P2X7 expression, we cloned and characterized 2334 bp of the 5′-flanking region of the murine *P2rx7* gene (from −2114 to +220). Bioinformatics analysis showed that the *P2rx7* gene promoter, unlike most type II eukaryotic gene promoters, does not contain TATA or CAAT boxes. It is well established that genes lacking a typical TATA box in their promoter sequence depend on multiple upstream regulator sequences for their activation (52). Software analysis of putative transcription factor binding indicated that the 5′-proximal regulatory region of the murine *P2rx7* gene contains several putative regulatory elements including AP1 (activator protein 1), CREB (c-AMP-responsive element-binding protein), E-box, HIF (hypoxia-inducible factor), SP1, STAT (signal transducer and activator of transcription), TCF/LEF1, and YY1F (activator/repressor binding to transcription initiation site), suggesting that P2X7 expression is tightly regulated at the transcriptional level. The most striking feature revealed by the *in silico* analysis of *P2rx7* promoter is the presence of seven putative SP1 motifs, most of them located close to the TSS. The Sp1 family of transcription factors recognizes GC and GT boxes at the DNA and has been widely described as general transcription factors frequently involved in transcriptional regulation of gene promoters that lack consensus TATA and CAAT boxes (38). Transfection experiments using different 5′-flanking sequences linked to the luciferase gene showed that 266 bp of the mouse *P2rx7* gene (from −249 to +17) contain the minimal promoter region. This fragment comprises the TSS and four putative SP1 sites (named SP1a, -b, -c, and -d, respectively). By deletion analysis, this

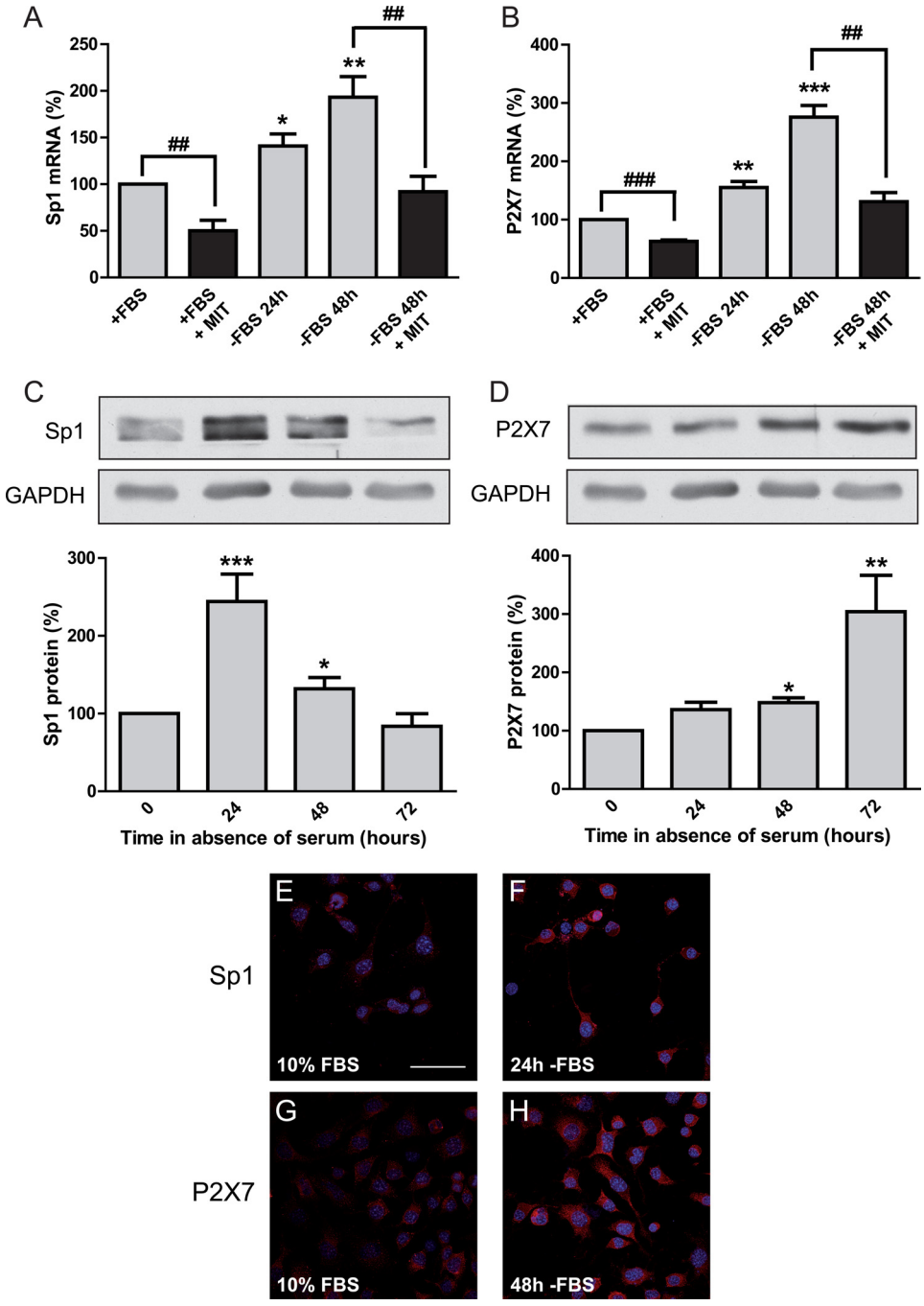

FIGURE 10. **Up-regulation of P2X7 receptor expression under serum deprivation.** Changes in Sp1 (*A*) and P2X7 (*B*) transcript levels in N2a cells cultured under serum deprivation for 24 or 48 h are shown. In some cases 300 nM mithramycin A (*MIT*) treatment was performed. Total RNA was extracted and analyzed for Sp1 and P2X7 mRNA by Q-PCR. The values represent the mean ± S.E. of three independent experiments in duplicate or triplicate. $*p < 0.05$, $**p < 0.01$, $***p < 0.001$ *versus* control (ANOVA with the post hoc Newman-Keuls test); ##, $p < 0.01$; ###, $p < 0.001$ (Student's *t* test). Changes in Sp1 (*C*) and P2X7 (*D*) protein levels under serum deprivation during the whole detection period are shown. SDS-PAGE was performed to analyze Sp1 and P2X7 receptor expression in cell lysates from N2a cells cultured for 0, 24, 48, or 72 h in the absence of serum (FBS). GAPDH was used as internal loading control. The values represent the mean ± S.E. of three independent experiments in duplicate or triplicate. $*p < 0.05$; $**p < 0.01$; $***p < 0.001$ *versus* control (ANOVA with the post hoc Newman-Keuls test). N2a cells were cultured in the presence or absence of serum for 24 or 48 h. Afterward, cells were fixed and immunostained with antibodies against Sp1 (*E* and *F*, *red*) or P2X7 (*G* and *H*, *red*). Nuclei were labeled with DAPI (*blue*). *Scale bar* = 50 μm.

region of maximum promoter activity could be subdivided into two segments, F2 (−148 to −41 bp), which increased promoter efficiency 3-fold compared with complete F fragment, and a proximal segment F3 (−50 to +49 bp), which displayed a significant promoter activity similar to that exerted by complete F construct. These findings indicate that the major elements responsible for transcriptional activation must be confined to these regions. Interestingly, both F2 and F3 constructs contains putative SP1 sites (SP1c and SP1d, respectively) that are structurally identical to the consensus site (G/T)GGGCGG(G/A)(G/A)(C/T) (53), although SP1d is located in the reverse strand. It is well established that DNA methylation of CpG islands is an important mechanism for transcriptional regulation of multiple genes in mammals (54–56). Methylation degree of CpG

islands contained within the SP1 consensus elements may interfere with the binding of Sp1 to DNA, modulating the Sp1-dependent transcription of genes (36). Bioinformatics analysis revealed that the 5′-proximal regulatory region of the murine *P2rx7* gene lacks CpG islands, so we ruled out that methylation of SP1 sites located into the promoter region could be interfering Sp1 binding to DNA. However, we cannot discard an epigenetic control of *P2rx7* gene as frequently CpG regions outside the active promoter can regulate transcription by modulation of DNA methylation. Indeed, the presence of a CpG-rich 547-bp region downstream of the active promoter of the human *P2RX7* gene that regulates its transcription has been previously reported (29).

Our data from site-directed mutation showed that replacement of two nucleotides in both SP1c and SP1d was enough to completely block the reporter activity. Therefore, we investigated whether SP1 binding sites identified in the murine promoter were also present in the upstream sequence of P2X7 genes from other mammals, as relevant transcriptional regulatory elements often show conservation between species (57). The species analyzed included rat, macaque, chimpanzee, orangutan, and human. Sequence alignment showed conserved SP1c and SP1d sites in identical positions across all species examined, suggesting that the involvement of Sp factors in the regulation of P2X7 transcription has been conserved during evolution. We notice that P2X7 receptor gene is highly polymorphic, with 40 coding variants reported in humans and more than 12 non-synonymous SNPs characterized for their effect on function (58). At least eight SNPs in *P2RX7* confer loss-of-function in the P2X7 signaling pathway, giving rise to severe functional defects (20, 59). Only two variants have been shown to confer gain of function (26). Currently, five SNPs have also been identified in the *P2RX7* promoter, although none of them appears to be associated with an altered ATP response phenotype (27). However, support for a regulatory role for the promoter SNPs comes from the fact that a positive association between a *P2RX7* promoter polymorphism (−762, T/C) and a major susceptibility to tuberculosis has been reported (60). Based on this precedent, we speculate that the presence of promoter SNPs in the region containing SP1c and/or SP1d could alter binding of Sp1 transcription factor, resulting in a decrease in P2X7 receptor gene transcription. Analysis of new promoter polymorphisms on P2X7 receptor function could be relevant to identify the regulatory mechanisms underlying the heterogeneity in ATP responsiveness observed within human populations.

Currently the Sp1 family of transcription factors consists of nine proteins (Sp1–9), with Sp1 being the first member indentified and cloned (38). Often, for several cell types and promoters, Sp1 and Sp3 have been reported as the major GC/GT box binding activities, being broadly expressed in most cells and tissues (61). It is well known that Sp1 can be regulated by glycosylation (62) and phosphorylation (53) and can directly interact with the basal transcription machinery to induce Sp1-dependent transcription of target genes (63). However, although Sp3 was found to be highly homologous to Sp1 with similar affinities for GC/GT boxes, there are some striking functional differences. Sp3 has been shown to act as a transcriptional activator in some cellular contexts, whereas in other experimental conditions Sp3 remains inactive or represses transcription driven by Sp1 or other transcription factors (61). Given the dual nature of Sp3, our experiments were focused on Sp1 protein as the classical transcriptional activator of GC box-containing genes. Overexpression of Sp1 protein increased gene promoter activity in N2a cells, resulting in a significant increase in luciferase activity and endogenous P2X7 mRNA and protein levels. Similar results were obtained in the macrophage cell line RAW264.7 indicating that the regulation of P2X7 expression by Sp1 is not restricted to neuronal cells. As expected, SP1c and SP1d mutations were able to disrupt Sp1-enhanced promoter activity in both N2a and RAW264.7 cells, suggesting that Sp1 binds to SP1c and SP1d sites to positively regulate *P2rx7* gene expression. The role of Sp1 as a key factor necessary for the basal activation of *P2rx7* gene transcription has been also corroborated by either Sp1 overexpression or interference of endogenous Sp1 protein in neuroblastoma cells.

Mithramycin A is an antibiotic isolated from various strains of the bacterium *Streptomyces* that has been used in the past in the treatment of several types of cancer including testicular carcinoma, chronic myeloid leukemia, and acute myeloid leukemia (64). More recently, mithramycin has been used in combination with other drugs such as apoptosis-inducing agents, chemotherapeutic drugs, or antiangiogenic compounds as a novel therapy for pancreatic cancer and other tumors (44). Here we show that neuroblastoma cells, macrophages, and primary cultures of cortical neurons and astrocytes treated with mithramycin A underwent a reduction in endogenous P2X7 receptor levels. The mechanism of action of mithramycin involves a non-covalently binding to GC-rich DNA sequences, preventing Sp1 from binding to a variety of promoters of genes involved in cell death, cell migration, and immune recognition of tumor cells (65). Noteworthy, high levels of P2X7 receptor expression have been found in various cancer cells, including human primary neuroblastoma tumors and neuroblastoma cell lines where P2X7 receptors support tumor growth (13, 51, 66). Although the source of extracellular ATP required to keep a tonic P2X7 receptor activation remains unclear, the exocytotic release of ATP coupled to P2X7 receptor stimulation has been demonstrated in neuroblastoma cells (67). In addition, a growing number of studies suggest a noticeable convergence between genes involved in transformation and those necessary for some types of neurodegeneration. In this line, mithramycin has been reported to prolong survival in mice models of Huntington disease (68–72) and to protect against dopaminergic neurotoxicity after methamphetamine administration (73). In addition, mutant huntingtin has been reported to inhibit Sp1-medianted gene transcription (74, 75), and human *huntingtin* gene expression is transcriptionally regulated by Sp1 (76). P2X7 receptors are also implicated in the development of several neurodegenerative pathologies such as Huntington and Alzheimer disease (9, 77, 78). Moreover, P2X7 receptors regulate both axonal development in hippocampal neurons and differentiation of neuroblastoma cells through a Ca^{2+}/calmodulin-dependent kinase II-related mechanism (7, 8). Our analysis of the expression of the P2X7 receptor in newborn *P2rx7*-EGFP mice, where the brain cytoarchitecture is still in progress, showed a good correlation between the presence of P2X7 receptors and

the cellular content in Sp1 factor. These data are in agreement with previous studies reporting that Sp1 is essential for early embryonic development (79) and that the level of Sp1 rises during development in the neural tissue of early fetuses (80). These evidences point to Sp1 as an important regulator of cellular processes during brain development and differentiation.

Serum deprivation has been described to enhance open chromatin accessibility, facilitating exposure of SP1 binding sites. Furthermore, Sp1 binding to its regulatory SP1 sites acts as a docking partner for recruiting RNA polymerase II to the promoter, which in turn results in up-regulation of gene expression (41). According to this premise, an increase in P2X7 expression after serum withdrawal could be correlated with an increase in Sp1 binding to SP1 sites at the *P2rx7* promoter. To confirm this hypothesis, we analyzed both P2X7 and Sp1 levels in differentiated *versus* proliferated N2a cells. Serum deprivation resulted in a significant increase in Sp1 mRNA followed by an expected increase in the transcript levels of P2X7 receptor. Both increases were completely abolished by mithramycin A treatment, indicating that both *Sp1* and *P2rx7* genes are being transcriptionally up-regulated by Sp1 binding to their promoters. We notice that the Sp1 and P2X7 proteins are enhanced under serum deprivation, but the increments observed were not synchronized. This evidence could be relevant in explaining why in newborn *P2rx7*-EGFP mice brains some EGFP-positive cells do not simultaneously express high levels of Sp1 protein.

In conclusion, regulation of P2X7 receptor expression may play a very important role in the development of different pathologies, including cancer and neurodegenerative diseases. By cloning and functionally characterizing the *P2rx7* gene promoter, our experiments provide the first molecular evidence that Sp1 plays an important role in the control of *P2rx7* gene expression in the nervous system. Therefore, we suggest that the gene encoding P2X7 subunit could be just one of the thousands of genes implicated in the control of cell growth, differentiation, and cell death whose expression is transcriptionally regulated by Sp1 (81, 82). Future studies will be focused on clarifying the role of Sp1 in the control of P2X7 receptor expression during brain development and disease.

Acknowledgments—We thank Dr. Maiken Nedergaard (University of Rochester Medical School, Rochester, NY) for kindly providing the P2rx7-EGFP mice and Dr. Lisardo Boscá (Instituto de Investigaciones Biomédicas Alberto Sols, Consejo Superior de Investigaciones Científicas-Universidad Autonoma de Madrid, Madrid, Spain) for providing the phosphatidylethanolamine-labeled anti CD11 antibody. We also thank María Diez-Zaera for technical assistance and the staff of the Genomic Service at Universidad Complutense de Madrid for help in DNA sequencing.

REFERENCES

1. Coddou, C., Yan, Z., Obsil, T., Huidobro-Toro, J. P., and Stojilkovic, S. S. (2011) Activation and regulation of purinergic P2X receptor channels. *Pharmacol. Rev.* **63,** 641–683
2. Torres, G. E., Egan, T. M., and Voigt, M. M. (1999) Hetero-oligomeric assembly of P2X receptor subunits. Specificities exist with regard to possible partners. *J. Biol. Chem.* **274,** 6653–6659
3. North, R. A. (2002) Molecular physiology of P2X receptors. *Physiol. Rev.* **82,** 1013–1067
4. Burnstock, G., Krügel, U., Abbracchio, M. P., and Illes, P. (2011) Purinergic signalling. From normal behaviour to pathological brain function. *Prog. Neurobiol.* **95,** 229–274
5. León, D., Hervás, C., and Miras-Portugal, M. T. (2006) P2Y1 and P2X7 receptors induce calcium/calmodulin-dependent protein kinase II phosphorylation in cerebellar granule neurons. *Eur. J. Neurosci.* **23,** 2999–3013
6. Ortega, F., Pérez-Sen, R., Delicado, E. G., and Miras-Portugal, M. T. (2009) P2X7 nucleotide receptor is coupled to GSK-3 inhibition and neuroprotection in cerebellar granule neurons. *Neurotox Res.* **15,** 193–204
7. Díaz-Hernandez, M., del Puerto, A., Díaz-Hernandez, J. I., Diez-Zaera, M., Lucas, J. J., Garrido, J. J., and Miras-Portugal, M. T. (2008) Inhibition of the ATP-gated P2X7 receptor promotes axonal growth and branching in cultured hippocampal neurons. *J. Cell Sci.* **121,** 3717–3728
8. Gómez-Villafuertes, R., del Puerto, A., Díaz-Hernández, M., Bustillo, D., Díaz-Hernández, J. I., Huerta, P. G., Artalejo, A. R., Garrido, J. J., and Miras-Portugal, M. T. (2009) Ca^{2+}/calmodulin-dependent kinase II signalling cascade mediates P2X7 receptor-dependent inhibition of neurite-genesis in neuroblastoma cells. *FEBS J.* **276,** 5307–5325
9. Diaz-Hernandez, J. I., Gomez-Villafuertes, R., León-Otegui, M., Hontecillas-Prieto, L., Del Puerto, A., Trejo, J. L., Lucas, J. J., Garrido, J. J., Gualix, J., Miras-Portugal, M. T., and Diaz-Hernandez, M. (2012) *In vivo* P2X7 inhibition reduces amyloid plaques in Alzheimer's disease through GSK3β and secretases. *Neurobiol. Aging* **33,** 1816–1828
10. Díaz-Hernández, M., Díez-Zaera, M., Sánchez-Nogueiro, J., Gómez-Villafuertes, R., Canals, J. M., Alberch, J., Miras-Portugal, M. T., and Lucas, J. J. (2009) Altered P2X7-receptor level and function in mouse models of Huntington's disease and therapeutic efficacy of antagonist administration. *FASEB J.* **23,** 1893–1906
11. Skaper, S. D., Debetto, P., and Giusti, P. (2010) The P2X7 purinergic receptor. From physiology to neurological disorders. *FASEB J.* **24,** 337–345
12. Tsuda, M., Tozaki-Saitoh, H., and Inoue, K. (2010) Pain and purinergic signaling. *Brain Res. Rev.* **63,** 222–232
13. Raffaghello, L., Chiozzi, P., Falzoni, S., Di Virgilio, F., and Pistoia, V. (2006) The P2X7 receptor sustains the growth of human neuroblastoma cells through a substance P-dependent mechanism. *Cancer Res.* **66,** 907–914
14. Di Virgilio, F., Ferrari, D., and Adinolfi, E. (2009) P2X(7). A growth-promoting receptor-implications for cancer. *Purinergic Signal* **5,** 251–256
15. Surprenant, A., Rassendren, F., Kawashima, E., North, R. A., and Buell, G. (1996) The cytolytic P2Z receptor for extracellular ATP identified as a P2X receptor (P2X7). *Science* **272,** 735–738
16. Rassendren, F., Buell, G. N., Virginio, C., Collo, G., North, R. A., and Surprenant, A. (1997) The permeabilizing ATP receptor, P2X7. Cloning and expression of a human cDNA. *J. Biol. Chem.* **272,** 5482–5486
17. Chessell, I. P., Simon, J., Hibell, A. D., Michel, A. D., Barnard, E. A., and Humphrey, P. P. (1998) Cloning and functional characterization of the mouse P2X7 receptor. *FEBS Lett.* **439,** 26–30
18. Gu, B. J., Zhang, W., Worthington, R. A., Sluyter, R., Dao-Ung, P., Petrou, S., Barden, J. A., and Wiley, J. S. (2001) A Glu-496 to Ala polymorphism leads to loss of function of the human P2X7 receptor. *J. Biol. Chem.* **276,** 11135–11142
19. Wiley, J. S., Dao-Ung, L. P., Li, C., Shemon, A. N., Gu, B. J., Smart, M. L., Fuller, S. J., Barden, J. A., Petrou, S., and Sluyter, R. (2003) An Ile-568 to Asn polymorphism prevents normal trafficking and function of the human P2X7 receptor. *J. Biol. Chem.* **278,** 17108–17113
20. Gu, B. J., Sluyter, R., Skarratt, K. K., Shemon, A. N., Dao-Ung, L. P., Fuller, S. J., Barden, J. A., Clarke, A. L., Petrou, S., and Wiley, J. S. (2004) An Arg-307 to Gln polymorphism within the ATP-binding site causes loss of function of the human P2X7 receptor. *J. Biol. Chem.* **279,** 31287–31295
21. Skarratt, K. K., Fuller, S. J., Sluyter, R., Dao-Ung, L. P., Gu, B. J., and Wiley, J. S. (2005) A 5′ intronic splice site polymorphism leads to a null allele of the P2X7 gene in 1–2% of the Caucasian population. *FEBS Lett.* **579,** 2675–2678
22. Cabrini, G., Falzoni, S., Forchap, S. L., Pellegatti, P., Balboni, A., Agostini, P., Cuneo, A., Castoldi, G., Baricordi, O. R., and Di Virgilio, F. (2005) A His-155 to Tyr polymorphism confers gain-of-function to the human P2X7 receptor of human leukemic lymphocytes. *J. Immunol.* **175,** 82–89
23. Shemon, A. N., Sluyter, R., Fernando, S. L., Clarke, A. L., Dao-Ung, L. P., Skarratt, K. K., Saunders, B. M., Tan, K. S., Gu, B. J., Fuller, S. J., Britton,

W. J., Petrou, S., and Wiley, J. S. (2006) A Thr-357 to Ser polymorphism in homozygous and compound heterozygous subjects causes absent or reduced P2X7 function and impairs ATP-induced mycobacterial killing by macrophages. *J. Biol. Chem.* **281,** 2079–2086
24. Eslick, G. D., Thampan, B. V., Nalos, M., McLean, A. S., and Sluyter, R. (2009) Circulating interleukin-18 concentrations and a loss-of-function P2X7 polymorphism in heart failure. *Int. J. Cardiol.* **137,** 81–83
25. Sun, C., Chu, J., Singh, S., and Salter, R. D. (2010) Identification and characterization of a novel variant of the human P2X(7) receptor resulting in gain of function. *Purinergic Signal.* **6,** 31–45
26. Stokes, L., Fuller, S. J., Sluyter, R., Skarratt, K. K., Gu, B. J., and Wiley, J. S. (2010) Two haplotypes of the P2X(7) receptor containing the Ala-348 to Thr polymorphism exhibit a gain-of-function effect and enhanced interleukin-1β secretion. *FASEB J.* **24,** 2916–2927
27. Li, C. M., Campbell, S. J., Kumararatne, D. S., Hill, A. V., and Lammas, D. A. (2002) Response heterogeneity of human macrophages to ATP is associated with P2X7 receptor expression but not to polymorphisms in the P2RX7 promoter. *FEBS Lett.* **531,** 127–131
28. Buell, G. N., Talabot, F., Gos, A., Lorenz, J., Lai, E., Morris, M. A., and Antonarakis, S. E. (1998) Gene structure and chromosomal localization of the human P2X7 receptor. *Receptors Channels* **5,** 347–354
29. Zhou, L., Luo, L., Qi, X., Li, X., and Gorodeski, G. I. (2009) Regulation of P2X(7) gene transcription. *Purinergic Signal* **5,** 409–426
30. Gong, S., Zheng, C., Doughty, M. L., Losos, K., Didkovsky, N., Schambra, U. B., Nowak, N. J., Joyner, A., Leblanc, G., Hatten, M. E., and Heintz, N. (2003) A gene expression atlas of the central nervous system based on bacterial artificial chromosomes. *Nature* **425,** 917–925
31. Banker, G., and Goslin, K. (1988) Developments in neuronal cell culture. *Nature* **336,** 185–186
32. Velasco, M., Díaz-Guerra, M. J., Díaz-Achirica, P., Andreu, D., Rivas, L., and Boscá, L. (1997) Macrophage triggering with cecropin A- and melittin-derived peptides induces type II nitric oxide synthase expression. *J. Immunol.* **158,** 4437–4443
33. Marban, C., Suzanne, S., Dequiedt, F., de Walque, S., Redel, L., Van Lint, C., Aunis, D., and Rohr, O. (2007) Recruitment of chromatin-modifying enzymes by CTIP2 promotes HIV-1 transcriptional silencing. *EMBO J.* **26,** 412–423
34. Carrasquero, L. M., Delicado, E. G., Sánchez-Ruiloba, L., Iglesias, T., and Miras-Portugal, M. T. (2010) Mechanisms of protein kinase D activation in response to P2Y(2) and P2X7 receptors in primary astrocytes. *Glia* **58,** 984–995
35. Nicke, A., Kuan, Y. H., Masin, M., Rettinger, J., Marquez-Klaka, B., Bender, O., Górecki, D. C., Murrell-Lagnado, R. D., and Soto, F. (2009) A functional P2X7 splice variant with an alternative transmembrane domain 1 escapes gene inactivation in P2X7 knock-out mice. *J. Biol. Chem.* **284,** 25813–25822
36. Clark, S. J., Harrison, J., and Molloy, P. L. (1997) Sp1 binding is inhibited by (m)Cp(m)CpG methylation. *Gene* **195,** 67–71
37. Suske, G. (1999) The Sp-family of transcription factors. *Gene* **238,** 291–300
38. Suske, G., Bruford, E., and Philipsen, S. (2005) Mammalian SP/KLF transcription factors. Bring in the family. *Genomics* **85,** 551–556
39. Ferrari, D., Pizzirani, C., Adinolfi, E., Lemoli, R. M., Curti, A., Idzko, M., Panther, E., and Di Virgilio, F. (2006) The P2X7 receptor. A key player in IL-1 processing and release. *J. Immunol.* **176,** 3877–3883
40. Christensen, M. A., Zhou, W., Qing, H., Lehman, A., Philipsen, S., and Song, W. (2004) Transcriptional regulation of BACE1, the β-amyloid precursor protein β-secretase, by Sp1. *Mol. Cell. Biol.* **24,** 865–874
41. Pan, Q., Yang, S., Wei, Y., Sun, F., and Li, Z. (2010) SP1 acts as a key factor, contributes to up-regulation of ADAM23 expression under serum deprivation. *Biochem. Biophys. Res. Commun.* **401,** 306–312
42. Nicolás, M., Noé, V., Jensen, K. B., and Ciudad, C. J. (2001) Cloning and characterization of the 5′-flanking region of the human transcription factor Sp1 gene. *J. Biol. Chem.* **276,** 22126–22132
43. Tapias, A., Auriol, J., Forget, D., Enzlin, J. H., Schärer, O. D., Coin, F., Coulombe, B., and Egly, J. M. (2004) Ordered conformational changes in damaged DNA induced by nucleotide excision repair factors. *J. Biol. Chem.* **279,** 19074–19083
44. Jia, Z., Zhang, J., Wei, D., Wang, L., Yuan, P., Le, X., Li, Q., Yao, J., and Xie, K. (2007) Molecular basis of the synergistic antiangiogenic activity of bevacizumab and mithramycin A. *Cancer Res.* **67,** 4878–4885
45. Sperlágh, B., Vizi, E. S., Wirkner, K., and Illes, P. (2006) P2X7 receptors in the nervous system. *Prog. Neurobiol.* **78,** 327–346
46. Pankratov, Y., Lalo, U., Krishtal, O. A., and Verkhratsky, A. (2009) P2X receptors and synaptic plasticity. *Neuroscience* **158,** 137–148
47. Sperlágh, B., Heinrich, A., and Csölle, C. (2007) P2 receptor-mediated modulation of neurotransmitter release. An update. *Purinergic Signal* **3,** 269–284
48. Abbracchio, M. P., Burnstock, G., Verkhratsky, A., and Zimmermann, H. (2009) Purinergic signalling in the nervous system. An overview. *Trends Neurosci.* **32,** 19–29
49. Ortega, F., Pérez-Sen, R., Morente, V., Delicado, E. G., and Miras-Portugal, M. T. (2010) P2X7, NMDA, and BDNF receptors converge on GSK3 phosphorylation and cooperate to promote survival in cerebellar granule neurons. *Cell. Mol. Life Sci.* **67,** 1723–1733
50. Ortega, F., Pérez-Sen, R., Delicado, E. G., and Teresa Miras-Portugal, M. (2011) ERK1/2 activation is involved in the neuroprotective action of P2Y13 and P2X7 receptors against glutamate excitotoxicity in cerebellar granule neurons. *Neuropharmacology* **61,** 1210–1221
51. Sun, S. H. (2010) Roles of P2X7 receptor in glial and neuroblastoma cells. The therapeutic potential of P2X7 receptor antagonists. *Mol. Neurobiol.* **41,** 351–355
52. Azizkhan, J. C., Jensen, D. E., Pierce, A. J., and Wade, M. (1993) Transcription from TATA-less promoters. Dihydrofolate reductase as a model. *Crit. Rev. Eukaryot. Gene Expr.* **3,** 229–254
53. Tan, N. Y., and Khachigian, L. M. (2009) Sp1 phosphorylation and its regulation of gene transcription. *Mol. Cell. Biol.* **29,** 2483–2488
54. Bird, A. P. (1986) CpG-rich islands and the function of DNA methylation. *Nature* **321,** 209–213
55. Larsen, F., Gundersen, G., Lopez, R., and Prydz, H. (1992) CpG islands as gene markers in the human genome. *Genomics* **13,** 1095–1107
56. Siegfried, Z., Eden, S., Mendelsohn, M., Feng, X., Tsuberi, B. Z., and Cedar, H. (1999) DNA methylation represses transcription *in vivo*. *Nat. Genet.* **22,** 203–206
57. Liu, Y., Liu, X. S., Wei, L., Altman, R. B., and Batzoglou, S. (2004) Eukaryotic regulatory element conservation analysis and identification using comparative genomics. *Genome Res.* **14,** 451–458
58. Jørgensen, N. R., Husted, L. B., Skarratt, K. K., Stokes, L., Tofteng, C. L., Kvist, T., Jensen, J. E., Eiken, P., Brixen, K., Fuller, S., Clifton-Bligh, R., Gartland, A., Schwarz, P., Langdahl, B. L., and Wiley, J. S. (2012) Single-nucleotide polymorphisms in the P2X7 receptor gene are associated with post-menopausal bone loss and vertebral fractures. *Eur. J. Hum. Genet.* **20,** 675–681
59. Fuller, S. J., Stokes, L., Skarratt, K. K., Gu, B. J., and Wiley, J. S. (2009) Genetics of the P2X7 receptor and human disease. *Purinergic Signal* **5,** 257–262
60. Li, C. M., Campbell, S. J., Kumararatne, D. S., Bellamy, R., Ruwende, C., McAdam, K. P., Hill, A. V., and Lammas, D. A. (2002) Association of a polymorphism in the P2X7 gene with tuberculosis in a Gambian population. *J. Infect Dis.* **186,** 1458–1462
61. Bouwman, P., and Philipsen, S. (2002) Regulation of the activity of Sp1-related transcription factors. *Mol. Cell. Endocrinol.* **195,** 27–38
62. Roos, M. D., Su, K., Baker, J. R., and Kudlow, J. E. (1997) O glycosylation of an Sp1-derived peptide blocks known Sp1 protein interactions. *Mol. Cell. Biol.* **17,** 6472–6480
63. Emili, A., Greenblatt, J., and Ingles, C. J. (1994) Species-specific interaction of the glutamine-rich activation domains of Sp1 with the TATA box-binding protein. *Mol. Cell. Biol.* **14,** 1582–1593
64. Koller, C. A., and Miller, D. M. (1986) Preliminary observations on the therapy of the myeloid blast phase of chronic granulocytic leukemia with plicamycin and hydroxyurea. *N. Engl. J. Med.* **315,** 1433–1438
65. Seznec, J., Silkenstedt, B., and Naumann, U. (2011) Therapeutic effects of the Sp1 inhibitor mithramycin A in glioblastoma. *J. Neurooncol.* **101,** 365–377
66. Adinolfi, E., Raffaghello, L., Giuliani, A. L., Cavazzini, L., Capece, M., Chiozzi, P., Bianchi, G., Kroemer, G., Pistoia, V., and Di Virgilio, F. (2012)

Expression of P2X7 receptor increases *in vivo* tumor growth. *Cancer Res.* **72,** 2957–2969
67. Gutiérrez-Martín, Y., Bustillo, D., Gómez-Villafuertes, R., Sánchez-Nogueiro, J., Torregrosa-Hetland, C., Binz, T., Gutiérrez, L. M., Miras-Portugal, M. T., and Artalejo, A. R. (2011) P2X7 receptors trigger ATP exocytosis and modify secretory vesicle dynamics in neuroblastoma cells. *J. Biol. Chem.* **286,** 11370–11381
68. Chatterjee, S., Zaman, K., Ryu, H., Conforto, A., and Ratan, R. R. (2001) Sequence-selective DNA binding drugs mithramycin A and chromomycin A3 are potent inhibitors of neuronal apoptosis induced by oxidative stress and DNA damage in cortical neurons. *Ann Neurol.* **49,** 345–354
69. Ferrante, R. J., Ryu, H., Kubilus, J. K., D'Mello, S., Sugars, K. L., Lee, J., Lu, P., Smith, K., Browne, S., Beal, M. F., Kristal, B. S., Stavrovskaya, I. G., Hewett, S., Rubinsztein, D. C., Langley, B., and Ratan, R. R. (2004) Chemotherapy for the brain. The antitumor antibiotic mithramycin prolongs survival in a mouse model of Huntington's disease. *J. Neurosci.* **24,** 10335–10342
70. Qiu, Z., Norflus, F., Singh, B., Swindell, M. K., Buzescu, R., Bejarano, M., Chopra, R., Zucker, B., Benn, C. L., DiRocco, D. P., Cha, J. H., Ferrante, R. J., and Hersch, S. M. (2006) Sp1 is up-regulated in cellular and transgenic models of Huntington disease, and its reduction is neuroprotective. *J. Biol. Chem.* **281,** 16672–16680
71. Ryu, H., Lee, J., Hagerty, S. W., Soh, B. Y., McAlpin, S. E., Cormier, K. A., Smith, K. M., and Ferrante, R. J. (2006) ESET/SETDB1 gene expression and histone H3 (K9) trimethylation in Huntington's disease. *Proc. Natl. Acad. Sci. U.S.A.* **103,** 19176–19181
72. Stack, E. C., Del Signore, S. J., Luthi-Carter, R., Soh, B. Y., Goldstein, D. R., Matson, S., Goodrich, S., Markey, A. L., Cormier, K., Hagerty, S. W., Smith, K., Ryu, H., and Ferrante, R. J. (2007) Modulation of nucleosome dynamics in Huntington's disease. *Hum. Mol. Genet.* **16,** 1164–1175
73. Hagiwara, H., Iyo, M., and Hashimoto, K. (2009) Mithramycin protects against dopaminergic neurotoxicity in the mouse brain after administration of methamphetamine. *Brain Res.* **1301,** 189–196
74. Dunah, A. W., Jeong, H., Griffin, A., Kim, Y. M., Standaert, D. G., Hersch, S. M., Mouradian, M. M., Young, A. B., Tanese, N., and Krainc, D. (2002) Sp1 and TAFII130 transcriptional activity disrupted in early Huntington's disease. *Science* **296,** 2238–2243
75. Li, S. H., Cheng, A. L., Zhou, H., Lam, S., Rao, M., Li, H., and Li, X. J. (2002) Interaction of Huntington disease protein with transcriptional activator Sp1. *Mol. Cell. Biol.* **22,** 1277–1287
76. Wang, R., Luo, Y., Ly, P. T., Cai, F., Zhou, W., Zou, H., and Song, W. (2012) Sp1 regulates human huntingtin gene expression. *J. Mol. Neurosci.* **47,** 311–321
77. Engel, T., Gomez-Villafuertes, R., Tanaka, K., Mesuret, G., Sanz-Rodriguez, A., Garcia-Huerta, P., Miras-Portugal, M. T., Henshall, D. C., and Diaz-Hernandez, M. (2012) Seizure suppression and neuroprotection by targeting the purinergic P2X7 receptor during status epilepticus in mice. *FASEB J.* **26,** 1616–1628
78. León-Otegui, M., Gómez-Villafuertes, R., Díaz-Hernández, J. I., Díaz-Hernández, M., Miras-Portugal, M. T., and Gualix, J. (2011) Opposite effects of P2X7 and P2Y2 nucleotide receptors on α-secretase-dependent APP processing in Neuro-2a cells. *FEBS Lett.* **585,** 2255–2262
79. Marin, M., Karis, A., Visser, P., Grosveld, F., and Philipsen, S. (1997) Transcription factor Sp1 is essential for early embryonic development but dispensable for cell growth and differentiation. *Cell* **89,** 619–628
80. Saffer, J. D., Jackson, S. P., and Annarella, M. B. (1991) Developmental expression of Sp1 in the mouse. *Mol. Cell. Biol.* **11,** 2189–2199
81. Yoo, J., Jeong, M. J., Kwon, B. M., Hur, M. W., Park, Y. M., and Han, M. Y. (2002) Activation of dynamin I gene expression by Sp1 and Sp3 is required for neuronal differentiation of N1E-115 cells. *J. Biol. Chem.* **277,** 11904–11909
82. Li, L., and Davie, J. R. (2010) The role of Sp1 and Sp3 in normal and cancer cell biology. *Ann. Anat.* **192,** 275–283

Relevance of the MEK/ERK Signaling Pathway in the Metabolism of Activated Macrophages: A Metabolomic Approach

Paqui G. Través, Pedro de Atauri, Silvia Marín, María Pimentel-Santillana, Juan-Carlos Rodríguez-Prados, Igor Marín de Mas, Vitaly A. Selivanov, Paloma Martín-Sanz, Lisardo Boscá and Marta Cascante

J Immunol 2012; 188:1402-1410; Prepublished online 21 December 2011;
doi: 10.4049/jimmunol.1101781
http://www.jimmunol.org/content/188/3/1402

The Journal of Immunology is published twice each month by
The American Association of Immunologists, Inc.,
9650 Rockville Pike, Bethesda, MD 20814-3994.

Print ISSN: 0022-1767 Online ISSN: 1550-6606.

Relevance of the MEK/ERK Signaling Pathway in the Metabolism of Activated Macrophages: A Metabolomic Approach

Paqui G. Través,* Pedro de Atauri,[†,‡,1] Silvia Marín,[†,‡,1] María Pimentel-Santillana,* Juan-Carlos Rodríguez-Prados,[†] Igor Marín de Mas,[†,‡] Vitaly A. Selivanov,[†,‡] Paloma Martín-Sanz,[*,§] Lisardo Boscá,[*,§] and Marta Cascante[†,‡]

The activation of immune cells in response to a pathogen involves a succession of signaling events leading to gene and protein expression, which requires metabolic changes to match the energy demands. The metabolic profile associated with the MAPK cascade (ERK1/2, p38, and JNK) in macrophages was studied, and the effect of its inhibition on the specific metabolic pattern of LPS stimulation was characterized. A [1,2-[^{13}C]$_2$]glucose tracer-based metabolomic approach was used to examine the metabolic flux distribution in these cells after MEK/ERK inhibition. Bioinformatic tools were used to analyze changes in mass isotopomer distribution and changes in glucose and glutamine consumption and lactate production in basal and LPS-stimulated conditions in the presence and absence of the selective inhibitor of the MEK/ERK cascade, PD325901. Results showed that PD325901-mediated ERK1/2 inhibition significantly decreased glucose consumption and lactate production but did not affect glutamine consumption. These changes were accompanied by a decrease in the glycolytic flux, consistent with the observed decrease in fructose-2,6-bisphosphate concentration. The oxidative and nonoxidative pentose phosphate pathways and the ratio between them also decreased. However, tricarboxylic acid cycle flux did not change significantly. LPS activation led to the opposite responses, although all of these were suppressed by PD325901. However, LPS also induced a small decrease in pentose phosphate pathway fluxes and an increase in glutamine consumption that were not affected by PD325901. We concluded that inhibition of the MEK/ERK cascade interferes with central metabolism, and this cross-talk between signal transduction and metabolism also occurs in the presence of LPS. ***The Journal of Immunology*****, 2012, 188: 1402–1410.**

Macrophages have important roles in innate and acquired immunity, as well as in tissue homeostasis (1, 2). Their activation is a complex process involving signaling events triggered by multiple inflammatory mediators, including exogenous factors, such as LPS, and endogenous mediators, such as cytokines and chemokines. Cytokines are major regulators of macrophage activation that limit the amount of inflammation and, thus, prevent toxicity and tissue damage (3, 4). Failure to induce an inflammatory response promotes unrestricted microbial proliferation and the development of serious infections, whereas excessive production of proinflammatory mediators may also be life threatening, as observed in patients with severe sepsis or septic shock. Therefore, immune responses must be tightly regulated (3, 5, 6).

NF-κB and MAPK signaling pathways (ERK, JNK, and p38) play a key role in the activation and regulation of innate and adaptive immune responses. For example, macrophages activate MEK/ERK cascade in response to bacterial infection. MEK/ERK signaling is involved in the activation of oxidative and nitrosative bursts, endosomal trafficking, and proinflammatory macrophage polarization (1, 3, 7–9). Therefore, MEK/ERK signaling is likely to enhance macrophage activity against intracellular pathogens (10–12). The MEK/ERK pathway in macrophages is one of the most widely studied intracellular signaling cascades involved in LPS-induced proinflammatory responses (10). In addition to this, the effect of inhibition of p38 and JNK with the selective inhibitors BIRB796 and BI78D3, respectively, has been evaluated (12, 13).

*Instituto de Investigaciones Biomédicas Alberto Sols, Consejo Superior de Investigaciones Científicas-Universidad Autónoma de Madrid, 28029 Madrid, Spain; [†]Department of Biochemistry and Molecular Biology, Faculty of Biology, University of Barcelona, 08028 Barcelona, Spain; [‡]Institute of Biomedicine, University of Barcelona, 08036 Barcelona, Spain; and [§]Centro de Investigación Biomédica en Red de Enfermedades Hepáticas y Digestivas, 08028 Barcelona, Spain

[1]P.d.A. and S.M. contributed equally to this work.

Received for publication June 17, 2011. Accepted for publication November 16, 2011.

This work was supported by Grants SAF2008-00164, BFU2011-24760, and PIB2010BZ-00540 from Spanish Ministry of Science and Innovation, Red Temática de Investigación Cooperativa en Cáncer, the Instituto de Salud Carlos III, Spanish Ministry of Science and Innovation and European Regional Development Fund "Una manera de hacer Europa" ISCIII-RTICC (RD6/0020/0046), and FIS-RECAVA (RD06/0014/0006) and CIBERehd founded by Instituto de Salud Carlos III, the European Commission (FP7) Etherpath KBBE Grant Agreement 222639, and by Agència de Gestió d'Ajuts Universitaris i de Recerca-Generalitat de Catalunya (Grant 2009SGR1308, 2009 CTP 00026, and Icrea Academia award 2010 to M.C.).

Address correspondence and reprint requests to Dr. Lisardo Boscá or Dr. Marta Cascante, Instituto de Investigaciones Biomédicas "Alberto Sols," Consejo Superior de Investigaciones Científicas-Universidad Autónoma de Madrid, Arturo Duperier 4, 28029 Madrid, Spain (L.B.) or Department of Biochemistry and Molecular Biology, Faculty of Biology, Universitat de Barcelona, Edifici Nou, Planta-2, Avinguda Diagona l645, 08028 Barcelona, Spain (M.C.). E-mail addresses: lbosca@iib.uam.es (L.B.) and marta.cascante@ub.edu (M.C.)

Abbreviations used in this article: COX-2, cyclooxygenase 2; DAF-2DA, 4,5-diaminofluorescein diacetate; DCFH-DA, dichlorofluorescein diacetate; FBPase-2, fructose-2,6-bisphosphatase; Fru-1,6-P_2, fructose-1,6-bisphosphate; Fru-2,6-P_2, fructose-2,6-bisphosphate; G6PDH, glucose-6-phosphate dehydrogenase; L-PFK-2, liver-type-PFK-2; Mal, malate; NOS-2, NO synthase 2; Oaa, oxaloacetate; PDH, pyruvate dehydrogenase; PFK-1, 6-phosphofructo-1-kinase; PFK-2, 6-phosphofructo-2-kinase; 6PGDH, 6-phospho-D-gluconate dehydrogenase; PI, propidium iodide; PPP, pentose phosphate pathway; Pyr, pyruvate; ROS, reactive oxygen species; TCA, tricarboxylic acid; uPFK-2, PFKB3 isoenzyme of PFK-2.

www.jimmunol.org/cgi/doi/10.4049/jimmunol.1101781

Immune activation rapidly and substantially enhances metabolic outputs (14, 15). Macrophage activation is followed by rapid changes in nutrient flux, which also seems to be necessary for immune activation, indicating that signals produced by immune cells might directly regulate their metabolism. Indeed, studies have highlighted a key role for activated macrophages in controlling energy metabolism and insulin action (15–17). For example, low-grade chronic inflammation is associated with accumulation of macrophages in adipose tissue and predisposition to insulin resistance (15, 18).

In the current study, we aimed to characterize changes in the central carbon metabolic network induced by ERK inhibition and provide a tool to analyze the metabolic flux distribution in macrophages as cross-talk between signal transduction and metabolic events. For this purpose, we used LPS as a model of proinflammatory activation and PD325901 as a selective inhibitor of the MEK/ERK cascade (12). To determine the metabolic state of the cells, we used a tracer-based metabolomics approach with [1,2-[^{13}C]$_2$]glucose as the carbon source. Mass isotopomer distribution analysis of key metabolites has been described as a powerful tool to map metabolic flux distribution in several cellular models (19, 20). By tracking the changes in metabolic fluxes induced by ERK signaling modulators, we observed details of the cross-talk between inflammatory signal transduction and metabolic networks. Similar results on glycolytic metabolism were observed in a macrophage cell line in primary cultures of murine peritoneal macrophages and in human monocytes/macrophages.

Materials and Methods

Materials

The murine macrophage cell line RAW 264.7 was obtained from the American Type Culture Collection (Manassas, VA). RPMI 1640, FBS, cell culture, and chemical reagents were obtained from Lonza (Cologne, Germany); PD325901, BIRB796, and BI78D3 were from Calbiochem (San Diego, CA). [1,2-[^{13}C]$_2$]glucose (>99% enriched) was from Isotec (Miamisburg, OH). LPS and reagents for metabolite derivatization were from Sigma-Aldrich (St. Louis, MO). Abs were from Santa Cruz Biotech (Santa Cruz, CA), Cell Signaling (Danvers, MA), or Sigma-Aldrich.

Cell culture conditions

RAW 264.7 cells were cultured in RPMI 1640 supplemented with glutamine (2 mM), 10% FBS, and antibiotics (100 U/ml penicillin, 100 μg/ml streptomycin, and 50 μg/ml gentamicin) at 37˚C in 5% CO_2. When cells reached 80% subconfluency, the medium was replaced with a medium containing only 2% FBS. After overnight serum reduction, cell cultures were loaded with [1,2-[^{13}C]$_2$]glucose and treated with 0.5 μM PD325901 and 500 ng/ml LPS for the indicated periods of time. The same procedure was used for studies with p38 and JNK inhibitors but in the absence of labeled glucose. Following incubation, the medium was removed, and cells were scraped off the dishes and processed for RNA, proteins, and intracellular metabolites. Murine peritoneal macrophages and human monocyte/macrophages were prepared (14, 21) and were used as described for the RAW 264.7 cells.

Flow cytometry

Cells were harvested and washed in PBS. After centrifugation at 4˚C for 5 min and 1000 × *g*, cells were resuspended in Annexin V binding buffer (10 mM HEPES [pH 7.4], 140 mM NaCl, 2.5 mM $CaCl_2$) and labeled with Annexin V^{FITC} solution and/or propidium iodide (PI) (100 μg/ml) for 15 min at room temperature in the dark. PI is impermeable to living and early apoptotic cells but stains necrotic and apoptotic dying cells with impaired membrane integrity in contrast to Annexin V, which stains early apoptotic cells.

6-Phosphofructo-2-kinase activity assay

Cells (grown in 6-cm dishes) were homogenized in 1 ml a medium containing 20 mM potassium phosphate ([pH 7.4], 4˚C), 1 mM DTT, 50 mM NaF, 0.5 phenylmethanesulfonyl fluoride, 10 μM leupeptin, and 5% poly (ethylene)glycol. After centrifugation in an Eppendorf centrifuge (15 min), poly(ethylene)glycol was added to the supernatant up to 15% (mass/vol) to fully precipitate the 6-phosphofructo-2-kinase (PFK-2). After resuspension of the pellet in the extraction medium, PFK-2 activity was assayed at pH 8.5 with 5 mM MgATP, 5 mM fructose-6-phosphate, and 15 mM glucose-6-phosphate. One unit of PFK-2 activity is the amount of enzyme that catalyzes the formation of 1 pmol Fru-2,6-bisphosphate (Fru-2,6-P_2)/min (22).

Metabolite assays

Fru-2,6-P_2 was extracted from cells (cultured in 24-well plates) after homogenization in 100 μl 50 mM NaOH, followed by heating at 80˚C for 10 min. The metabolite was measured by the activation of the pyrophosphate-dependent 6-phosphofructo-1-kinase (PFK-1) (22). Glucose and lactate were measured enzymatically in the culture medium (23). Glutamine was determined after deamination to glutamate, which was measured enzymatically using the enzyme glutamate dehydrogenase (23). NO release was determined spectrophotometrically by the accumulation of nitrite and nitrate in the medium (phenol red-free), as described before (14).

Preparation of cell extracts

Cells (grown in six-well dishes) were washed twice with ice-cold PBS and homogenized in 0.2 ml buffer containing 10 mM Tris-HCl (pH 7.5), 1 mM $MgCl_2$, 1 mM EGTA, 10% glycerol, 0.5% CHAPS, 1 mM 2-ME, 0.1 mM PMSF, and a protease inhibitor mixture (Sigma-Aldrich). The extracts were vortexed for 30 min at 4˚C and centrifuged for 10 min at 13,000 × *g*. The supernatants were stored at −20˚C. Protein levels were determined using the Bio-Rad detergent-compatible protein reagent (Richmond, CA). All steps were carried out at 4˚C.

Western blot analysis

Samples of cell extracts containing equal amounts of protein (30 μg/lane) were boiled in 250 mM Tris-HCl (pH 6.8), 2% SDS, 10% glycerol, and 2% 2-ME and separated in 10% SDS-PAGE. The gels were blotted onto a polyvinylidene fluoride membrane (GE Healthcare, Barcelona, Spain) and processed as recommended by the supplier of the Abs against the murine Ags: phospho-ERK1/2 (9101s), phospho-p38 (9211s), phospho-JNK (9251s), NO synthase 2 (NOS-2; sc-7271), cyclooxygenase 2 (COX-2; sc-1999), liver-type–PFK-2 (L–PFK-2) (sc-10096), and β-actin (A-5441). For PFKB3 isoenzyme of PFK-2 (uPFK-2), specific peptides of the isoenzyme were used to generate polyclonal Abs by immunizing rabbits (New Zealand White) with multiple intradermal injections of 300 μg Ag in 1 ml CFA, followed by boosters with 100 μg Ag in IFA. The blots were developed by the ECL protocol (Amersham), and different exposure times were used for each blot with a charged-coupling device camera in a luminescent-image analyzer (Molecular Imager, Bio-Rad) to ensure linearity of the band intensities.

RNA isolation and RT-PCR analysis

One microgram of total RNA, extracted with TRIzol Reagent (Invitrogen) according to the manufacturer's instructions, was reverse transcribed using Transcriptor First Strand cDNA Synthesis Kit for RT-PCR, following the instructions of the manufacturer (Roche). Real-time PCR was conducted with SYBR Green on a MyiQ real-time PCR System (Bio-Rad), using the SYBR Green method. PCR thermocycling parameters (24) were 95˚C for 10 min, 40 cycles of 95˚C for 15 s, and 60˚C for 1 min. All samples were analyzed for 36B4 expression in parallel. Each sample was run in duplicate and was normalized to 36B4. The replicates were then averaged, and fold induction was determined on ΔΔCt-based fold-change calculations. Primer sequences are available on request.

Measurement of reactive oxygen species and NO synthesis

The generation of reactive oxygen species (ROS) was monitored using dichlorofluorescein diacetate (DCFH-DA). Cells were preincubated with 10 μM DCFH-DA for 15 min and fluorescence was measured using a cell cytometer. For fluorometric NO determination, the cell-permeable fluorophore 4,5-diaminofluorescein diacetate (DAF-2DA) was used. Cells were preincubated with 10 μM DAF-2DA for 15 min, and DAF-2DA fluorescence was measured in a cell cytometer.

Metabolite isolation and isotopologue analysis

Glucose, lactate, and glutamate from the incubation medium were purified, derivatized, and analyzed, as previously described (19). Thus, glucose was purified from culture medium using a tandem set of Dowex-1X8/Dowex-50WX8 (Sigma-Aldrich) ion-exchange columns and converted to its aldonitrile pentaacetate derivative. The ion cluster around m/z 328 was

monitored (carbons 1 to 6 of glucose, chemical ionization). Lactate from the cell culture media was extracted by ethyl acetate after acidification with HCl. Lactate was derivatized to its propylamide-heptafluorobutyric form, and the cluster around m/z 328 (carbons 1 to 3 of lactate, chemical ionization) was monitored. Glutamate was separated from the medium using ion-exchange chromatography and converted to its n-trifluoroacetyl-n-butyl derivative. The ion clusters around m/z 198 (carbons 2 to 5 of glutamate, electron impact ionization) and m/z 152 (carbons 2 to 4 of glutamate, electron impact ionization) were monitored. RNA ribose was purified, derivatized, and analyzed, as previously described (20). In detail, RNA ribose was isolated by acid hydrolysis of cellular RNA after TRIzol purification of cell extracts. Ribose isolated from RNA was derivatized to its aldonitrile acetate form using hydroxylamine in pyridine and acetic anhydride, and the ion cluster around the m/z 256 (carbons 1 to 5 of ribose, chemical ionization) was monitored. Spectral data were corrected using regression analysis to extract natural [^{13}C] enrichment from the results (25). Measurement of [^{13}C] label distribution determined the different relative distribution percentages of isotopologues, and m0 (molecules without any [^{13}C] labels), m1 (molecules with one [^{13}C]), m2 (with two [^{13}C]), and so forth were reported as molar fractions.

Gas chromatography/mass spectrometry

Mass spectral data were obtained on a QP2010 mass selective detector connected to a GC-2010 gas chromatograph (Shimadzu Scientific Instruments) using helium as the gas carrier and isobutane 0.0016 Pa as the reagent gas in chemical-ionization analysis. Settings were as follows: gas chromatograph inlet, 250°C for glucose, ribose, and glutamate and 200°C for lactate; transfer line, 250°C; and mass chromatography source, 200°C. A Varian VF-5 capillary column (30 m in length, 250 μm in diameter, and with a 0.25-μm film thickness) was used to analyze all of the compounds. In vitro experiments were carried out using duplicate cultures each time for each treatment regimen. Mass spectral analyses were carried out by three independent automated injections of 1 μl each sample and were accepted only if the standard sample deviation was <1% of the normalized peak intensity.

Estimation of internal fluxes based on the measured [^{13}C] redistribution

Each ^{13}C-labeled metabolite corresponds to a different isotopomer, which differs only in the labeling state of its individual atoms (26). For a specific metabolite, the number of possible isotopomers, 2^n, depends on the number, *n*, of carbons for each metabolite. The relative abundance of product isotopomers depends on the labeled status of the substrates (50% [1,2-[^{13}C]$_2$]glucose) and the flux distribution throughout the metabolic network (27–29). Isotopomer abundances can be predicted by solving a system of isotopomer mass balance equations, where each equation describes the dependency of each isotopomer abundance on fluxes and isotopomer abundance of other metabolites (30). The space of solution for each condition (vehicle, LPS, PD325901, and PD325901+LPS) is scanned by solving the system of equations for feasible combinations of flux values for all reaction steps. All combinations satisfied the constraints associated with network topology described below, stoichiometry for each reaction, and measured fluxes for glucose consumption, lactate production, and glutamine consumption (23). Also, total [^{13}C] enrichment of ribose ($\sum$m = m1+m2+m3) was applied to fix the differential de novo RNA synthesis (step D in Fig. 5) among the analyzed conditions (Table I). For reversible reactions, exchange fluxes, which account for the cycle through the forward and backward reactions (29, 31), were considered in addition to the net reactions. Ratios m1/(m1+m2) and m2/(m1+m2) for lactate and glutamate C2–C4 and C2–C5 fragments and m1/(m1+m2+m3), m2/(m1+m2+m3), and m3/(m1+m2+m3) for ribose measured experimentally (Table I) and predicted for different flux distributions were compared (least squares). The 20 combinations of flux distributions with a best fitting were taken for each case (vehicle, PD325901, LPS, and PD325901+LPS).

Network structure

The assumed network scheme corresponds to those in Fig. 5. Each solid arrow indicates a reversible or irreversible reaction step catalyzed by an enzyme (or transporter) or one block of enzymes. Dashed lines indicate regulatory connections (product inhibition by glucose-6-phosphate and activation of pyruvate kinase by fructose-1,6-bisphosphate (Fru-1,6-P$_2$). Letters correspond to the reaction steps. Reaction steps A–P account for glycolysis, as well as pentose phosphate pathway (PPP) and tricarboxylic acid (TCA) cycle enzyme-catalyzed reactions. Some reactions are neglected and grouped into blocks (e.g., reaction step F representing the block from GAPDH to pyruvate kinase), and others are assumed to be involved in rapid equilibriums (e.g., glucose-6-phosphate isomerase). Metabolites are combined into pools: a first pool for hexose-phosphates, including glucose-6-phosphate and fructose-6-phosphate; a second pool for pentose-phosphates accounting for ribose-5-phosphate, ribulose-5-phosphate, and xylulose-5-phosphate; and a third pool for oxaloacetate (Oaa) and malate (Mal). The rest of the metabolic intermediaries are Fru-1,6-P$_2$, dihydroxyacetonephosphate, GAPDH, sedoheptulose-7-phosphate, erythrose-4-phosphate, pyruvate (Pyr), acetyl-CoA, citrate, 2-oxoglutarate, and succinyl-CoA. Reaction steps A, D, T, U, X, Y, and Z represent the inputs and outputs of the metabolic system.

Estimation of flux dependencies on enzyme activities

Estimation of flux dependencies on enzyme activities are based on the identification of control coefficients with fixed signs. The sign and magnitude of control coefficients depend on the topology of the network, the stoichiometry of the reactions, and the magnitudes of fluxes and of regulatory dependencies (enzyme–substrate affinity, inhibitions, and activations) (23). Magnitudes of regulatory dependencies are unknown, but the sign of some control coefficients are fixed, irrespective of these magnitudes. Others are sign indeterminate, meaning that they can be positive and negative, and some are always zero.

Statistical analysis

The data shown are the means ± SD of three or four experiments. Statistical significance was estimated with the Student *t* test for unpaired observations. Significance of isotopologue data (Table I) was analyzed using two-way ANOVA.

Results

Characterization of macrophage activation after ERK1/2 inhibition

To characterize the response of RAW 264.7 cells to the MEK/ERK selective inhibitor PD325901 (12) and LPS activation, several functional markers were used. Fig. 1*A* shows the dose-dependent inhibition of ERK1/2 phosphorylation by PD325901 in LPS-activated cells. The inhibitor significantly decreased LPS-induced NOS-2 and COX-2 protein levels (Fig. 1*B*), as well as nitrite plus nitrate accumulation in the medium (Fig. 1*C*). At the metabolic level, PD325901 decreased the basal levels of Fru-2,6-P$_2$, a potent activator of the glycolytic flux, and impaired its increase induced by LPS (Fig. 1*D*). This was associated with a decrease in the expression of the highly active uPFK-2 isoform induced by LPS and, concomitantly, a reduction in total PFK-2/fructose-2,6-bisphosphatase (FBPase-2) activity (Fig. 1*E*). Similar results in terms of ERK inhibition, NOS-2 and COX-2 expression, and changes in PFK-2 isoenzymes were observed with the MEK/ERK inhibitors SL327 and PD98059 (data not shown). Changes in mRNA correlated with those observed for protein levels of NOS-2, COX-2, uPFK-2, and L–PFK-2 (Fig. 1*F*). Moreover, to reinforce the specific effect of ERK1/2 inhibition on LPS activation, an increase in IL-12p40 (IL-12) and decrease in TNF-α mRNA levels were observed (Fig. 1*G*), as described before (32). PD325901 impaired LPS induction of IL-1β and IL-6 mRNA levels (Fig. 1*G*) but did not affect the levels of the chemokines CXCL-1 and CXCL-10 (Fig. 1*H*). Because cell activation might interfere with viability, the percentage of apoptotic cells was determined by measuring Annexin V and PI staining. PD325901 moderately influenced cell viability in resting macrophages but enhanced apoptosis in LPS-activated cells (Fig. 2*A*). Moreover, PD325901 decreased cell numbers at 18 h but did not significantly affect the percentage of cells gating at the S, G$_2$, and M phases of the cell cycle, which was <18% (Fig. 2*A*). The oxidation of DCFH-DA and DAF during LPS activation was measured at 18 h. PD325901 moderately increased the oxidation of both probes but impaired the large changes that accompany LPS activation (Fig. 2*B*). An image of cells after 18 h of treatment is shown in Fig. 2*C*.

To characterize the metabolic changes induced by ERK1/2 inhibition, RAW 264.7 cells were treated with 0.5 μM of PD325901

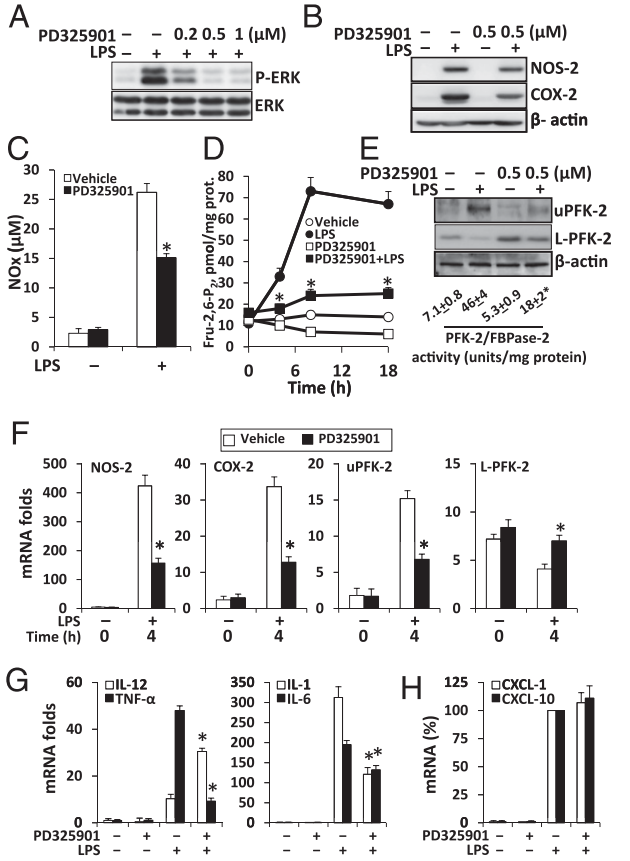

FIGURE 1. Effect of MEK/ERK inhibition on LPS activation of RAW 264.7 macrophages. Cells were maintained overnight in 2% FBS and treated with the indicated concentrations of PD325901 10 min before activation with 500 ng/ml LPS. The levels of phospho-ERK1/2 were determined at 30 min (*A*), and the levels of NOS-2, COX-2 (*B*), and nitrite plus nitrate in the medium (NOx) were determined after 18 h (*C*). *D*, The time course of the intracellular levels of Fru-2,6-P_2 was evaluated after treatment with 0.5 μM PD325901 and 500 ng/ml LPS. *E*, The protein levels of uPFK-2 and L-PFK-2 and the PFK-2/FBPase-2 activity were determined at 18 h. *F*, The mRNA levels of the indicated genes were determined at 0 and 4 h after LPS activation. The mRNA levels of IL-12, activated upon ERK1/2 inhibition, and TNF-α, IL-1β, IL-6 (*G*), and the chemokines CXCL-1 and CXCL-10 (*H*) were determined at 4 h after treatment. Results are representative blots for four experiments or the mean ± SD of four experiments. $^*p < 0.01$ versus no PD325901.

and/or 500 ng/ml of LPS. Glucose and glutamine consumptions and lactate production after 1, 4, and 8 h of incubation are presented in Fig. 3*A*. Both glucose consumption and lactate production were lower in the presence of PD325901, whereas glutamine consumption was not affected. LPS stimulation increased glucose consumption and lactate production but did not induce these effects in the presence of PD325901. Interestingly, LPS increased glutamine consumption, regardless of the presence of PD325901. The ratios between lactate production and glucose consumption, as well as glucose/glutamine consumption are shown (Fig. 3*B*). Because glucose-6-phosphate dehydrogenase (G6PDH) and 6-phospho-D-gluconate dehydrogenase (6PGDH) activities might be affected by PD325901 in LPS-activated cells, the time course of their activity was measured, with a modest transient increase at 8 h, independent of PD325901 treatment (Fig. 3*C*). In addition to RAW 264.7 cells, the effect of the inhibition of ERK on LPS-dependent activation of glycolysis was investigated in peritoneal murine macrophages and in human monocyte/macrophages. As Fig. 3*D* shows, LPS challenge promoted uPFK-2 expression and an increase in Fru-2,6-P_2 levels in these macrophages. Treatment with PD325901 blunted the effect of LPS on both uPFK-2 expression and Fru-2,6-P_2 increase. In addition to this, good correlations between uPFK-2/Fru-2,6-P_2 levels and glucose consumption and lactate production were observed in the three types of macrophages analyzed (Fig. 3*E*).

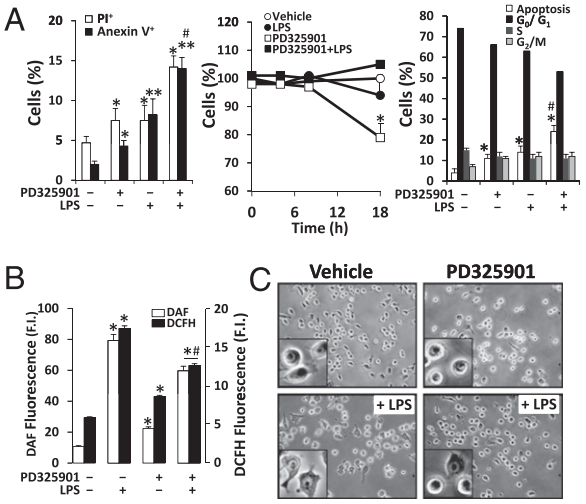

FIGURE 2. Effect of MEK/ERK inhibition on cell viability and oxidative stress. Cells were pretreated with 0.5 μM PD325901 10 min before activation with 500 ng/ml LPS. *A*, After 8 h of treatment, the percentage of cells positive for PI and Annexin V staining was determined (*left panel*). The time course of the cell density (*center panel*) and the cell cycle distribution at 18 h (*right panel*) were determined. *B*, The changes in fluorescence of DAF and DCFH-DA were determined at 18 h. *C*, A representative photograph of macrophages treated for 18 h with PD325901 and LPS at low cell density. Original magnification ×100; ×400 *inset*). Results show the mean ± SD of three experiments. $^*p < 0.05$, $^{**}p < 0.01$ versus the untreated condition. $^{\#}p < 0.01$ versus no PD325901.

Inhibition of p38 and JNK MAPKs with selective inhibitors was also evaluated in RAW 264.7 cells. The p38 inhibitor BIRB796 did not significantly affect cell viability at 0.5 μM (Fig. 4*A*; previous p38 inhibitors exhibited cytotoxic effects) and suppressed p38 phosphorylation (Fig. 4*B*). However, the selective JNK inhibitor BI78D3 significantly decreased cell viability at the minimal concentration required to suppress JNK phosphorylation in response to LPS (Fig. 4*A*, 4*B*). p38 inhibition did not influence the LPS-dependent uPFK-2 expression (Fig. 4*C*), the increase in Fru-2,6-P_2 levels, or the glycolytic flux in RAW 264.7 cells (Fig. 4*D*). With regard to JNK inhibition, it is difficult to draw conclusions about the effects on cell viability. Although treatment with BI78D3 decreased uPFK-2 levels at 8 h after LPS treatment (Fig. 4*C*), the Fru-2,6-P_2 levels at 8 h were 81% of those of LPS (Fig. 4*D*), which contrasts with the 69% inhibition observed after MEK/ERK inhibition (Fig. 1*D*).

Measured isotopologue distribution

The metabolism of [1,2-[^{13}C]$_2$]glucose causes rearrangement, exchange, or loss of the [^{13}C] label, which is incorporated into the glucose metabolic intermediates in specific patterns. The [^{13}C] label enrichment of these intermediates also depends on the dilution of their unlabeled counterparts. Thus, a specific isotopologue distribution provides information on the flux of metabolites along the forward and reverse pathways of substrate cycles. RAW 264.7 cells treated with 0.5 μM of PD325901 and/or 500 ng/ml of LPS were incubated for 18 h with 10 mM glucose 50% enriched in [1,2-[^{13}C]$_2$]-D-glucose, and the isotopologue distributions were measured (Table I).

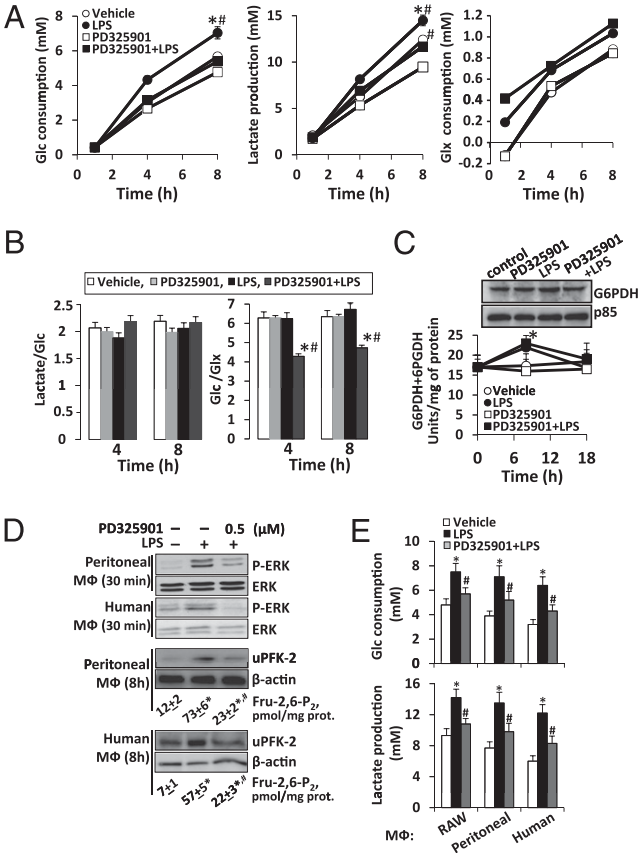

FIGURE 3. Effect of MEK/ERK inhibition on LPS-activation of metabolic fluxes in macrophages. RAW 264.7 cells were pretreated with 0.5 μM PD325901 10 min before activation with 500 ng/ml LPS. *A*, The glucose and glutamate consumption and lactate production were determined at the indicated times. *B*, The ratios between lactate and glucose and glucose and glutamate concentrations at 4 and 8 h after activation. *C*, G6PDH+6PGDH activities were determined at the indicated times, and a blot showing the protein levels at 18 h is shown. *D*, The effect of 0.5 μM PD325901 on LPS activation in peritoneal murine macrophages and human monocyte/macrophages was analyzed in terms of ERK phosphorylation (30 min), as well as uPFK-2 expression and Fru-2,6-P_2 levels (8 h). *E*, Glucose consumption and lactate release were determined at 8 h. Results show the mean ± SD of four experiments. $^{*}p < 0.01$ versus the untreated condition; $^{\#}p < 0.05$ versus no PD325901.

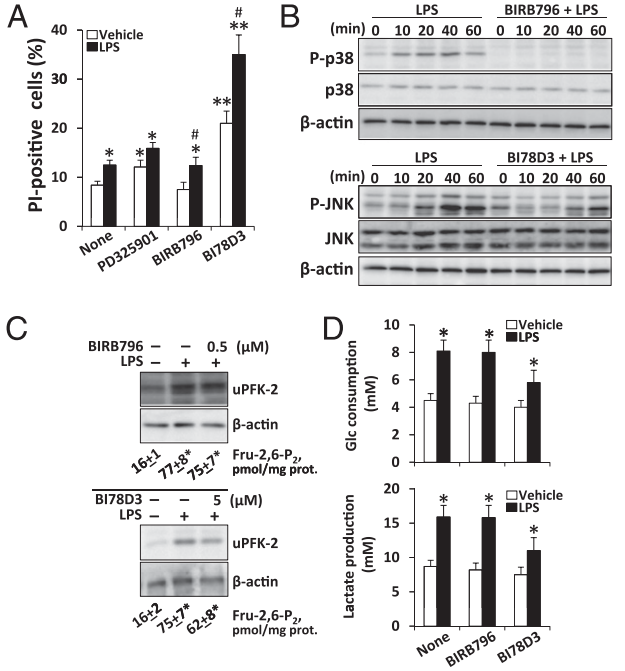

FIGURE 4. Effect of MAPK inhibition on LPS activation of metabolic fluxes in macrophages. RAW 264.7 cells were pretreated with 0.5 μM BIRB796 (p38 inhibitor) or 5 μM BI78D3 (JNK inhibitor) 10 min before activation with 500 ng/ml LPS. *A*, Cell viability was determined at 8 h by PI staining. *B*, MAPK inhibition was determined at the indicated times. The effect of MAPK inhibitors on LPS activation was analyzed in terms of uPFK-2 expression and Fru-2,6-P_2 levels (*C*), as well as glucose consumption and lactate release at 8 h (*D*). Results show the mean ± SD of three experiments. $^{*}p < 0.05$, $^{**}p < 0.01$ versus the untreated condition; $^{\#}p < 0.05$ versus no MAPK inhibitor.

Glucose and lactate in the medium. Glucose enrichment was not significantly affected either by PD325901 or LPS treatment alone or in combination (data not shown), indicating that the macrophages did not release newly synthesized glucose into the medium. With regard to lactate, [^{13}C] incorporation through glycolysis results in the formation of lactate with two [^{13}C] (m2 lactate). m1 lactate mainly originates from the decarboxylation of [^{13}C] caused by the metabolism of [1,2-[^{13}C]$_2$]glucose through the oxidative branch of the PPP and its subsequent recycling to glycolysis through the nonoxidative branch of PPP or by the action of Pyr cycling (mediated by phosphoenolpyruvate carboxykinase or malic enzyme). The parameter PPC (PPC = [m1/m2]/[3+(m1/m2)]) that represents the contribution of these last two pathways over glycolysis was lower after activation with LPS, regardless of the presence of PD325901. This suggested that MEK inhibition did not affect the relative contribution of these pathways to lactate formation.

Ribose in RNA. Pentose phosphates can be synthesized from glucose or glycolytic intermediates through two pathways: the oxidative and nonoxidative branches of the PPP. The ratio of m1/m2 among the different ribose isotopologue fractions represents the contribution of the oxidative versus the nonoxidative branch of PPP. This ratio changes from 1.29 in control to 1.10 in the presence of PD325901, 1.08 after LPS activation, and 1.13 in the presence of both, indicating a similar decrease in the oxidative branch of ribose synthesis in all cases. A part of RNA ribose was not synthesized de novo, because the nonlabeled nucleotides that existed before the incubation were reused in subsequent generations. This reused part contributed to the value of the nonlabeled fraction (m0) of defined RNA ribose. The lower m0 value found in control and LPS conditions suggested that PD325901 addition resulted in diminishing de novo synthesis of nucleotides.

Glutamate in the medium. Label distribution in glutamate allows us to estimate the relative contributions of pyruvate carboxylase and pyruvate dehydrogenase (PDH) to the TCA cycle (19). The fact that glutamate was mainly labeled at the fourth and fifth positions in all incubation conditions demonstrated that [^{13}C] from [1,2-[^{13}C]$_2$]glucose entered the TCA cycle, mainly by PDH in RAW 264.7 cells, regardless of treatment. Furthermore, glutamate labeling increased in the presence of PD325901 and/or LPS, indicating that both stimuli and their combination increased the exchange between glutamate and α-ketoglutarate.

Estimation of internal fluxes

Mass isotopomer distribution analysis was completed with a numerical estimation of internal fluxes. To reveal the profiles of internal metabolic fluxes that underlie the isotopologue distributions corresponding to ERK1/2 inhibition in resting or activated cells, we analyzed the label distributions using the approach described in *Materials and Methods*. The metabolic network ana-

Table I. Isotopologue distribution in different metabolites

Metabolite	Vehicle	LPS	PD325901	PD325901+LPS
Lactate C1–C3				
m0	0.783 ± 0.0033	0.783 ± 0.0116	0.790 ± 0.004	0.772 ± 0.006*,#
m1	0.0200 ± 0.0033	0.0156 ± 0.0026**	0.0184 ± 0.0016	0.0173 ± 0.0020
m2	0.198 ± 0.004	0.212 ± 0.006**	0.190 ± 0.004**	0.211 ± 0.004*
PPC	0.033 ± 0.006	0.024 ± 0.004**	0.031 ± 0.003	0.027 ± 0.003*
Ribose C1–C5				
m0	0.752 ± 0.006	0.766 ± 0.002	0.801 ± 0.005**	0.771 ± 0.003*
m1	0.121 ± 0.004	0.103 ± 0.003*	0.092 ± 0.004**	0.102 ± 0.001**
m2	0.0938 ± 0.0026	0.0954 ± 0.0012	0.0840 ± 0.0012*	0.0905 ± 0.0017
m3	0.0206 ± 0.0015	0.0212 ± 0.0006	0.010 ± 0.0086*	0.0234 ± 0.0019
m1/m2	1.29 ± 0.00	1.08 ± 0.05**	1.10 ± 0.06**	1.13 ± 0.02**
Glutamate C2–C5				
m0	0.974 ± 0.001	0.959 ± 0.002**	0.960 ± 0.003**	0.956 ± 0.002**,#
m1	0.0050 ± 0.0006	0.0111 ± 0.0008**	0.0079 ± 0.0020**	0.0099 ± 0.0008**
m2	0.0201 ± 0.0005	0.0287 ± 0.0009**	0.0308 ± 0.0012**	0.033 ± 0.0006**,##
Glutamate C2–C4				
m0	0.975 ± 0.001	0.960 ± 0.001**	0.960 ± 0.003**	0.956 ± 0.001**,##
m1	0.0245 ± 0.0007	0.0390 ± 0.0013**	0.0390 ± 0.0026**	0.0435 ± 0.0015**,##
m2	0.0007 ± 0.0003	0.0011 ± 0.0005	0.0007 ± 0.0012	0.0006 ± 0.0006
Contributions to TCA cycle				
Pyruvate carboxylase	0.04 ± 0.01	0.04 ± 0.02	0.01 ± 0.04*	0.02 ± 0.02
PDH	0.96 ± 0.01	0.96 ± 0.02	0.99 ± 0.04*	0.98 ± 0.02

Isotopologue distribution of lactate (fragment C1–C3) and glutamate (fragments C2–C5 and C2–C4) secreted into the culture medium and RNA ribose (fragment C1–C5) after 18 h without LPS or PD325901 (vehicle) or with LPS and PD325901 individually or in combination. PPC parameter was estimated from the formula (m1/m2)/{3 + (m1/m2)} using lactate isotopologue fractions. Pyruvate carboxylase and PDH contributions to TCA cycle were estimated using $m2_{C2–C4}/m2_{C2–C5}$ and $(m2_{C2–C5} - m2_{C2–C4})/m2_{C2–C5}$, respectively. Values are expressed as mean ± SD.

*$p < 0.05$, **$p < 0.01$ versus the untreated condition; #$p < 0.05$, ##$p < 0.01$ versus no PD325901.

lyzed is depicted in Fig. 5, and the resulting numerical estimation of fluxes throughout the main steps in the metabolic network is presented in Fig. 6. The flux profile results indicated that RAW 264.7 cells under basal conditions were mainly glycolytic, having most of the consumed glucose (flux through A) converted into lactate (flux through T). The consumed glutamine in the TCA cycle (flux through U) was transformed to Oaa-Mal (fluxes through O and P), mainly recycled to Pyr (flux through R), and excreted into the medium as lactate. Flux through PDH (flux through L) was ~40–80 times lower than that from the triose phosphate pool to Pyr (flux through F), suggesting that glucose and glutamine are mainly rerouted to lactate, and only ~1.25–2.5% of the Pyr produced from glucose enters the TCA cycle in RAW 264.7 cells. The incubation of RAW 264.7 cells with PD325901 produced a clear decrease in almost all the analyzed fluxes. Furthermore, LPS increased the glycolytic flux, although this was inhibited by PD325901. With regard to PPP fluxes, observed differences in fluxes through B, G, H, and I showed a clear decrease in the presence of PD325901. A smaller decrease in the PPP fluxes was induced by LPS and when cells were coincubated with PD325901 and LPS. These differences in flux profiles are consistent with the different consumptions and productions of glucose, lactate, and glutamine and de novo synthesis of nucleotides.

Flux dependencies on enzyme activities

At a specific network description of central carbon metabolism with a particular topology, reaction stoichiometry, flux values and sign

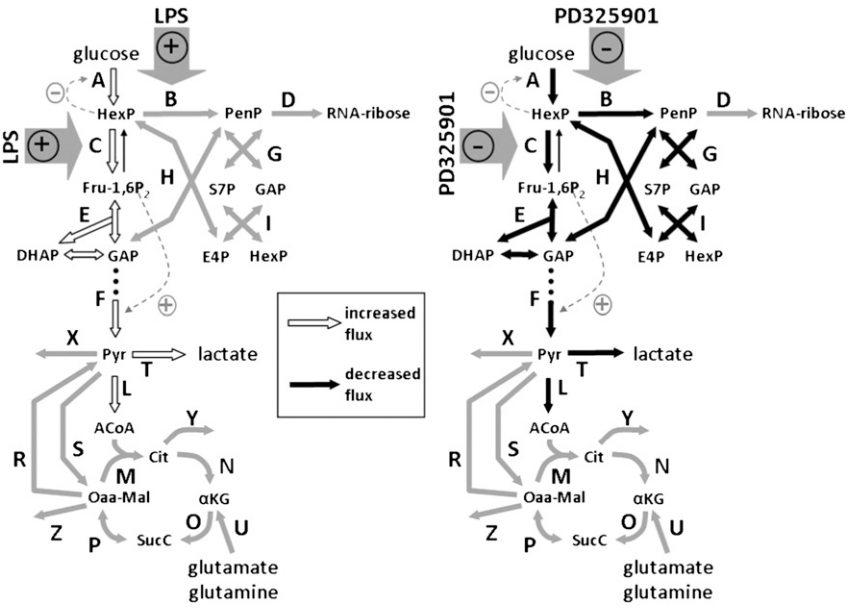

FIGURE 5. Cross-talk between MEK/ERK and key aspects of macrophage metabolism. Gray arrows represent the proposed activities that are regulated by signal transduction throughout MEK/ERK after incubation with PD325901 (*right panel*) or LPS (*left panel*). Positive (+) or negative (−) symbols predict activation or inhibition, respectively. ACoA, acetyl-CoA; Cit, citrate; DHAP, dihydroxyacetonephosphate; E4P, erythrose-4-phosphate; GAP, Fru-1,6P_2, glyceraldehyde-3-phosphate; HexP, hexose phosphates; αKG, 2-oxoglutarate; PenP, pentose phosphates; S7P, sedoheptulose-7-phosphate; SucC, succinyl-CoA.

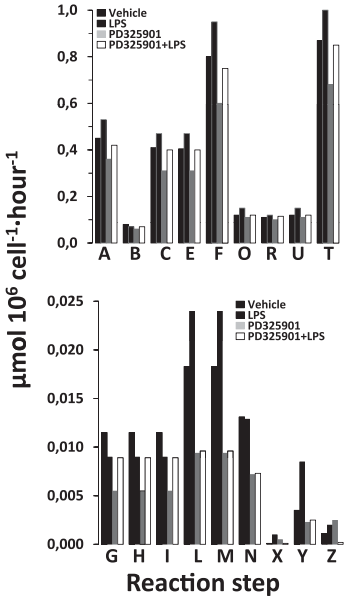

FIGURE 6. Metabolic fluxes in RAW 264.7 cells. Estimation of internal fluxes based on measured [^{13}C] redistribution. Bars are the median of the best 20 flux distributions corresponding to vehicle, LPS, PD325901, and PD325901 + LPS. Letters correspond to the reaction steps in the network schemes in Fig. 5.

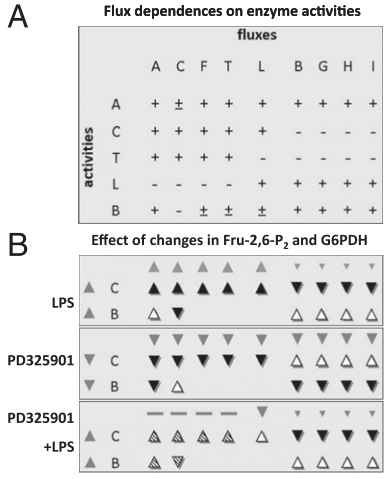

FIGURE 7. Flux dependencies on enzyme activities. Flux dependencies on enzyme activities (*A*) and compatibility of changes in fluxes with changes in enzyme activities (C, PFK-1; B, G6PDH+6PGDH) (*B*). "+," "−," and "±" predict the direction of changes in fluxes with respect to the direction of changes in enzyme activities: +, same direction; −, opposite direction; ±, indeterminate. Increase-decrease symbols ("▲", "▼", "–") refer to an increase or decrease in enzyme activity or flux: ▲, increase; ▼, decrease; –, no change. In *B*, gray symbols refer to observed changes in fluxes or activities. Black or white symbols identify compatibility in the direction of changes in fluxes and activities with the predicted dependencies in *A*: black, compatible or satisfied prediction; white, noncompatible or nonsatisfied prediction; filled, only compatible with very small (not observed) changes in fluxes.

of the regulatory dependencies (positive for enzyme-substrate dependencies and activations, and negative for inhibitions), dependencies among specific activities and the flux through a specific reaction depend on the relative magnitudes of the regulatory dependencies, which are unknown. However, some of these dependencies can be mainly positive or negative (23). A positive dependency indicates that a change in the enzyme activity is compatible or predicts a change in the flux that follows the same direction, irrespective of the magnitude of the regulatory dependencies. This means that an increase in the activity will induce an increase in the flux, whereas decreasing the activity will also decrease the flux. In contrast, a negative dependency indicates that changes in the activity will induce an inverse effect on the changes in the flux. Fig. 7*A* shows some of these sign-fixed dependencies for the main glycolytic and PPP fluxes with respect to changes in the activities of glucose uptake + hexokinase (reaction step A in Fig. 5), PFK-1 (reaction step C in Fig. 5), lactate dehydrogenase + lactate exchange (reaction step T in Fig. 5), PDH (reaction step L in Fig. 5), and G6PDH+6PGDH (reaction step B in Fig. 5).

The analysis of the compatibility of the measured changes in enzyme activities in the context of topology, stoichiometry, fluxes, and regulations affecting the central carbon metabolism provides fundamental information for interpreting the effects of LPS stimulation and PD325901 inhibition. Changes in glycolytic activity by regulating PFK-1 activity (reaction step C) are expected as a consequence of the changes in basal levels of Fru-2,6-P_2 (Fig. 1*D*), which is a potent activator of the glycolytic flux. More modest changes in G6PDH and 6PGDH activities (reaction step B) were recorded (Fig. 3*C*). Fig. 7*B* shows the compatibility of the direction of these changes in enzyme activities and the direction of changes in fluxes. In cells treated with PD325901, the decrease in PFK-1 (reaction step C) activity alone explains the decrease in the glycolytic fluxes (reaction steps A, C, F, T, and L) but not the changes in PPP fluxes (reaction steps B, G, H, and I). In contrast, a decrease in the activities of G6PDH+6PGDH (reaction step B) alone explains the observed changes in PPP fluxes but not all of the changes observed in glycolytic fluxes. Interestingly, this showed that changes in PFK-1 and G6PDH+6PGDH occur simultaneously, as has been experimentally observed, and could explain the changes in both glycolytic and PPP fluxes. In cells treated with LPS, the strong PFK-1 activation that follows the high levels of Fru-2,6-P_2 observed could qualitatively explain all of the changes in glycolytic and PPP fluxes. An increase in the activities of G6PDH+6PGDH alone will result in an increase in PPP fluxes, but this was not observed, given that the high levels of Fru-2,6-P_2 favored PFK-1 activation in the resulting flux profile. When cells were treated simultaneously with PD325901 and LPS, the slight increase in Fru-2,6-P_2 was not sufficient to activate the glycolytic flux profile characteristic of PFK-1 activation. The slight decrease in the PPP fluxes observed can be explained by the combined effect of changes in both PFK-1 and G6PDH+6PGDH activities.

Discussion

A detailed [1,2-[^{13}C]$_2$]glucose tracer-based metabolomics approach, together with measured changes in glucose and glutamine consumption and lactate production, was used to characterize the effects of MEK/ERK inhibition on the basic metabolic response to LPS stimulation in macrophages. One of our previous studies showed that classic versus alternative macrophage activation involved the expression of specific sets of metabolic enzymes intended to cope with the energy demands of the activated cells (14). However, the finding that a single hit (i.e., MEK inhibition) might influence the LPS response in metabolic terms offers a new view on the cross-talk between cell activation and basic energy metabolism. Moreover, these effects on MEK/ERK inhibition were also observed in cultured peritoneal macrophages and in human monocytes differentiated to macrophages (21, 24). From a bioenergetics point of view, macrophages are essentially glycolytic cells (16, 33, 34) using anaerobic glycolysis to metabolize glucose. One of the regulators of glucose metabolism in macrophages is the increase in Fru-2,6-P_2 levels, which activates the flux through

PFK-1 (14, 35). In many glycolytic cells, Fru-2,6-P_2 levels are tightly regulated through balancing PFK-2/FBPase-2 activities. Four genes encode the PFK-2/FBPase-2 in mammals. The L-type is encoded by the *PFKB1* gene and is mainly expressed in the liver and muscle. The uPFK-2 is encoded by the *PFKB3* gene and has a predominantly kinase activity, with lower bisphosphatase activity. This gene is induced by hypoxia and regulated by phosphorylation, playing a role in the high glycolytic rate of various cell types, such as cancer cells (35, 36). In macrophages, innate and classic activation, but not the alternative IL-4/IL-13 stimulation, switches the expression of the PFK-2/FBPase-2 isoform from *PFKB1* prevailing in resting cells to *PFKB3*, resulting in an increase in Fru-2,6-P_2 levels and glycolytic flux (14). Interestingly, MEK/ERK inhibition impaired the LPS-dependent expression of uPFK-2, thus decreasing Fru-2,6-P_2 levels, PFK-2 activity, and, as expected, glucose consumption and lactate production but without changes in glutamine/glutamate consumption. The ability of the MEK/ERK pathway to prevent the switch from L–PFK-2 to uPFK-2 in response to LPS was unexpected and revealed fine tuning of macrophage activation. Other changes induced by LPS, such as a decrease in PPP fluxes, were not affected by PD325901. Indeed, using the same approach, a selective p38 inhibitor (12) did not interfere with the LPS enhancement of glycolytic flux, including the increase in uPFK-2/Fru-2,6-P_2 levels. However, the lack of a JNK inhibitor preserving cell viability complicates this study in these cells. Even though, analysis of lactate release and uPFK-2/Fru-2,6-P_2 levels in cells treated with BI78D3 and activated with LPS suggests a minor (if any) effect of JNK inhibition on carbon metabolism in RAW 264.7 cells.

The cross-talk between MEK/ERK and central carbon metabolism is summarized in Fig. 5. From an analytical point of view, macrophage activation with LPS is characterized by enhanced flux through PFK-1, via a Fru-2,6-P_2 increase, and explains the increases in the glycolytic pathway and the decrease in the reactions in the PPP. However, the transient (peak at 8h), but statistically significant, increase in activity through the G6PDH+6PGDH block should lead to changes in the opposite direction, which are likely to mediate the decrease in fluxes throughout the PPP via increased PFK-1 activity. Interestingly, the flux profile changed following PD325901 inhibition, with or without LPS, and could not be explained by the change in PFK-1 alone. Changes in both PFK-1 and in G6PDH+6PGDH are required to explain the observed flux profile. Indeed, an additional regulator of the cross-talk at the Fru-2,6-P_2 level is the expression of TIGAR, a p53-inducible enzyme that hydrolyzes Fru-2,6-P_2 to fructose-6-phosphate (37, 38). We investigated whether TIGAR was regulated by p53 levels in macrophages. However, p53 was only upregulated at the end of the activation process (data not shown), when there was a large increase in the synthesis of ROS and reactive nitrogen species. Interestingly, MEK/ERK inhibition decreased ROS production by LPS-activated macrophages, confirming an interference of this MAPK on the LPS-dependent activation program of the macrophage. However, at the same time, MEK/ERK inhibition moderately enhanced (8 h) or maintained (18 h) the metabolic flux through the G6PDH pathway, excluding a sequential dependence of these pathways during activation. In agreement with these results, p66Shc-deficient mice, which exhibit an attenuated ROS synthesis due to a defect in the activation of the NADPH oxidase complex, also exhibit a marked reduction in ERK activation (39).

Finally, ERK1/2 activation in macrophages under proinflammatory conditions has been associated with different pathophysiological situations, ranging from cancer to insulin resistance. For example, macrophage infiltration increases during tumor progression in mouse models of lung cancer, but the combined inhibition of MEK and PI3K ablated macrophage-mediated increases in epithelial growth, enhancing animal survival (40); in contrast, it was shown that the proinflammatory cytokine IL-1β reduces insulin receptor substrate 1 expression and prevents Akt activation, leading to insulin resistance through a mechanism that is partly mediated by ERK activation (41–43). Therefore, ERK1/2 regulation appears to be an important mediator of macrophage function.

In summary, the presented quantitative analysis revealed many more details about the metabolic effects of the signaling regulators studied, showing that the exploration of metabolic effects provides important details that cannot be shown by only qualitative analysis of experimental data. Our work is an example of quantitative analysis of the cross-talk between signal transduction and metabolism in RAW 264.7 cells.

Acknowledgments

We thank Verónica Terrón for technical help.

Disclosures

The authors have no financial conflicts of interest.

References

1. Gordon, S., and F. O. Martinez. 2010. Alternative activation of macrophages: mechanism and functions. *Immunity* 32: 593–604.
2. Gordon, S. 2007. The macrophage: past, present and future. *Eur. J. Immunol.* 37 (Suppl. 1): S9–S17.
3. Nathan, C. 2002. Points of control in inflammation. *Nature* 420: 846–852.
4. Hu, X., S. D. Chakravarty, and L. B. Ivashkiv. 2008. Regulation of interferon and Toll-like receptor signaling during macrophage activation by opposing feedforward and feedback inhibition mechanisms. *Immunol. Rev.* 226: 41–56.
5. Martinez, F. O., A. Sica, A. Mantovani, and M. Locati. 2008. Macrophage activation and polarization. *Front. Biosci.* 13: 453–461.
6. Pasare, C., and R. Medzhitov. 2004. Toll-like receptors: linking innate and adaptive immunity. *Microbes Infect.* 6: 1382–1387.
7. Mantovani, A., A. Sica, S. Sozzani, P. Allavena, A. Vecchi, and M. Locati. 2004. The chemokine system in diverse forms of macrophage activation and polarization. *Trends Immunol.* 25: 677–686.
8. Nathan, C., and A. Ding. 2010. Nonresolving inflammation. *Cell* 140: 871–882.
9. Martinez, F. O., S. Gordon, M. Locati, and A. Mantovani. 2006. Transcriptional profiling of the human monocyte-to-macrophage differentiation and polarization: new molecules and patterns of gene expression. *J. Immunol.* 177: 7303–7311.
10. Rao, K. M. 2001. MAP kinase activation in macrophages. *J. Leukoc. Biol.* 69: 3–10.
11. Rao, K. M., T. Meighan, and L. Bowman. 2002. Role of mitogen-activated protein kinase activation in the production of inflammatory mediators: differences between primary rat alveolar macrophages and macrophage cell lines. *J. Toxicol. Environ. Health A* 65: 757–768.
12. Bain, J., L. Plater, M. Elliott, N. Shpiro, C. J. Hastie, H. McLauchlan, I. Klevernic, J. S. Arthur, D. R. Alessi, and P. Cohen. 2007. The selectivity of protein kinase inhibitors: a further update. *Biochem. J.* 408: 297–315.
13. Stebbins, J. L., S. K. De, T. Machleidt, B. Becattini, J. Vazquez, C. Kuntzen, L. H. Chen, J. F. Cellitti, M. Riel-Mehan, A. Emdadi, et al. 2008. Identification of a new JNK inhibitor targeting the JNK-JIP interaction site. *Proc. Natl. Acad. Sci. USA* 105: 16809–16813.
14. Rodríguez-Prados, J. C., P. G. Través, J. Cuenca, D. Rico, J. Aragonés, P. Martín-Sanz, M. Cascante, and L. Boscá. 2010. Substrate fate in activated macrophages: a comparison between innate, classic, and alternative activation. *J. Immunol.* 185: 605–614.
15. Odegaard, J. I., R. R. Ricardo-Gonzalez, A. Red Eagle, D. Vats, C. R. Morel, M. H. Goforth, V. Subramanian, L. Mukundan, A. W. Ferrante, and A. Chawla. 2008. Alternative M2 activation of Kupffer cells by PPARdelta ameliorates obesity-induced insulin resistance. *Cell Metab.* 7: 496–507.
16. Wu, G. Y., C. J. Field, and E. B. Marliss. 1991. Glucose and glutamine metabolism in rat macrophages: enhanced glycolysis and unaltered glutaminolysis in spontaneously diabetic BB rats. *Biochim. Biophys. Acta* 1115: 166–173.
17. Rosa, L. F., Y. Cury, and R. Curi. 1992. Effects of insulin, glucocorticoids and thyroid hormones on the activities of key enzymes of glycolysis, glutaminolysis, the pentose-phosphate pathway and the Krebs cycle in rat macrophages. *J. Endocrinol.* 135: 213–219.
18. Zeyda, M., and T. M. Stulnig. 2007. Adipose tissue macrophages. *Immunol. Lett.* 112: 61–67.
19. Marin, S., W. N. Lee, S. Bassilian, S. Lim, L. G. Boros, J. J. Centelles, J. M. FernAndez-Novell, J. J. Guinovart, and M. Cascante. 2004. Dynamic profiling of the glucose metabolic network in fasted rat hepatocytes using [1,2-13C2]glucose. *Biochem. J.* 381: 287–294.
20. Ramos-Montoya, A., W. N. Lee, S. Bassilian, S. Lim, R. V. Trebukhina, M. V. Kazhyna, C. J. Ciudad, V. Noé, J. J. Centelles, and M. Cascante. 2006.

Pentose phosphate cycle oxidative and nonoxidative balance: A new vulnerable target for overcoming drug resistance in cancer. *Int. J. Cancer* 119: 2733–2741.
21. Prieto, P., J. Cuenca, P. G. Través, M. Fernández-Velasco, P. Martín-Sanz, and L. Boscá. 2010. Lipoxin A4 impairment of apoptotic signaling in macrophages: implication of the PI3K/Akt and the ERK/Nrf-2 defense pathways. *Cell Death Differ.* 17: 1179–1188.
22. Martin-Sanz, P., M. Cascales, and L. Boscá. 1989. Glucagon-induced changes in fructose 2,6-bisphosphate and 6-phosphofructo-2-kinase in cultured rat foetal hepatocytes. *Biochem. J.* 257: 795–799.
23. de Atauri, P., A. Benito, P. Vizán, M. Zanuy, R. Mangues, S. Marín, and M. Cascante. 2011. Carbon metabolism and the sign of control coefficients in metabolic adaptations underlying K-ras transformation. *Biochim. Biophys. Acta* 1807: 746–754.
24. Traves, P. G., S. Hortelano, M. Zeini, T. H. Chao, T. Lam, S. T. Neuteboom, E. A. Theodorakis, M. A. Palladino, A. Castrillo, and L. Bosca. 2007. Selective activation of liver X receptors by acanthoic acid-related diterpenes. *Mol. Pharmacol.* 71: 1545–1553.
25. Lee, W. N., L. O. Byerley, E. A. Bergner, and J. Edmond. 1991. Mass isotopomer analysis: theoretical and practical considerations. *Biol. Mass Spectrom.* 20: 451–458.
26. Schmidt, K., M. Carlsen, J. Nielsen, and J. Villadsen. 1997. Modeling isotopomer distributions in biochemical networks using isotopomer mapping matrices. *Biotechnol. Bioeng.* 55: 831–840.
27. Cascante, M., and S. Marin. 2008. Metabolomics and fluxomics approaches. *Essays Biochem.* 45: 67–81.
28. Sauer, U. 2006. Metabolic networks in motion: 13C-based flux analysis. *Mol. Syst. Biol.* 2: 62.
29. Wiechert, W., M. Möllney, S. Petersen, and A. A. de Graaf. 2001. A universal framework for 13C metabolic flux analysis. *Metab. Eng.* 3: 265–283.
30. Wiechert, W., M. Möllney, N. Isermann, M. Wurzel, and A. A. de Graaf. 1999. Bidirectional reaction steps in metabolic networks: III. Explicit solution and analysis of isotopomer labeling systems. *Biotechnol. Bioeng.* 66: 69–85.
31. Wiechert, W. 2007. The thermodynamic meaning of metabolic exchange fluxes. *Biophys. J.* 93: 2255–2264.
32. Feng, G. J., H. S. Goodridge, M. M. Harnett, X. Q. Wei, A. V. Nikolaev, A. P. Higson, and F. Y. Liew. 1999. Extracellular signal-related kinase (ERK) and p38 mitogen-activated protein (MAP) kinases differentially regulate the lipopolysaccharide-mediated induction of inducible nitric oxide synthase and IL-12 in macrophages: *Leishmania* phosphoglycans subvert macrophage IL-12 production by targeting ERK MAP kinase. *J. Immunol.* 163: 6403–6412.
33. Bustos, R., and F. Sobrino. 1992. Stimulation of glycolysis as an activation signal in rat peritoneal macrophages. Effect of glucocorticoids on this process. *Biochem. J.* 282: 299–303.
34. Newsholme, P., S. Gordon, and E. A. Newsholme. 1987. Rates of utilization and fates of glucose, glutamine, pyruvate, fatty acids and ketone bodies by mouse macrophages. *Biochem. J.* 242: 631–636.
35. Bando, H., T. Atsumi, T. Nishio, H. Niwa, S. Mishima, C. Shimizu, N. Yoshioka, R. Bucala, and T. Koike. 2005. Phosphorylation of the 6-phosphofructo-2-kinase/fructose 2,6-bisphosphatase/PFKFB3 family of glycolytic regulators in human cancer. *Clin. Cancer Res.* 11: 5784–5792.
36. Calvo, M. N., R. Bartrons, E. Castaño, J. C. Perales, A. Navarro-Sabaté, and A. Manzano. 2006. PFKFB3 gene silencing decreases glycolysis, induces cell-cycle delay and inhibits anchorage-independent growth in HeLa cells. *FEBS Lett.* 580: 3308–3314.
37. Bensaad, K., E. C. Cheung, and K. H. Vousden. 2009. Modulation of intracellular ROS levels by TIGAR controls autophagy. *EMBO J.* 28: 3015–3026.
38. Li, H., and G. Jogl. 2009. Structural and biochemical studies of TIGAR (TP53-induced glycolysis and apoptosis regulator). *J. Biol. Chem.* 284: 1748–1754.
39. Tomilov, A. A., V. Bicocca, R. A. Schoenfeld, M. Giorgio, E. Migliaccio, J. J. Ramsey, K. Hagopian, P. G. Pelicci, and G. A. Cortopassi. 2010. Decreased superoxide production in macrophages of long-lived p66Shc knock-out mice. *J. Biol. Chem.* 285: 1153–1165.
40. Fritz, J. M., L. D. Dwyer-Nield, and A. M. Malkinson. 2011. Stimulation of neoplastic mouse lung cell proliferation by alveolar macrophage-derived, insulin-like growth factor-1 can be blocked by inhibiting MEK and PI3K activation. *Mol. Cancer* 10: 76.
41. Barbarroja, N., R. López-Pedrera, M. D. Mayas, E. García-Fuentes, L. Garrido-Sánchez, M. Macías-González, R. El Bekay, A. Vidal-Puig, and F. J. Tinahones. 2010. The obese healthy paradox: is inflammation the answer? *Biochem. J.* 430: 141–149.
42. Jager, J., T. Grémeaux, M. Cormont, Y. Le Marchand-Brustel, and J. F. Tanti. 2007. Interleukin-1beta-induced insulin resistance in adipocytes through down-regulation of insulin receptor substrate-1 expression. *Endocrinology* 148: 241–251.
43. Kopp, A., C. Buechler, M. Bala, M. Neumeier, J. Schölmerich, and A. Schäffler. 2010. Toll-like receptor ligands cause proinflammatory and prodiabetic activation of adipocytes via phosphorylation of extracellular signal-regulated kinase and c-Jun N-terminal kinase but not interferon regulatory factor-3. *Endocrinology* 151: 1097–1108.

THE JOURNAL OF IMMUNOLOGY

Selective Impairment of P2Y Signaling by Prostaglandin E_2 in Macrophages: Implications for Ca^{2+}-Dependent Responses

Paqui G. Través, María Pimentel-Santillana, Luz María G. Carrasquero, Raquel Pérez-Sen, Esmerilda G. Delicado, Alfonso Luque, Manuel Izquierdo, Paloma Martín-Sanz, María Teresa Miras-Portugal and Lisardo Boscá

J Immunol published online 11 March 2013
http://www.jimmunol.org/content/early/2013/03/10/jimmunol.1203029

The Journal of Immunology is published twice each month by The American Association of Immunologists, Inc., 9650 Rockville Pike, Bethesda, MD 20814-3994.

Print ISSN: 0022-1767 Online ISSN: 1550-6606.

Published March 11, 2013, doi:10.4049/jimmunol.1203029

Selective Impairment of P2Y Signaling by Prostaglandin E_2 in Macrophages: Implications for Ca^{2+}-Dependent Responses

Paqui G. Través,*,†,[1] María Pimentel-Santillana,†,[1] Luz María G. Carrasquero,*,[1] Raquel Pérez-Sen,* Esmerilda G. Delicado,* Alfonso Luque,‡ Manuel Izquierdo,† Paloma Martín-Sanz,†,§ María Teresa Miras-Portugal,* and Lisardo Boscá*,†,§

Extracellular nucleotides have been recognized as important modulators of inflammation via their action on specific pyrimidine receptors (P2). This regulation coexists with the temporal framework of proinflammatory and proresolution mediators released by the cells involved in the inflammatory response, including macrophages. Under proinflammatory conditions, the expression of cyclooxygenase-2 leads to the release of large amounts of PGs, such as PGE_2, that exert their effects through EP receptors and other intracellular targets. The effect of these PGs on P2 receptors expressed in murine and human macrophages was investigated. In thioglycollate-elicited and alternatively activated macrophages, PGE_2 selectively impairs P2Y but not P2X7 Ca^{2+} mobilization. This effect is absent in LPS-activated cells and is specific for PGE_2 because it cannot be reproduced by other PGs with cyclopentenone structure. The inhibition of P2Y responses by PGE_2 involves the activation of nPKCs (PKCε) and PKD that can be abrogated by selective inhibitors or by expression of dominant-negative forms of PKD. The inhibition of P2Y signaling by PGE_2 has an impact on the cell migration elicited by P2Y agonists in thioglycollate-elicited and alternatively activated macrophages, which provide new clues to understand the resolution phase of inflammation, when accumulation of PGE_2, anti-inflammatory and proresolving mediators occurs. ***The Journal of Immunology*****, 2013, 190: 000–000.**

Under inflammatory conditions or in early stages of many diseases characterized by the occurrence of associated inflammatory processes, several chemical mediators accumulate at sites of tissue damage. One of these molecules is PGE_2, which activates specific G protein–coupled membrane receptors (EP receptors). Four different receptors, EP1–EP4, can be distinguished pharmacologically (1); however, in addition to EP-mediated effects, PGs may exert other EP-independent actions (2). In addition to PGs, nucleotides can be released during the course of inflammatory responses and activate immune cells, such as monocytes, macrophages, and lymphocytes (3). These extracellular nucleotides exert several effects on immune cells and are involved in cytoskeleton reorganization, cell migration, phagocytosis, or exocytosis (3–6). Extracellular nucleotides can also play tissue-specific roles. In brains, they have been involved in different pathologies affecting immune cells (microglia), such as neuropathic pain for which a potent pharmacological therapy is under development (for a review, see Refs. 7–9). These actions of nucleotides are mediated by specific receptors, namely P2 receptors, which are classified in two major families: G protein–coupled P2Y receptors and ionotropic P2X receptors (10–12). Currently, eight subtypes of P2Y ($P2Y_{1,2,4,6,11,12,13,14}$) and seven subtypes of P2X (P2X1–7) have been cloned and characterized (for a review, see Ref. 13).

There are several examples of cross-regulation between the purinergic system and inflammatory molecules. In macrophages, it has been described that UTP potentiates PGE_2 release, which is involved in the enhancement of NO synthase 2 induction by LPS (14). In platelets, a cross-desensitization between ADP and thromboxane receptor signaling has been reported previously (4), and there is mounting evidence supporting that these interactions play important roles in several inflammatory and degenerative disorders, such as multiple sclerosis, amyotrophic lateral sclerosis, or Alzheimer's disease (15–18). In these pathologies, extracellular ATP exerts proinflammatory actions provoking cytokine release and PGs production (19). Recent studies have revealed that prostanoids exert both proinflammatory and anti-inflammatory actions through regulation of gene expression (2, 20), and it has been shown that PGE_2 is a potent inhibitor of the purinergic signaling mediated by some purinergic receptors (21). Although this modulation could play an important role in the anti-inflammatory effects of PGE_2, less is known about the underlying cross-talk between PGs and P2 signaling. In particular, because macrophage activation can be polarized into proinflammatory ("classically activated" or M1, using microbial stimuli such as LPS, or cytokines such as IFN-γ) or anti-inflammatory/proresolution ("alternatively activated" or M2, using IL-4 and/or IL-13 as stimuli)

*Departamento de Bioquímica y Biología Molecular IV, Facultad de Veterinaria e Instituto Universitario de Investigación en Neuroquímica, Instituto de Investigación Sanitaria del Hospital Clínico San Carlos, Universidad Complutense Madrid, 28040 Madrid, Spain; †Instituto de Investigaciones Biomédicas Alberto Sols, Centro Mixto Consejo Superior de Investigaciones Científicas-Universidad Autónoma, 28029 Madrid, Spain; ‡Centro de Investigación en Sanidad Animal-Instituto Nacional de Investigación y Tecnología Agraria y Alimentaria, Valdeolmos, 28020 Madrid, Spain; and §Centro de Investigación Biomédica en Red de Enfermedades Hepáticas y Digestivas, 08036 Barcelona, Spain

[1]P.G.T., M.P.-S., and L.M.G.C. contributed equally to this work.

Received for publication November 2, 2012. Accepted for publication February 11, 2013.

This work was supported by Grants BFU2011-24760 and BFU2011-24743 from Ministerio de Economía y Competitividad, Grant S2010/BMD-2378 from Comunidad de Madrid, and Fondo de Investigación Sanitaria-Red Cardiovascular (RECAVA) Grant RD06/0014/0025 and Fundación Marcelino Botín (to M.T.M.-P.). RECAVA and Centro de Investigación Biomédica en Red de Enfermedades Hepáticas y Digestivas are funded by the Instituto de Salud Carlos III.

Address correspondence and reprint requests to Dr. Lisardo Boscá, Instituto de Investigaciones Biomédicas Alberto Sols, Centro Mixto Consejo Superior de Investigaciones Científicas-Universidad Autónoma, Arturo Duperier 4, 28029 Madrid, Spain. E-mail address: lbosca@iib.uam.es

The online version of this article contains supplemental material.

Abbreviations used in this article: COX-2, cyclooxygenase-2; KO, knockout; PK, protein kinase; RFU, relative fluorescence unit; WT, wild-type.

commitment (22–25), understanding the contributions of P2 receptors to these adaptive responses of macrophages would provide insight into the regulation of the inflammatory signaling. In this work, we analyze the effect of PGE_2 on the main P2 receptors expressed in peritoneal macrophages. In these cells, PGE_2 selectively impairs P2Y but not P2X7 signaling. In addition, our data point to nPKCs and PKD as the main contributors to the desensitization of P2Y receptors by PGE_2. Interestingly, these effects are observed in thioglycollate-elicited and alternatively activated macrophages but not in cells challenged with LPS. Downstream Ca^{2+}-dependent events activated upon P2Y stimulation are desensitized by PGE_2 in these cells. Finally, in thioglycollate-elicited and alternatively activated macrophages, PGE_2 significantly affects the cell migration induced by P2Y agonists, providing new clues to understand the resolution phase of inflammation, when PGE_2, anti-inflammatory, and proresolving mediators accumulate in the local microenvironment.

Materials and Methods

Materials

ATP, UTP, UDP, α,β-meATP, 2MeSADP, BzATP, PPADS, and anti–β-actin Ab were purchased from Sigma-Aldrich (St. Louis, MO). A438079 was obtained from Tocris Bioscience (Ellisville, MO). DFU was from Merck (Rahway, NJ). PGs were from Cayman Chemical (Ann Arbor, MI). Gö6976, Gö6983, Gö6850, and inhibitors of standard signaling pathways were from Calbiochem (San Diego, CA). Fura 2-AM was from Invitrogen (Carlsbad, CA). Different cytokines were obtained from PeproTech (London, U.K.). Abs against $P2Y_2$, $P2Y_4$, $P2Y_6$, and $P2X_7$ receptors were from Alomone Labs (Jerusalem, Israel), anti-GAPDH was from Ambion (Austin, TX), and other Abs were from Santa Cruz Biotechnology (Santa Cruz, CA), Cell Signaling Technology (Danvers, MA), or from the sources described previously (25). Reagents for electrophoresis were obtained from Bio-Rad (Hercules, CA) and Sigma-Aldrich. Tissue culture dishes were from Falcon (Lincoln Park, NJ), and culture medium was from Invitrogen.

Animals and cell lines

Eight- to 12-wk-old male wild-type (WT) C57BL/6 mice were housed under a 12-h light/dark cycle and food and water was provided ad libitum. Animals were cared for according to a protocol approved by the Ethical Committee of our institution (following directive 2010/63/EU of the European Parliament). Cyclooxygenase-2 (COX-2) and P2X7-deficient mice were used as described previously (26–28). Elicited peritoneal macrophages were obtained from male mice 4 d after i.p. administration of 2.5 ml 3% thioglycollate broth essentially as described previously (29). Cells were seeded onto 15-mm-diameter coverslips in 12-multiwell plates at a density of 2×10^5 cells/well or in 60-mm petri dishes at 4×10^6 cells/plate and cultured with RPMI 1640 medium supplemented with 10% heat-inactivated FBS and antibiotics (100 U/ml penicillin and 100 μg/ml streptomycin) at 37°C in an humidified atmosphere with 5% CO_2. After 2-h incubation, nonadherent cells were removed. Adherent cells were maintained in culture conditions and used within 2 d after plating. The murine macrophage cell line RAW 264.7 was maintained in culture and used as described for peritoneal macrophages.

Isolation of human monocytes

PBMCs were isolated from buffy coats of healthy donors by centrifugation on Ficoll–Hypaque Plus (GE Healthcare, Barcelona, Spain) following the manufacturer's protocol. $CD14^+$ cells were obtained using immunomagnetic isolation (Miltenyi Biotec, Bergisch Gladbach, Germany). Cells were maintained for 4 h at 1×10^6 cells/ml in DMEM supplemented with antibiotics (100 IU/ml penicillin and 100 μg/ml streptomycin). After this period, the supernatant was removed, and adherent cells were cultured in the same medium supplemented with 10% heat-inactivated FBS. Cells were maintained overnight with this medium and differentiated to macrophages with human M-CSF (20 ng/ml; PeproTech) for 7 d.

Calcium microfluorimetric analysis in single cells

Macrophages attached to coverslips were incubated in Locke's solution (140 mM NaCl, 4.5 mM KCl, 2.5 mM $CaCl_2$, 1.2 mM KH_2PO_4, 1.2 mM $MgSO_4$, 5.5 mM glucose, and 10 mM HEPES [pH 7.4]) supplemented with 1 mg/ml BSA and loaded with 5–7 μM fura 2-AM for 45 min at 37°C. Once washed in fresh Locke's solution, a coverslip was placed in a small superfusion chamber, and the cells were imaged through a NIKON TE-200 microscope with a Plan Fluor ×20/0.5 objective and were stimulated for 30 s with a variety of purinergic receptor agonists at near-maximal effective concentrations: 100 μM ATP (10–12), 100 μM UTP (1, 30, 31), 10 μM UDP (32), 10 μM 2MeSADP (33), 100 μM α,β-meATP (34), or 300 μM BzATP (28, 31). In other studies, prostanoids (5 μM PGA_1, PGD_2, PGE_2, or $15dPGJ_2$) were applied for 5 min before nucleotides superfusion in the presence of prostanoids. When purinergic or prostanoid receptors antagonists or PKC inhibitors were used, they were preincubated at the indicated concentrations and for the required times (as specified in the text and figure legends) and kept during prostanoid incubation and/or purinergic agonist stimulation. Cells were illuminated at 340 and 380 nm, and the emitted light was isolated by a dichroic mirror (430 nm) and a 510-nm band-pass filter (Ω Optical, Brattleboro, VT). Images were obtained with an ORCA-ER C 47 42-80 camera from Hamamatsu (Hamamatsu City, Japan) controlled by MetaFluor 6.2r & PC software (Universal Imaging, Cambridge, U.K.). Exposure time was 300 ms, and the change in the wavelength of incoming light from 340 to 380 nm was carried out in <5 ms. Fluorescence images were acquired at a sampling frequency of 2 Hz and processed by averaging signals from small elliptical regions within individual cells. Background signals were subtracted from each wavelength, and the F_{340}/F_{380} ratio was calculated (34). The values are calculated on the basis of the magnitude of the initial peak that represents the initial transient components. Alternatively, in some cases, calcium mobilization was measured using the nonratiometric Fluo-4 direct probe (Invitrogen) and following the instructions of the supplier. In this case, the changes in fluorescence were measured in a fluorescence microscope (Observer Z1, Plan Apochromat objective; Zeiss) equipped with a Cascade1K camera, analyzed using the Axiovision 4.8 imaging program, and expressed as relative fluorescence units (RFU); ΔRFU is (maximal fluorescence − minimal fluorescence)/minimal fluorescence of the cells.

Generation of RAW 264.7 macrophages overexpressing COX-2

RAW 264.7 cells were transfected with the murine COX-2 gene under the control of the CMV promoter and a geneticin (G418) resistance gene. These cells expressed the COX-2 transgene and continuously released PGE_2 into the culture medium.

Cell culture and transient transfections

RAW 264.7 macrophages were maintained in RPMI 1640 medium containing 100 U/ml penicillin, 100 μg/ml streptomycin, and 10% heat-inactivated FBS. Before experiments, the medium was replaced but containing 2% FBS. For transient transfections, cells were grown at 80% confluence and transfected with a GFP-encoding plasmid in combination with a CMV-driven vector containing different PKC/PKD1 isotypes (1:5 plasmid ratio). Plasmids directing the expression of constitutive PKC isotypes were referred as PKC-α*, δ*, and ζ* (35). A murine GFP–PKD1 vector was used to determine the intracellular PKD1 localization. Cells were transfected using the Cell Line Nucleofector Kit V and following the manufacturer's instructions (Amaxa). After nucleofection, cells were maintained in culture overnight, and calcium mobilization was measured using Fluo-4 direct (Invitrogen) in the GFP-positive population.

Determination of PGE_2 and cAMP levels

PGE_2 levels were measured in the culture medium, and endogenous cAMP levels were measured using specific immunoassay kits (GE Healthcare).

RNA isolation and RT-PCR analysis

One microgram of total RNA, extracted with TRIzol reagent (Invitrogen), was reverse transcribed using a Transcriptor First-Strand cDNA Synthesis kit for RT-PCR following the indications of the manufacturer (Roche). Real-time PCR was conducted with SYBR Green (Applied Biosystems, Foster City, CA) on a MyiQ Real-Time PCR System (Bio-Rad). The TaqMan probes for mouse $P2Y_2$, $P2Y_4$, $P2Y_6$, and $P2X_7$ used in this study were purchased from Applied Biosystems, and experiments for validation of amplification efficiency were performed for each TaqMan primers/probe set, according to Refs. 36 and 37). PCR thermocycling parameters were 95°C for 10 min, 40 cycles of 95°C for 15 s, and 60°C for 1 min. Each sample was run in duplicate and was normalized with the expression of 36B4. The fold induction was determined in a ΔΔCt based fold-change calculations (relative quantity, RQ, is $2^{-\Delta\Delta Ct}$).

Preparation of total protein cell extracts

Cells were homogenized in a medium containing 10 mM Tris-HCl (pH 7.5), 1 mM $MgCl_2$, 1 mM EGTA, 10% glycerol, 0.5% CHAPS, 1 mM 2-ME, and 0.1 mM PMSF and a protease and phosphatase inhibitor mixture

(Sigma-Aldrich). The extracts were vortexed for 30 min at 4°C, and after centrifuging for 20 min at 13,000 × *g*, the supernatants were stored at −20°C. Protein levels were determined with Bradford reagent (Bio-Rad).

Western blotting

Protein extracts were boiled in loading buffer (250 mM Tris-HCl [pH 6.8], 2% SDS, 10% glycerol, and 2% 2-ME), and 30 μg protein were subjected to 8–10% SDS-PAGE electrophoresis gels. Proteins were transferred to polyvinylidene difluoride membranes (GE Healthcare). Membranes were incubated for 1 h with low-fat milk powder (5%) in PBS (10 mM Tris-HCl [pH 7.4] and 150 mM NaCl) containing 0.1% Tween 20. Blots were incubated overnight at 4°C with primary Abs against $P2Y_2$, $P2Y_4$, $P2Y_6$, or $P2X_7$ receptors (1:500 dilution) or the indicated Abs, as described previously (25). The blots were developed by ECL Advance protocol (GE Healthcare), and different exposure times were performed for each blot with a charge-coupled device camera in a luminescent image analyzer (Molecular Imager; Bio-Rad) to ensure the linearity of the band intensities. Values of densitometry were determined using Quantity One software (Bio-Rad).

Macrophage migration analysis

Transwell assays. Migration assays were performed in 24 Transwells (uncoated 8-μm porous Transwells), according to the manufacturer's instructions (Corning, Corning, NY). Briefly, 5×10^4 peritoneal macrophages were seeded in the upper chambers. Cells were allowed to attach for 2-3 h, and unattached cells were removed by thorough washing with PBS. After 24 h, cells were starved overnight. Macrophages were stimulated with combinations of PGE_2 and UTP (in the upper chamber), and media with serum (10% FBS), MCP-1 (PeproTech), or UTP were added into lower chamber (600 μl) as chemoattractants. The plates were incubated at 37°C overnight. The membrane was fixed with paraformaldehyde (4% [pH 7.2]) and stained with crystal violet solution (Sigma-Aldrich). The number of cells that migrated completely through the 8-μm pores was determined in three random fields. The migration assays were performed in triplicate.

In vitro wound-healing cell migration assay. A total of 5×10^5 macrophages were seeded in a 24-well plate to form a confluent monolayer. After 18 h with LPS (250 ng/ml) or IL-4/IL-13 (20 ng/ml each), the wound was made by scraping a conventional pipette tip across the monolayer. Cells were washed with PBS, stimulated with combinations of PGE_2 and UTP, and refreshed with medium supplemented with or without 10% FBS, MCP-1, or UTP to induce the migration. Photographs of two random fields were taken at the indicated time points, and the cells were counted to calculate the average number of cells that had migrated per equal surface.

Statistical analysis

The values in graphs correspond to the means ± SD. The statistical significance was estimated with a Student *t* test for unpaired observation. Data were analyzed by the SPSS for Windows statistical package, version 9.0.1.

Results

Pyrimidine nucleotides and BzATP induce intracellular calcium increases in peritoneal macrophages

The changes in intracellular-free calcium concentration ($[Ca^{2+}]_i$) elicited by a variety of purinergic receptor agonists in Fura 2–loaded cells were analyzed (see *Materials and Methods* for details on the concentrations used). As Fig. 1A shows, almost all cells responded to ATP stimulation even in the absence of extracellular Ca^{2+} (Fig. 1B, second trace), indicating the participation of functional metabotropic (P2Y) and ionotropic (P2X) receptors, respectively (10–12). A similar percentage of cells also responded to UTP, a $P2Y_2/P2Y_4$ receptor agonist. The $P2Y_6$ receptor agonist UDP elicited intracellular Ca^{2+} increases, and 15% of the cells responded to 2MeSADP, which activates $P2Y_1$, $P2Y_{12}$, and $P2Y_{13}$ receptors. In addition, α,β-meATP, a P2X1/P2X3 agonist, induced slight calcium

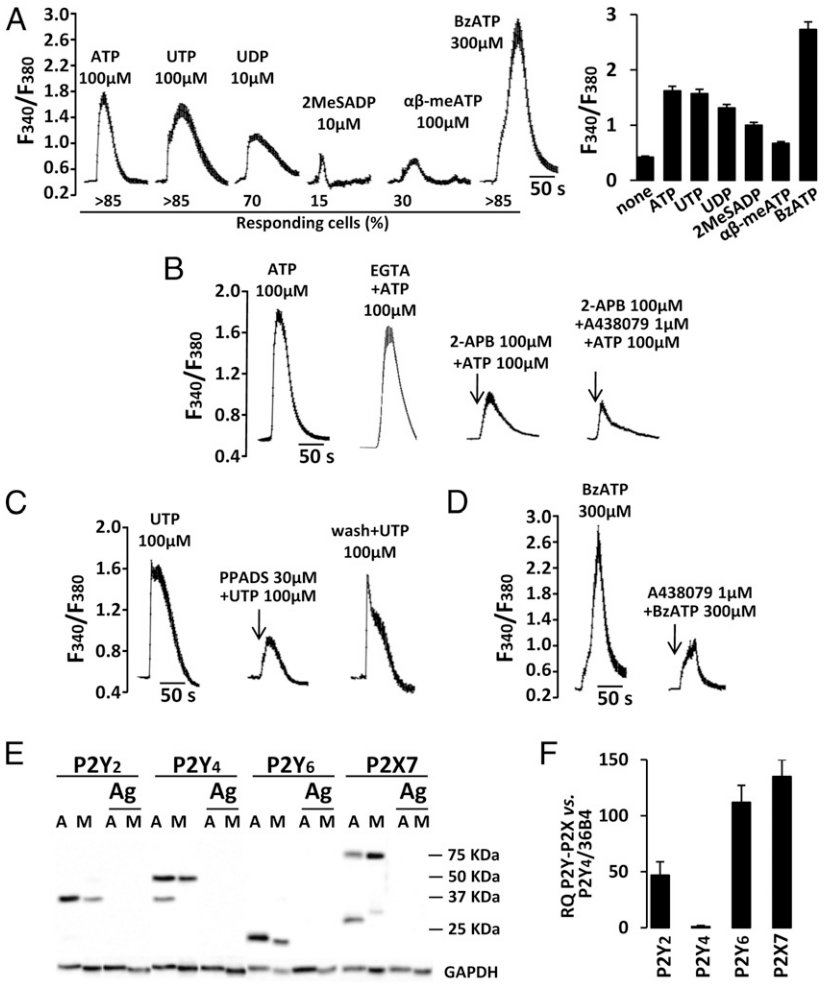

FIGURE 1. Characterization of the response of thioglycollate-elicited peritoneal macrophages to P2 agonists. Cells were mounted in coverslips, and the response to the indicated P2 agonists was determined on a single-cell basis. A representative trace, the percentage of responding cells and the mean ± SD of the fluorescence ratio changes in responding cells are represented (**A**). The pharmacological characterization of the ATP receptors was carried out in the presence (first trace) and absence of extracellular Ca^{2+} plus 100 μM EGTA (second trace) and using the IP3 receptor inhibitor 2-APB (100 μM, 3 min) or the P2X7 antagonist A438079 (1 μM, 3 min) (**B**). The nonselective P2 antagonist PPADS (30 μM, 3 min) (**C**) and the response to BzATP (**D**) was analyzed. The expression levels of the indicated P2 receptors were determined by immunoblot, using specific Abs and astrocyte (*lane A*) extracts as controls confronted to macrophages (*lane M*). The presence of the immunogen (Ag lanes) in the incubation blot was used to ensure specificity (**E**). Comparative real-time PCR was used to determine the relative mRNA levels of $P2Y_2$, $P2Y_4$, $P2Y_6$, and $P2X_7$. Each sample was normalized using 36B4 as housekeeping (**F**). Results show a representative experiment out of five (A–D) or three (E, F) independent preparations.

mobilization (30% of cells). In contrast, BzATP, which activates the P2X7 receptor channel, triggered a substantial calcium response. We also checked the presence of functional P2 receptors using pharmacological approaches: the potent selective P2X7 antagonist A438079 and 2-APB, an inhibitor of the IP3 receptors and store-operated Ca^{2+} channels (38), reduced the response to ATP (Fig. 1B). The response to UTP was inhibited by PPADS, which has been reported to depress responses mediated by metabotropic ($P2Y_1$, $P2Y_4$, and $P2Y_{13}$) and ionotropic (P2X1–3, P2X5, and P2X7) receptors in a reversible manner (Fig. 1C). As shown in Fig. 1D, BzATP-induced Ca^{2+} flux was markedly reduced when A438079 was administered shortly before BzATP challenge, confirming the presence of an active P2X7 receptor. The presence of $P2Y_2$, $P2Y_4$, $P2Y_6$, and $P2X_7$ receptors was confirmed by immunoblot using specific Abs (Fig. 1E), and comparative real-time PCR indicated that $P2Y_6$ and P2X7 mRNA was more represented in thioglycollate-elicited cells (Fig. 1F).

PGE$_2$ modulates P2Y$_4$ and P2Y$_6$ receptors activity but not the P2X7

We were interested in studying the effect of PGs on P2 signaling, because these lipids are important regulators of macrophage function. Preliminary experiments using a transgenic macrophage cell line (RAW 264.7 cells) in which the COX-2 gene was constitutively expressed in the absence of additional stimuli (TG-RAW), showed a continuous release of PGE_2 into the culture medium, a situation that was not observed in macrophages from WT animals or lacking COX-2 ($cox2^{-/-}$) (Supplemental Fig. 1A). Interestingly, overexpression of COX-2 resulted in a decrease in the number of cells showing Ca^{2+} mobilization in response to ATP, UTP, UDP, and 2MeSADP but not in response to BzATP (Supplemental Fig. 1B, *upper panel*). No inhibition was observed when the cells were treated with the selective COX-2 inhibitor DFU (Supplemental Fig. 1B, *lower panel*). Moreover, a decrease in the amplitude of the calcium response to UTP was observed in the presence of active COX-2 (Supplemental Fig. 1B, *upper inset*). The time course of the effect of the addition of DFU to the cell cultures (Supplemental Fig. 1C, *right panel*) suggests rapid actions of PGs on P2 signaling. To test whether this effect of COX-2 was PGE_2 dependent, time-course experiments adding exogenous PGE_2 to the cell cultures were performed (Supplemental Fig. 1C, *left panel*). The exogenous addition of PGE_2 inhibited Ca^{2+} fluxes mediated by ATP after only 30 min, although this addition of PGE_2 did not influence the expression level of various P2Y and P2X receptors in macrophages (Supplemental Fig. 1D).

PGE$_2$ but not other PGs with cyclopentenone structure modulates P2Y receptors activity

To analyze the interplay between PGE_2 and Ca^{2+} mobilization, macrophages were treated with PGE_2, and $[Ca^{2+}]_i$ fluxes were measured. PGE_2 inhibited $[Ca^{2+}]_i$ increase elicited by ATP, UTP, or UDP in a reversible manner (Fig. 2A). In contrast, the response triggered by BzATP (P2X7 agonist) was not affected by PGE_2 pretreatment. Other PGs with cyclopentenone structure (PGA_1, PGD_2, and $15dPGJ_2$) failed to decrease significantly UTP-dependent $[Ca^{2+}]_i$ increases (Fig. 2B, 2C). Moreover, the effect of PGE_2 on UTP-dependent Ca^{2+} mobilization was not reproduced by agonists of the EP2/EP3 PG receptors (butaprost/sulprostone) or suppressed by an antagonist of the EP4 receptor (AH238488) in the presence of PGE_2 (Fig. 2D), suggesting an EP-independent effect. Analysis of the cAMP accumulation and UTP-dependent Ca^{2+} mobilization by PGE_2 in macrophages showed independent $EC_{0.5}$ values (Fig. 2E), suggesting that EP receptors were not involved in the mechanism of action of PGE_2 on P2Y signaling. Interestingly, PGE_2 did not alter the Ca^{2+} mobilization elicited by ionomycin but suppressed the response induced by thapsigargin, indicating an interference with Ca^{2+} mobilization from intracellular stores (Fig. 2F, 2G).

PGE$_2$ modulates P2 responses via PKC signaling

To further investigate the signaling pathway involved in the modulation of P2 receptors by PGE_2, we used inhibitors of MAPKs, PI3K, GSK3, and PKA, or challenge with activators of PKA (DiBuAMPc) and PKC (PDBu). As shown in Fig. 3A, pretreatment with the inhibitors or the PKA activator DiBuAMPc did not prevent the effect of PGE_2 on UTP-induced Ca^{2+} mobilization. However, activation of PKC/PKD with PDBu reduced UTP-dependent $[Ca^{2+}]_i$ rise to similar levels than preincubation with PGE_2. Treatment with α-PDD, an inactive analog of PDBu, did not modify the response to UTP. These data suggest that PKCs/PKDs might be involved in P2Y receptors inhibition by PGE_2. To determine the PKC isoforms implicated in this regulatory effect, different PKC inhibitors were used (Fig. 3B). Gö6983 and Gö6976 at 10 nM (cPKC inhibitors) did not affect the response to PGE_2, suggesting that cPKCs were not involved in the process. However, Gö6976 at 100 nM (inhibitor of PKD but not nPKCs), CID755673 (PKD inhibitor), and to a lesser extent Gö6850 (cPKCs and nPKCs inhibitor) attenuated the PGE_2 inhibition of UTP-induced $[Ca^{2+}]_i$ mobilization, suggesting the involvement of nPKCs and PKD in the mechanism of action of PGE_2. In agreement with these data, transfection of the macrophage cell line RAW 264.7 with different isoforms of PKCs, including constitutively active constructs (denoted by a *) revealed that both PKCε and PKD1 attenuated the Ca^{2+} mobilization by UTP. Moreover, transfection with a dominant-negative PKD1 isoform reversed the PGE_2-induced inhibition of Ca^{2+} flux (Fig. 3C). Indeed, a delayed mobilization of PKD1 to the plasma membrane induced by PDBu in GFP–PKD1-transfected cells was observed after treatment of RAW 246.7 cells with PGE_2 but not with PGD_2 (Fig. 3D). In addition, PGE_2 promoted a time-dependent phosphorylation of PKD1 (Fig. 3E). Taken together, these results suggest that phospho-PKD1 is interacting with intracellular membranes in response to PGE_2, delaying the shift toward the plasma membrane upon challenge with PDBu. These data are in agreement with previous reports on alternative subcellular localizations of PKD1 (39). Furthermore, from a functional point of view, treatment of macrophages with PGE_2 significantly decreased the phosphorylation of ACC and AMPKα, two well-known targets of Ca^{2+}-mobilization (Fig. 3E–G).

Differential modulation of P2Y-dependent Ca^{2+} mobilization in innate and alternatively activated macrophages

Thioglycollate-elicited peritoneal macrophages were activated with LPS or IL-4/IL-13, and the response of P2Y receptors to PGE_2 was analyzed. Fig. 4A shows the activation profiling of the cells used to determine the response to UTP and BzATP as representatives of the P2Y and P2X7 challenges, respectively. As Fig. 4B shows, control and IL-4/IL-13–activated macrophages exhibited a significant inhibition of UTP (but not BzATP) Ca^{2+} mobilization after treatment with PGE_2. However, this was not the case in cells challenged with LPS (Fig. 4C, *left*). Because COX-2 is expressed in these cells and PGE_2 accumulates in the culture medium, an experiment was carried out in the presence of the selective COX-2 inhibitor DFU. Under these conditions, PGE_2 challenge was unable to modify the UTP response. Similar effects were observed at 5 h after challenge with LPS, a condition in which COX-2 expression and the synthesis of PGE_2 are negligible. Indeed, LPS, but not IL4/IL13 activated macrophages from P2X7-deficient animals exhibited a similar loss of response to PGE_2 as the WT cells in terms of changes in Ca^{2+} mobilization upon UTP challenge (Fig. 4D).

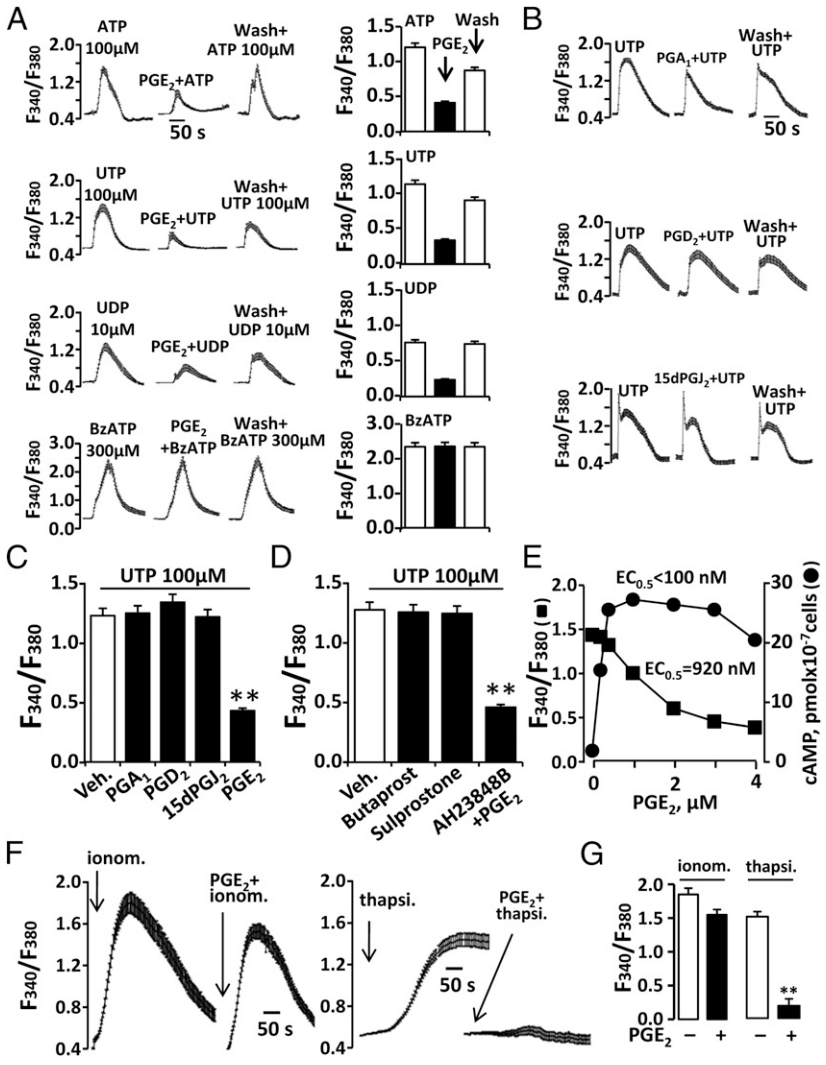

FIGURE 2. Characterization of PGE_2 inhibition of P2-dependent Ca^{2+} mobilization in peritoneal macrophages. Cells were mounted in coverslips and the response to the indicated P2 agonists was determined. Incubation with 5 μM PGE_2 decreased the P2Y responses. After the cell layer was washed with medium to remove the PG, the response to the P2 agonists was restored (**A**). Effect of different PGs (assayed at 5 μM) on the response to Ca^{2+} mobilization by 100 μM UTP (**B**). Quantitative analysis of the response to Ca^{2+} mobilization by UTP of different PGs (**C**) and of agonists or antagonists of the EP receptors (**D**). The ability of PGE_2 to mobilize calcium and to increase cAMP levels was determined in the same experiment (**E**). The effects of PGE_2 on Ca^{2+} mobilization in response to ionomycin (1 μM) and thapsigargin (500 nM) were determined (**F**, **G**). Results show a representative trace and the mean ± SD of three experiments (A–D, F, G) or the means of a representative experiment out of two (E). $^{**}p < 0.001$ versus the same condition in the absence of preincubation with PGE_2.

PGE_2 inhibits P2Y/Ca^{2+}-dependent cell migration

Analysis of macrophage signaling in response to UTP stimulation was carried out in nontreated (thioglycollate-elicited) and LPS or IL-4/IL-13–activated macrophages from P2X7 knockout (KO) mice. As Fig. 5 shows, treatment of thioglycollate-elicited or M2 macrophages with PGE_2 increased phospho-PKCε (S729) labeling. In parallel, we observed a reduction in the phosphorylation of ACC, CaMKII, AKT, and to a lesser extent AMPK, all these phosphoenzymes potentially modulated by Ca^{2+} mobilization. However, LPS activated macrophages exhibited PKCε phosphorylation that was not regulated by PGE_2. At this point, we also examined the functional responses of these macrophages. Extracellular nucleotides are known to induce cell migration (3, 5). As Fig. 5B shows, Transwell migration analysis of thioglycollate-elicited macrophages showed a response that was increased in cells treated with UTP, a process that was attenuated after pretreatment with PGE_2. In addition, "wound-healing" migration assays (Fig. 5C, 5D) showed a significant impairment of migration in thioglycollate-elicited or IL-4/IL-13–treated macrophages challenged with PGE_2 when analyzed at 2 and 4 h after treatment with UTP.

Human monocytes activated with LPS show a time-dependent desensitization to Ca^{2+} mobilization by UTP upon challenge with PGE_2

To determine whether the regulation of $[Ca^{2+}]_i$ by P2Y receptor was also present in human macrophages, blood monocytes were differentiated into macrophages, and the response to combinatorial treatment with UTP and PGE_2 was investigated. As Fig. 6A shows, ~80% of resting and LPS or human IL-4/human IL-10/human IL-13–activated human macrophages responded to UTP challenge. Interestingly, preincubation with 5 μM PGE_2 significantly decreased the response to UTP of resting and M2-activated cells (Fig. 6B). However, in LPS-activated macrophages, a time-dependent blockade to the PGE_2 response was observed during the initial 4-h activation period (Fig. 6C). Indeed, treatment of these cells with PDBu, but not with α-PDD, significantly decreased the response to UTP challenge in resting and M2 macrophages but not in cells treated with LPS (Fig. 6D). Under these conditions, PGE_2 promoted a modest but significant phosphorylation of PKD1 at S916 in resting but not in LPS-activated cells (Fig. 6E). These results suggest that human macrophages exhibit a modulation of UTP responses by PGE_2 reminiscent to that observed in rodent peritoneal macrophages (Fig. 7).

Discussion

The identification of extracellular nucleotides (i.e., ATP and UTP) as innate immune regulators acting via the P2 receptors is a well-accepted paradigm in the modulation of the inflammatory response (3, 13, 40, 41). Activation of P2 receptors induces a rise in $[Ca^{2+}]_i$, which in turn has an impact on the activation of other transmembrane ion fluxes, on intracellular signaling via Ca^{2+}-sensing targets, and on metabolic and mitochondrial changes required for

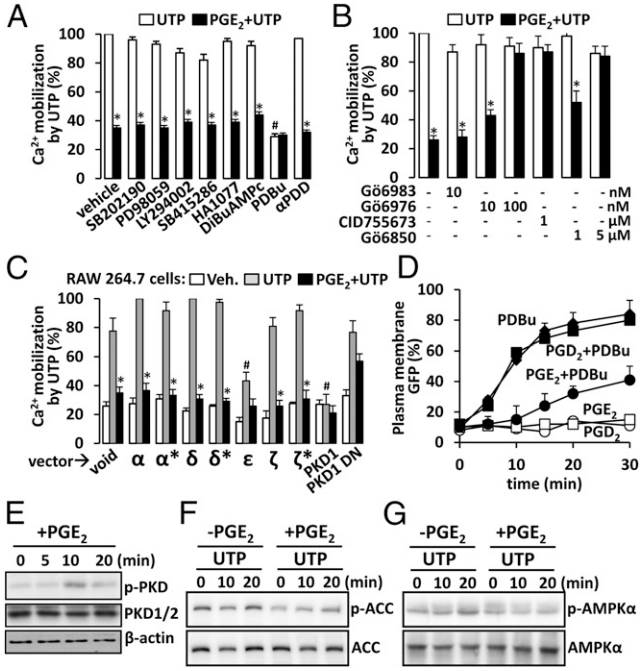

FIGURE 3. Characterization of targeting of different signaling pathways on the effect of PGE_2 on Ca^{2+} mobilization by UTP in peritoneal macrophages. Cells were treated for 15 min with the indicated inhibitors of the MAPK, PI3K, GSK3, and PKA pathways or the PKA and PKC activators DiBuAMPc (5 μM), PDBu (200 nM), and the non-PKC activator phorbol α-PDD (200 nM). Cells were then incubated for an additional 10-min period with 5 μM PGE_2, and the response to 100 μM UTP in terms of Ca^{2+} mobilization was determined (**A**). Analysis of the effect of isotype-specific PKC/PKD inhibitors on Ca^{2+} mobilization in response to UTP (**B**). RAW 264.7 cells were transfected with a GFP-encoding vector, and the indicated PKC or PKD constructs and the Ca^{2+} mobilization by UTP were determined in GFP-positive cells, using the nonratiometric Fluo-4 assay (**C**). RAW cells expressing GFP–PKD1 were treated for 10 min with 5 μM PGE_2 or PGD_2 and then challenged with 100 nM PDBu to induced the translocation of PKD1 to the plasma membrane, and the accumulation of the fluorescence in this compartment was quantified (**D**). In peritoneal macrophages, challenge with 5 μM PGE_2 was able to promote PKD1 phosphorylation in S956 (**E**). The effect of PGE_2 on the inhibition of UTP-dependent Ca^{2+} mobilization was also observed in the impaired phosphorylation of ACC (**F**) and AMPKα (**G**). Results show the mean ± SD of three experiments (A–D) or a representative blot (E–G) out of four experiments. $^*p < 0.001$ versus the same condition in the absence of preincubation with PGE_2 (A–C); $\#p < 0.001$ versus the corresponding control conditions in the absence of activators (E) or versus the same condition in transfections with the void vector (C).

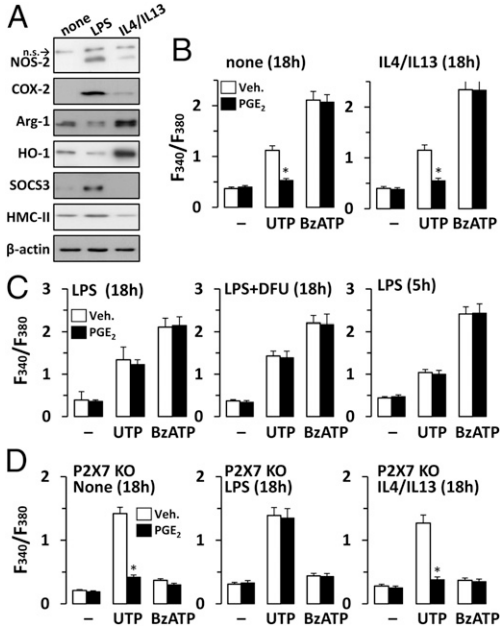

FIGURE 4. Classic but not alternative activation of macrophages impairs the effect of PGE_2 on P2Y-dependent activation of macrophages. The basic activation profile of macrophages activated with 250 ng/ml LPS or 20 ng/ml IL-4 plus IL-13 was determined by Western blot analysis at 18 h (**A**). Macrophages from WT or P2X7-deficient mice (P2X7 KO) were prepared, and after the indicated time of culture in the presence or absence of LPS or IL-4/IL-13, cells were treated for 10 min with 5 μM PGE_2, and the Ca^{2+} responses to UTP (100 μM) or BzATP (300 μM) were determined using the dual excitation 340/380-nm protocol as described in *Materials and Methods* (**B**–**D**). Results show a representative blot (A) and the mean ± SD of the maximal fluorescence ratio changes of four experiments [20–40 cells per experiment (B–D)]. $^*p < 0.001$ versus the same condition in the absence of PGE_2 (B–D).

the specific regulation of macrophage functions (25, 42–44). Several members of the P2Y and P2X receptors have been identified in cells of the immune system (40, 44). Indeed, P2 agonists are increasingly viewed as a new class of innate immune system mediators following their release at sites of inflammation as a result of infection or cell damage. Local elevated concentrations of ATP are thought to mediate most of its effects through binding to the P2X7 receptor, whereas UTP and UDP can act through $P2Y_2$/$P2Y_4$ and $P2Y_6$, respectively (15, 45–47). Although the $P2Y_2$ receptor appears to be the dominant target for UTP in resident macrophages (30), our data suggest that $P2Y_4$ receptor could be also involved in UTP-dependent calcium responses in peritoneal macrophages, as supported by the high expression of both $P2Y_4$ and $P2Y_6$ receptors and the sensitivity to PPADS antagonism. Even the contribution of $P2Y_2$/$P2Y_4$ or $P2Y_4$/$P2Y_6$ heteromers can be considered (48). A relevant aspect in this context of P2 heterogeneity is the potential cross-talk between the P2X and P2Y families of receptors. One of such examples is the synergism between both families in the activation of dendritic cells, which is necessary for the efficient initiation of immune responses. In addition to Ag, the presence of P2 agonists coming from necrotic cells results in a synergistic activation and maturation of dendritic cells and, therefore, in a more efficient signaling in T cells, leading to a higher expression of proinflammatory mediators and adhesion molecules (3, 49, 50).

In macrophages, much attention has been paid to P2X7 signaling because this receptor is highly expressed in these cells, and it has been involved in the regulation of stress signals (19, 44). It is well known that P2X7 activation by ATP participates in the regulation of the innate response in macrophages, including the killing of intracellular pathogens, the release and maturation of proinflammatory cytokines (i.e., IL-1β and IL-18) (51–55), and the increase in PGE_2 levels (19). The mechanisms involved in these actions implicate a rise in Ca^{2+} influx and in the activation of the MAPK signaling pathways (56–58). However, less is known regarding the role of P2Y receptors in macrophage function. In the present work, we provide new data on the fine regulation of P2Y signaling in macrophages using specific pharmacological agonists and antagonists and cells derived from P2X7 KO mice, discounting possible interferences via this receptor. Moreover, our data reveal a previously unrecognized interplay between PGs and P2Y responses in the context of macrophage activation, polarization, and resolution of the inflammation. We have extensively characterized the expression of $P2Y_2$, $P2Y_4$, and $P2Y_6$ in thioglycollate-elicited macrophages, using functional and immu-

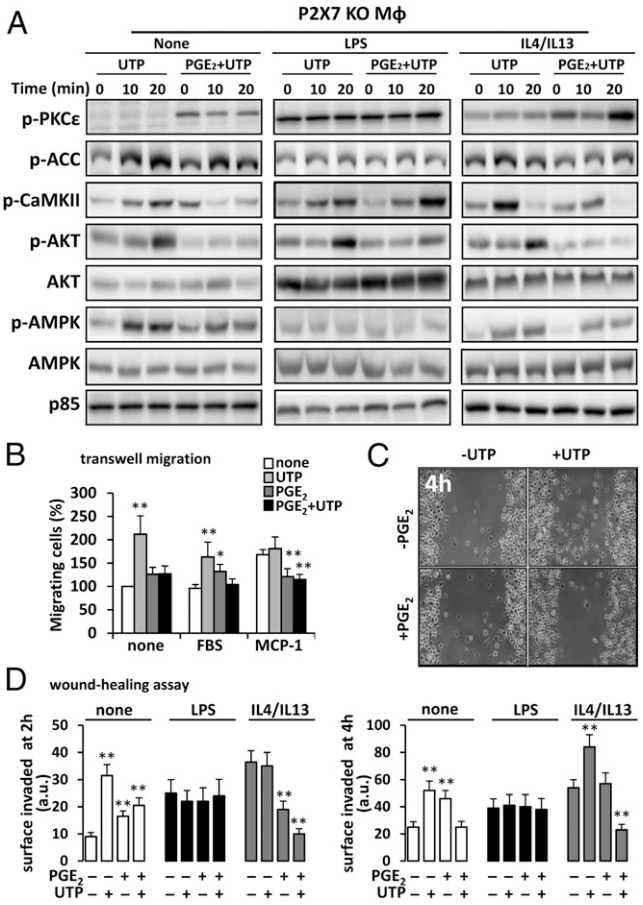

FIGURE 5. Characterization of the effect of PGE_2 on the Ca^{2+}-dependent P2 signaling and functional responses in macrophages from P2X7-deficient mice activated with LPS or IL-4 + IL-13. Macrophages from P2X7 KO mice were activated with 250 ng/ml LPS or 20 ng/ml IL-4 + IL-13. After 18 h in culture, cells were treated for 10 min in the absence or presence of 5 μM PGE_2, and upon UTP challenge (100 μM), the levels of the indicated phosphoproteins were determined by Western blot analysis (**A**). The capacity of these cells to migrate in Transwell was determined after incubation with PGE_2 and UTP (100 μM). The migration was measured after 18 h of incubation in the absence or presence of 10% FBS or 10 ng/ml MCP-1 in the lower wells (**B**). Wound-healing–like experiments were carried out after standard scratch of the cell dishes and analysis of the cell replenishment at 2 and 5 h. A representative migration of thioglycollate-elicited macrophages at 2 h is shown in (**C**; magnification ×10), and the effect of LPS or IL-4/IL-13 priming on the repair capacity was determined after 18 h of polarization and preincubation for 10 min with PGE_2 and stimulation for 2 and 4 h with UTP (**D**). Results show a representative blot or image (A, C) out of three or the mean ± SD of four experiments (B, D). $*p < 0.05$, $**p < 0.001$ versus the same condition in the absence of treatment.

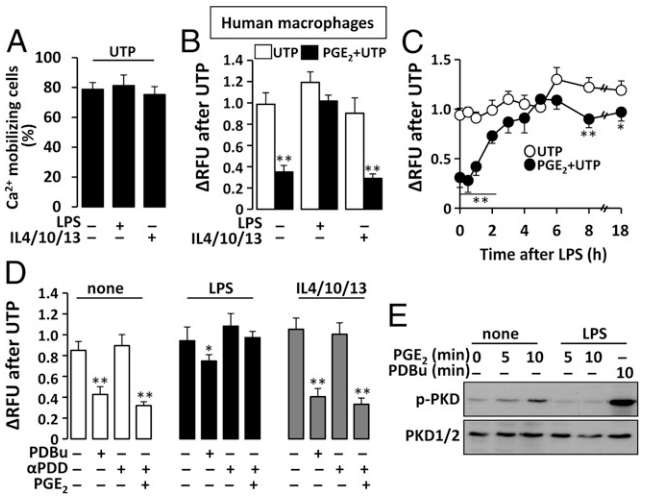

FIGURE 6. Characterization of the effect of PGE_2 on the Ca^{2+}-dependent UTP-signaling in human macrophages. Human monocytes were differentiated into macrophages with human M-CSF. Cells were activated with 250 ng/ml LPS or 20 ng/ml human IL-4, IL-10, and IL-13. After 18 h of incubation, cells were loaded with Fluo-4, and the percentage of Ca^{2+}-mobilizing cells in response to UTP was determined (**A**). Cells were also preincubated for 10 min with 5 μM PGE_2, and the response to 100 μM UTP was determined (**B**). The time course of the inhibitory response to PGE_2 challenge in macrophages activated with LPS was analyzed after incubation of the cells with the PG and UTP (**C**). The effect of treatment for 10 min with PDBu (200 nM) on the Ca^{2+} mobilization in response to UTP of resting and LPS or IL-4/10/13–activated macrophages (18h) was determined. The inactive phorbol α-PDD was used as negative control for PKC activation (**D**). The phosphorylation of human PKD1 in S916 was determined by immunoblot in cells treated for 18h in the absence or presence of LPS. Cells were incubated with 5 μM PGE_2 or 200 nM PDBu for the indicated periods of time (**E**). Results show the mean ± SD of three experiments (A–D) or a representative blot (E). $*p < 0.05$, $**p < 0.001$ versus the same condition in the absence of PGE_2 (B, C) or in the absence of treatment (D). ΔRFU is (maximal fluorescence − minimal fluorescence)/minimal fluorescence of the cells.

nological approaches. In view of the confusion in the literature regarding the role of PGs on P2 signaling and macrophage activation (20, 21, 59–63), we studied the role of these bioactive lipids on UTP- and ATP-dependent P2 responses. Preliminary experiments in macrophages carrying a COX-2 transgene revealed a rapid blockade of Ca^{2+} mobilization induced by P2Y agonists that could be ascribed to the accumulation of PGE_2 in the culture medium. Indeed, when these experiments were performed in mouse embryo fibroblasts from the WT, the COX-2–deficient mice, or in these mouse embryo fibroblasts but carrying a COX-2 transgene, the release of PGE_2 impaired UTP-dependent Ca^{2+} mobilization responses, whereas the presence in the incubation medium of the selective COX-2 inhibitor DFU restored the UTP response (data not shown), which suggests the occurrence of this regulation of P2 receptors by PGE_2 in other cells, in addition to macrophages. Moreover, this regulation of P2Y by PGs was also observed in macrophages from P2X7-deficient mice, suggesting that this response is independent of P2X7 receptors. Even more, macrophages challenged with specific agonists of the P2X7 receptors failed to show the inhibitory effect of PGE_2 in Ca^{2+} mobilization. A schematic representation of this cross-regulation between PGE_2 and P2Y receptors in macrophages is shown in Fig. 7.

Although M1- and M2-activated macrophages exhibit similar expression levels of purinergic receptors (64), other changes have been described in macrophage polarization with respect to purinergic receptor signaling. LPS-treated macrophages (M1) show a rapid and sustained suppression of phospholipase C β1 and β2 expression that could affect P2 receptor signaling (65). It is well established that in M1 macrophages P2X7 receptor induce the release of IL-1β (52, 54). In addition to this, during macrophage transition from M1 to M2 phenotype, it has been described the uncoupling of P2X7 receptor signaling to reactive oxygen species production, NLRP-3 inflammasome/caspase-1 cascade activation, and IL-β release. The effect of extracellular ATP on anti-inflammatory phenotype progression does not involve P2Y/P2X receptor–mediated processes but is dependent on pyrophosphate ATP chains, which induce actin cytoskeletal rearrangements/actin filaments clustering that trap inflammasome complex (54). In agreement with this, ectonucleotidases seem to play a role in the

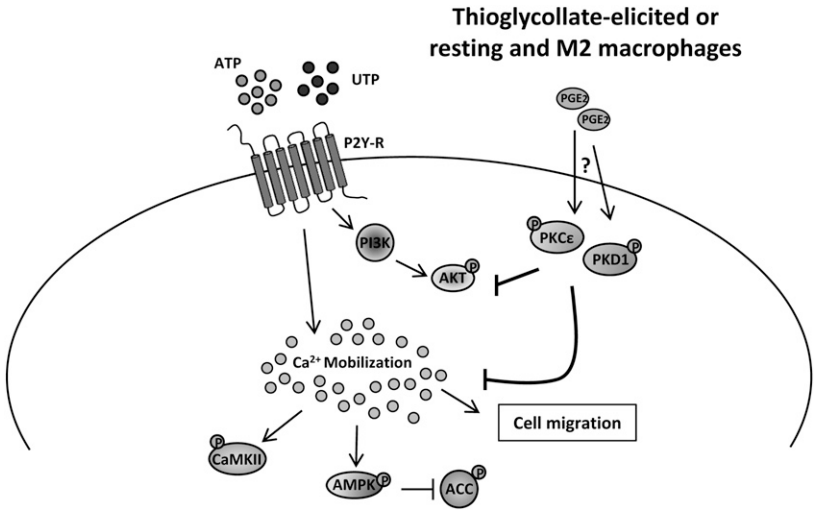

FIGURE 7. Schematic representation of the effect of PGE_2 on the Ca^{2+}-dependent ATP/UTP signaling. Thioglycollate-elicited or M2 activated murine or "resting" human macrophages exhibit a cross-regulation between PGE_2 and P2Y signaling that is independent of the PG receptors (EP-R) expressed at the plasma membrane level. PGE_2 interferes with P2Y-R signaling through a PKCε/PKD1 activation pathway.

transition from M1 to M2 state during inflammatory resolution or to be involved in the functions played by different macrophages. In fact, in parallel with increased expression of NTPDase 1, 3, and ecto-5′-nucleotidase, higher ATP hydrolytic activity has been detected in M2 macrophages, favoring adenosine production that functions as a negative feedback modulator to limit inflammation (64). Our data add additional insights on the M1 versus M2 responses showing that M1 polarization suppresses the inhibitory effect of PGE_2 on Ca^{2+} mobilization: This indicates that classic or innate activation promote a yet unidentified signaling that abrogates the action of PGE_2 on P2Y receptors. This effect was observed in both rodent and human macrophages, although the mechanisms that impair the response to PGE_2 in LPS-activated macrophages remain unclear; kinetic analysis of the time required to suppress this response upon LPS challenge indicates that a 2-h signaling period is necessary to abolish PGE_2 sensitivity, suggesting that this is not the result of the rapid signaling elicited after TLR4 engagement but because of secondary events in the signaling process that remain unknown. One possibility is via alterations in the PKD1 signaling (31). Regarding the physiopathological relevance of the modulation of P2Y receptors by PGs, we have investigated the consequences of distal events because of the impairment of Ca^{2+} mobilization in thioglycollate-elicited and alternatively activated macrophages. The response to PGE_2 might participate in the attenuation of the inflammatory response contributing to promote resolution, because the blockade in Ca^{2+} mobilization has an important reflect in terms of activation of different signaling pathways, including key regulators such as PKCs and energetic metabolism via AMPK activation and ACC inhibition. In line with this potential action of PGE_2, the absence of response in M1-activated macrophages provides a certain protection on the energetic demands typical for these cells (25, 66). Moreover, from a functional point of view, we have investigated the impact of PGE_2 on P2Y-dependent migration. Recent data suggest that both P2Y and P2X receptors participate in the phagocytic process of dying cells exerted by the macrophages (5). Indeed, these observations are in agreement with the fact that P2 receptors participate in a wide range of phagocytic and chemotactic actions, as described for $P2Y_{2,4,6}$ receptors in the phagocytosis of apoptotic bodies by microglial cells (67).

Regarding the mechanism of regulation of P2Y receptors by PGE_2 in thioglycollate-elicited macrophages, our data show that this PG promotes a rapid and transient phosphorylation of PKD1 and pharmacological inhibition of this kinase constitutes a sufficient condition to block the effects of PGE_2 on UTP-dependent Ca^{2+} mobilization. PKDs are expressed ubiquitously and regulate diverse cellular processes such as oxidative stress, gene expression, cell survival, vesicle trafficking, and P2X7 signaling (31), although its precise function in macrophages remains poorly characterized. PKD1 appears to be the specific isotype regulated by extracellular ligands in macrophages (68); therefore, it is conceivable that PGE_2 controls the activity of this particular isotype. Indeed, an association of PKD1 with TLR9 and in general with the MyD88-dependent proinflammatory immune responses has been described previously (68–70). Previous data from the literature described that activation of PKCδ acts as an upstream PKD1 activation step (69). However, using the macrophage cell line RAW 264.7 transfected with a constitutively active PKCδ construct, it was not possible to mimic the effects of PGE_2 on UTP-dependent Ca^{2+} mobilization. Interestingly, overexpression of PKCε, but not other classical, new, or atypical PKCs, was sufficient to mimic PGE_2 effects on P2Y receptors. Ancillary overexpression of PKD1 blunted the effect of UTP on Ca^{2+} mobilization, but when a vector encoding a catalytically inactive form of PKD1 was expressed, the response to UTP persisted, and the inhibitory effect of PGE_2 was significantly decreased. Taken together, these data suggest that PKD is involved in the regulation of P2Y signaling. Importantly, human macrophages behaved like the rodent counterparts in terms of Ca^{2+} mobilization by P2Y receptors in response to UTP, including the desensitization after M1 polarization and the phosphorylation of PKD1 at S916 in response to PGE_2. This phosphorylation at S916 has been reported to correspond to a fully activated PKD1 (71). Activation of PKD1 has been associated with activation of upstream PKCs and/or activation of G proteins and various receptor–associated tyrosine kinases. The mechanisms involved in the PGE_2-dependent PKD1 activation might involve a transient rise in activators, perhaps in the concentration of DAGs at several membrane compartments, including the Golgi, as it has been reported in other cell types (39, 70). In agreement with this suggestion, the experiments in cells expressing GFP–PKD1 failed to show a PGE_2-dependent mobilization of the GFP–PKD1 toward the plasma membrane, which suggests that other compartments are more relevant in mediating the signaling of the phospho–S916-PKD1 involved in P2Y blockade of Ca^{2+} mobilization. Moreover, the observation that PGE_2 delays the PDBu-induced mobilization of GFP–PKD1 toward the plasma membrane is in support of this suggestion. These data suggest that PKD may participate in the interplay between P2Y and P2X receptors (31), and indeed, an inverse signaling has been described linking P2X4 receptor engagement in the activa-

tion of phospholipase A_2 and in the release of PGE_2 that might participate in the intercellular interplay between P2X and P2Y receptors (72). In conclusion, our work provides a new mechanism of regulation of P2Y activity in macrophages, involving the participation of PGE_2, and with a functional implication in basic biological responses of the macrophage, such as metabolic activation and migration. Unraveling the molecular signatures associated with PGE_2 accumulation in the course of the inflammatory reaction might help to understand the complex network of interaction orchestrated by macrophages to control inflammation.

Disclosures

The authors have no financial conflicts of interest.

References

1. Sugimoto, Y., and S. Narumiya. 2007. Prostaglandin E receptors. *J. Biol. Chem.* 282: 11613–11617.
2. Scher, J. U., and M. H. Pillinger. 2009. The anti-inflammatory effects of prostaglandins. *J. Investig. Med.* 57: 703–708.
3. Elliott, M. R., F. B. Chekeni, P. C. Trampont, E. R. Lazarowski, A. Kadl, S. F. Walk, D. Park, R. I. Woodson, M. Ostankovich, P. Sharma, et al. 2009. Nucleotides released by apoptotic cells act as a find-me signal to promote phagocytic clearance. *Nature* 461: 282–286.
4. Barton, J. F., A. R. Hardy, A. W. Poole, and S. J. Mundell. 2008. Reciprocal regulation of platelet responses to P2Y and thromboxane receptor activation. *J. Thromb. Haemost.* 6: 534–543.
5. Marques-da-Silva, C., G. Burnstock, D. M. Ojcius, and R. Coutinho-Silva. 2011. Purinergic receptor agonists modulate phagocytosis and clearance of apoptotic cells in macrophages. *Immunobiology* 216: 1–11.
6. Marteau, F., D. Communi, J. M. Boeynaems, and N. Suarez Gonzalez. 2004. Involvement of multiple P2Y receptors and signaling pathways in the action of adenine nucleotides diphosphates on human monocyte-derived dendritic cells. *J. Leukoc. Biol.* 76: 796–803.
7. Beggs, S., T. Trang, and M. W. Salter. 2012. $P2X4R^+$ microglia drive neuropathic pain. *Nat. Neurosci.* 15: 1068–1073.
8. Hansen, R. R., A. Nasser, S. Falk, S. B. Baldvinsson, P. H. Ohlsson, J. M. Bahl, M. F. Jarvis, M. Ding, and A. M. Heegaard. 2012. Chronic administration of the selective P2X3, P2X2/3 receptor antagonist, A-317491, transiently attenuates cancer-induced bone pain in mice. *Eur. J. Pharmacol.* 688: 27–34.
9. Tsuda, M., S. Beggs, M. W. Salter, and K. Inoue. 2013. Microglia and intractable chronic pain. *Glia* 61: 55-61.
10. Ralevic, V., and G. Burnstock. 1998. Receptors for purines and pyrimidines. *Pharmacol. Rev.* 50: 413–492.
11. North, R. A. 2002. Molecular physiology of P2X receptors. *Physiol. Rev.* 82: 1013–1067.
12. Abbracchio, M. P., G. Burnstock, J. M. Boeynaems, E. A. Barnard, J. L. Boyer, C. Kennedy, G. E. Knight, M. Fumagalli, C. Gachet, K. A. Jacobson, and G. A. Weisman. 2006. International Union of Pharmacology LVIII: update on the P2Y G protein-coupled nucleotide receptors: from molecular mechanisms and pathophysiology to therapy. *Pharmacol. Rev.* 58: 281–341.
13. Vitiello, L., S. Gorini, G. Rosano, and A. la Sala. 2012. Immunoregulation through extracellular nucleotides. *Blood* 120: 511–518.
14. Chen, B. C., and W. W. Lin. 2000. Pyrimidinoceptor potentiation of macrophage PGE_2 release involved in the induction of nitric oxide synthase. *Br. J. Pharmacol.* 130: 777–786.
15. Raouf, R., A. J. Chabot-Doré, A. R. Ase, D. Blais, and P. Séguéla. 2007. Differential regulation of microglial P2X4 and P2X7 ATP receptors following LPS-induced activation. *Neuropharmacology* 53: 496–504.
16. Xu, J., M. Chalimoniuk, Y. Shu, A. Simonyi, A. Y. Sun, F. A. Gonzalez, G. A. Weisman, W. G. Wood, and G. Y. Sun. 2003. Prostaglandin E_2 production in astrocytes: regulation by cytokines, extracellular ATP, and oxidative agents. *Prostaglandins Leukot. Essent. Fatty Acids* 69: 437–448.
17. Yiangou, Y., P. Facer, P. Durrenberger, I. P. Chessell, A. Naylor, C. Bountra, R. R. Banati, and P. Anand. 2006. COX-2, CB2 and P2X7-immunoreactivities are increased in activated microglial cells/macrophages of multiple sclerosis and amyotrophic lateral sclerosis spinal cord. *BMC Neurol.* 6: 12.
18. León-Otegui, M., R. Gómez-Villafuertes, J. I. Díaz-Hernández, M. Díaz-Hernández, M. T. Miras-Portugal, and J. Gualix. 2011. Opposite effects of P2X7 and P2Y2 nucleotide receptors on α-secretase-dependent APP processing in Neuro-2a cells. *FEBS Lett.* 585: 2255–2262.
19. Barberà-Cremades, M., A. Baroja-Mazo, A. I. Gomez, F. Machado, F. Di Virgilio, and P. Pelegrín. 2012. P2X7 receptor-stimulation causes fever via PGE2 and IL-1β release. *FASEB J.* 26: 2951–2962.
20. Narumiya, S. 2009. Prostanoids and inflammation: a new concept arising from receptor knockout mice. *J. Mol. Med.* 87: 1015–1022.
21. Ito, M., and I. Matsuoka. 2008. Regulation of purinergic signaling by prostaglandin E_2 in murine macrophages. *J. Pharmacol. Sci.* 107: 443–450.
22. Gordon, S., and F. O. Martinez. 2010. Alternative activation of macrophages: mechanism and functions. *Immunity* 32: 593–604.
23. Mantovani, A. 2010. Molecular pathways linking inflammation and cancer. *Curr. Mol. Med.* 10: 369–373.
24. Mantovani, A., C. Garlanda, and M. Locati. 2009. Macrophage diversity and polarization in atherosclerosis: a question of balance. *Arterioscler. Thromb. Vasc. Biol.* 29: 1419–1423.
25. Rodríguez-Prados, J. C., P. G. Través, J. Cuenca, D. Rico, J. Aragonés, P. Martín-Sanz, M. Cascante, and L. Boscá. 2010. Substrate fate in activated macrophages: a comparison between innate, classic, and alternative activation. *J. Immunol.* 185: 605–614.
26. Lim, H., B. C. Paria, S. K. Das, J. E. Dinchuk, R. Langenbach, J. M. Trzaskos, and S. K. Dey. 1997. Multiple female reproductive failures in cyclooxygenase 2-deficient mice. *Cell* 91: 197–208.
27. Solle, M., J. Labasi, D. G. Perregaux, E. Stam, N. Petrushova, B. H. Koller, R. J. Griffiths, and C. A. Gabel. 2001. Altered cytokine production in mice lacking $P2X_7$ receptors. *J. Biol. Chem.* 276: 125–132.
28. Sánchez-Nogueiro, J., P. Marín-García, and M. T. Miras-Portugal. 2005. Characterization of a functional $P2X_7$-like receptor in cerebellar granule neurons from $P2X_7$ knockout mice. *FEBS Lett.* 579: 3783–3788.
29. Zeini, M., P. G. Través, R. López-Fontal, C. Pantoja, A. Matheu, M. Serrano, L. Boscá, and S. Hortelano. 2006. Specific contribution of $p19^{ARF}$ to nitric oxide-dependent apoptosis. *J. Immunol.* 177: 3327–3336.
30. del Rey, A., V. Renigunta, A. H. Dalpke, J. Leipziger, J. E. Matos, B. Robaye, M. Zuzarte, A. Kavelaars, and P. J. Hanley. 2006. Knock-out mice reveal the contributions of P2Y and P2X receptors to nucleotide-induced Ca^{2+} signaling in macrophages. *J. Biol. Chem.* 281: 35147–35155.
31. Carrasquero, L. M., E. G. Delicado, L. Sánchez-Ruiloba, T. Iglesias, and M. T. Miras-Portugal. 2010. Mechanisms of protein kinase D activation in response to P2Y(2) and P2X7 receptors in primary astrocytes. *Glia* 58: 984–995.
32. Jiménez, A. I., E. Castro, D. Communi, J. M. Boeynaems, E. G. Delicado, and M. T. Miras-Portugal. 2000. Coexpression of several types of metabotropic nucleotide receptors in single cerebellar astrocytes. *J. Neurochem.* 75: 2071–2079.
33. Carrasquero, L. M., E. G. Delicado, A. I. Jiménez, R. Pérez-Sen, and M. T. Miras-Portugal. 2005. Cerebellar astrocytes co-express several ADP receptors: presence of functional P2Y(13)-like receptors. *Purinergic Signal.* 1: 153–159.
34. Hervás, C., R. Pérez-Sen, and M. T. Miras-Portugal. 2003. Coexpression of functional P2X and P2Y nucleotide receptors in single cerebellar granule cells. *J. Neurosci. Res.* 73: 384–399.
35. Díaz-Guerra, M. J., O. G. Bodelón, M. Velasco, R. Whelan, P. J. Parker, and L. Boscá. 1996. Up-regulation of protein kinase C-ε promotes the expression of cytokine-inducible nitric oxide synthase in RAW 264.7 cells. *J. Biol. Chem.* 271: 32028–32033.
36. Marín-García, P., J. Sánchez-Nogueiro, A. Diez, M. León-Otegui, M. Linares, P. García-Palencia, J. M. Bautista, and M. T. Miras-Portugal. 2009. Altered nucleotide receptor expression in a murine model of cerebral malaria. *J. Infect. Dis.* 200: 1279–1288.
37. Sánchez-Nogueiro, J., P. Marín-García, D. León, M. León-Otegui, E. Salas, R. Gómez-Villafuertes, J. Gualix, and M. T. Miras-Portugal. 2009. Axodendritic fibres of mouse cerebellar granule neurons exhibit a diversity of functional P2X receptors. *Neurochem. Int.* 55: 671–682.
38. Nelson, D. W., R. J. Gregg, M. E. Kort, A. Perez-Medrano, E. A. Voight, Y. Wang, G. Grayson, M. T. Namovic, D. L. Donnelly-Roberts, W. Niforatos, et al. 2006. Structure-activity relationship studies on a series of novel, substituted 1-benzyl-5-phenyltetrazole P2X7 antagonists. *J. Med. Chem.* 49: 3659–3666.
39. Kunkel, M. T., and A. C. Newton. 2010. Calcium transduces plasma membrane receptor signals to produce diacylglycerol at Golgi membranes. *J. Biol. Chem.* 285: 22748–22752.
40. Kessler, S., W. G. Clauss, A. Günther, W. Kummer, and M. Fronius. 2011. Expression and functional characterization of P2X receptors in mouse alveolar macrophages. *Pflugers Arch.* 462: 419–430.
41. Hazleton, J. E., J. W. Berman, and E. A. Eugenin. 2012. Purinergic receptors are required for HIV-1 infection of primary human macrophages. *J. Immunol.* 188: 4488–4495.
42. la Sala, A., D. Ferrari, S. Corinti, A. Cavani, F. Di Virgilio, and G. Girolomoni. 2001. Extracellular ATP induces a distorted maturation of dendritic cells and inhibits their capacity to initiate Th1 responses. *J. Immunol.* 166: 1611–1617.
43. Aga, M., C. J. Johnson, A. P. Hart, A. G. Guadarrama, M. Suresh, J. Svaren, P. J. Bertics, and B. J. Darien. 2002. Modulation of monocyte signaling and pore formation in response to agonists of the nucleotide receptor $P2X_7$. *J. Leukoc. Biol.* 72: 222–232.
44. Coutinho-Silva, R., D. M. Ojcius, D. C. Górecki, P. M. Persechini, R. C. Bisaggio, A. N. Mendes, J. Marks, G. Burnstock, and P. M. Dunn. 2005. Multiple P2X and P2Y receptor subtypes in mouse J774, spleen and peritoneal macrophages. *Biochem. Pharmacol.* 69: 641–655.
45. Ostrom, R. S., C. Gregorian, and P. A. Insel. 2000. Cellular release of and response to ATP as key determinants of the set-point of signal transduction pathways. *J. Biol. Chem.* 275: 11735–11739.
46. Seregi, A., S. Doll, A. Schobert, and G. Hertting. 1992. Functionally diverse purinergic P2Y-receptors mediate prostanoid synthesis in cultured rat astrocytes: the role of ATP-induced phosphatidyl-inositol breakdown. *Eicosanoids* 5(Suppl.): S19–S22.
47. Zhang, Z., Z. Wang, H. Ren, M. Yue, K. Huang, H. Gu, M. Liu, B. Du, and M. Qian. 2011. $P2Y_6$ agonist uridine 5′-diphosphate promotes host defense against bacterial infection via monocyte chemoattractant protein-1-mediated monocytes/macrophages recruitment. *J. Immunol.* 186: 5376–5387.
48. D'Ambrosi, N., M. Iafrate, E. Saba, P. Rosa, and C. Volonté. 2007. Comparative analysis of P2Y4 and P2Y6 receptor architecture in native and transfected neuronal systems. *Biochim. Biophys. Acta* 1768: 1592–1599.

49. Shin, A., T. Toy, S. Rothenfusser, N. Robson, J. Vorac, M. Dauer, M. Stuplich, S. Endres, J. Cebon, E. Maraskovsky, and M. Schnurr. 2008. P2Y receptor signaling regulates phenotype and IFN-α secretion of human plasmacytoid dendritic cells. *Blood* 111: 3062–3069.
50. Wai, L. E., J. A. Garcia, O. M. Martinez, and S. M. Krams. 2011. Distinct roles for the NK cell-activating receptors in mediating interactions with dendritic cells and tumor cells. *J. Immunol.* 186: 222–229.
51. Ferrari, D., P. Chiozzi, S. Falzoni, S. Hanau, and F. Di Virgilio. 1997. Purinergic modulation of interleukin-1β release from microglial cells stimulated with bacterial endotoxin. *J. Exp. Med.* 185: 579–582.
52. Ferrari, D., C. Pizzirani, E. Adinolfi, R. M. Lemoli, A. Curti, M. Idzko, E. Panther, and F. Di Virgilio. 2006. The P2X7 receptor: a key player in IL-1 processing and release. *J. Immunol.* 176: 3877–3883.
53. Mehta, V. B., J. Hart, and M. D. Wewers. 2001. ATP-stimulated release of interleukin (IL)-1β and IL-18 requires priming by lipopolysaccharide and is independent of caspase-1 cleavage. *J. Biol. Chem.* 276: 3820–3826.
54. Pelegrin, P., and A. Surprenant. 2009. Dynamics of macrophage polarization reveal new mechanism to inhibit IL-1β release through pyrophosphates. *EMBO J.* 28: 2114–2127.
55. Perregaux, D. G., P. McNiff, R. Laliberte, M. Conklyn, and C. A. Gabel. 2000. ATP acts as an agonist to promote stimulus-induced secretion of IL-1 β and IL-18 in human blood. *J. Immunol.* 165: 4615–4623.
56. Gu, B. J., B. M. Saunders, S. Petrou, and J. S. Wiley. 2011. P2X$_7$ is a scavenger receptor for apoptotic cells in the absence of its ligand, extracellular ATP. *J. Immunol.* 187: 2365–2375.
57. Hanley, P. J., M. Kronlage, C. Kirschning, A. del Rey, F. Di Virgilio, J. Leipziger, I. P. Chessell, S. Sargin, M. A. Filippov, O. Lindemann, et al. 2012. Transient P2X7 receptor activation triggers macrophage death independent of Toll-like receptors 2 and 4, caspase-1, and pannexin-1 proteins. *J. Biol. Chem.* 287: 10650–10663.
58. Lemaire, I., S. Falzoni, B. Zhang, P. Pellegatti, and F. Di Virgilio. 2011. The P2X7 receptor and Pannexin-1 are both required for the promotion of multinucleated macrophages by the inflammatory cytokine GM-CSF. *J. Immunol.* 187: 3878–3887.
59. Okonogi, K., T. W. Gettys, R. J. Uhing, W. C. Tarry, D. O. Adams, and V. Prpic. 1991. Inhibition of prostaglandin E$_2$-stimulated cAMP accumulation by lipopolysaccharide in murine peritoneal macrophages. *J. Biol. Chem.* 266: 10305–10312.
60. Brambilla, R., J. T. Neary, F. Cattabeni, L. Cottini, G. D'Ippolito, P. C. Schiller, and M. P. Abbracchio. 2002. Induction of COX-2 and reactive gliosis by P2Y receptors in rat cortical astrocytes is dependent on ERK1/2 but independent of calcium signalling. *J. Neurochem.* 83: 1285–1296.
61. Wihlborg, A. K., M. Malmsjö, A. Eyjolfsson, R. Gustafsson, K. Jacobson, and D. Erlinge. 2003. Extracellular nucleotides induce vasodilatation in human arteries via prostaglandins, nitric oxide and endothelium-derived hyperpolarising factor. *Br. J. Pharmacol.* 138: 1451–1458.
62. Costa-Junior, H. M., A. N. Mendes, G. H. Davis, C. M. da Cruz, A. L. Ventura, C. H. Serezani, L. H. Faccioli, A. Nomizo, C. G. Freire-de-Lima, C. Rda. Bisaggio, and P. M. Persechini. 2009. ATP-induced apoptosis involves a Ca^{2+}-independent phospholipase A2 and 5-lipoxygenase in macrophages. *Prostaglandins Other Lipid Mediat.* 88: 51–61.
63. Xia, M., and Y. Zhu. 2011. Signaling pathways of ATP-induced PGE$_2$ release in spinal cord astrocytes are EGFR transactivation-dependent. *Glia* 59: 664–674.
64. Zanin, R. F., E. Braganhol, L. S. Bergamin, L. F. Campesato, A. Z. Filho, J. C. Moreira, F. B. Morrone, J. Sévigny, M. R. Schetinger, A. T. de Souza Wyse, and A. M. Battastini. 2012. Differential macrophage activation alters the expression profile of NTPDase and ecto-5′-nucleotidase. *PLoS ONE* 7: e31205.
65. Grinberg, S., G. Hasko, D. Wu, and S. J. Leibovich. 2009. Suppression of PLCβ2 by endotoxin plays a role in the adenosine A(2A) receptor-mediated switch of macrophages from an inflammatory to an angiogenic phenotype. *Am. J. Pathol.* 175: 2439–2453.
66. Través, P. G., P. de Atauri, S. Marín, M. Pimentel-Santillana, J. C. Rodríguez-Prados, I. Marín de Mas, V. A. Selivanov, P. Martín-Sanz, L. Boscá, and M. Cascante. 2012. Relevance of the MEK/ERK signaling pathway in the metabolism of activated macrophages: a metabolomic approach. *J. Immunol.* 188: 1402–1410.
67. Koizumi, S., Y. Shigemoto-Mogami, K. Nasu-Tada, Y. Shinozaki, K. Ohsawa, M. Tsuda, B. V. Joshi, K. A. Jacobson, S. Kohsaka, and K. Inoue. 2007. UDP acting at P2Y6 receptors is a mediator of microglial phagocytosis. *Nature* 446: 1091–1095.
68. Park, J. E., Y. I. Kim, and A. K. Yi. 2009. Protein kinase D1 is essential for MyD88-dependent TLR signaling pathway. *J. Immunol.* 182: 6316–6327.
69. Matthews, S. A., M. N. Navarro, L. V. Sinclair, E. Emslie, C. Feijoo-Carnero, and D. A. Cantrell. 2010. Unique functions for protein kinase D1 and protein kinase D2 in mammalian cells. *Biochem. J.* 432: 153–163.
70. Newton, R. H., S. Leverrier, S. Srikanth, Y. Gwack, M. D. Cahalan, and C. M. Walsh. 2011. Protein kinase D orchestrates the activation of DRAK2 in response to TCR-induced Ca^{2+} influx and mitochondrial reactive oxygen generation. *J. Immunol.* 186: 940–950.
71. Lavalle, C. R., K. Bravo-Altamirano, K. V. Giridhar, J. Chen, E. Sharlow, J. S. Lazo, P. Wipf, and Q. J. Wang. 2010. Novel protein kinase D inhibitors cause potent arrest in prostate cancer cell growth and motility. *BMC Chem. Biol.* 10: 5.
72. Ulmann, L., H. Hirbec, and F. Rassendren. 2010. P2X4 receptors mediate PGE$_2$ release by tissue-resident macrophages and initiate inflammatory pain. *EMBO J.* 29: 2290–2300.